DEORPHANIZATION AND CHARACTERIZATION OF SEA LAMPREY OLFACTORY TRACE AMINE-ASSOCIATED RECEPTORS

By

Liang Jia

A DISSERTATION

Submitted to
Michigan State University
in partial fulfillment of the requirements
for the degree of

Fisheries and Wildlife —Doctor of Philosophy

2022

ABSTRACT

DEORPHANIZATION AND CHARACTERIZATION OF SEA LAMPREY OLFACTORY TRACE AMINE-ASSOCIATED RECEPTORS

By

Liang Jia

The sense of smell plays an important role in mediating diverse behaviors in the animal kingdom. Odor detection in the sea lamprey is mediated by a limited number of odorant receptors (ORs) and trace amine-associated receptors (TAARs). Upon binding with odorants, the receptors are activated and subsequently activate the downstream neuronal signaling cascade that transforms the chemical information into electrophysiological signals. Odorous biogenic amines, when enriched in biological excretions, stimulate TAARs of the main olfactory epithelium and evoke innate behaviors in animals. I hypothesized that these biogenic amines are potent ligands for lamprey TAARs, and characterized the structural basis for amine recognition in these receptors. Chapter 1 describes discovery that spermine, an odorous polyamine in semen, serves as a sex pheromone in sea lamprey. Spermine potently stimulates the lamprey olfactory system, activates TAAR348 receptor, and attracts ovulated females. A novel antagonist to this receptor inhibits olfactory and female behavioral responses to spermine. This discovery elucidates a mechanism that male animals recruit mates through the release of chemical cues in ejaculates. In chapter 2, I demonstrated that two clades of independently evolved TAARs, represented by sea lamprey TAAR365 (sTAAR365) and mouse TAAR9 (mTAAR9), share a similar response profile. The results suggest a conserved mechanism whereby independently evolved TAAR receptors utilize convergent structural bases to detect various biogenic polyamines. In chapter 3, I found that a cadaverine-responsive sea lamprey TAAR receptor, TAAR346a, exhibits high basal activity when heterologously expressed in HEK293T cells. Triethylamine serves as an inverse agonist for TAAR346a that can specifically

attenuate its high basal activity. These data support a model in which the inverse agonist recognizes only one of the two orthosteric sites used by the agonist as it elicits its inhibitory effect on the basal activity of the receptor. Further evidence was provided to highlight the importance of interhelical interactions in modulating ligand-independent activation of TAAR346a. Thus, this thesis contributes to a better understanding of sea lamprey olfaction and the structural basis of TAARs for amine recognition in vertebrate animals.

Dedicated to my wife Ya Wang, daughter Yige Jia and my parents.
Thank you for supporting and loving me each and every day.

ACKNOWLEDGEMENTS

The completion of this dissertation would not ever happen without the help of Li lab. I am deeply grateful for their support. First, I would like to thank my supervisor Dr. Weiming Li for his invaluable supervision, supports and encouragement during the research of my PhD degree. His immense knowledge and experience have encouraged me and evoked my scientific curiosity. Many thanks to my co-adviser and committee member, Dr. Richard R. Neubig, who read numerous of my revisions and provided invaluable feedback on my manuscripts. Also, I would like to thank my committee members, Dr. Yu-Wen Chung-Davidson and Dr. Cheryl A. Murphy for their guidance, selfless help and assistance to make this project possible.

I would like to thank all the members in the Li Lab. It is my pleasure to be a member of this great family. It is their kind help and support that have made my study and life in the Michigan State a wonderful time. In particular, I am extremely grateful to my colleagues, collaborators, and friends, Dr. Anne M. Scott, Dr. Qian Li, Dr. Shengju Li, Dr. Ke Li, Wenxuan Dai, Dr. Yao Zu, Dr. Jianfeng Ren, Dr. Qinghua Zhang, Dr. Edmund Ellsworth, and Dr. Zhe Zhang for their technical support and collaborative efforts during data collection. I would also like to thank the staff in the core facility of Department of Pharmacology and Toxicology for their technical assistance.

Additionally, I would like to express my sincere gratitude to the staff in the Department of Fisheries and Wildlife, particularly Jill Cruth for her kind help during my PhD study. I would like to also thank the Hammond Bay Biological Station for providing research specimens. My appreciation also goes out to the Michigan State University, the Great Lakes Fishery Commission, and the SHOU & MSU Joint Research Center for their generous funding.

And finally, I own my deepest gratitude to my parents, my wife, Ya Wang, and my daughter,

Yige Jia, for their unconditional love, unfailing support, and continuous encouragement.

TABLE OF CONTENTS

LIST OF TABLES

LIST OF FIGURES

KEY TO ABBREVATIONS

ACIII	type III adenylyl cyclase
AOB	accessory olfactory bulb
AR	adrenergic receptor
BSA	bovine serum albumin
CAD	cadaverine
cAMP	cyclic adenosine monophosphate
CAM	constitutively active mutant
cGMP	cyclic guanosine monophosphate
CNG	cyclic nucleotide gated ion channel
CRE	cyclic-adenosine monophosphate response element
DIC	differential interference contrast
DIG	digoxigenin
DkPES	3,12-diketo-4,6-petromyzonene-24-sulfate
DLR	diencephalic locomotor region
DMEM	Dulbecco's Modified Eagle Medium
ECL	extracellular loop
EC_{50}	half-maximal effective concentration
EGFP	enhanced green fluorescent protein
E_{max}	maximal efficacy
EOG	electro-olfactogram
EPL	external plexiform layer

ESI-MS/MS	electrospray ionization mass spectrometry
ESP	exocrine gland secreted peptide
ETC	external tufted cell
FBS	fetal bovine serum
FPR	formyl peptide receptor-related receptor
$G_{\alpha olf}$	olfactory G protein
GABA	gamma-aminobutryric acid
GC	granule cell
GC-D	guanylyl cyclase D
GCL	granule cell layer
GFP	green fluorescent protein
GL	glomerular layer
GPCR	G-protein coupled receptor
GR	gustatory receptor
HEK293T	human embryonic kidney 293T
HTS	high-throughput screening
ICL	intracellular loop;
IC_{50}	half-maximal inhibitory concentration
IPL	internal plexiform layer
IR	ionotropic odor receptor
IS	internal standard
JGC	juxtaglomerular cell
3kACA	3-keto allocholic acid

3kPZS	3-keto petromyzonol sulfate
LCR	locus control region
LOT	lateral olfactory tract
MC	mitral cell
MCL	mitral cell layer
MHC	major histocompatibility complex
MLR	mesencephalic locomotor region
MOE	main olfactory epithelium
MRM	multiple reaction monitoring
mRTPs	mouse receptor transporting proteins
MS222	3-aminobenzoic acid ethyl ester
mTAAR9	mouse trace amine-associated receptor 9
M/TC	mitral and tufted cell
MUP	major urinary protein
nap-spermine	1-naphthylacetyl spermine
NBT/BCIP	nitro blue tetrazolium and 5-bromo-4-chloro-3-indolyl phosphate
OFL	olfactory fiber layer
ONL	olfactory nerve layer
OR	odorant receptor
OSN	olfactory sensory neuron
PADS	petromyzonamine disulfate
PGC	periglomerular cell
PSDS	petromyzosterol disulfate

PUT	putrescine
PZS	petromyzonol sulfate
RT	room temperature
SAC	short axon cell
Sp-d_8	[$^2H_8$]-spermine
SPD	spermidine
SPM	spermine
SSC	saline-sodium citrate
sTAAR365	sea lamprey trace amine-associated receptor 365
SV40	simian virus 40
TA	trace amine
TAAR	trace amine-associated receptor
TC	tufted cell
TCA	trichloroacetic acid
TEA	triethylamine
TM	transmembrane
TR-FRET	time-resolved fluorescence energy transfer
TSHR	thyroid stimulating hormone receptor
UHPLC-MS/MS	ultrahigh performance liquid chromatography-tandem mass spectrometry
VNO	vomeronasal organ
V1R	vomeronasal type 1 receptor
V2R	vomeronasal type 2 receptor

INTRODUCTION TO DISSERTATION

GENERAL INTRODUCTION

Sensory systems, including olfaction, gustation, vision, hearing, and touch, allow living organisms to perceive external stimuli from the surrounding environment. Among these sensory systems, the sense of smell plays a critical role in the perception and discrimination of a great number of environmental odors in the animal kingdom, ranging from invertebrates to mammals [1-3]. These odors serve as chemical cues that modulate social behaviors and physiological functions of many species. Animals show corresponding behavioral responses upon detection of specific odors that alarm environmental risks or facilitate chemical communications among conspecifics and interspecies, such as locating food, identifying kin, avoiding predators, recognizing territory, mating, and navigation [4-8].

The sense of smell is well conserved in living organisms. Bacteria and prokaryotes have specialized chemoreceptive mechanisms in response to environmental chemicals [9-11]. The specialized chemoception receptor enables *E. coli* to detect an attractant stimulus and show corresponding attraction movement. For humans, the sense of smell influences the living quality and is involved in the differentiation of thousands of airborne odors with high sensitivity [12]. Olfactory perception relies on the interaction between a given odorant and paired receptors and results in appropriate behavioral responses, such as attraction and aversion. The olfactory system detects and discriminates tens of thousands of structurally distinct odorants through a repertoire of chemosensory receptor proteins, which are expressed at the cilia of olfactory sensory neurons (OSNs) in the olfactory epithelium of vertebrates, or the antenna and maxillary palp of insects [13]. Since the discovery of olfactory receptor genes [14], great strides have been made in understanding the molecular basis of olfaction. Upon binding an odorant, the receptors are activated, leading to

the activation of the downstream neuronal signaling cascade that transforms the chemical information into electrophysiological signals (Figure I-1). Consequentially, the electrical signals are transmitted along the axons of OSNs projecting to the main and/or accessary olfactory bulb of vertebrates or the antennal lobe of insects (the second relay station of the neural circuit), followed by mitral/turfed mediated projections to the primary olfactory cortex, finally resulting in corresponding physiological and behavioral outputs [1-3].

Olfactory perception relies on the recognition of odors by olfactory receptors that were first reported by Drs. Linda Buck and Richard Axel in 1991, who were awarded the 2004 Nobel Prize in Physiology or Medicine for their pioneering work on olfaction [14]. Genes encoding olfactory receptors are variable among vertebrate species that have undergone rapid evolution with gene duplication, degeneration, and pseudogenization [15, 16]. Previous studies have shown that the size of olfactory receptor repertoires is correlated with species-specific habitat adaptations [15, 16]. Olfactory receptors constitute the largest and most diverse family of G protein-coupled receptors (GPCRs) in mammals [16]. Two subfamilies of GPCRs serving as olfactory receptors are highly expressed at the cilia of OSNs in the main olfactory epithelium (MOE): odorant receptors (ORs) and trace amine-associated receptors (TAARs) [14, 17, 18]. ORs are encoded by the largest mammalian gene family. In contrast, genes encoding TAARs constitute a much smaller repertoire in comparison with that of ORs. Phylogenetic analysis has indicated that TAARs are well conserved in vertebrates and distantly related to biogenic amine receptors [17], suggesting that TAARs may have a distinct function to specifically detect volatile amines with high sensitivity.

Our current understanding of ligand selectivity of TAARs relies on studies of a small number of deorphanized TAARs in several species, including mouse, zebrafish, rat, and human [18-27]. One of the primary roadblocks currently under the investigation of TAARs is a lack of identified

agonists. In addition, the expression of TAARs in nonolfactory cells is affected to a great extent by endoplasmic reticulum retention and protein folding impairment [28]. Recently, the whole-genome sequencing and a well-established heterologous expressing system have enabled us to perform high-throughput screening for novel ligands of orphan TAARs that allow a better understanding of olfactory TAAR mediated chemosensory perception [29, 30]. The other blockade slowing down the understanding of olfaction is a lack of crystal structure for olfactory receptors. Despite many OR agonists that have been identified, the structural basis of ORs for ligand recognition is based on studies of a limited number of ORs. Several highly variable residues in transmembrane helices III, V, and VI are involved in ligand binding in ORs [31-33]. However, the structural determinants of ligand recognition by most TAARs remain largely elusive.

The sea lamprey (*Petromyzon marinus*), one of the most primitive extant vertebrates, is an ideal species for the study of chemical communication. Sea lamprey possess a well-developed olfactory system that shows high sensitivity and specificity to olfactory stimuli. The olfactory organ in adult sea lamprey has a large nasal sac with lamellar folds containing both a main olfactory epithelium (the main olfactory organ) and tubular diverticula (the accessory olfactory organ) [34]. More importantly, the sea lamprey has a limited-repertoire of TAAR-like receptors (hereafter TAARs) expressed at the cilia of OSNs [29]. Hence, the sea lamprey provides a good model to elucidate biogenic amines detected by TAARs and their corresponding olfactory outputs. This thesis aims to develop a better understanding of amine agonists, inverse agonists, and antagonists for TAARs, physiological functions and behavioral responses of these amine ligands, and the structural basis of TAARs for amine recognition. Agonists and antagonists for TAARs identified in this study may provide potential approaches either for sea lamprey population control in the Great Lakes or conservation in the Atlantic Ocean.

The purpose of this chapter is to summarize the current knowledge on vertebrate olfactory systems, with an emphasis on olfactory receptors and sensory neurons in sea lamprey. The understanding of the main olfactory pathway and sensory input processing mechanism from olfactory sensory neurons to the olfactory bulb, olfactory circuits to higher brain centers, and olfactory-driven behavioral output are also discussed.

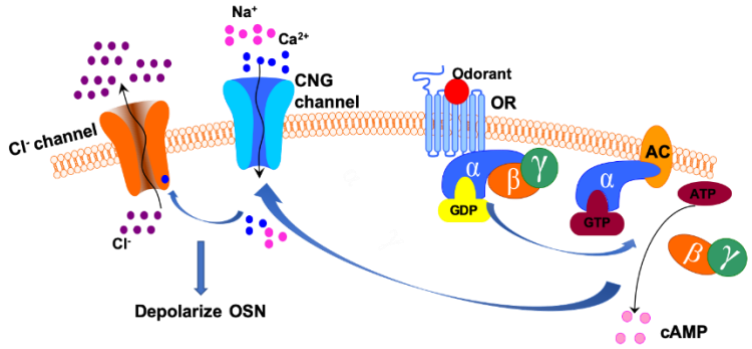

Figure I-1. Schematic diagram illustrating the endogenous OR signal transduction pathway in the olfactory sensory neurons

On an OSN, an odorant binds to an OR at sensory cilia, and the odorant-bound OR is coupled with the olfactory specific G protein $G_{\alpha olf}$, which consequently activates type III adenylyl cyclase (ACIII) resulting in an increase of cellular cAMP production. The cAMP subsequently leads to the opening of cAMP-sensitive cyclic nucleotide-gated (CNG) channels, which cause sodium and calcium influx, depolarize the neuron and consequentially open the calcium-gated chloride ion channels. The chloride ion outflux results in further membrane depolarization of OSNs that generates action potentials. OSN, olfactory sensory neurons; AC, adenylyl cyclase; OR, odorant receptor; CNG channel, cAMP-sensitive cyclic nucleotide-gated channel.

OLFACTORY ANATOMY IS WELL CONSERVED IN VERTEBRATE ANIMALS

The olfactory system is an important sensory system in vertebrates, ranging from lamprey to mammals, and plays a critical role in the perception and discrimination of a great number of environmental stimuli. Almost all-natural olfactory stimuli are composed of larger numbers of complex odor mixtures. For example, the olfactory epithelium of humans expresses around ~400 intact olfactory receptors [13], and, with a combinatorial manner, it is speculated that humans can discriminate at least a trillion olfactory stimuli [12]. Although the sea lamprey genome encodes a much smaller olfactory receptor repertoire [29], sea lamprey still relies heavily on chemical cues for migration and reproduction. Similarly, teleost fish can detect soluble odorants in the water and exhibit fundamental behaviors [35-37].

The peripheral olfactory system exhibits many common features at the signal transduction level among vertebrates, but some species have species-specific anatomical structures of the olfactory organ. For example, a peripheral olfactory organ containing the main olfactory epithelium appears to be well conserved among vertebrates. Also, most vertebrates, including lamprey, commonly utilize a G-protein $G_{\alpha olf}$ mediated signal transduction cascade to convey olfactory signals. For unique features of the olfactory system, the sea lamprey possesses a two-chambered nasal pit that is integrated into a single nostril on top of the skull [34]. In contrast, teleost fish possess two nasal cavities, with an anterior nostril (water entrance) and a posterior nostril (water exit) at each nasal cavity [37]. Moreover, lamprey have a unique feature in having a main olfactory organ and a primordial accessory olfactory organ [34]. Whereas, cartilaginous fish and teleost fish only have a main olfactory organ, and a vomeronasal organ is observed in the lungfish [35]. Although the vomeronasal organ is absent from the olfactory system of jawless and

teleost fishes, genomic mining revealed that molecular components of the vomeronasal organ are well-conserved in genomes of sea lamprey and teleosts [29, 36, 37]. In contrast, mammals, reptiles, and amphibians have a dual olfactory system that is composed of a main olfactory organ and a vomeronasal organ.

Olfactory sensory neurons perceive odor information by expressing a given olfactory receptor at the cilia extending into the mucosa of the nasal cavity. Each olfactory sensory neuron is destined to express a single type of olfactory receptor from the receptor repertoire, which is referred to as the "one neuron-one receptor" hypothesis [38]. However, several recent studies have challenged the "one neuron-one receptor" hypothesis, showing that immature sensory neurons can express multiple olfactory receptor genes from different chromosomes [39]. Moreover, contradictory results have also been reported in *Drosophila* [40]. However, most mature olfactory sensory neurons in mice only express one of the ~1000 olfactory receptor genes, suggesting the "one neuron-one receptor" hypothesis seems to be valid in mature neurons.

Upon the activation of olfactory sensory neurons by a given odorant, the activated neurons generate an action potential and project olfactory signals to a symmetrically distributed forebrain structure, the olfactory bulb (OB) [41]. The axons from a population of olfactory sensory neurons expressing the same olfactory receptor converge to a glomerular structure in the olfactory bulb [41, 42]. This topographic pattern of axonal convergence from olfactory sensory neurons to the olfactory bulb is well-conserved in vertebrates and is referred to as the "one receptor -one glomerulus" hypothesis [41-44]. The sensory inputs are integrated, synapsed in the glomeruli, and consequently relayed to higher neural processing centers. The general anatomy of the olfactory bulb exhibits many common features among various vertebrate species, including lamprey. Each glomerulus receives signal inputs from sensory neurons expressing the same odorant receptors,

and then may synapse with interneurons and projection neurons, and transmits signals to higher olfactory processing centers in the brain, where olfactory signals are interpreted to corresponding behavioral responses.

OLFACTORY RECEPTORS TYPES AND THEIR LIGANDS

The olfactory system has a remarkable capacity to detect numerous chemical cues in the natural environment. The olfactory epithelium contains millions of olfactory sensory neurons that extend a single dendrite toward the surface of the epithelium [37, 38]. Olfactory sensory neurons detect odorants at specialized cilia that are located at the apical part of the dendrite, being equipped with the requisite chemosensory receptors and signaling cascade components [39]. At the olfactory sensory neurons, chemical information of a given odorant is converted into biological signals via the activation of paired olfactory receptors [40-44].

The repertoire of olfactory receptors varies extensively among different vertebrate species [45-49]. The genomic DNA contains multiple types of genes encoding the olfactory receptor proteins, a superfamily of the seven-transmembrane G-protein coupled receptors (GPCRs) [14, 18, 45]. In addition, very few neurons express the non-GPCR receptor guanylyl cyclase D (GC-D, Gucy2d) and utilize a noncanonical cyclic guanosine monophosphate (cGMP)-mediated signaling cascade to process the olfactory inputs [45]. Two subfamilies of GPCRs, odorant receptors (ORs) and trace amine-associated receptors (TAARs) serve as chemosensory receptors expressed in the main olfactory epithelium [14, 18]. Whilst, sensory neurons in the vomeronasal organ utilize three subsets of GPCRs, vomeronasal type 1 receptor (V1R), vomeronasal type 2 receptor (V2R), and formyl peptide receptor-related receptors (FPR), to detect olfactory stimuli [45].

Odorant receptors (ORs)

Odorant receptor genes are present in the genome of all vertebrates, including the lamprey [14, 29, 46]. The number of OR genes is much smaller in teleost fish and lamprey than in mammals. The zebrafish has the largest known OR repertoire in teleosts, containing ~134 intact OR genes

and 21 pseudogenes [45, 47]. As with tetrapod animals, the zebrafish ORs are distributed throughout the genome and are generally clustered [45]. The sea lamprey genome contains 27 intact OR genes that are expressed in the olfactory epithelium of both parasitic and adult animals [29]. By contrast, amphibian species have a larger OR repertoire, exhibiting the selective pressure of ORs in amphibians and terrestrial animals [45]. Amphibians and terrestrial animals seem to have evolved a large number of ORs for the detection of tremendous volatile odorants, allowing transformation from aquatic to terrestrial habitat [47]. Meanwhile, these species still maintain the ability to detect water-soluble odorants. However, marine mammals that had evolved from a common terrestrial ancestor, including whales and dolphins, lose a great number of ORs (express as pseudogenes) for the adaption of aquatic habitat [47, 48]. The human genome has ~1000 OR genes, but over 60% are believed to be pseudogenes [13]. Likewise, rodents have a similar OR repertoire in size as that of humans, but only containing about 20% pseudogenes, which may underlie a reduced olfaction dependence in humans relative to mice [45].

Odorant receptors are predominantly expressed in sensory neurons of the main olfactory epithelium [49]. A single OR can detect multiple odorants and a given odorant can be recognized by multiple ORs. ORs exhibit a canonical structure of seven transmembrane (TM) α-helices, containing a glycosylation site in the extracellular N-terminal and interhelical disulfide bonds between the extracellular loops (ECLs) [32]. ORs possess several conserved structural motifs that differentiate themselves from other GPCRs, such as an LHTPMY motif in the intracellular loop 1 (ICL1), a MAYDRYVAIC motif at the end of TM3, an FSTCSSH motif at the beginning of TM6, and a PMLNPF motif in TM7 [49, 50]. Moreover, ORs have highly variable amino acids in TMs that are responsible for the selectivity of ligand recognition [27, 31-33, 50]. Many ORs possess a broad ligand spectrum compared with non-olfactory GPCRs, allowing ORs to detect various

structurally similar odorants [50]. For example, human ORs can detect distinct small molecular odorants with a hydrophobic structure, suggesting that the recognition of these odorants to ORs likely rely on hydrophobic interactions [50]. Generally, ORs can detect various odorants sharing a common structural basis or functional group, and meanwhile utilize highly variable residues to determine ligand selectivity [32, 33, 50, 51].

Odorant receptors utilize the heterotrimeric G-protein subunit $G_{\alpha olf}$, type III adenylyl cyclase (ACIII), CNG ion channel, and calcium-gated chloride ion channel to mediate odor signal transduction [51]. Upon odorant binding, the OR shifts into an active conformation that allows to be coupled with the olfactory specific G protein $G_{\alpha olf}$ and in turn activates adenylyl cyclase III (AC III) to produce cAMP, an intracellular second messenger in olfactory sensory neurons [52]. Cytoplasmic cAMP directly leads to the opening of cAMP-sensitive cyclic nucleotide-gated channels (CNG channels). The activated CNG channels permit the influx of Ca^{2+} and Na^{+}, which in turn triggers the opening of calcium-gated chloride ion channels. The Ca^{2+} and Na^{+} influx and the movement of Cl^{-} outward depolarize the olfactory sensory neurons to generate action potentials [53, 54].

Phylogenetic analysis has suggested that vertebrate ORs are categorized into nine groups (including α, β, γ, δ, ε, ζ, η, θ, and κ) and each group has evolved respectively from an ancestral gene [45, 55]. Remarkably, an explosion of gene numbers in the α and γ clades was observed in tetrapod species and are referred to class I and class II ORs, respectively [55]. This expansion suggests that the evolution of class I and class II OR repertoires played an important role in the evolutionary adaption of vertebrates from aquatic to terrestrial environments [47, 48]. The sea lamprey ORs are classified as class I ORs, suggesting that the evolutionary separation of class I and class II ORs antedates the divergence of jawless and jawed vertebrates [29, 45, 55]. The

remnant seven groups of ORs primarily exist in the teleost and amphibian genomes. Notably, ORs from groups β, δ, ε, and ζ, are clarified into the class I ORs, but η, θ, and κ groups neither belong to class I nor class II ORs [45, 55]. Thus, these findings suggest that ORs of the β, δ, ε, ζ, η, θ, and κ groups mainly serve to recognize water-soluble odorants, while α and γ ORs are responsible for the detection of airborne odorants [45].

Trace amine-associated receptors (TAARs)

Besides ORs, additional classes of olfactory receptors were suspected to express in sensory neurons of the main olfactory epithelium for odor detection. In 2006, the second class of olfactory GPCRs, trace amine-associated receptors (TAARs), were efficiently expressed in the MOE of mice and served as olfactory receptors for the detection of volatile amines [18]. TAARs are a subfamily of class-A (rhodopsin-like) GPCRs that were initially identified in 2001 for the detection of trace amines (TAs), a series of intermediate products at very low concentration for the synthesis of biogenic amines, in the nervous system of vertebrates [56, 57]. The deorphanization of TAARs showed that one member of TAARs (TAAR1) specifically expressed in the central nervous systems and peripheral tissues exhibits high sensitivity to phenyl-ethanolamine and tryptamine [56, 57]. However, all other TAARs (excluding TAAR1) display functional dichotomy and are highly expressed in the murine olfactory system [18]. Thus, all TAARs except TAAR1 are known as olfactory TAARs, being responsible for the detection of volatile amines.

Trace amine-associated receptors are thought to have arisen from a common ancestor before the divergence of jawed vertebrates and jawless fish [45]. The classical TAAR fingerprint motif (NSxxNPxxYxxxYxWF) in the TM7 is present in most gnathostome TAARs but is partially conserved in the sea lamprey TAARs [17]. Thus, it remains controversial how TAAR genes arose during vertebrate evolution. Moreover, most TAARs, from lamprey to mammal, contain the amine

recognition motif (DW motif), a highly conserved amine recognition motif in biogenic amine receptors [58, 59]. The DW motif consists of a negatively charged aspartate ($D^{3.32}$) in the TM3 and a hydrophobic tryptophan ($W^{7.40}$) in the TM7. The $D^{3.32}$ residue contributes a deprotonated carboxyl group to form a salt bridge with the amino group of ligands [40, 58], whereas the tryptophan $W^{7.40}$ serves to stabilize the hydrophobic backbone of ligands [59]. As lamprey TAARs play critical roles in mediating chemosensory function [29], we speculate that TAARs have arisen early in jawless fish evolution. The number of olfactory TAAR genes is highly variable among the species examined [60]. As with ORs, TAAR genes lack introns in the coding region and disperse at a specific region in the mouse genome, forming a single cluster [55, 60]. In contrast, the TAAR genes of sea lamprey and teleost fish are located on multiple chromosomes [29, 55, 60]. In all vertebrate species, the TAAR repertoires are much smaller than the OR repertoires. Mammals, amphibians, reptiles, as well as birds, have a limited number of TAAR genes [60-62]. Humans have 6 intact TAAR genes, while mice possess 15 functional TAARs, and rats contain 17 intact TAAR genes [55, 60]. Strikingly, the dog genome has been shown to have 2 intact TAAR genes for an animal with a keen sense of smell [60]. However, there is a large expansion in the repertoire of TAAR genes in teleost fishes, such as zebrafish, medaka, and stickleback, conceivably due to a genome duplication that occurred in these teleost species [62, 63]. The zebrafish has a similar size repertoire encoding TAARs (109 intact genes) and ORs (155 intact genes) [63]. In jawless fish, the sea lamprey genome has a similar number of TAAR genes as with ORs (27 intact OR genes), containing 26 intact TAAR genes and 2 pseudogenes [29]. Several of these TAAR genes are expressed in the main olfactory organ of lamprey [29]. Phylogenetic analysis has been shown that TAAR genes are distantly related to aminergic receptors, but are distinct from canonical ORs [55]. Up to now, the origin of TAAR genes is still debatable. Some groups believed that TAARs had

emerged before the separation of jawless and jawed vertebrates, and are likely evolved from a common ancestor (5-hydroxytryptamine receptor 4) [29, 60]. The TAAR phylogenetic tree suggests that lamprey TAAR genes converge into a monophyletic branch out of the jawed TAAR clade, sharing a high bootstrap probability (99%) [60]. In addition, lamprey TAAR genes have been shown to encode proteins that serve as olfactory receptors in the lamprey olfactory epithelium, which appears to support that TAAR genes are present in jawless vertebrates [29]. However, others argued that TAAR genes initially arose in elephant sharks, probably as lamprey TAAR clade is closely related with aminergic receptors [17]. The phylogenetic tree of TAARs classified the TAAR family into five jawed vertebrate-specific subfamilies (subfamilies I-V) and a lamprey-specific subfamily [60]. The large expansion of teleost TAAR genes mainly occurred in the subfamily I TAARs [60]. TAAR1 genes from various species examined converged into a monophyletic clade (subfamily IV) and are presumed to respond to trace amines in the nervous system, suggesting that the "non-olfactory type" function is well conserved in this subfamily of TAAR genes [55, 60]. All other TAARs, like ORs, serve as olfactory type receptors that recognize diverse volatile amines and elicit distinct behaviors [18, 19, 64, 65].

All TAARs (excluding TAAR1) are expressed in a minority of sensory neurons in the mouse olfactory epithelium, abiding by the "one neuron-one receptor" hypothesis [18-20]. Each sensory neuron expressing a unique TAAR gene does not co-express other TAARs or ORs [18]. Although TAAR genes are not phylogenetically related to canonical ORs, TAAR sensory neurons express key factors of canonical OR signal transduction cascade, including $G_{\alpha olf}$, ACIII, and CNG channels, suggesting that TAARs may utilize a similar mechanism to evoke amine responses as ORs [18]. This is supported by expressing TAARs in a heterologous expression system that TAARs are coupled to $G_{\alpha olf}$ to initiate cAMP cascade [18, 26, 27, 64]. In addition, TAAR sensory neurons in

a $G_{\alpha olf}$-knockout mouse strain showed no olfactory responses to odor stimuli [65]. Also, olfactory responses to volatile amines were absent in neurons with ACIII or the CNG channel defect [66, 67]. However, additional pieces of evidence have been shown that the non-olfactory TAAR1 utilizes a different signaling pathway (by coupling to $G_{\alpha s}$) to induce intracellular cAMP production and further activate downstream pathways [68].

Our current understanding of the structural basis of olfactory TAARs for ligand specificity and selectivity is based on several studies [18, 19, 23, 25-27, 64, 68], including those on 8 mouse TAARs, 6 rat TAARs, 2 primate TAARs, and 12 zebrafish TAARs. A number of olfactory TAARs are broadly activated by some structurally related ligands, while some TAARs are narrowly tuned for specific odorants [19]. Mouse TAAR3 recognizes isoamylamine and isobutylamine with high sensitivity and specificity [20]. β-phenylethylamine is able to specifically activate mouse TAAR4 and rat TAAR4 [18]. TAAR5 of mouse, rat, macaque, and human shows robust response to trimethylamine [18, 19, 68, 69]. Mouse TAAR9 is broadly tuned by monoamines, diamines, and polyamines, including triethylamine, cadaverine, spermine, and spermidine [19]. Mouse TAAR7e and TAAR7f share great sequence identity and can be activated by structurally related ligands. Mouse TAAR7e specifically responds to N, N-dimethylphenylethylamine and 5-methoxy-N, N-dimethyltryptamine, whereas N, N-dimethylcyclohexylamine selectively activates mouse TAAR7f [64]. Mutational analysis showed that the TAAR7e mutant with swapped residues from TAAR7f at positions 3.37 and 3.38 reverses receptor activity for N, N-dimethylcyclohexylamine, and vice versa [64]. Other examples in regard to the molecular basis of ligand selectivity are delineated in zebrafish olfactory TAARs. The two aspartates $Asp^{3.32}$ and $Asp^{5.42}$ in TAAR13a, TAAR13c, TAAR13d, TAAR13e, and TAAR14d serve as a di-cation recognition motif for the detection of diamines [27]. However, receptors that contain $Asp^{3.32}$ or $Asp^{5.42}$, including TAAR10a, TAAR12h,

TAAR12i, TAAR16c, TAAR16e, and TAAR16f, can be activated by monoamines. Interestingly, mutations of $Asp^{5.42}$ enable the receptor to detect a monoamine ligand, 3-methoxytyramine [27]. Moreover, the $Asp^{6.58}$ residue functions as an allosteric binding site for cadaverine recognition. Mutation of $Asp^{6.58}$ creates a supersensitive receptor that exhibits a significant increase in affinity of cadaverine [58]. To date, the structural basis of a TAAR receptor recognizes amines with one or two amino groups having been examined. However, how TAAR receptors recognize polyamines with three or four amino groups has not been determined.

Moreover, these volatile amines for TAARs are produced by the decarboxylation of amino acids and therefore are enriched in rotten tissues and body fluids (such as urine and semen) of many organisms [21, 26]. Behavioral trials have suggested that volatile amines are involved in mediating intraspecies and interspecies chemical communication. TAARs responded to these amines can elicit innate behavioral responses, such as attraction or aversion [18, 21, 26, 27, 64, 69]. Using a heterologous cell expression system, several groups have identified various ligands for many vertebrate TAARs, with a half-maximal effective concentration (EC_{50}) value ranging from 10^{-7} to 10^{-4} molar [18, 19, 26, 27, 64]. Consistently, the electrophysiological recordings of neurons expressing TAARs validated ligands identified from heterologous screening, but the *in vivo* recording of TAAR sensory neurons are more sensitive to various amines, with the EC_{50} values at nanomolar concentrations [65, 70]. In addition, TAAR sensory neurons are broadly tuned for amines in the *in vivo* analysis. Knockout of the mouse olfactory TAAR gene cluster results in severe defects in amine detection [20]. However, a single TAAR gene deficit only reduces the behavioral sensitivity to its most potent ligand [20].

Guanylyl cyclase-D

The non-GPCR olfactory guanylyl cyclase D (GC-D) was initially identified from the rat

olfactory epithelium in 1995 [71]. The GC-D transcripts are restrictedly expressed in a minority of olfactory sensory neurons (less than 0.1%) that are randomly scattered among OR at the posterior of the main olfactory epithelium [72, 73]. Like OR and TAAR expressing neurons, these rare GC-D neurons exhibit a canonical bipolar morphology [71-73]. The GC-D neurons project their axons to glomeruli at the caudal part of the olfactory bulb, forming a necklace structure [72]. Being distinct from OR- and TAAR-expressing sensory neurons, the GC-D neurons do not co-express components of the canonical $G_{\alpha olf}$ signaling pathway, including $G_{\alpha olf}$, ACIII, and CNG channels [72]. Instead, this small group of neurons was found to express GC-D and cGMP-sensitive CNG channels, suggesting that these neurons may use cGMP cascade to mediate olfactory signal transduction [71, 72].

Evolutionary analysis has revealed that the GC-D gene *Gucy2d* is pseudogenized in the primate lineage, probably because the GC-D neuron mediated olfactory function is degenerated in primates [74]. GC-D neurons have been shown to respond to diverse ligands, including carbon dioxide, carbon disulfide, and natriuretic peptides [75-77]. Carbon dioxide is considered to function as an important environmental cue, and its concentrations are relevant to the presence of prey and predator [76]. When exposed to carbon dioxide, GC-D neurons exhibit an increase in intracellular cGMP level followed by the opening of cGMP-sensitive CNG channels, which results in an increase in neuronal action potential [76]. Furthermore, it has been shown that GC-D neurons display extremely high sensitivity to carbon disulfide, which is thought to be associated with food selection behavior in rodents [77]. GC-D neurons are able to detect carbon disulfide with a threshold less than micromolar, whereas carbon dioxide exhibits a much higher threshold at a millimolar range [76, 77]. In addition, GC-D neurons have been shown to respond to two kinds of natriuretic peptides, uroguanylin and guanylyn [75]. Uroguanylin and guanylyn are proposed to

be present in excreted urine, and consistently, GC-D neurons are able to be activated by diluted urine [75]. More importantly, GC-D neurons had impaired responses to natriuretic peptides when knockout the expression of GC-D and cGMP-specific CNG channel genes, suggesting that natriuretic peptides activate GC-D neurons through the cGMP signaling [75]. Taken together, these findings suggest that urinary natriuretic peptides serve as physiological stimulants that are critical for the activation of GC-D neurons.

Vomeronasal Receptors (V1Rs and V2Rs)

In addition to the main olfactory organ, a vomeronasal organ (VNO) was found to be present in most tetrapod animals and functions as an accessory olfactory organ for the detection of pheromones [78-81]. The VNO is located above the nasal palate, connecting to the nasal cavity via a duct [78]. The olfactory stimuli are pumped into the VNO via this duct and then distributed to the VNO lumen, where VNO sensory neurons recognize these odorants [78-81]. The VNO deficit can cause the abrogation of social and sexual behaviors, suggesting that the VNO plays an important role in sensing pheromones and allelochemicals of intra- and interspecies [78]. VNO sensory neurons are located in a crescent-shaped olfactory epithelium and project their axons to distinct regions of the accessory olfactory bulb (AOB) [79].

Vomeronasal organ neurons express three different types of olfactory GPCRs for the detection of pheromones, including vomeronasal type 1 receptors (V1Rs), vomeronasal type 2 receptors (V2Rs), and formyl peptide receptors (FPRs) [81-85]. Although lamprey and teleost fish do not contain VNO, the sea lamprey genome has been shown to contain an intact V1R gene [29]. Moreover, it has been suggested that V1Rs and V2Rs are expressed in the MOE of teleost fish, although mammalian V1Rs and V2Rs are expressed in the vomeronasal neuroepithelium of VNO [82-85]. Two types of G proteins, $G_{\alpha i2}$ and $G_{\alpha o}$, have been shown to be expressed in V1R- and

V2R-expressing VNO neurons, respectively [81-85]. V1R-expressing neurons co-express $G_{\alpha i2}$ in the apical layer of the VNO epithelium [81, 82], whereas $G_{\alpha o}$ is co-expressed with V2Rs in the VNO neurons found at the basal layer of the VNO epithelium [83-85]. As with ORs and TAARs, V1R genes are intron-less and generally clustered on chromosomes [86, 87]. Each VNO neuron monoallelically expresses a single V1R gene. V2R genes, a typical class C GPRCs, are encoded by multiple exons and can be coordinately expressed in individual sensory neurons [88]. V2Rs have a much longer hydrophobic N-terminal extracellular domain that is thought to be involved in ligand recognition [88].

Phylogenetic analysis has indicated that V1R genes exhibit no significant sequence homology with V2Rs gene and can be classified into three clades (Clade 1: mammals and amphibians; Clades 2 and 3: teleost fish and amphibians) [89-93]. It suggests that V1R genes emerged after the separation of jawless fish and jawed vertebrates [90]. Evolutionary analysis of vertebrate V1Rs suggested that V1Rs are distantly related to bitter taste receptors, while V2Rs are distantly related to sweet/umami taste receptors and metabotropic glutamate receptors [89]. The number of V1R genes shows significant variation among vertebrate species [90, 91]. V1R genes expanded greatly in mammals that have a well-developed VNO, for example, mouse (239), rat (109), rabbit (159), and opossum (98) [90, 91]. However, the V1R repertoire size exhibits tremendous variation among mammalian species. In contrast to mammals, teleosts have the V1R gene families that are of similar sizes [92, 93]. Most V1R genes are absent or pseudogenized in the primate lineage [91]. The human genome contains about 200 V1R pseudogenes and four intact V1R genes [91]. This conceivably is because primate animals possess a degenerated VNO system. In humans, it has been shown that the VNO deteriorates largely before birth and its anatomical structure is fragmentary [94]. These findings suggest that the deterioration of VNO had evolved synchronically with the

pseudogenization of V1R genes in humans [94]. More interestingly, though rodents and dogs have a functional VNO, the dog genome has a much smaller V1R repertoire than rodent animals [91]. In contrast to what has been observed in many species, several ruminant V1R orthologs are expressed in sensory neurons at the MOE and VON [91], suggesting that both the MOE and VNO are involved in the detection of V1R ligands in ruminants. Though a previous study has identified 4 V1R-like genes in the sea lamprey genome, one of the four V1R-like genes was identified as a pseudogene, and two of them were classified into the OR family [29]. Thus, we conclude that the sea lamprey contains one intact V1R-like gene, which is consistent with the results preciously described in several teleost species [95]. However, several groups examined the genome of several teleost fish and identified five additional V1Rs that were overlooked in the previous study [92]. In contrast to teleost fish, rodents appear to possess a much larger V1R gene repertoire [90]. However, the chicken genome does not encode any V1R genes, conceivably due to the lack of VNO in birds [91].

Since the discovery of V1R genes, the vast majority of V1Rs are still orphan genes. Several V1R ligands have been identified in the investigation of apical V1R expressing neurons [96-103]. V1Rs expressing neurons typically respond to pheromones with high sensitivity in mice [96]. Compounds derived from mouse urine, such as 2-hepatanone, 6-hydroxyl-6-methyl-3-heptanone, n-pentylacetate, and isobutylamine, are able to specifically activate the V1Rb2 expressing neurons in mice and function as pheromones to accelerate estrus and induce animals into puberty [97-102]. Behavioral trials revealed that knockout mice lacking the *V1Ra* and *V1Rb* gene clusters exhibit a significant reduction in aggression behavior [103]. Moreover, mutant animals completely lost the electrophysiological responses to stimuli (6-hydroxyl-6-methyl-3-heptanone, n-pentylacetate, and isobutylamine) [103].

The phylogenetic analysis of V2Rs suggested that V2R genes are divided into five subfamilies [88]. As with the V1R gene repertoire, the V2R repertoire also greatly expanded in rodents [88]. The mouse and rat genomes contain about ~120 and ~ 80 intact V2R genes, respectively [88]. However, no intact V2Rs have been identified in humans, macaque, chimpanzee, dog, cow, goat, and chicken, suggesting that the V2R genes are lost in these species [88-90]. Notably, no V2R genes have been identified in sea lamprey [29], but V2R genes are present in teleost fish, indicating the V2R genes emerged after the divergence of jawless and jawed vertebrates [92]. The V2R gene repertoire of jawed animals displays a striking variation in size. Frogs have the largest V2R gene family, with ~250 intact genes [91]. In addition, zebrafish, fugu, and pufferfish contain 44, 18, and 4 functional V2R genes, respectively [93].

Most V2Rs are expressed in a group of neurons in the basal layer of VNO that are broadly tuned to major histocompatibility complex peptides (MHCs) and exocrine gland secreted peptides (ESPs) [104, 105]. Direct evidence has been provided by the studies of V2Rp5 and V2R1b deficient mice. The male mouse excreted a lacrimal peptide (ESP1) that serves as a male pheromone to activate V2Rp5 and induce a specific sexual behavior in females [104]. Moreover, the V2R1b expressing neurons are tuned to detect MHC peptides [105]. Mice lacking the V2Rp5 or V2R1b gene exhibit a significant reduction of the response to ESP1 or MHC peptides [104, 105]. In addition, VNO neurons at the basal layer of VNO epithelium can respond to major urinary proteins (MUPs), suggesting that V2Rs may contribute to the recognition of MUPs [100]. On the other hand, V2R expressing microvillus neurons are thought to be involved in amino acids detection in teleost fish [106, 107]. Thus, V2Rs in teleost fish and mammals appear to evolve for the detection of specific environmental odors.

Formyl Peptide Receptors (FPRs)

Formyl peptide receptors (FPRs), a subfamily of GPCRs, were initially identified in the immune system of mammals, where they recognize formylated peptides in response to inflammation [108]. Recent studies have shown that FPRs also may function as VNO olfactory receptors in rodents [109, 110]. Phylogenetic analysis revealed that FPR genes cluster into a monophyletic clade and are classified into three subfamilies, including FPR1, FPRL1, and FPRL2 [111]. Vomeronasal FPRs exhibit no significant sequence similarity with ORs, TAARs, or V1/2Rs [111]. In rodents, vomeronasal FPR genes form a single gene cluster that is closely adjacent to V1/2R gene clusters [109, 110]. Vomeronasal FPRs are monoallelically expressed in a small group of VNO sensory neurons that appear to lack other olfactory receptors (V1Rs or V2Rs) [109, 110]. Seven *FPRL1* genes clustered on chromosome 17 were discovered in mice, including *FPR-rs1*, *FPR-rs2* (a non-olfactory gene), *FPR-rs3*, *FPR-rs4*, *FPR-rs5* (a pseudogene), *FPR-rs6*, and *FPR-rs7* [109, 110]. Among these FPRs, FPR-rs3/4/6/7 are predominantly expressed in the apical layer of VNO sensory neurons, while FPR-rs1 is confined to sensory neurons in the basal VNO layer [109, 110, 112]. The signal transduction mechanism of FPR expressing neurons is similar to what has been observed in V1Rs or V2Rs [113]. Notably, the determinant of signaling pathways for individual FRP genes seems to be associated with the different subsets of VNO neurons. FPR-rs1 expressing neurons are co-expressed with $G_{\alpha o}$, whereas apical neurons expressing the other FPRs co-express $G_{\alpha i2}$ [113].

Vomeronasal FPRs have been demonstrated to be involved in the detection of microbial metabolites and mitochondria-derived peptides, including ND1-6T, ND1-6I, and N-formyl methionine-leucine-phenylalanine [113, 114]. However, the specific roles of FPRs in mediating behavioral responses in rodents are largely unknown. The physiological dichotomy of FPRs,

serving as olfactory and immune-related receptors, highlights their potential connections between olfactory and immune systems.

OLFACTORY SENSORY NEURONS

In vertebrates, the initial action of olfactory sense takes place at the main olfactory epithelium (MOE). The MOE is composed of three primary cell types, including olfactory sensory neurons (OSNs), supporting cells, and basal cells [115]. OSNs are short-lived cells that are replaced every few months [115]. These neurons possess a bipolar morphology with a single dendrite and axon. The OSNs extend a single dendrite to the apical layer of MOE. The dendrite emanates from a 5-7 μm cell body embedded in the lower two-thirds of the neuroepithelium and terminates in a knob swelling with a bunch of sensory cilia [117-119]. Thus, the initial event of odor recognition proceeds along with the interaction between odorants and their relevant receptors at the cilia. OSN axons from the basal pole project to a specific location in the olfactory bulb, forming a glomerular structure [41, 42]. Likewise, axons of VNO sensory neurons converge on the accessory olfactory bulb (AOB) [115].

Mammalian OSNs are made up of two cell populations: ciliated and microvillous neurons [115]. Ciliated neurons constitute a majority of sensory neurons in the OME. These cells are primarily located at deep positions of MOE and have long dendrites with a bunch of cilia extending towards the surface of the neuroepithelium. In contrast, microvillous neurons are mainly positioned in the neuroepithelium of VNO and possess intermediate-length dendrites carrying microvilli [115]. As with mammals, the MOE of teleost fish contains both ciliated and microvillous neurons [116]. In addition, teleost fish possess a third OSN population, known as the fish-specific crypt cells [106]. These egg-shaped neurons are located in the apical layer of the neuroepithelium. Therefore, teleost OSNs are made up of three morphologically distinct cell types located in the MOE of the nasal cavity [106, 116]: 1) ciliated cells that have long dendrites with cilia and are

located in the deep layer of MOE; 2) microvillous cells that possess intermediate-length dendrites with microvilli and positioned in the intermediate layer of MOE; and 3) crypt cells that contain both microvilli and cilia and are embedded in the apical surface of MOE. Similarly, sea lamprey OSNs exhibit polymorphisms as the neuron morphology observed in teleost [117]. Three types of OSNs are present in the MOE of the sea lamprey, including tall, intermediate, and short OSNs [117]. The tall OSNs in sea lamprey are the predominant morphotype neurons in the MOE and have a similar morphology to teleost ciliated OSNs [117]. The intermediate and short neurons are less prominent morphotypes in the MOE [117]. The intermediate neurons possess a fusiform-shaped cell body and share a similar morphology with teleost microvillous OSNs [117]. The short neurons have an egg-like shape and are located at the apical layer of MOE, which are highly similar to those teleost-specific crypt cells [117].

Ciliated neurons are known to co-express ORs or TAARs with the olfactory-specific $G_{\alpha olf}$ and primarily respond to amino acids and bile acids by using the canonical cAMP-mediated signaling pathway [106, 118, 119]. Microvillous neurons selectively express V1/2Rs with the G protein $G_{\alpha i}$/ $G_{\alpha o}$ and have been shown to respond to nucleotides and amino acids [106, 120, 121]. Crypt cells have been shown to express a V1R-like *ORA4* gene in zebrafish and appear to be involved in the recognition of amino acids, bile acids, and pheromones [122-125].

Most OSNs only express one type of functional olfactory receptor in vertebrates, following the “one neuron-one receptor” hypothesis [38, 40]. Chemosensory receptor genes are clustered at various loci that spread over most chromosomes [38, 40]. A locus control region (LCR) was proposed to explain the potential mechanism of monoallelic expression in OSNs [126]. The LCR is a cis-regulatory element that is involved in the transcriptional regulation of multiple genes at a specific cluster [127]. The LCR is likely to form a complex with nuclear factors, such as Lhx2,

Emx2, and Olf/Ebf (O/E proteins), that modifies the chromatin structure near the OR cluster and initiates the transcription of one OR gene in each OSN [128]. However, the physical interaction between LCR and OR promoter could not prevent the transcription of an additional OR gene from another OR cluster [129]. Therefore, OSNs might have evolved a negative feedback mechanism to ensure no further transcription of other OR genes [129]. It has been shown that epigenetic-mediated transcriptional silencing plays an important role in precluding multiple expressions of OR genes in each OSN [129]. Two silent trimethyl marks, H3K9me3 and H4K20me3, are found to be associated with the silencing of OR-gene clusters [129]. These two silent markers are abundantly present in inactivated OR clusters, but are significantly reduced in an activated OR-gene region [129]. When functional OR protein is expressed, the OR relevant molecules transmit negative feedback signals (such as methylation and phosphorylation) at OR promoters, OR enhancers, and transcription factors, to inhibit further activation of other OR genes [126-129].

NEURAL CIRCUITS IN THE OLFACTORY BULB

Most mammals possess two parallel olfactory systems that are anatomically and functionally disparate, the main and vomeronasal olfactory systems [130]. The main olfactory system primarily recognizes volatile odors that are transduced to the main olfactory bulb [130]. In contrast, non-volatile odors are detected by the vomeronasal olfactory system and then are relayed to the accessory olfactory bulb (AOB) [130]. Lower vertebrates, such as jawless and teleost fish, do not possess the vomeronasal organ. However, a recent study has reported that the jawless lamprey has a primordial accessory olfactory organ [34]. The MOB is a symmetric cylindrical-like structure connected to the forebrain. The MOB functions as a relay station to receive and integrate olfactory inputs from different OSNs in the MOE, and then synapses in the olfactory cortex [130]. Thus, it plays important roles in mediating olfactory functions, including odor coding, sorting synaptic inputs, synaptic connection with the olfactory cortex, and receiving neuromodulatory inputs from higher neural centers.

The mammalian MOB is made up of six laminated layers, from superficial to deep, including olfactory nerve layer (ONL), glomerular layer (GL), external plexiform layer (EPL), mitral cell layer (MCL), internal plexiform layer (IPL), and granule cell layer (GCL) [130]. The teleost OB shares a similar organization as the mammalian MOB, lacking two concentrated neuropils (EPL and IPL) [131]. In the mammalian MOB, the ONL is made up of olfactory nerve fibers and axons from OSNs [132, 133]. An odorant activates its paired OSNs, eliciting neural action potentials that pass along olfactory nerve fibers and converge on the GL, by forming a spherical-shaped glomerulus [132, 133]. The glomerulus is considered to be a functional unit of the olfactory system [130]. The OSNs that respond to the same ligand synapse in a set of glomeruli located at a specific

region of MOB [134-139]. Each glomerulus contains a population of output neurons (mitral and tufted cells, M/TCs) and intrinsic GL neurons (referred to as juxtaglomerular cells, JGCs) [140]. The GL neurons are primarily comprised of three neuron types: external tufted cells (ETCs), periglomerular cells (PGCs), and short axon cells (SACs) [140]. Most of these JGCs are serving as interneurons, whereas a minority of ETCs function as output neurons [141]. The EPL contains numerous tufted cells (TCs), some interneurons, and neural networks of dendrodendritic synapses between M/TCs and granule cells (GCs) [141]. Moreover, the thin MCL is made up of numerous mitral cells and granule cells [142, 143]. Mitral cells (MCs) have a similar morphology as TCs, but the lateral dendrites of MCs are more extensive [142, 143]. The dendrites of M/TCs receive axonal inputs from olfactory nerve fibers within the glomeruli, whereas M/TC lateral dendrites form dendrodendritic synapses with GCs and interneurons from EPL [142, 143]. The IPL is relatively thin and contains interneurons, SACs, and M/TC axons [140, 141]. The most internal layer, the GCL is made up of a large number of local interneurons, the small axon-less granule cells [130]. Notably, these GCs are also present in the MCL and use the gamma-aminobutryric acid (GABA) as an inhibitory neurotransmitter [164]. The apical dendrites of GCs receive dendrodendritic synapses from M/TCs and in turn may synapse in M/TCs [140-143]. GCs also can receive inputs from M/TC axons and other GCL interneurons [140-143]. These local interneurons make axodendritic synapses onto M/TCs that mediate feedback or feedforward inhibition [140-143].

The OB of teleost fish is comprised of four layers, including the olfactory nerve layer (ONL), glomerular layer (GL), mitral cell layer (MCL), and granule cell layer (GCL) [131]. The local interneurons ETCs and PGCs are not present in the GL of teleost fish. The teleost MCL is primarily comprised of mitral cells, and in some species another type of projection neuron is referred to as

ruffed cells [144, 145]. Mitral cells extend dendrites into the GL and form axodendritic synapses with OSN axons within glomeruli. In zebrafish, mitral cells receive synaptic inputs from OSNs within the glomeruli and project to telencephalon and diencephalon [146, 147]. In contrast, ruffed cells are not innervated by OSN axons directly. These cells receive axodendritic synapses from GCs in the GCL, which in turn make dendrodendritic synapses onto mitral cells [131, 148]. Moreover, mitral cells also receive inhibitory synapses from GC dendrites [149]. In zebrafish, GCs make dendrodendritic synapses onto mitral and ruffed cells that inhibit the activation of mitral and ruffed cells [149]. In goldfish, ruffed cells exhibit spontaneous activity that can be inhibited by GCs [150].

In addition to the MOB, rodents have a distinct structure known as the accessory olfactory bulb (AOB), which is located at the posterior of the forebrain [151]. Unlike the MOB, the AOB receives neural inputs from OSNs in the vomeronasal organ. The AOB has a laminated structure as with the MOB, and sensory inputs from the VNO directly project to the GL of AOB [151]. The axons of OSNs expressing V1Rs primarily project to the anterior portion of the GL in AOB [82]. In contrast, the posterior portion of GL receives sensory inputs from OSNs expressing V2Rs [83-85]. The EPL and MCL of AOB have no conspicuous boundary, and therefore, these two layers are combined in an external cellular layer (ECL) [152]. Mitral cells are the primary cell type in the ECL and spread over the entire ECL [152, 153]. Besides mitral cells, the ECL also contains other projection neurons, such as tufted cells, external granule cells [152]. As with the ECL, the IPL and GCL of AOB are integrated into an internal cellular layer (ICL) [152, 153]. The ICL locates at the deep of the lateral olfactory tract and is glutted with local granule cells [152]. These granule cells in the AOB have a similar morphology to their counterparts in the MOB and are proposed to be involved in the lateral olfactory tract between the olfactory bulb and olfactory cortex [151-153].

The MOB not only processes sensory inputs from the OSNs but also receives synaptic inputs from serotonergic, cholinergic, and noradrenergic neurons in higher brain centers. It has been shown that the zebrafish OB receives serotonergic inputs from raphe serotonergic neurons [154]. Serotonergic fibers are primarily present in the GL and make synapses onto PGC and M/TC dendrites [155]. Serotonin can facilitate interneuron excitability but reduce the excitation of mitral and ruffed cells [154, 155]. Male pheromone treatment can significantly reduce serotonin concentrations in the brainstem of female sea lamprey that might be able to explain the increased swimming rate in females [156]. Cholinergic fibers are mainly dense in the GL and IPL of the MOB [157]. Moreover, it has been shown that an increasing of acetylcholine in the MOB is able to promote odor discrimination [158]. In contrast, odor adaption and discrimination are impaired when muscarinic antagonists are applied to the MOB [159, 160]. Noradrenergic projections to the MOB arise from the locus coeruleus of the brainstem and mainly converge on the IPL and GCL by acting on various adrenergic receptors [161, 162]. Odor stimulation can activate neurons in the locus coeruleus and in turn elicit rapid increases of norepinephrine concentrations in the MOB [163]. Low concentrations of norepinephrine suppress the activity of GCs via α2 adrenergic receptors, which in turn enhance the excitation of MCs [164]. While high levels of norepinephrine exert opposite effects mainly by means of α1 adrenergic receptors [165]. Therefore, these neuromodulatory inputs from the forebrain and brainstem terminate in most MOB layers and modulate multiple neuronal activities.

OLFACTORY SYSTEM IN SEA LAMPREY

Sea lamprey undergo a complex life cycle, including a prolonged larval phase, a radical metamorphosis phase, a parasitic phase, a migrating phase, and a spawning phase [166]. Following the completion of metamorphosis, juveniles migrate downstream from rivers and streams to the ocean or lakes for parasitic feeding, where sea lamprey rely on multiple sensory systems to locate hosts and avoid predators [167]. Among these senses, the olfactory sense of lamprey appears to be essential for various physiological functions. Relative to its brain size, the sea lamprey appears to have the largest olfactory organ among vertebrate species [168]. Parasitic adults rely on the olfactory sense to detect hosts released amino acids and amines [168]. When fully grown, parasitic adults cease feeding and migrate upstream to rivers and streams, where they become sexually mature, mate, and die. During the adult phase, the olfactory sense plays critical roles in the recognition of stream odors and mating pheromones [6, 166, 169, 170]. Steam odors are thought to be a mixture of larval pheromones. It has been shown that the landlocked lampreys fail to locate migration rivers when they become anosmic [171]. Upon spermiation, sexually mature males release sex pheromones that attract ovulatory females for mating [6, 166, 169]. Once ovulatory females arrive at the spawning nest, they move from nest to nest and spawn intermittently for approximately 1 week before the mature adults die [166].

During the metamorphosis phase, the olfactory organ undergoes a remarkable remodeling process, developing from an epithelial tube into a nasal sac [172-174]. The olfactory organ is located on top of the skeleton at the front of brain and has a single deep nasal sac with two chambers. Each nasal chamber is made up of many lamellar-like olfactory epithelia (MOE) and tubular diverticula (an accessory olfactory organ, AOO) that contain three morphotypes of OSNs

[117, 175]. These polymorphic sensory neurons are found in the olfactory epithelium of both metamorphic and adult lampreys [175]. As in teleost fish, tall OSNs in sea lamprey are predominantly present in the MOE, whereas intermediate and short OSNs are less prominent [175]. The main olfactory epithelium and accessory olfactory organ of sea lamprey contain representatives of most chemosensory receptor gene families, including OR, TAAR, and V1R [29, 34]. Moreover, the sea lamprey possesses a laminated olfactory bulb to receive sensory inputs from OSNs in the main and accessory olfactory epithelium [117]. As with teleost fish, molecular features of odors are encoded by glomerular units in the lamprey OB, allowing the animal to discriminate various odors. The adults can detect bile acids at very low concentrations and discriminate a proton change of two structurally similar bile acids for distinct behavioral responses [5, 169, 176]. Therefore, the olfactory sense is essential for sea lamprey to orientate migratory streams, locate spawning nests, and lure mates.

Anatomical analysis of the lamprey OB has revealed that the OB in lamprey is made up of four concentric layers, including olfactory fiber layer (OFL), glomerular layer with mitral cells (GL), granule cell layer (GCL), and ependymal cells layer (EC) [177]. The apical dendrites of mitral cells in the GL receive direct synaptic inputs from OSNs. The same morphotype OSNs from different species may project to distinct spatial regions (medial/lateral regions) of the olfactory bulb and higher brain centers [117, 178-180]. In sea lamprey, OSN axons from the main olfactory epithelium project primarily to the medial and lateral portions of the OB [117]. OSNs from the AOO mainly project their axons to the medial region of the olfactory bulb [117]. Excluding the medial region, all other regions of the lamprey OB express olfactory-specific G-protein $G_{\alpha olf}$, suggesting that the medial region likely express other G proteins (G_i/G_o) [181]. Projection neurons in the medial portion of OB synapse with the posterior tuberculum (PT), a caudal ventral region

of the diencephalon, serving as a relay station between olfactory input and locomotor output [182]. Neurons in the PT project their axons to the mesencephalic locomotor region (MLR) in the mesencephalon [182]. The MLR neurons make synaptic connections onto reticulospinal neurons in the rhombencephalon that activate the locomotion of the spinal cord in sea lamprey [183]. In contrast, projection neurons in the non-medial region extended axons to the lateral pallium and other prosencephalon portions, suggesting that these OB regions are not involved in mediating locomotion in sea lamprey [182, 184]. Thus, projection neurons in the medial and non-medial region of the olfactory bulb project their axons to distinct regions of higher brain centers, showing no overlap in sea lamprey.

PHEROMONE COMMUNICATION IN SEA LAMPREY

Anadromous fish primarily rely on the olfactory sense to mediate migratory and reproductive behaviors [171, 185-188]. Some anadromous fishes (e.g. salmonids, sturgeons) return to their natal streams for spawning, whereas the sea lamprey chooses another strategy during migration, known as the "suitable river strategy" [171, 185-188]. There is strong evidence that sea lamprey rely on the density of larval population, and not the natal streams they came from, in selecting spawning habitats [189-192]. Migratory adults selectively enter spawning streams by tracking larval odors and other steam odors [171, 189]. Electro-olfactogram (EOG) recordings have shown that adult lampreys exhibit sensitive and specific olfactory responses to larvae excreted bile acids, such as petromyzonol sulfate (PZS), petromyzonamine disulfate (PADS), and petromyzosterol disulfate (PSDS) [171, 189, 191]. The mixture of these bile acids induces behavioral preferences in laboratory trials, similar to those induced by larval odors [193-196]. However, a single compound of these bile acids alone fails to replicate larval-odor induced behavioral activities in the natural field [196]. A recent study has demonstrated that (+) -(2S,3S,5R)-tetrahydro-3-hydroxy-5-[(1R)-1-hydroxyhexyl]-2-furanoctanoic acid, a fatty acid derivative, serves as a critical component of lamprey migratory pheromone [6]. A chemosynthetic imitation of this migratory pheromone can elicit robust olfactory responses of adult sea lampreys and is able to reproduce larvae-odor induced behavioral activities in a tributary stream [6]. Moreover, lampreys display acute olfactory responses to amino acid L-arginine, which appears to serve as a feeding attractant [166].

When migratory adults enter the spawning stream, the presence of mating pheromones and the increased water temperature influence the maturation of different batches of migrants [197, 198]. Migratory males first arrive at the spawning stream and set about building nests. Upon sexual

maturation, spermiating males release a male mating pheromone that specifically attracts ovulatory females to the spawning nests over long distances [5]. The lamprey male mating pheromone is made up of multiple components that possess various physiological functions [199-202]. The bile acid 3-keto petromyzonol sulfate (3kPZS) is a major component of male mating pheromone that is released via their gills [202]. 3kPZS has been shown to be highly attractive to ovulated females in both laboratory and field trials [5, 169]. Ovulated females exhibit high olfactory sensitivity to 3kPZS, with a detection threshold of 10^{-13} M [5, 169]. Moreover, exposure of sexually immature adults to 3kPZS significantly accelerates sexual maturation [197]. In addition to 3kPZS, male mating pheromone contains other components that may elicit other behavioral responses, such as attraction, mating search, and nest retention [199]. It has been shown that males release another bile acid, 3,12-diketo-4,6-petromyzonene-24-sulfate (DkPES), serving as a minor component of male mating pheromone [200]. Nests applied with the mixture of DkPES and 3kPZS at a specific ratio (2∶29.8 or 10∶29.8) show more attraction to ovulated females than nests baited with 3 KPZS alone [200]. These results suggest that DkPES serves as a potent male pheromone that is involved in a close-range communication in sea lamprey. Moreover, 3-keto allocholic acid (3kACA), a 3kPZS analog, is identified as a minor component of male mating pheromone that may function as a puberty inhibitory pheromone in sea lamprey [198]. EOG recordings have demonstrated that 3kACA shows robust olfactory responses in adult lampreys but was proven to be invalid in behavioral responses [201]. Notably, spermiating male washing is more attractive to ovulated females, suggesting that male mating pheromone contains additional unknown components [199].

Upon spermiation, genes encoding enzymes for bile acid anabolism are up-regulated in males, which in turn increase the production of 3kPZS and its precursor petromyzonol sulfate (PZS) [176]. These two bile acids are excreted from gill glandular cells, and spermiating males release much

more 3kPZS than PZS [202]. However, the larvae odors contain more PZS than 3kPZS [176]. PZS functions as an antagonist for 3kPZS that enable ovulated females to discriminate larval odor from the male mating pheromone [176]. Thus, PZS appears to be an essential odor that plays an important role in mediating olfactory and behavioral responses in sea lamprey.

Besides the above-mentioned pheromones, milt released by spermiating males appears to be a reliable source of a male sex pheromone. Seminal plasma contains aphrodisiac and/or anti-aphrodisiac molecules that are essential for sexual attractiveness, physiology, and sexual behaviors in pacific herring, bitterling, snakes, and insects [203-210]. During the spawning season, spermiating males are aggregated on riverine gravel nests and release milt frequently for a week. Thus, seminal components released along with the milt could serve as olfactory cues for ovulatory females to locate the presence of spermiating males. However, no specific aphrodisiac molecules have been identified from semen and their molecular mechanisms in mediating mating behaviors remain unknown.

In general, when the parasitic lamprey in lakes or the Atlantic Ocean cease feeding, they follow larval odors (e.g. 3kPZS and PZS) and river plumes migrating into tributaries with suitable nursery habitats. Several weeks after entering spawning ground, males become sexually mature and set about constructing spawning nests. At this moment, spermiating males release the major component of mating pheromone 3kPZS that attract ovulated females over a long distance. Spermiating males also simultaneously release a smaller amount of PZS that cooperates with abundant 3kPZS at a specific ratio to allow ovulated females to recognize spawning habitats.

SEXUAL DIMORPHICSM OF BEHAVIORAL RESPONSES IN SEA LAMPREY

Detection of sex pheromone is important for sexual behaviors in vertebrates. Sea lamprey display sexually dimorphism in the response to the stimulation of mating pheromone, both behaviorally and physiologically [211]. Upon sexual maturation, male sea lampreys release the male-specific sex pheromone 3kPZS that only elicits preference and searching behavior in ovulated females [5, 211]. More interestingly, 3kPZS treatment can elicit great excitatory responses of reticulospinal (RS) cells [212-214]. These RS neurons in the hindbrain are thought to be locomotion commanders that are able to activate spinal locomotor networks in sea lamprey [212-214]. Moreover, adult European river lamprey possess another diencephalic locomotor center in the ventral thalamus that can make synapses onto RS neurons [215]. In sea lamprey, 3kPZS-induced excitatory responses of RS cells could be recorded in both males and females [182]. The dichotomy of 3kPZS-induced behavioral responses probably is mediated by the activity of RS neurons, which may be modulated by neurotransmitters concentrations from higher brain regions.

Neurotransmitters have been shown to play essential roles in mediating motoneuron and premotor interneuron activities in lamprey [216, 217]. Injections of serotonergic and dopaminergic compounds drastically affect motor function and loco motivity of sea lamprey [218, 219]. Sea lamprey exposed to 3kPZS exhibits serotonin sexual dimorphism in the brain [156]. 3kPZS treatment causes a significant increase of serotonin levels in the forebrain of adult females, whereas serotonin is not detectable in the forebrain of adult males [156]. In contrast, a reduction of serotonin level is observed in the brainstem of adult females but has no significant difference in adult males [156]. Therefore, serotonin levels in the forebrain and brainstem appear to be important to regulate sex-specific behaviors in sea lamprey.

Moreover, dopaminergic chemicals can also modulate odor-evoked locomotion in sea lamprey. Dopaminergic neurons are extensively present in the medial portion of OB, the posterior tuberculum, and the dorsal hypothalamic nucleus [219]. Injections of dopamine receptor D1 and D2 agonists in the medial OB cause a significant decrease of RS neuron responses to olfactory nerve stimulation [219]. In contrast, injection of a dopamine receptor D2 antagonist in the medial OB results in a significant increase of RS cell activation [219]. Thus, odor-evoked locomotion in sea lamprey is affected by dopaminergic networks in the OB. In addition, olfactory outputs to specific areas of higher brain centers seem to be glutamatergic dependent [182]. The glutamate receptor antagonist (CNQX) can inhibit 3kPZS-induced RS cell responses [182]. Sea lamprey possess two olfactory neural pathways in response to odor-induced locomotion, the medial OB-PT pathway and the lateral pallium-PT pathway [182]. Injection of CNQX in the medial OB significantly abrogates RS cell responses to stimulation, whereas no significant differences are observed in the lateral pallium [182]. Moreover, injection of glutamate in the PT can cause swimming behavior in sea lamprey, indicating that the medial OB-PT neural circuit has an important role in modulating pheromone-evoked locomotion in sea lamprey [182]. Interestingly, RS cells also receive inputs from the diencephalic locomotor region (DLR), whereas injection of CNQX in the DLR has no inhibitory effect on RS cell responses [220]. Thus, these observations suggest that sex pheromone-induced sexually dimorphic behaviors in sea lamprey probably are modulated by multiple components. These differences in the nervous system may help explain 3kPZS-induced sexually dimorphic behaviors in sea lamprey.

STRUCTURAL BASIS OF CONSTITUTIVELY ACTIVE GPCRs

G protein-coupled receptors (GPCRs) are activated by extracellular substances, such as hormones, biogenic amines, pheromones, and neurotransmitters, and transform extracellular stimuli into intracellular signals via an intracellular guanine nucleotide-binding protein (G protein), which in turn activates an intracellular signaling cascade to elicit physiological responses. GPCRs display various degrees of basal activity. Most GPCRs are agonist-dependent with low basal activity, whereas some GPCRs are constitutively active in the absence of agonists. β2-adrenergic receptor (β2-AR) is the first GPCR reported to show constitutive activity that can couple to heterotrimeric G_s protein in the absence of ligand [221]. Moreover, neuroblastoma cells expressing the endogenous δ-opioid receptor exhibit robust basal activity that can be inhibited by some negative antagonists (also known as inverse agonists) [222]. In addition to these wildtype constitutively active GPCRs, many mutant GPCRs (constitutively active mutants, CAMs) possess considerable basal activities. The Lefkowitz laboratory performed a series of research showing that β2-AR, α_{1B}-AR, and α_1-AR mutant receptors exhibit a significant increase of constitutive activity [223-226]. They proposed a ternary complex model to elucidate the activation of GPCRs [224]. The wildtype receptor is stabilized in equilibrium between an inactive and an active conformation. Upon ligand binding, an agonist appears to shift the receptor into an active conformation (R* state), whereas an inverse agonist prefers to stabilize the receptor into an inactive conformation (R state) [227]. Evidence from molecular dynamics and mutational analysis suggested that GPCRs rely on the deprotonation of the DRY motif to shift into an active state. Substitution of the $D^{3.49}$ residue to all other amino acids in α_{1B}-AR causes the constitutive activation of the receptor [228, 229]. Mutant receptors that disrupt the interaction between $D^{3.49}$

and $R^{3.50}$ result in the constitutive activation of α_{1B}-AR [228, 229]. Moreover, mutation of the A^{293} residue to all other amino acids leads to a significant increase in basal activity of α_{1B}-AR [230]. The mutation probably causes a movement of the N-terminal portion of the third intracellular loop 3 and in turn enforces the outwards movement of $R^{3.50}$ that stabilizes the receptor in an active conformation. Similar to α_{1B}-AR, α_{1A}- AR seems to possess a parallel structural basis for receptor activation [231]. However, numbers of studies on β2-AR have demonstrated that intramolecular interactions are involved in constraining the receptor in an inactive conformation, and disruption of these intramolecular interactions can lead to the constitutive activation of β2-AR [232, 233]. The charge-neutralizing mutation of the $D^{3.49}$ residue results in the constitutive activation of β2-AR [233]. The activated β2-AR crystal structure has demonstrated that the $Arg^{3.50}$ residue of the DRY motif moves outwards to form new cation–π interactions with Tyr^{219} and Tyr^{326}, and the Tyr^{391} residue of the G protein α subunit, leading to the constitutive activation of β2-AR [234-236].

The first report of the thyroid-stimulating hormone receptor (TSHR) CAM was identified in the investigation of thyroid adenoma [237]. Two somatic mutations (D6.30G and A6.34I) in TM6 of TSHR lead to the constitutive activation of the receptor and in turn cause hyperthyroidism [237]. Mutation of the Ser^{281} residue in the extracellular loop to S281T and S281N results in an increase of cAMP accumulation [238]. Substitution of the highly conserved $Gly^{1.49}$ to G1.49S generates a TSHR CAM [239]. This mutant shows constitutive activity with an accumulation of second messengers cAMP and inositol phosphate (IP3). However, mutation of the Ile^{691} residue to I691F at the C-terminal tail elicits constitutive activity for stimulation of IP3, but hardly affects basal cAMP production [240]. In contrast, mutation of the $A^{6.34}$ residue to A6.34V in the third intracellular loop causes loss of basal IP3 accumulation, and instead, the mutant exhibits a significant increase of cAMP production and an increased constitutive activation for stimulation

of adenylyl cyclase [240]. These findings suggest that the $Ala^{6.34}$ residue is critical for $G_{\alpha q}$ coupling. Moreover, mutations breaking down the interaction between the extracellular loop and the N-terminal tail shift the TSHR into an active conformation [238]. In addition, multiple TSHR CAMs have been identified in the research of thyroid adenoma and hyperthyroidism, showing that CAM mutations predominantly occur in all seven transmembrane domains and the second and third intracellular loops [241-245].

Notably, some mutants of constitutively active GPCRs lose basal activity and have been verified to be associated with physiological dysfunctions. Mutations of the constitutively active melanocortin-4 receptor (MC4R) result in the loss of basal activity and can cause obesity [246]. Mutations (R7H, T11S, R18C, R18H, and R18L) in the extracellular N-terminal lead to a significant decrease of basal activity but have no effects on ligand affinity [246]. Moreover, the N-terminal deletion mutant completely abrogates the basal activity of the receptor but shows normal responses to the α-melanocyte-stimulating hormone [246]. These findings indicate that the extracellular N-terminal portion of MC4R plays an important role in mediating the receptor constitutive activity. Besides the extracellular N-terminal, mutations (I2.62S, I2.62T, A154D, F5.48L, and N6.30S) in the transmembrane segments and intracellular loop result in a significant decrease of basal activity [247]. More interestingly, MC4R mutants (H158R, P230L, S3.30L, and L6.40Q) identified from some obese patients exhibit much higher basal activity [248-252]. As hyperfunction or hypofunction in GPCR basal activity may lead to various dysfunctions, it is important for GPCRs to be stabilized in a proper conformation.

It has been demonstrated that OSNs display varying degrees of action potential firing rates in the absence of stimuli, suggesting that these intrinsic currents are receptor-dependent [253-256]. Physiological evidence with mouse OSNs showed that an antagonist of mI7-receptor inhibits the

basal current noise of mI7-OSNs, thus likely serving as an inverse agonist [256]. Moreover, odorant receptors also play an important role in mediating the topographic projection of activated glomeruli in the OB [257]. Agonist-independent GPCR activity can determine anterior-posterior axon targeting of OSNs [257], indicating that the constitutive activity of odorant receptor could be essential for modulating both short- and long-term olfactory functions. In addition, it has been indicated that the basal activity of the odorant receptor is G protein dependent [257]. HEK293T cells expressing different odorant receptors with G_s exhibit varying degrees of constitutive activity. Thus, G_s appears to be more efficient in mediating the basal activity than G_{olf}. However, whether olfactory TAARs are constitutively active and the molecular mechanisms of olfactory receptor constitutive activation are largely unknown.

OVERVIEW OF DISSERTATION

Trace amine-associated receptors (TAARs) are a class of important olfactory receptors that plays essential roles in detecting volatile amines and mediating stereotyped behaviors in vertebrates. A number of TAARs have been demonstrated to be expressed in the MOE of adult sea lampreys [29], suggesting that lamprey TAARs are essential olfactory receptors for the detection of ecologically important amines. However, the response profiles of TAARs in sea lamprey and how TAARs recognize odorous amines have not been determined. None of these lamprey TAARs have been deorphanized yet, *in vivo* or *in intro*. Therefore, this dissertation sets out to identify ligands for sea lamprey TAARs and characterize structural basis of TAARs for amine recognition. This thesis uses the sea lamprey olfactory TAARs as research objects to examine their ligands, behavioral responses, the molecular basis for ligand recognition, and the structural determinants of ligand-independent receptor activation.

Chapter 1 describes spermine in semen of male sea lamprey acts as a sex pheromone. This chapter has been published in *PLOS Biology* and I am a co-first author for the article. Upon spermiation, male sea lamprey typically releases milt frequently for a week. Biogenic amines generated by microbial decarboxylation of amino acids, such as triethylamine, cadaverine, and putrescine, are thought to be important environmental substances existing in the river plumes. These amines also (cadaverine, putrescine, spermine, and spermidine) contribute to smell of semen [258, 259]. Thus, amines from semen could be a reliable source of sex pheromone for male adults to attract ovulated females. Firstly, we found that sea lamprey milt contains abundant spermine, especially in the seminal plasma. EOG recordings revealed that spermine evokes concentration-dependent responses in the olfactory epithelium of adult lampreys with a highly sensitive threshold.

A two-choice maze confirmed that this compound is only attractive to ovulatory females. These results highly suggest that spermine in the male semen acts as a male sex pheromone. Using a well-established cAMP response element (CRE)-driven luciferase reporter assay (Figure I-2) [30], we examined cellular responses of 26 lamprey TAARs to the stimulation of 10 μM spermine. We found that only TAAR348 exhibits robust responses to spermine in a concentration-dependent manner. In particular, I identified a spermine antagonist (cyclen) from 22 spermine analogs that is able to inhibit spermine-induced cellular, olfactory, and behavioral responses. Moreover, a spermine structural analog (1-naphthylacetyl spermine) was identified as a distinct TAAR348 agonist that can mimic spermine effects, producing identical cellular, olfactory, and behavioral responses. Taken together, these results support a specific role for TAAR348 in mediating the pheromonal responses of spermine.

Chapter 2 delineates a conserved mechanism whereby two independently evolved TAARs recognize various polyamines with distinct motifs via a conserved binding site. This chapter has been published in the *Journal of Biological Chemistry* and I am the first author for the article. Many olfactory receptors are broadly tuned for structurally related ligands, whereas some receptors are activated by specific odorants. As with this theory, I identified a sea lamprey TAAR (sTAAR365) that is broadly tuned for biogenic polyamines (cadaverine, putrescine, and spermine), sharing a similar response profile as mouse TAAR9 (cadaverine, spermine, and spermidine). Docking and site-directed mutagenesis analyses showed that both sTAAR365 and mTAAR9 recognize two amino groups of cadaverine with the conserved $Asp^{3.32}$ and $Tyr^{6.51}$ residues. sTAAR365, which has remarkable sensitivity for cadaverine (EC50 = 4 nM), uses an extra residue, $Thr^{7.42}$, to stabilize ligand binding. These cadaverine recognition sites also interact with amines with four and three amino groups (spermine and spermidine, respectively). $Glu^{7.36}$ of sTAAR365

cooperates with Asp$^{3.32}$ and Thr$^{7.42}$ to recognize spermine, whereas mTAAR9 recognizes spermidine through an additional aromatic residue, Tyr$^{7.43}$. These results suggest a conserved mechanism whereby independently evolved TAAR receptors recognize amines with two, three, or four amino groups using the same recognition sites, at which sTAAR365 and mTAAR9 evolved distinct motifs. These motifs interact directly with the amino groups of the polyamines, a class of potent and ecologically important odorants, mediating olfactory signaling.

Chapter 3 presents the structural determinants for ligand-dependent and ligand-independent activation of an olfactory trace amine-associated receptor. This chapter has been prepared for a manuscript and I am the first author for the article. Using the above-mentioned strategy, I burrowed deep into the basal activity of all other lamprey TAARs. I identified a sea lamprey olfactory TAAR receptor (TAAR346a) that shows considerable constitutive activity when heterologously expressed in HEK293T cells. Cadaverine was found to be an agonist for TAAR346a, whereas a monoamine (triethylamine) was identified as an inverse agonist that can specifically attenuate the constitutive activity of TAAR346a. Further evidence with modeling and site-directed mutagenesis provides structural insights into the activation of TAAR346a. One negatively-charged residue in TM5, Asp$^{5.42}$, is required for the inverse agonist recognition. Along with Asp$^{5.42}$, the highly conserved aspartate Asp$^{3.32}$ composes a di-cationic recognition motif for cadaverine binding. Our results support a model in which the inverse agonist recognizes only one (Asp$^{5.42}$) of the two orthosteric sites (Asp$^{3.32}$ and Asp$^{5.42}$) used by the agonist as it elicits its inhibitory effect on the basal activity of the receptor. Moreover, interhelical hydrogen bond networks among TMs of TAAR346a appear to function as an activation switch for the constitutive activation of the receptor. In contrast, residues involved in the hydrophobic core and ionic lock are suggested to be associated with a relatively inactive conformation.

Taken together, studies presented in this dissertation provide physiological, behavioral, and molecular evidence to support that biogenic amines are potent odorants for sea lamprey olfactory trace amine-associated receptors and can mediate sea lamprey physiology and behavioral responses. By combining data with homology modeling and site-directed mutagenesis analyses, this thesis proposes molecular mechanisms whereby sea lamprey TAARs respond to biogenic polyamines. These discoveries will help to complete the story on how biogenic amines with one through four amino groups are recognized by GPCRs.

Chapter 1 of this dissertation, entitled "Spermine in semen of male sea lamprey acts as a sex pheromone" by Scott AM, Zhang Z, Jia L et al. (2019) in the journal of *PLOS Biology*, is the achievement of joint research cooperated with Dr. Anne M. Scott and Dr. Zhe Zhang under the supervision of Dr. Richard R. Neubig and Dr. Weiming Li. Chapter 2 of this dissertation is the outcome of joint research in collaboration with Dr. Shengju Li under the supervision of Dr. Richard R. Neubig, Dr. Qian Li, and Dr. Weiming Li, which contributes to a published manuscript as a first author entitled "Convergent olfactory trace amine-associated receptors detect biogenic polyamines with distinct motifs via a conserved binding site" by Jia L, Li S, Dai W et al. (2021) in the *journal of Biological Chemistry*. Chapter 3 of this dissertation contributes to a manuscript entitled "Structural determinants of ligand-dependent and ligand-independent activation of an olfactory trace amine-associated receptor". This manuscript is undertaken by the author under the supervision of Dr. Richard R. Neubig and Dr. Weiming Li and is in preparation for submission to the *journal of Biological Chemistry*.

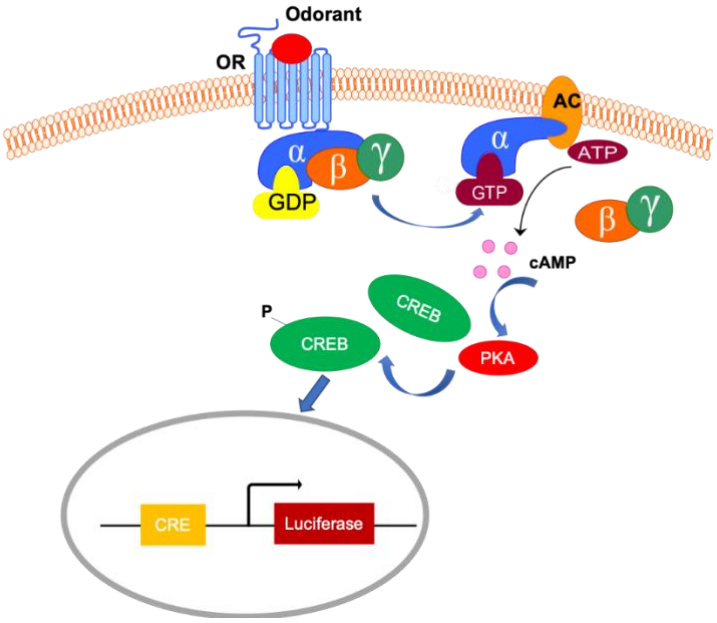

Figure I-2. Schematic diagram illustrating the heterologous OR signal transduction pathway for the initial screening

Upon an odorant binding to an OR, the odorant-bound OR transforms into an active state, allowing the receptor to be coupled with the olfactory specific G protein $G_{\alpha olf}$. $G_{\alpha olf}$ consequently activates adenylyl cyclase (AC) that results in the accumulation of cellular cAMP. cAMP elicits the activation of protein kinase A (PKA), which in turn phosphorylates and activates the transcription factor, cAMP response element-binding protein (CREB). The activated CREB binds to cAMP response element (CRE) and induces the expression of luciferase reporter gene that could be quantified by luminescence detection method. AC, adenylyl cyclase; CRE, cAMP response element; CREB, cAMP response element-binding protein; OR, odorant receptor; PKA, protein kinase A.

REFERENCES

REFERENCES

1. Hildebrand J G, Shepherd G M. Mechanisms of olfactory discrimination: Converging Evidence for Common Principles Across Phyla. Annual Review of Neuroscience.1997;20(1):595-631.

2. Ache B W, Young J M. Olfaction: Diverse Species, Conserved Principles. Neuron. 2005;48(3): 417-430.

3. Rinaldi A C. The scent of life: The exquisite complexity of the sense of smell in animals and humans. EMBO Reports. 2007;8(7):629-633.

4. Wallace K J, Rosen J B. Predator odor as an unconditioned fear stimulus in rats: elicitation of freezing by trimethylthiazoline, a component of fox feces. Behavioral neuroscience. 2000;114(5): 912.

5. Johnson N S, Yun S S, Thompson H T, et al. A synthesized pheromone induces upstream movement in female sea lamprey and summons them into traps. Proceedings of the National Academy of Sciences. 2009;106(4):1021-1026.

6. Li K, Brant C O, Huertas M, et al. Fatty-acid derivative acts as a sea lamprey migratory pheromone. Proceedings of the National Academy of Sciences. 2018;115(34):8603-8608.

7. McMeniman C J, Corfas R A, Matthews B J, et al. Multimodal integration of carbon dioxide and other sensory cues drives mosquito attraction to humans. Cell. 2014;156(5):1060-1071.

8. Vickers N J. Mechanisms of animal navigation in odor plumes. The Biological Bulletin. 2000; 198(2):203-212.

9. Adler J. Chemoreceptors in Bacteria. Science. 1969;166(3913):1588-1597.

10. De Palo G, Endres R G. Unraveling Adaptation in Eukaryotic Pathways: Lessons from Protocells. PLOS Computational Biology. 2013;9(10).

11. Derby C D, Kozma M T, Senatore A, et al. Molecular Mechanisms of Reception and Perireception in Crustacean Chemoreception: A Comparative Review. Chemical Senses. 2016; 41(5):381-398.

12. Bushdid C, Magnasco M O, Vosshall L B, et al. Humans Can Discriminate More than 1 Trillion Olfactory Stimuli. Science. 2014;343(6177):1370-1372.

13. Malnic B, Godfrey P A, Buck L B, et al. The human olfactory receptor gene family. Proceedings of the National Academy of Sciences of the United States of America. 2004;101(8): 2584-2589.

14. Buck L B, Axel R. A novel multigene family may encode odorant receptors: A molecular basis for odor recognition. Cell. 1991;65(1):175-187.

15. Gilad Y, Man O, Paabo S, et al. Human specific loss of olfactory receptor genes. Proceedings of the National Academy of Sciences of the United States of America. 2003;100(6):3324-3327.

16. Trimmer C, Keller A, Murphy N R, et al. Genetic variation across the human olfactory receptor repertoire alters odor perception. Proceedings of the National Academy of Sciences of the United States of America. 2019;116(19):9475-9480.

17. Hussain A, Saraiva L R, Korsching S I, et al. Positive Darwinian selection and the birth of an olfactory receptor clade in teleosts. Proceedings of the National Academy of Sciences of the United States of America. 2009;106(11):4313-4318.

18. Liberles S D, Buck L B. A second class of chemosensory receptors in the olfactory epithelium. Nature. 2006;442(7103):645-650.

19. Saraiva L R, Kondoh K, Ye X, et al. Combinatorial effects of odorants on mouse behavior. Proceedings of the National Academy of Sciences of the United States of America. 2016;113(23).

20. Dewan A, Pacifico R, Zhan R, et al. Non-redundant coding of aversive odours in the main olfactory pathway. Nature. 2013;497(7450):486-489.

21. Li Q, Korzan W J, Ferrero D M, et al. Synchronous Evolution of an Odor Biosynthesis Pathway and Behavioral Response. Current Biology. 2013;23(1):11-20.

22. Tan E S, Groban E S, Jacobson M P, et al. Toward Deciphering the Code to Aminergic G Protein-Coupled Receptor Drug Design. Chemistry & Biology. 2008;15(4):343-353.

23. Staubert C, Boselt I, Bohnekamp J, et al. Structural and Functional Evolution of the Trace Amine-Associated Receptors TAAR3, TAAR4 and TAAR5 in Primates. PLOS ONE. 2010;5(6).

24. Muhlhaus J, Dinter J, Nurnberg D, et al. Analysis of Human TAAR8 and Murine Taar8b Mediated Signaling Pathways and Expression Profile. International Journal of Molecular Sciences. 2014;15(11):20638-20655.

25. Dinter J, Muhlhaus J, Wienchol C L, et al. Inverse Agonistic Action of 3-Iodothyronamine at the Human Trace Amine-Associated Receptor 5. PLOS ONE. 2015;10(2).

26. Hussain A, Saraiva L R, Ferrero D M, et al. High-affinity olfactory receptor for the death-associated odor cadaverine. Proceedings of the National Academy of Sciences of the United States of America. 2013;110(48):19579-19584.

27. Li Q, Tachiebaffour Y, Liu Z, et al. Non-classical amine recognition evolved in a large clade of olfactory receptors. eLife. 2015;4,e10441.

28. Ikegami K, De March C A, Nagai M H, et al. Structural instability and divergence from conserved residues underlie intracellular retention of mammalian odorant receptors. Proceedings of the National Academy of Sciences of the United States of America. 2020;117(6):2957-2967.

29. Libants S V, Carr K M, Wu H, et al. The sea lamprey Petromyzon marinus genome reveals the early origin of several chemosensory receptor families in the vertebrate lineage. BMC Evolutionary Biology. 2009;9(1):180-180.

30. Zhuang H, Matsunami H. Evaluating cell-surface expression and measuring activation of mammalian odorant receptors in heterologous cells. Nature Protocols. 2008;3(9):1402-1413.

31. Reisert J, Restrepo D. Molecular Tuning of Odorant Receptors and Its Implication for Odor Signal Processing. Chemical Senses. 2009;34(7):535-545.

32. Kato A, Touhara K. Mammalian olfactory receptors: pharmacology, G protein coupling and desensitization. Cellular and Molecular Life Sciences. 2009;66(23):3743-3753.

33. Katada S, Hirokawa T, Oka Y, et al. Structural Basis for a Broad But Selective Ligand Spectrum of a Mouse Olfactory Receptor: Mapping the Odorant-Binding Site. The Journal of Neuroscience. 2005;25(7):1806-1815.

34. Chang S, Chungdavidson Y W, Libants S V, et al. The sea lamprey has a primordial accessory olfactory system. BMC Evolutionary Biology. 2013;13(1):172-172.

35. Gonzalez A, Morona R, Lopez J M, et al. Lungfishes, Like Tetrapods, Possess a Vomeronasal System. Frontiers in Neuroanatomy. 2010;4:130.

36. Grus W E, Zhang J. Origin of the Genetic Components of the Vomeronasal System in the Common Ancestor of all Extant Vertebrates. Molecular Biology and Evolution. 2009;26(2):407-419.

37. Olivares J, Schmachtenberg O. An update on anatomy and function of the teleost olfactory system. PeerJ. 2019;7:e7808.

38. Serizawa S, Miyamichi K, Sakano H, et al. One neuron–one receptor rule in the mouse olfactory system. Trends in Genetics. 2004;20(12):648-653.

39. Hanchate N K, Kondoh K, Lu Z, et al. Single-cell transcriptomics reveals receptor transformations during olfactory neurogenesis. Science. 2015;350(6265):1251-1255.

40. Spehr M, Leinderszufall T. One Neuron–Multiple Receptors: Increased Complexity in Olfactory Coding? Science Signaling. 2005;2005(285).

41. Vassar R, Chao S K, Sitcheran R, et al. Topographic organization of sensory projections to the olfactory bulb. Cell. 1994;79(6):981-991.

42. Mori K. Grouping of odorant receptors: odour maps in the mammalian olfactory bulb. Biochemical Society Transactions. 2001;31(1):134-136.

43. Ahuja G, Ivandic I, Salturk M, et al. Zebrafish crypt neurons project to a single, identified mediodorsal glomerulus. Scientific Reports. 2013;3(1):2063-2063.

44. Takeuchi H, Sakano H. Neural map formation in the mouse olfactory system. Cellular and Molecular Life Sciences. 2014;71(16):3049-3057.

45. Nei M, Niimura Y, Nozawa M, et al. The evolution of animal chemosensory receptor gene repertoires: roles of chance and necessity. Nature Reviews Genetics. 2008;9(12):951-963.

46. Niimura Y, Matsui A, Touhara K, et al. Extreme expansion of the olfactory receptor gene repertoire in African elephants and evolutionary dynamics of orthologous gene groups in 13 placental mammals. Genome Research. 2014;24(9):1485-1496.

47. Freitag J, Ludwig G, Andreini I, et al. Olfactory receptors in aquatic and terrestrial vertebrates. Journal of Comparative Physiology A-neuroethology Sensory Neural and Behavioral Physiology. 1998;183(5):635-650.

48. Kishida T, Kubota S, Shirayama Y, et al. The olfactory receptor gene repertoires in secondary-adapted marine vertebrates: evidence for reduction of the functional proportions in cetaceans. Biology Letters. 2007;3(4):428-430.

49. Fleischer J, Breer H, Strotmann J, et al. Mammalian olfactory receptors. Frontiers in Cellular Neuroscience. 2009;9-9.

50. Abaffy T, Malhotra A, Luetje C W, et al. The Molecular Basis for Ligand Specificity in a Mouse Olfactory Receptor A NETWORK OF FUNCTIONALLY IMPORTANT RESIDUES. Journal of Biological Chemistry. 2007;282(2):1216-1224.

51. Mombaerts P. Genes and ligands for odorant, vomeronasal and taste receptors. Nature Reviews Neuroscience. 2004;5(4):263-278.

52. Breer H, Boekhoff I, Tareilus E, et al. Rapid kinetics of second messenger formation in olfactory transduction. Nature. 1990;345(6270):65-68.

53. Kurahashi T, Yau K. Co-existence of cationic and chloride components in odorant-induced current of vertebrate olfactory receptor cells. Nature. 1993;363(6424):71-74.

54. Lowe G, Gold G H. Nonlinear amplification by calcium-dependent chloride channels in olfactory receptor cells. Nature. 1993;366(6452):283-286.

55. Niimura Y, Nei M. Evolutionary dynamics of olfactory receptor genes in fishes and tetrapods. Proceedings of the National Academy of Sciences of the United States of America. 2005;02(17): 6039-6044.

56. Borowsky B, Adham N, Jones K A, et al. Trace amines: Identification of a family of mammalian G protein-coupled receptors. Proceedings of the National Academy of Sciences of the United States of America. 2001;98(16):8966-8971.

57. Bunzow J R, Sonders M S, Arttamangkul S, et al. Amphetamine, 3,4-methylenedioxymethamphetamine, lysergic acid diethylamide, and metabolites of the

catecholamine neurotransmitters are agonists of a rat trace amine receptor. Molecular Pharmacology. 2001;60(6):1181-1188.

58. Sharma K, Ahuja G, Hussain A, et al. Elimination of a ligand gating site generates a supersensitive olfactory receptor. Scientific Reports. 2016;6(1):28359-28359.

59. Huang E S. Construction of a sequence motif characteristic of aminergic G protein–coupled receptors. Protein Science. 2003;12(7):1360-1367.

60. Hashiguchi Y, Nishida M. Evolution of Trace Amine–Associated Receptor (TAAR) Gene Family in Vertebrates: Lineage-Specific Expansions and Degradations of a Second Class of Vertebrate Chemosensory Receptors Expressed in the Olfactory Epithelium. Molecular Biology and Evolution. 2007;24(9):2099-2107.

61. Lagerstrom M C, Hellstrom A R, Gloriam D E, et al. The G protein-coupled receptor subset of the chicken genome. PLOS Computational Biology. 2006;2(6).

62. Tessarolo J A, Tabesh M J, Nesbitt M, et al. Genomic Organization and Evolution of the Trace Amine-Associated Receptor (TAAR) Repertoire in Atlantic Salmon (Salmo salar). G3: Genes, Genomes, Genetics. 2014;4(6):1135-1141.

63. Gloriam D E, Bjarnadottir T K, Yan Y, et al. The repertoire of trace amine G-protein-coupled receptors: large expansion in zebrafish. Molecular Phylogenetics and Evolution. 2005;35(2):470-482.

64. Ferrero D M, Wacker D, Roque M A, et al. Agonists for 13 Trace Amine-Associated Receptors provide insight into the molecular basis of odor selectivity. ACS Chemical Biology. 2012;7(7): 1184-1189.

65. Zhang J, Pacifico R, Cawley D, et al. Ultrasensitive Detection of Amines by a Trace Amine-Associated Receptor. The Journal of Neuroscience. 2013;33(7):3228-3239.

66. Brunet L J, Gold G H, Ngai J, et al. General anosmia caused by a targeted disruption of the mouse olfactory cyclic nucleotide-gated cation channel. Neuron. 1996;17(4):681-693.

67. Wong S T, Trinh K, Hacker B M, et al. Disruption of the Type III Adenylyl Cyclase Gene Leads to Peripheral and Behavioral Anosmia in Transgenic Mice. Neuron. 2000;27(3):487-497.

68. Wallrabenstein I, Kuklan J, Weber L, et al. Human Trace Amine-Associated Receptor TAAR5 Can Be Activated by Trimethylamine. PLOS ONE. 2013;8(2).

69. Ferrero, D. M., Lemon, J. K., Fluegge, D., Pashkovski, S. L., Korzan, W. J., Datta, S. R., Spehr, M., Fendt, M., and Liberles, S. D. Detection and avoidance of a carnivore odor by prey. Proc. Natl. Acad. Sci. U. S. A. 2011;108,11235–11240.

70. Pacifico R, Dewan A, Cawley D, et al. An Olfactory Subsystem that Mediates High-Sensitivity Detection of Volatile Amines. Cell Reports. 2012;2(1):76-88.

71. Fulle H, Vassar R, Foster D C, et al. A receptor guanylyl cyclase expressed specifically in olfactory sensory neurons. Proceedings of the National Academy of Sciences of the United States of America. 1995;92(8):3571-3575.

72. Juilfs D M, Fulle H, Zhao A Z, et al. A subset of olfactory neurons that selectively express cGMP-stimulated phosphodiesterase (PDE2) and guanylyl cyclase-D define a unique olfactory signal transduction pathway. Proceedings of the National Academy of Sciences of the United States of America. 1997;94(7):3388-3395.

73. Zufall F, Munger S D. Receptor guanylyl cyclases in mammalian olfactory function. Molecular and Cellular Biochemistry. 2010;334(1):191-197.

74. Young J M, Waters H, Dong C, et al. Degeneration of the olfactory guanylyl cyclase D gene during primate evolution. PLOS ONE. 2007;2(9).

75. Leinderszufall T, Cockerham R E, Michalakis S, et al. Contribution of the receptor guanylyl cyclase GC-D to chemosensory function in the olfactory epithelium. Proceedings of the National Academy of Sciences of the United States of America. 2007;104(36):14507-14512.

76. Hu J, Zhong C, Ding C, et al. Detection of Near-Atmospheric Concentrations of CO_2 by an Olfactory Subsystem in the Mouse. Science. 2007;317(5840):953-957.

77. Munger S D, Leinderszufall T, Mcdougall L M, et al. An olfactory subsystem that detects carbon disulfide and mediates food-related social learning. Current Biology. 2010;20(16):1438-1444.

78. Halpern M. The organization and function of the vomeronasal system. Annual Review of Neuroscience. 1987;10(1):325-362.

79. Meredith M. Sensory processing in the main and accessory olfactory systems: comparisons and contrasts. The Journal of Steroid Biochemistry and Molecular Biology. 1991;39(4):601-614.

80. Halpern M, Martinezmarcos A. Structure and function of the vomeronasal system: an update. Progress in Neurobiology. 2003;70(3):245-318.

81. Halpern M, Shapiro L S, Jia C, et al. Differential localization of G proteins in the opossum vomeronasal system. Brain Research. 1995;677(1):157-161.

82. Dulac C, Axel R. A novel family of genes encoding putative pheromone receptors in mammals. Cell. 1995;83(2):195-206.

83. Matsunami, H., Buck, L. B. A multigene family encoding a diverse array of putative pheromone receptors in mammals. Cell. 1997;90(4):775-784.

84. Herrada G, Dulac C. A Novel Family of Putative Pheromone Receptors in Mammals with a Topographically Organized and Sexually Dimorphic Distribution. Cell. 1997;90(4):763-773.

85. Ryba N J, Tirindelli R. A New Multigene Family of Putative Pheromone Receptors. Neuron. 1997;19(2):371-379.

86. Roppolo D, Vollery S, Kan C, et al. Gene cluster lock after pheromone receptor gene choice. The EMBO Journal. 2007; 26(14):3423-3430.

87. Capello L, Roppolo D, Jungo V P, et al. A common gene exclusion mechanism used by two chemosensory systems. European Journal of Neuroscience. 2009;29(4):671-678.

88. Yang H, Shi P, Zhang Y, et al. Composition and evolution of the V2r vomeronasal receptor gene repertoire in mice and rats. Genomics. 2005;86(3):306-315.

89. Bjarnadottir T K, Fredriksson R, Schioth H B, et al. The gene repertoire and the common evolutionary history of glutamate, pheromone (V2R), taste (1) and other related G protein-coupled receptors. Gene. 2005;70-84.

90. Rodriguez I, Punta K D, Rothman A, et al. Multiple new and isolated families within the mouse superfamily of V1r vomeronasal receptors. Nature Neuroscience. 2002;5(2):134-140.

91. Grus W E, Shi P, Zhang Y, et al. Dramatic variation of the vomeronasal pheromone receptor gene repertoire among five orders of placental and marsupial mammals. Proceedings of the National Academy of Sciences of the United States of America. 2005;102(16):5767-5772.

92. Saraiva L R, Korsching S I. A novel olfactory receptor gene family in teleost fish. Genome Research. 2007;17(10):1448-1457.

93. Hashiguchi Y, Furuta Y, Nishida M, et al. Evolutionary Patterns and Selective Pressures of Odorant/Pheromone Receptor Gene Families in Teleost Fishes. PLOS ONE. 2008;3(12).

94. Trotier D, Eloit C, Wassef M, et al. The Vomeronasal Cavity in Adult Humans. Chemical Senses. 2000;25(4):369-380.

95. Pfister P, Rodriguez I. Olfactory expression of a single and highly variable V1r pheromone receptor-like gene in fish species. Proceedings of the National Academy of Sciences of the United States of America. 2005;102(15):5489-5494.

96. Leinderszufall T, Lane A P, Puche A C, et al. Ultrasensitive pheromone detection by mammalian vomeronasal neurons. Nature. 2000;405(6788):792-796.

97. Jemiolo B, Harvey S, Novotny M V, et al. Promotion of the Whitten effect in female mice by synthetic analogs of male urinary constituents. Proceedings of the National Academy of Sciences of the United States of America. 1986;83(12):4576-4579.

98. Jemiolo B, Andreolini F, Xie T, et al. Puberty-affecting synthetic analogs of urinary chemosignals in the house mouse, Mus domesticus. Physiology & Behavior. 1989;46(2):293-298.

99. Novotny M V, Jemiolo B, Wiesler D, et al. A unique urinary constituent, 6-hydroxy-6-methyl-3-heptanone, is a pheromone that accelerates puberty in female mice. Chemistry & Biology. 1999; 6(6):377-383.

100. Novotny M V, Ma W, Wiesler D, et al. Positive identification of the puberty-accelerating pheromone of the house mouse: the volatile ligands associating with the major urinary protein. Proceedings of The Royal Society B: Biological Sciences. 1999;266(1432):2017-2022.

101. Boschat C, Pelofi C, Randin O, et al. Pheromone detection mediated by a V1r vomeronasal receptor. Nature Neuroscience. 2002;5(12):1261-1262.

102. Tirindelli R, Dibattista M, Pifferi S, et al. From Pheromones to Behavior. Physiological Reviews. 2009;89(3):921-956.

103. Punta K D, Leinderszufall T, Rodriguez I, et al. Deficient pheromone responses in mice lacking a cluster of vomeronasal receptor genes. Nature. 2002;419(6902):70-74.

104. Haga S, Hattori T, Sato T, et al. The male mouse pheromone ESP1 enhances female sexual receptive behaviour through a specific vomeronasal receptor. Nature. 2010;466(7302):118-122.

105. Leinderszufall T, Brennan P A, Widmayer P, et al. MHC Class I Peptides as Chemosensory Signals in the Vomeronasal Organ. Science. 2004;306(5698):1033-1037.

106. Hansen A, Rolen S H, Anderson K, et al. Correlation between Olfactory Receptor Cell Type and Function in the Channel Catfish. The Journal of Neuroscience. 2003;23(28):9328-9339.

107. Hansen A, Anderson K, Finger T E, et al. Differential distribution of olfactory receptor neurons in goldfish: structural and molecular correlates. The Journal of Comparative Neurology. 2004;477(4):347-359.

108. Soehnlein O, Lindbom L. Phagocyte partnership during the onset and resolution of inflammation. Nature Reviews Immunology. 2010;10(6):427-439.

109. Riviere S, Challet L, Fluegge D, et al. Formyl peptide receptor-like proteins are a novel family of vomeronasal chemosensors. Nature. 2009;459(7246):574-577.

110. Liberles S D, Horowitz L F, Kuang D, et al. Formyl peptide receptors are candidate chemosensory receptors in the vomeronasal organ. Proceedings of the National Academy of Sciences of the United States of America. 2009;106(24):9842-9847.

111. Yang H, Shi P. Molecular and evolutionary analyses of formyl peptide receptors suggest the absence of VNO-specific FPRs in primates. Journal of Genetics and Genomics. 2010;37(12):771-778.

112. Ackels T, Der Weid B T, Rodriguez I, et al. Physiological characterization of formyl peptide receptor expressing cells in the mouse vomeronasal organ. Frontiers in Neuroanatomy. 2014;134-134.

113. Chamero P, Katsoulidou V, Hendrix P, et al. G protein G(alpha)o is essential for vomeronasal function and aggressive behavior in mice. Proceedings of the National Academy of Sciences of the United States of America. 2011;108(31):12898-12903.

114. Kolaczkowska E, Kubes P. Neutrophil recruitment and function in health and inflammation. Nature Reviews Immunology. 2013;13(3):159-175.

115. Ma M. Encoding Olfactory Signals via Multiple Chemosensory Systems. Critical Reviews in Biochemistry and Molecular Biology. 2007;42(6):463-480.

116. Hansen A, Zielinski B S. Diversity in the olfactory epithelium of bony fishes: Development, lamellar arrangement, sensory neuron cell types and transduction components. Journal of Neurocytology. 2005;34(3):183-208.

117. Ren X, Chang S, Laframboise A J, et al. Projections from the accessory olfactory organ into the medial region of the olfactory bulb in the sea lamprey (Petromyzon marinus): A novel vertebrate sensory structure? The Journal of Comparative Neurology. 2009;516(2):105-116.

118. Sato K, Suzuki N. Whole-cell Response Characteristics of Ciliated and Microvillous Olfactory Receptor Neurons to Amino Acids, Pheromone Candidates and Urine in Rainbow Trout. Chemical Senses. 2001;26(9):1145-1156.

119. Schmachtenberg O, Bacigalupo J. Olfactory transduction in ciliated receptor neurons of the Cabinza grunt, Isacia conceptionis (teleostei: haemulidae). European Journal of Neuroscience. 2004;20(12):3378-3386.

120. Alioto T S, Ngai J. The repertoire of olfactory C family G protein-coupled receptors in zebrafish: candidate chemosensory receptors for amino acids. BMC Genomics. 2006;7(1):309-309.

121. Yoshihara, Y. Molecular genetic dissection of the zebrafish olfactory system. In Chemosensory Systems in Mammals, Fishes, and Insects. Springer. 2008; 1-19.

122. Oka Y, Saraiva L R, Korsching S I, et al. Crypt Neurons Express a Single V1R-Related ora Gene. Chemical Senses. 2012;37(3):219-227.

123. Schmachtenberg O. Histological and electrophysiological properties of crypt cells from the olfactory epithelium of the marine teleost Trachurus symmetricus. The Journal of Comparative Neurology. 2006;495(1):113-121.

124. Vielma A H, Ardiles A O, Delgado L M, et al. The elusive crypt olfactory receptor neuron: evidence for its stimulation by amino acids and cAMP pathway agonists. The Journal of Experimental Biology. 2008;211(15):2417-2422.

125. Bazaes A, Schmachtenberg O. Odorant tuning of olfactory crypt cells from juvenile and adult rainbow trout. The Journal of Experimental Biology. 2012;215(10):1740-1748.

126. Chess A, Simon I, Cedar H, et al. Allelic inactivation regulates olfactory receptor gene expression. Cell. 1994;78(5):823-834.
127. Grosveld F, Van Assendelft G B, Greaves D R, et al. Position-independent, high-level expression of the human β-globin gene in transgenic mice. Cell. 1987;51(6):975-985.

128. Serizawa S, Miyamichi K, Nakatani H, et al. Negative Feedback Regulation Ensures the One Receptor-One Olfactory Neuron Rule in Mouse. Science. 2003;302(5653):2088-2094.

129. Magklara A, Yen A, Colquitt B M, et al. An Epigenetic Signature for Monoallelic Olfactory Receptor Expression. Cell. 2011;145(4):555-570.

130. Shepherd G.M, Greer C.A. Olfactory bulb. In: Shepherd G.M, editor. The synaptic organization of the brain. Oxford University Press; New York.1998;159–204.

131. Satou M. Synaptic organization, local neuronal circuitry, and functional segregation of the teleost olfactory bulb. Progress in Neurobiology. 1990;34(2):115-142.

132. Wachowiak M, Shipley M T. Coding and synaptic processing of sensory information in the glomerular layer of the olfactory bulb. Seminars in Cell & Developmental Biology. 2006;17(4): 411-423.

133. Willhite D C, Nguyen K T, Masurkar A V, et al. Viral tracing identifies distributed columnar organization in the olfactory bulb. Proceedings of the National Academy of Sciences of the United States of America. 2006;103(33):12592-12597.

134. Ressler K J, Sullivan S L, Buck L B, et al. A zonal organization of odorant receptor gene expression in the olfactory epithelium. Cell. 1993;73(3):597-609.

135. Ressler K J, Sullivan S L, Buck L B, et al. Information coding in the olfactory system: Evidence for a stereotyped and highly organized epitope map in the olfactory bulb. Cell. 1994, 79(7):1245-1255.

136. Vassar R, Chao S K, Sitcheran R, et al. Topographic organization of sensory projections to the olfactory bulb. Cell. 1994;79(6):981-991.

137. Mombaerts P, Wang F, Dulac C, et al. Visualizing an Olfactory Sensory Map. Cell. 1996; 87(4):675-686.

138. Wang F, Nemes A, Mendelsohn M, et al. Odorant Receptors Govern the Formation of a Precise Topographic Map. Cell. 1998;93(1):47-60.

139. Potter S M, Zheng C, Koos D S, et al. Structure and Emergence of Specific Olfactory Glomeruli in the Mouse. The Journal of Neuroscience. 2001;21(24):9713-9723.

140. Pinching A J, Powell T P. The neuron types of the glomerular layer of the olfactory bulb. Journal of Cell Science. 1971;9(2):305-345.

141. Ennis, M., Hamilton, K. A., Hayar A. Neurochemistry of the main olfactory system. In Handbook of Neurochemistry and Molecular Neurobiology, 3rd Edition, Lajtha, A. (Ed). 2007, Vol. 20, Sensory Neurochemistry, Johnson, D. (Ed.). Heidelberg, Germany: Springer, pp. 137–204.

142. Frazier L L, Brunjes P C. Unilateral odor deprivation: early postnatal changes in olfactory bulb cell density and number. The Journal of Comparative Neurology. 1988;269(3):355-370.

143. Parrishaungst S, Shipley M T, Erdelyi F, et al. Quantitative analysis of neuronal diversity in the mouse olfactory bulb. The Journal of Comparative Neurology. 2007;501(6):825-836.

144. Doving, K. B. Functional properties of the fish olfactory system. In Progress in sensory physiology. Springer, Berlin, Heidelberg. 1986;6:39-104.

145. Kasumyan, A. O. The olfactory system in fish: structure, function, and role in behavior. Journal of Ichthyology. 2004;44(2), S180.

146. Fuller C L, Yettaw H K, Byrd C A, et al. Mitral cells in the olfactory bulb of adult zebrafish (Danio rerio): morphology and distribution. The Journal of Comparative Neurology. 2006;499(2): 218-230.

147. Miyasaka N, Morimoto K, Tsubokawa T, et al. From the Olfactory Bulb to Higher Brain Centers: Genetic Visualization of Secondary Olfactory Pathways in Zebrafish. The Journal of Neuroscience. 2009;29(15):4756-4767.

148. Kosaka T, Hama K. Synaptic organization in the teleost olfactory bulb. Journal de physiologie. 1982;78(8):707-719.

149. Kermen F, Franco L M, Wyatt C, et al. Neural circuits mediating olfactory-driven behavior in fish. Frontiers in Neural Circuits. 2013;62-62.

150. Zippel H P, Reschke C, Korff, et al. Simultaneous recordings from two physiologically different types of relay neurons, mitral cells and ruffed cells, in the olfactory bulb of goldfish. Cellular and Molecular Biology. 1999;45(3):327-337.

151. Meredith M, Oconnell R J. Efferent control of stimulus access to the hamster vomeronasal organ. The Journal of Physiology. 1979;286(1):301-316.

152. Larrivasahd J. The accessory olfactory bulb in the adult rat: a cytological study of its cell types, neuropil, neuronal modules, and interactions with the main olfactory system. The Journal of Comparative Neurology. 2008;510(3):309-350.

153. Takami S, Graziadei P P. Light microscopic golgi study of mitral/tufted cells in the accessory olfactory bulb of the adult rat. The Journal of Comparative Neurology. 1991;311(1):65-83.

154. Lillesaar C, Stigloher C, Tannhauser B, et al. Axonal projections originating from raphe serotonergic neurons in the developing and adult zebrafish, Danio rerio, using transgenics to

visualize raphe-specific pet1 expression. The Journal of Comparative Neurology. 2009;512(2): 158-182.
155. Gracia-Llanes F J, Blasco-Ibáñez J M, Nácher J, et al. Synaptic connectivity of serotonergic axons in the olfactory glomeruli of the rat olfactory bulb. Neuroscience. 2010;169(2):770-780.

156. Chungdavidson Y W, Wang H, Scott A M, et al. Pheromone 3kPZS evokes context-dependent serotonin sexual dimorphism in the brain of the sea lamprey (Petromyzon marinus). Integrative Zoology. 2015;10(1):91-101.

157. Mandairon, N., Ferretti, C. J., Stack, C. M., Rubin, D. B., Cleland, T. A., & Linster, C. Cholinergic modulation in the olfactory bulb influences spontaneous olfactory discrimination in adult rats. European Journal of Neuroscience. 2006;24(11):3234-3244.

158. Chaudhury, D., Escanilla, O., & Linster, C. Bulbar acetylcholine enhances neural and perceptual odor discrimination. Journal of Neuroscience. 2009;29(1):52-60.

159. Linster C, Cleland T A. Cholinergic modulation of sensory representations in the olfactory bulb. Neural Networks. 2002;15(4-6):709-717.

160. Wilson J M, Rempel J, Brownstone R M. Postnatal development of cholinergic synapses on mouse spinal motoneurons. Journal of Comparative Neurology. 2004;474(1):13-23.

161. Shipley M T, Halloran F J, de la Torre J. Surprisingly rich projection from locus coeruleus to the olfactory bulb in the rat. Brain research. 1985;329(1-2):294-299.

162. McLean J H, Shipley M T, Nickell W T, et al. Chemoanatomical organization of the noradrenergic input from locus coeruleus to the olfactory bulb of the adult rat. Journal of Comparative Neurology. 1989;285(3):339-349.

163. Linster C, Nai Q, Ennis M. Nonlinear effects of noradrenergic modulation of olfactory bulb function in adult rodents. Journal of neurophysiology. 2011;105(4):1432-1443.

164. Nai Q, Dong H W, Hayar A, et al. Noradrenergic regulation of GABAergic inhibition of main olfactory bulb mitral cells varies as a function of concentration and receptor subtype. Journal of neurophysiology. 2009;101(5):2472-2484.

165. Nai Q, Dong H W, Linster C, et al. Activation of α1 and α2 noradrenergic receptors exert opposing effects on excitability of main olfactory bulb granule cells. Neuroscience. 2010;169(2): 882-892.

166. Buchinger, T.J., Siefkes, M.J., Zielinski, B.S. et al. Chemical cues and pheromones in the sea lamprey (Petromyzon marinus). Front Zool. 2015; 12:32.

167. Kleerekoper H, Van Erkel G A. The olfactory apparatus of Petromyzon marinus. Canadian Journal of Zoology. 1960;38(1):209-223.

168. Kleerekoper H, Mogensen J. Role of olfaction in the orientation of Petromyzon marinus. I. Response to a single amine in prey's body odor. Physiol Zool. 1963;36:347–360.

169. Li W, Scott A P, Siefkes M J, et al. Bile Acid Secreted by Male Sea Lamprey That Acts as a Sex Pheromone. Science. 2002;296(5565):138-141.

170. Sorensen P W, Vrieze L A, Fine J M, et al. A multi-component migratory pheromone in the sea lamprey. Fish Physiology and Biochemistry. 2003:253-257.

171. Vrieze L A, Bjerselius R, Sorensen P W. Importance of the olfactory sense to migratory sea lampreys Petromyzon marinus seeking riverine spawning habitat. Journal of Fish Biology.2010; 76(4):949-964.

172. Kleerekoper H. The sense organs. In: Hardisty mw, Potter IC. The biology of lampreys. 1972; vol 2. Academic Press, New York, pp373-404.

173. Vandenbossche J, Seelye J G, Zielinski B S, et al. The Morphology of the Olfactory Epithelium in Larval, Juvenile and Upstream Migrant Stages of the Sea Lamprey, Petromyzon marinus. Brain Behavior and Evolution. 1995,45(1):19-24.

174. Vandenbossche J, Youson JH, Pohlman D, et al. Metamorphosis of the olfactory organ of the sea lamprey (Petromyzon marinus L.): Morphological changes and morphometric analysis. J Morphol. 1997;231(1):41-52.

175. Laframboise A J, Ren X, Chang S, et al. Olfactory sensory neurons in the sea lamprey display polymorphisms. Neuroscience Letters. 2007;414(3):277-281.

176. Buchinger T J, Scott A M, Fissette S D, et al. A pheromone antagonist liberates female sea lamprey from a sensory trap to enable reliable communication. Proceedings of the National Academy of Sciences. 2020;117(13):7284-7289.

177. Iwahori N, Kiyota E, Nakamura K, et al. A Golgi study on the olfactory bulb in the lamprey, Lampetra japonica. Neuroscience Research. 1987;5(2):126-139.

178. Northcutt R G, Puzdrowski R L. Projections of the Olfactory Bulb and Nerves Terminalis in the Silver Lamprey. Brain Behavior and Evolution. 1988;32(2):96-107.

179. Polenova O A, Vesselkin N P. Olfactory and nonolfactory projections in the river lamprey (Lampetra fluviatilis) telencephalon. Journal für Hirnforschung. 1993;34(2).

180. Chang S. The neural connectivity of olfactory bulb regions in ovulated female lampreys (Petromyzon marinus). M.Sc. thesis. 2006. University of Windsor.

181. Frontini A, Zaidi A U, Hua H, et al. Glomerular Territories in the Olfactory Bulb from the Larval Stage of the Sea Lamprey Petromyzon marinus. The Journal of Comparative Neurology. 2003;465(1):27-37.

182. Derjean D, Moussaddy A, Atallah E, et al. A Novel Neural Substrate for the Transformation of Olfactory Inputs Into Motor Output. PLOS Biology. 2010,8(12).

183. Dubuc R, Brocard F, Antri M, et al. Initiation of locomotion in lampreys. Brain Research Reviews. 2008;57(1):172-182.

184. Green W W. The neuroanatomical organization and chemosensory response characteristics of the olfactory bulb in the sea lamprey (Petromyzon marinus). Ph.D. Dissertation. 2013. University of Windsor.

185. Shoji T, Ueda H, Ohgami T, et al. Amino Acids Dissolved in Stream Water as Possible Home Stream Odorants for Masu Salmon. Chemical Senses. 2000;25(5):533-540.

186. Shoji T, Yamamoto Y, Nishikawa D, et al. Amino acids in stream water are essential for salmon homing migration. Fish Physiology and Biochemistry. 2003;28(1):249-251.

187. Johnson N S, Luehring M A, Siefkes M J, et al. Mating Pheromone Reception and Induced Behavior in Ovulating Female Sea Lampreys. North American Journal of Fisheries Management. 2006;26(1):88-96.

188. Yambe H, Kitamura S, Kamio M, et al. l-Kynurenine, an amino acid identified as a sex pheromone in the urine of ovulated female masu salmon. Proceedings of the National Academy of Sciences of the United States of America. 2006;103(42):15370-15374.

189. Moore H H, Schleen L P. Changes in Spawning Runs of Sea Lamprey (Petromyzon marinus) in Selected Streams of Lake Superior after Chemical Control. Canadian Journal of Fisheries and Aquatic Sciences. 1980; 37(11):1851-1860.

190. Bergstedt R A, Seelye J G. Evidence for Lack of Homing by Sea Lampreys. Transactions of The American Fisheries Society. 1995;124(2):235-239.

191. Li W, Sorensen P W, Gallaher D D, et al. The olfactory system of migratory adult sea lamprey (Petromyzon marinus) is specifically and acutely sensitive to unique bile acids released by conspecific larvae. The Journal of General Physiology. 1995;105(5):569-587.

192. Waldman J R, Grunwald C, Wirgin I, et al. Sea lamprey Petromyzon marinus: an exception to the rule of homing in anadromous fishes. Biology Letters. 2008;4(6):659-662.

193. Sorensen P W, Fine J M, Dvornikovs V, et al. Mixture of new sulfated steroids functions as a migratory pheromone in the sea lamprey. Nature Chemical Biology. 2005;1(6):324-328.

194. Fine J M, Sorensen P W. Isolation and biological activity of the multi-component sea lamprey migratory pheromone. Journal of Chemical Ecology. 2008;34(10):1259-1267.

195. Fine J M, Sorensen P W. Production and fate of the sea lamprey migratory pheromone. Fish Physiology and Biochemistry. 2010;36(4):1013-1020.

196. Meckley T D, Wagner C M, Luehring M A, et al. Field Evaluation of Larval Odor and Mixtures of Synthetic Pheromone Components for Attracting Migrating Sea Lampreys in Rivers. Journal of Chemical Ecology. 2012;38(8):1062-1069.

197. Chungdavidson Y W, Wang H, Siefkes M J, et al. Pheromonal bile acid 3-ketopetromyzonol sulfate primes the neuroendocrine system in sea lamprey. BMC Neuroscience. 2013;14(1):11-11.

198. Chungdavidson Y W, Wang H, Bryan M B, et al. An anti-steroidogenic inhibitory primer pheromone in male sea lamprey (Petromyzon marinus). General and Comparative Endocrinology. 2013;24-31.

199. Johnson N S, Yun S S, Buchinger T J, et al. Multiple functions of a multi-component mating pheromone in sea lamprey Petromyzon marinus. Journal of fish biology. 2012;80(3):538-554.

200. Li K, Brant CO, Siefkes MJ, Kruckman HG, Li W. Characterization of a novel bile alcohol sulfate released by sexually mature male Sea Lamprey (Petromyzon marinus). PLoS ONE. 2013;8.

201. Siefkes M J, Li W. Electrophysiological evidence for detection and discrimination of pheromonal bile acids by the olfactory epithelium of female sea lampreys (Petromyzon marinus). Journal of Comparative Physiology A-neuroethology Sensory Neural and Behavioral Physiology. 2004;190(3):193-199.

202. Li W, Scott A P, Siefkes M J, et al. A male pheromone in the sea lamprey (Petromyzon marinus): an overview. Fish Physiology and Biochemistry. 2003;28(1):259-262.

203. Carolsfeld J, Tester M, Kreiberg H, et al. Pheromone-Induced Spawning of Pacific Herring. Hormones and Behavior. 1997;31(3):256-268.

204. Avila F W, Sirot L K, Laflamme B A, et al. Insect seminal fluid proteins: identification and function. Annual Review of Entomology. 2011;56(1):21-40.

205. Shine R, Mason R T. An airborne sex pheromone in snakes. Biology Letters. 2012;8(2):183-185.

206. Perry J C, Sirot L K, Wigby S, et al. The seminal symphony: How to compose an ejaculate. Trends in Ecology and Evolution. 2013;28(7):414-422.

207. Gabrieli P, Kakani E G, Mitchell S N, et al. Sexual transfer of the steroid hormone 20E induces the postmating switch in Anopheles gambiae. Proceedings of the National Academy of Sciences of the United States of America. 2014;111(46):16353-16358.

208. Suarez S, Wolfner M. Seminal Plasma Plays Important Roles in Fertility. In: Jonge CD, Barratt C, editors. The Sperm Cell: Production, Maturation, Fertilization, Regeneration. Cambridge: Cambridge University Press. 2017;88–108.

209. Malouines C. Counter-perfume: using pheromones to prevent female remating. Biological Reviews. 2017;92(3): 570-1581.

210. Smith C, Spence R, Reichard M, et al. Sperm is a sexual ornament in rose bitterling. Journal of Evolutionary Biology. 2018; 31(11):1610-1622.

211. Siefkes M J, Winterstein S R, Li W, et al. Evidence that 3-keto petromyzonol sulphate specifically attracts ovulating female sea lamprey, Petromyzon marinus. Animal Behaviour. 2005; 70(5):1037-1045.

212. Sirota M G, Prisco G V, Dubuc R, et al. Stimulation of the mesencephalic locomotor region elicits controlled swimming in semi-intact lampreys. European Journal of Neuroscience. 2000; 12(11):4081-4092.

213. Ray D L, Brocard F, Bourcierlucas C, et al. Nicotinic activation of reticulospinal cells involved in the control of swimming in lampreys. European Journal of Neuroscience. 2003; 17(1):137-148.

214. Brocard F, Dubuc R. Differential Contribution of Reticulospinal Cells to the Control of Locomotion Induced By the Mesencephalic Locomotor Region. Journal of Neurophysiology. 2003; 90(3):1714-1727.

215. Manira A E, Pombal M A, Grillner S, et al. Diencephalic projection to reticulospinal neurons involved in the initiation of locomotion in adult lampreys Lampetra fluviatilis. The Journal of Comparative Neurology. 1997;389(4):603-616.

216. Harriswarrick R M, Cohen A H. Serotonin modulates the central pattern generator for locomotion in the isolated lamprey spinal cord. The Journal of Experimental Biology. 1985; 116(1):27-46.

217. Dongen P A, Grillner S, Hokfelt T, et al. 5-Hydroxytryptamine (serotonin) causes a reduction in the afterhyperpolarization following the action potential in lamprey motoneurons and premotor interneurons. Brain Research. 1986;366(1):320-325.

218. Kemnitz C P, Strauss T R, Hosford D M, et al. Modulation of swimming in the lamprey, Petromyzon marinus, by serotonergic and dopaminergic drugs. Neuroscience Letters. 1995;201(2): 115-118.

219. Beauséjour P A, Auclair F, Daghfous G, et al. Dopaminergic modulation of olfactory-evoked motor output in sea lampreys (Petromyzon marinus L.). Journal of Comparative Neurology. 2020; 528(1):118-138.

220. Ménard A, Grillner S. Diencephalic locomotor region in the lamprey--afferents and efferent control. J Neurophysiol. 2008;100(3):1343-1353.

221. Cerione RA, Sibley DR, Codina J, et al. Reconstitution of a hormone-sensitive adenylate cyclase system. The pure beta-adrenergic receptor and guanine nucleotide regulatory protein confer hormone responsiveness on the resolved catalytic unit. J Biol Chem. 1984;259(16):9979-9982.

222. Costa T, Herz A. Antagonists with negative intrinsic activity at delta opioid receptors coupled to GTP-binding proteins. Proceedings of the National Academy of Sciences of the United States of America. 1989;86(19):7321–7325.

223. Cotecchia S, Exum S, Caron M G, et al. Regions of the alpha 1-adrenergic receptor involved in coupling to phosphatidylinositol hydrolysis and enhanced sensitivity of biological function. Proceedings of the National Academy of Sciences of the United States of America. 1990;87(8): 2896–2900.

224. Samama P, Cotecchia S, Costa T, et al. A mutation-induced activated state of the beta 2-adrenergic receptor. Extending the ternary complex model. Journal of Biological Chemistry. 1993; 268(7):4625-4636.

225. Ren Q, Kurose H, Lefkowitz R J, et al. Constitutively active mutants of the α2-adrenergic receptor. Journal of Biological Chemistry. 1993;268:16483-16487.

226. Pei G, Samama P, Lohse M J, et al. A constitutively active mutant beta 2-adrenergic receptor is constitutively desensitized and phosphorylated. Proceedings of the National Academy of Sciences of the United States of America. 1994;91(7):2699-2702.

227. de Ligt RA, Kourounakis AP, IJzerman AP. Inverse agonism at G protein-coupled receptors: (patho)physiological relevance and implications for drug discovery. Br J Pharmacol. 2000;130(1):1-12.

228. Scheer A, Fanelli F, Costa T, et al. Constitutively active mutants of the alpha 1B-adrenergic receptor: role of highly conserved polar amino acids in receptor activation. The EMBO Journal. 1996;15(14):3566-3578.

229. Scheer A, Fanelli F, Costa T, et al. The activation process of the α1B-adrenergic receptor: Potential role of protonation and hydrophobicity of a highly conserved aspartate. Proceedings of the National Academy of Sciences of the United States of America. 1997;94(3):808-813.

230. Kjelsberg M A, Cotecchia S, Ostrowski J, et al. Constitutive activation of the alpha 1B-adrenergic receptor by all amino acid substitutions at a single site. Evidence for a region which constrains receptor activation. Journal of Biological Chemistry. 1992;267(3):1430-1433.

231. Rossier O, Abuin L, Fanelli F, et al. Inverse agonism and neutral antagonism at α1a-and α1b-adrenergic receptor subtypes. Molecular pharmacology. 1999;56(5):858-866.

232. Gether U, Ballesteros J A, Seifert R, et al. Structural Instability of a Constitutively Active G Protein-coupled Receptor AGONIST-INDEPENDENT ACTIVATION DUE TO CONFORMATIONAL FLEXIBILITY. Journal of Biological Chemistry. 1997;272(5):2587-2590.

233. Rasmussen S G, Jensen A, Liapakis G, et al. Mutation of a Highly Conserved Aspartic Acid in the β2 Adrenergic Receptor: Constitutive Activation, Structural Instability, and Conformational Rearrangement of Transmembrane Segment 6. Molecular Pharmacology. 1999;56(1):175-184.

234. Fritze O, Filipek S, Kuksa V A, et al. Role of the conserved NPxxY(x)5,6F motif in the rhodopsin ground state and during activation. Proceedings of the National Academy of Sciences of the United States of America. 2003;100(5):2290-2295.

235. Vogel R, Sakmar T P, Sheves M, et al. Coupling of Protonation Switches During Rhodopsin Activation. Photochemistry and Photobiology. 2007;83(2):286-292.

236. Hofmann K P, Scheerer P, Hildebrand P W, et al. A G protein-coupled receptor at work: the rhodopsin model. Trends in Biochemical Sciences. 2009;34(11):540-552.

237. Parma J, Duprez L, Van Sande J, et al. Somatic mutations in the thyrotropin receptor gene cause hyperfunctioning thyroid adenomas. Nature. 1993;365(6447):649-651.

238. Duprez L, Parma J, Costagliola S, et al. Constitutive activation of the TSH receptor by spontaneous mutations affecting the N-terminal extracellular domain. FEBS Letters. 1997;409(3): 469-474.

239. Biebermann H, Schoneberg T, Hess C, et al. The First Activating TSH Receptor Mutation in Transmembrane Domain 1 Identified in a Family with Nonautoimmune Hyperthyroidism. The Journal of Clinical Endocrinology and Metabolism. 2001;86(9):4429-4433.

240. Liu Z, Fan F, Xiao X, et al. Constitutive activation of the thyroid-stimulating hormone receptor (TSHR) by mutating Ile691 in the cytoplasmic tail segment. PLOS ONE. 2011;6(1).

241. Parma J, Van Sande J, Swillens S, et al. Somatic mutations causing constitutive activity of the thyrotropin receptor are the major cause of hyperfunctioning thyroid adenomas: identification of additional mutations activating both the cyclic adenosine 3',5'-monophosphate and inositol phosphate-Ca^{2+} cascades. Mol Endocrinol. 1995;9:725−733.

242. Tonacchera M, Van Sande J, Cetani F, et al. Functional characteristics of three new germline mutations of the thyrotropin receptor gene causing autosomal dominant toxic thyroid hyperplasia. The Journal of Clinical Endocrinology and Metabolism. 1996;81(2):547-554.

243. Schwab K O, Gerlich M, Broecker M, et al. Constitutively active germline mutation of the thyrotropin receptor gene as a cause of congenital hyperthyroidism. The Journal of Pediatrics. 1997;131(6):899-904.

244. Khoo D H, Parma J, Rajasoorya C, et al. A Germline Mutation of the Thyrotropin Receptor Gene Associated with Thyrotoxicosis and Mitral Valve Prolapse in a Chinese Family. The Journal of Clinical Endocrinology and Metabolism. 1999;84(4):1459-1462.

245. Lee T W, Cotecchia S, Milligan G, et al. Up-regulation of the levels of expression and function of a constitutively active mutant of the hamster alpha1B-adrenoceptor by ligands that act as inverse agonists. Biochemical Journal. 1997;325(3):733-739.

246. Srinivasan S, Lubranoberthelier C, Govaerts C, et al. Constitutive activity of the melanocortin-4 receptor is maintained by its N-terminal domain and plays a role in energy homeostasis in humans. Journal of Clinical Investigation. 2004;114(8):1158-1164.

247. Tao Y, Segaloff D L. Functional Analyses of Melanocortin-4 Receptor Mutations Identified from Patients with Binge Eating Disorder and Nonobese or Obese Subjects. The Journal of Clinical Endocrinology and Metabolism. 2005;90(10):5632-5638.

248. Vaisse C, Clement K, Durand E, et al. Melanocortin-4 receptor mutations are a frequent and heterogeneous cause of morbid obesity. Journal of Clinical Investigation. 2000;106(2):253-262.

249. Xiang Z, Litherland S A, Sorensen N B, et al. Pharmacological characterization of 40 human melanocortin-4 receptor polymorphisms with the endogenous proopiomelanocortin-derived agonists and the agouti-related protein (AGRP) antagonist. Biochemistry. 2006;45(23):7277-7288.

250. Hinney A, Hohmann S, Geller F, et al. Melanocortin-4 Receptor Gene: Case-Control Study and Transmission Disequilibrium Test Confirm that Functionally Relevant Mutations Are Compatible with a Major Gene Effect for Extreme Obesity. The Journal of Clinical Endocrinology and Metabolism. 2003;88(9):4258-4267.

251. Vallijaakola K, Lipsanennyman M, Oksanen L, et al. Identification and Characterization of Melanocortin-4 Receptor Gene Mutations in Morbidly Obese Finnish Children and Adults. The Journal of Clinical Endocrinology and Metabolism. 2004;89(2):940-945.

252. Hinney A, Bettecken T, Tarnow P, et al. Prevalence, Spectrum, and Functional Characterization of Melanocortin-4 Receptor Gene Mutations in a Representative Population-Based Sample and Obese Adults from Germany. The Journal of Clinical Endocrinology and Metabolism. 2006;91(5):1761-1769.

253. Trotier D, MacLeod P. Intracellular recordings from salamander olfactory receptor cells. Brain Res. 1983;268:225–237.

254. Frings S, Lindemann B. Current recording from sensory cilia of olfactory receptor cells in situ. I. The neuronal response to cyclic nucleotides. The Journal of General Physiology. 1991; 97(1):1-16.

255. Lowe G, Gold G H. OLFACTORY TRANSDUCTION IS INTRINSICALLY NOISY. Proceedings of the National Academy of Sciences of the United States of America. 1995;92(17): 7864-7868.

256. Reisert J. Origin of basal activity in mammalian olfactory receptor neurons. The Journal of General Physiology. 2010;136(5):529-540.

257. Nakashima A, Takeuchi H, Imai T, et al. Agonist-Independent GPCR Activity Regulates Anterior-Posterior Targeting of Olfactory Sensory Neurons. Cell. 2013;154(6):1314-1325.

258. van Leeuwenhoek, A. Observationes D. Anthonii Leeuwenhoek, de Natis e semine genitali Animalculis. Philos Trans R Soc London. 1678;12:1040-1043.

259. Heidari A, Gobato R. Putrescine, Cadaverine, Spermine and Spermidine–Enhanced Precatalyst Preparation Stabilization and Initiation (EPPSI) Nano Molecules. Parana Journal of Science and Education. 2018;4(5):1-14.

CHAPTER 1

SPERMINE IN SEMEN OF MALE SEA LAMPREY ACTS AS A SEX PHEROMONE

Scott AM[#], **Zhang Z**[#], **Jia L**[#], Li K, Zhang Q, Dexheimer T, Ellsworth E, Ren J, Chung-Davidson YW, Zu Y, Neubig RR, Li W. Spermine in semen of male sea lamprey acts as a sex pheromone. *PLoS Biol*. 2019 Jul 9;17(7): e3000332.
# These authors contributed equally to this work.

ABSTRACT

Semen is fundamental for sexual reproduction. The non-sperm part of ejaculated semen, or seminal plasma, facilitates the delivery of sperm to the eggs. The seminal plasma of some species with internal fertilization contains anti-aphrodisiac molecules that deter promiscuity in post-copulatory females, conferring fitness benefits to the ejaculating male. By contrast, in some taxa with external fertilization such as fish, exposure to semen promotes spawning behaviors. However, no specific compounds in semen have been identified as aphrodisiac pheromones. We sought to identify a pheromone from the milt (fish semen) of sea lamprey (*Petromyzon marinus*), a jawless fish that spawns in lek-like aggregations in which each spermiating male defends a nest, and ovulatory females move from nest to nest to mate. We postulated that milt compounds signal to ovulatory females the presence of spawning spermiating males. We determined that spermine, an odorous polyamine initially identified from human semen, is indeed a milt pheromone. At concentrations as low as 10^{-14} molar, spermine stimulated the lamprey olfactory system and attracted ovulatory females but did not attract males or pre-ovulatory females. We found spermine activated a trace amine-associated receptor (TAAR)-like receptor in the lamprey olfactory epithelium. A novel antagonist to that receptor nullified the attraction of ovulatory females to spermine. Our results elucidate a mechanism whereby a seminal plasma pheromone attracts ready-to-mate females and implicates a possible conservation of the olfactory detection of semen from jawless vertebrates to humans. Milt pheromones may also have management implications for sea lamprey populations.

INTRODUCTION

Semen is fundamental for sexual reproduction. Ejaculated semen contains sperm cells that are essential to fertilize eggs. The ejaculate confers reproductive advantages to males because the seminal plasma, the fluid compartment of semen, contains a myriad of molecules that alter the sexual attractiveness [1], physiology [2, 3], and sexual behavior of post-copulatory females [4]. For some animals with internal fertilization, ejaculate contains anti-aphrodisiac molecules that deter or inhibit other males from courting with copulated females to reduce sperm competition [1, 5]. Seminal molecules may also cause the females to cease mating and start laying eggs without further mating [6]. Many of these seminal molecules have been shown to be female hormones, or mimics of hormones, that regulate the reproductive physiology and behaviors of females [6]. Males gain reproductive advantages by investing in seminal molecules that suppress subsequent mating in already mated females [7].

In addition to the well-known anti-aphrodisiac function of seminal plasma in some species with internal fertilization, seminal plasma appears to be an aphrodisiac in some species with external fertilization in which seminal compounds stimulate mating behaviors. The milt (fish semen) of Pacific herring (*Clupea pallasii*) induces a series of reproductive behaviors in adults with elevated levels of steroid hormones despite no physical interaction occurring between the sexes when spawning [8]. In addition, female bitterling (*Rhodeus ocellatus*) increase egg deposition when exposed to milt [9]. The milt of these fishes likely contains pheromones that trigger the documented spawning behaviors. Evidence for this type of seminal pheromone remains limited to these 2 species. However, no specific molecules from semen have been identified with such a function, hampering a molecular understanding of how seminal plasma mediates

reproductive behaviors.

We hypothesize that male sea lamprey, a basal vertebrate that spawns with multiple mates in a lek-like system, release a milt-derived pheromone. During their spawning season, sexually mature male lampreys that express milt (spermiating males) congregate on riverine gravel patches. Each spermiating male builds a nest and releases a sex pheromone from its gills that attracts sexually mature female (ovulatory) sea lampreys [10, 11]. In the spawning lek, each male defends a nest, while females move from nest to nest to spawn intermittently for approximately 1 week before mature adults die [11, 12]. During that period, the gill-released sex pheromone alone is insufficient to attract and retain the females on the nest, but spawning pairs have been observed to remain together for an extended duration [11]. This indicates that additional factors contribute to the maintenance of spawning aggregations. Because males typically release milt frequently for a week, seminal molecules released along with sperm would be a reliable, localized signal for the presence of actively spawning males in the vicinity, likely within a mating aggregation.

In this study, we discovered that spermine in sea lamprey milt acts as a specific semen-derived sex pheromone that promotes mating behaviors. This polyamine, initially discovered as crystals in human semen by Antonie van Leeuwenhoek in 1678 [13], evokes olfactory responses in teleost fish [14, 15] and possibly humans [16]. We reasoned that emitted spermine reveals sperm availability and thus can serve as a signal that benefits males seeking multiple mating partners. Our data indicate that sea lamprey seminal plasma contains high levels of spermine that stimulates the lamprey olfactory system and attracts ovulatory females at subpicomolar concentrations. We found that spermine activates a specific trace amine-associated receptor (TAAR)-like receptor (TAAR348), whereas an antagonist to this receptor inhibits olfactory and female behavioral responses to spermine. We conclude that spermine is a male pheromone and postulate that

TAAR348 plays a role in mediating those responses to spermine.

RESULTS

Spermine was present in seminal plasma of sea lampreys

Previous studies found that spermine (see structure in the inset of Figure 1-1A) is more abundant in semen than any other tissue or fluid [17, 18]. To measure emitted spermine from adult sea lampreys, we optimized an ultrahigh performance liquid chromatography-tandem mass spectrometry (UHPLC–MS/MS) assay and found that sea lamprey milt contained 172 ± 21 ng g^{-1} of spermine (mean ± SEM, n = 6; Figure 1-1A). When milt was fractionated into the 2 components—seminal plasma and sperm—around 70% of the spermine was detected in the seminal plasma (Figure 1-1B). In comparison, spermine was not detected in the mixture of expressed ovarian fluid and eggs from ovulatory females (Figure 1-1A). Spermine was also not detected in appreciable quantities in water conditioned with either ovulatory females or spermiating males, indicating it is not likely released from gills, as is known to be the case for other lamprey sex pheromones (Table1-1; limit of quantification of spermine from water samples: 0.02 ng mL^{-1}) [11, 19]. Although spermine is a ubiquitous polyamine with wide-ranging cellular functions [13, 17, 18], our results indicate that milt—in particular the seminal plasma—is the main source of waterborne spermine from sexually mature male sea lampreys.

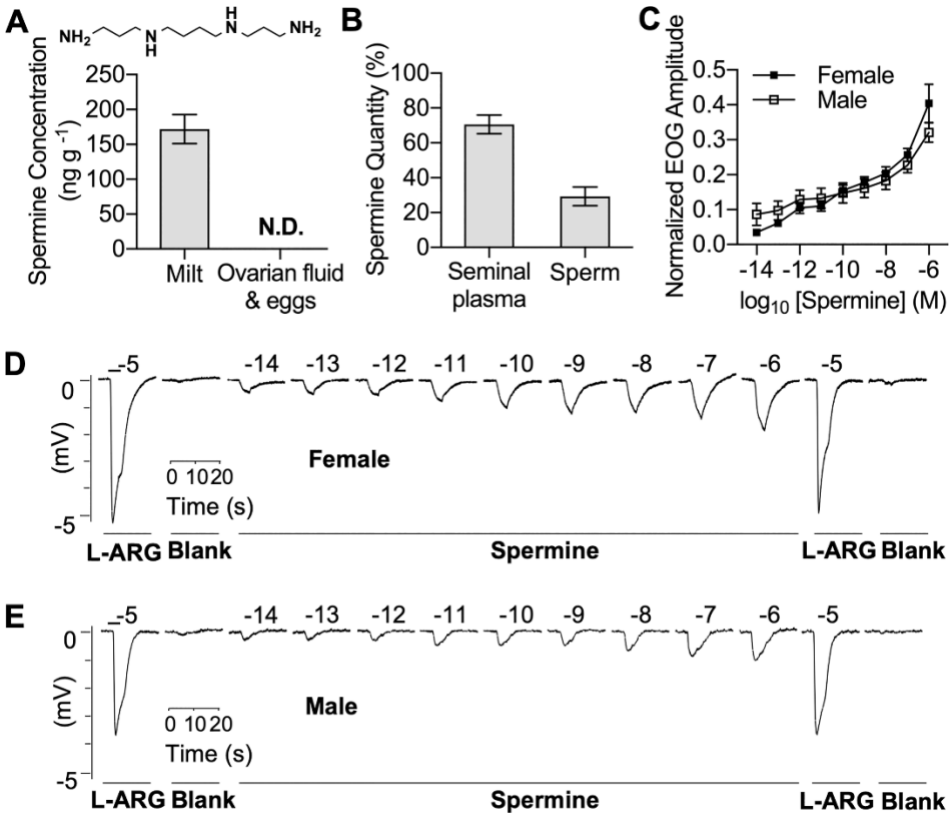

Figure 1-1. The seminal content and olfactory potency of spermine

(A) The concentration of spermine in sea lamprey milt and ovarian fluid with eggs (mean ± SEM, n = 6), measured with UHPLC–MS/MS. (Inset) Structure of spermine. (B) Percentage of spermine by weight in the milt components, seminal plasma and sperm, determined with UHPLC–MS/MS (mean ± SEM, n = 6). (C) Semi-logarithmic plot of normalized EOG amplitude (mean ± SEM) elicited by spermine (10^{-15} M to 10^{-6} M) in pre-ovulatory female (n = 10) and pre-spermiating male (n = 11) sea lampreys. The EOG response to spermine at each concentration was blank-subtracted and normalized to the response of 10^{-5} M L-ARG (standard) for each fish. (D) Representative EOG traces of pre-ovulatory female olfactory epithelia exposed to spermine at concentrations between 10^{-15} and 10^{-6} M. The number above each trace is the logarithmic value of the molar concentration of each stimulant. The bar above the L-ARG trace on the left represents the duration of odorant treatment. (E) EOG traces of pre-spermiating male olfactory epithelia exposed to spermine. Blank, vehicle solution; EOG, electro-olfactogram; L-ARG, L-arginine; N.D., not detectable; UHPLC–MS/MS, ultrahigh performance liquid chromatography-tandem mass spectrometry.

Sample ID	Concentration (ng mL^{-1})
Spermiating Male-1	N.D.
Spermiating Male-2	N.D.
Spermiating Male-3	0.12†
Spermiating Male-4	N.D.
Spermiating Male-5	N.D.
Spermiating Male-6	N.D.
Spermiating Male-7	N.D.
Spermiating Male-8	N.D.
Spermiating Male-9	N.D.
Ovulatory Female-1	N.D.
Ovulatory Female-2	N.D.
Ovulatory Female-3	N.D.
Ovulatory Female-4	N.D.
Ovulatory Female-5	N.D.
Ovulatory Female-6	N.D.
Ovulatory Female-7	N.D.
Ovulatory Female-8	N.D.
Ovulatory Female-9	N.D.
Ovulatory Female-10	N.D.

Table 1-1. The concentration of spermine in water conditioned with spermiating male and ovulatory female sea lampreys determined with UHPLC–MS/MS

The limit of spermine quantification with the UHPLC−MS/MS was 1.0 ng mL^{-1}. The water samples were concentrated 50 times prior to subjecting them to the UHPLC−MS/MS, so the limit of spermine quantification of the water samples was 0.02 ng mL^{-1}. †The handling of sea lampreys most likely resulted in the incidental release of expressible milt into the water sample. Adult lamprey skin is slippery. To transfer lampreys in and out of water sampling buckets, one needs to grip both head and tail regions of the lamprey, and accidental pressure on the abdomen is difficult to avoid. N.D., not detectable.

Spermine potently stimulated the olfactory system and attracted ovulatory females

Spermine evoked concentration-dependent responses in adult sea lamprey olfactory epithelia (Figure 1-1C, 1-1D, 1-1E), as recorded with electro-olfactogram (EOG). Spermine was highly stimulatory with a threshold of detection of 10^{-14} M for females ($p = 0.005$, paired t test, one tailed with a Bonferroni correction) and 10^{-13} M for males ($p = 0.005$, paired t test, one tailed with a Bonferroni correction; Figure S1-1). The threshold of detection was also estimated by fitting a linear regression on log-transformed EOG data using the formula $\log (N + 1.5) = a \log C + b$, where N is the normalized response, C is the concentration, and a and b are constants following a previously described approach by Hubbard and colleagues [20]. The threshold of detection is the value for x, where $y = 0.1761$ (i.e., log 1.5; $N = 0$). Using this approach, we calculated the spermine threshold of detection to be less than 10^{-14} M for both females and males (females: $10^{-14.9}$ M and males: $10^{-17.5}$ M). We decided to report the more conservative results from the paired t test approach as the spermine thresholds of detection.

To directly test the pheromone function of spermine, we examined the effect of spermine on adult sea lamprey behavior in a two-choice maze assay supplied with natural stream water (Figure S1-2). Ovulatory females preferred the channel activated with milt when applied to produce a final spermine concentration in the maze of 2.2×10^{-14} M, compared with the channel with the vehicle (Figure 1-2, $p = 0.008$). Likewise, ovulatory females were attracted to spermine at 10^{-14}, 2.2×10^{-14}, and 10^{-12} M compared with the vehicle (Figure 1-2, $p = 0.022$, $p = 0.003$, $p = 0.002$, respectively). Ovulatory females had similar behavioral preferences for milt and spermine at 10^{-14}, 2.2×10^{-14}, and 10^{-12} M ($p = 0.55$).

The behavioral effect of spermine was maturation specific and sex specific. When applied at 10^{-12} M, spermine was not attractive over the vehicle for pre-ovulatory females, spermiating males,

and pre-spermiating males (Figure 1-2, $p = 0.359$, $p = 1.00$, and $p = 0.600$, respectively). In contrast, milt itself attracted all adults, including pre-ovulatory females, spermiating males, and pre-spermiating males, over the vehicle (Figure 1-2, $p < 0.001$, $p = 0.023$, and $p = 0.004$, respectively). Our chemical, electrophysiological, and behavioral evidence demonstrates that spermine is a sex pheromone that specifically attracts ovulatory females.

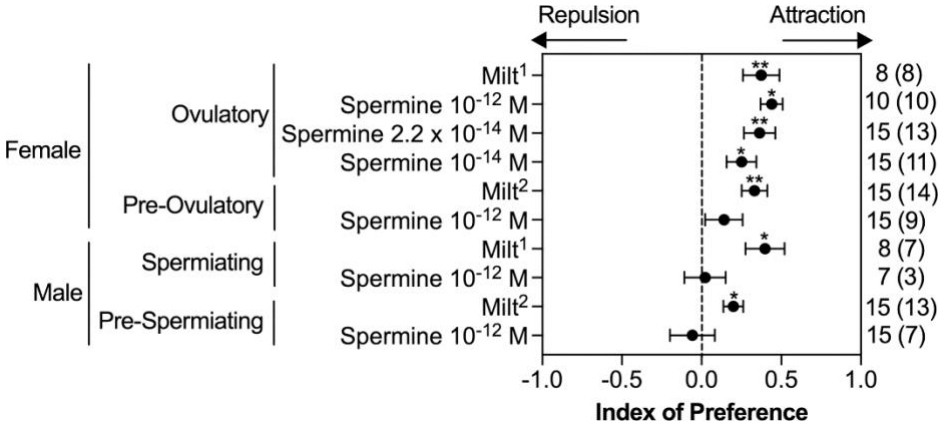

Figure 1-2. Adult sea lamprey behavioral responses to milt and spermine in a two-choice maze

The index of preference (mean ± SEM) was calculated as the value of [Ae ÷ (Ae + Be)–Ac ÷ (Ac + Bc)], where Bc is the cumulative amount of time spent in the control channel before odorant application, Be is the cumulative amount of time spent in the experimental channel before odorant application, Ac is the cumulative amount of time spent in the control channel after odorant application, and Ae is the cumulative amount of time spent in the experimental channel after odorant application in a two-choice maze (Figure S1-2; see Materials and methods). A positive index value indicates attraction, and a negative index value indicates repulsion. Significance was evaluated using a Wilcoxon signed-rank test. *$p < 0.05$. **$p < 0.01$. The number in the parentheses indicates the number of test subjects spending more time in the experimental channel out of the total sample size. Milt was applied to produce a final spermine concentration of (1) 2.2×10^{-14} M or (2) 3.8×10^{-14} M in the maze.

Spermine activated a single TAAR-like receptor expressed in HEK293T cells

Next, we sought to characterize the olfactory chemoreceptor(s) that detects spermine. We focused our search on TAARs, a family of receptors known to mediate olfactory responses to mono- and di-amines [21, 22] and to modify specific behaviors in vertebrates [21, 23]. The sea lamprey genome contains genes encoding 26 TAAR-like receptors [24]. We expressed these receptors in human embryonic kidney 293T (HEK293T) cells, a modified HEK293 cell line that expresses the simian virus 40 (SV40) large T antigen that efficiently amplifies the transcription vector with the receptor gene inserts, as described by Zhuang and colleagues [25] and measured the responses to spermine. This heterologous expression system has been used to express various G-protein-coupled receptors (GPCRs), including chemoreceptors from a variety of species. Of the 26 TAAR-like receptors, 21 appropriately targeted to the cell membrane, and of these, only TAAR-like 348 (TAAR348, hereafter) showed robust responses to 10 μM spermine (Figure 1-3A). Spermine did not activate any of the 22 sea lamprey odorant receptors (ORs) or 3 sea lamprey vomeronasal type 1 receptors (V1Rs) expressed in HEK293T cells (Figure S1-3).

Spermine stimulated cyclic-adenosine monophosphate (cAMP) production in HEK293T cells expressing TAAR348 in a concentration-dependent manner, but not in mock-transfected cells or cells with other TAARs (Figure 1-3B and 1-3C). TAAR348 gave robust responses to spermine with a half-maximal response occurring at 34 ± 1 μM (mean ± SEM; half-maximal effective concentration [EC_{50}]). TAAR348 also responded to 4 other amine variants (Figure S1-4A); however, they were at least 30-fold less potent and did not produce maximal responses at the highest concentration tested (30 μM; Figure S1-4B).

In situ hybridization results showed that *taar348* transcripts were located in a sparse population of olfactory sensory neurons (OSNs) in adult sea lampreys (Figure 1-3D and Figure

S1-5). The *taar348* probe hybridized to mRNA in a small subset of OSNs in the lamellae in middle sections along the rostral-caudal axis of the main olfactory epithelium but were not contained to certain olfactory epithelial zones as positive staining was sparsely distributed along the dorsoventral and lateral axes. Labeled intact neurons showed a tall morphology [26], homologous to teleost ciliated OSNs [27], with the cell bodies situated deeper in the olfactory epithelium and long dendrites projecting towards the epithelial surface. In comparison, no labeling was observed either in intermediate OSNs, homologous to teleost microvillous OSNs, which have a characteristic plump cell body and an intermediate soma position, or in short OSNs, homologous to teleost crypt OSNs, which have a rounded, egg-shape and are situated in the most apical layer of the epithelium [26, 27]. These data demonstrate that TAAR348 located in the olfactory epithelium is a cognate receptor of spermine with a high level of specificity.

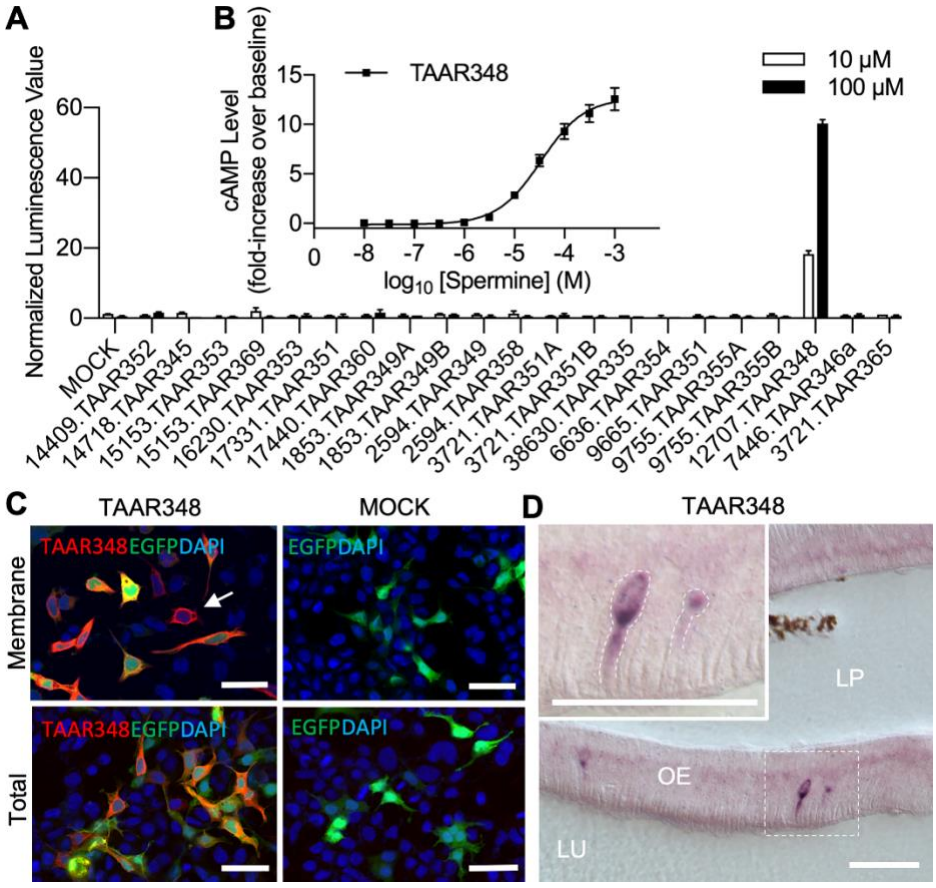

Figure 1-3. Spermine activated sea lamprey TAAR348

(A) HEK293T cells were incubated with TAAR plasmids or mock (empty vector) along with a CRE-luciferase reporter vector for 48 hours and subsequently stimulated with 10 or 100 μM spermine for 4 hours. Luciferase activity was indicated by luminescence value and was normalized to the response from the control stimuli DMSO (mean ± SEM, n = 2). (B) As an inset to (A), (B) shows spermine-induced cAMP production in HEK293T cells expressing TAAR348. The cAMP levels were measured with a TR-FRET assay and normalized to the cAMP level in buffer-treated cells (mean ± SEM, n = 5). Fold increase over basal level was calculated as [(measured cAMP − basal cAMP) ÷ basal cAMP] − 1. (C) TAAR348 targeted to HEK293T cell membrane as shown by the immunostained Rho-tag antibody (red) for total (bottom panel, with permeation using Triton X-100) or membrane-bound (top panel, without permeation) expression. Receptors located on the cell surface appeared as red rings around the nucleus (denoted with arrow). The nucleus was counterstained with DAPI (blue). EGFP was used as the negative control to evaluate transfection efficiency (green). Scale bar: 50 μm. (D) Representative olfactory receptor neurons expressing *taar348* (purple), labeled with a DIG-labeled antisense RNA probe in a cross-sectional view of the main olfactory epithelium of an adult female sea lamprey. The section was counterstained with Nuclear Fast Red. Scale bar: 50 μm. LP, lamina propria; LU, lumen; OE, olfactory epithelium.

A specific antagonist of TAAR348 reduced olfactory and nullified behavioral responses to spermine

Because genetic editing methods are not feasible in adult sea lamprey [28], we utilized pharmacologic tools to examine the role of TAAR348 in mediating the observed olfactory and behavioral responses to spermine in sea lampreys. We screened 22 structural analogs of spermine (Table 1-2) as potential antagonists of the TAAR348-mediated cAMP responses to spermine (Figure S1-6A). We found that cyclen (1,4,7,10-tetraazacyclododecane; see structure in the inset of Figure 1-4B) blocked the spermine-induced cAMP-stimulating activity. It inhibited spermine-induced cAMP production in HEK293T cells with TAAR348 in a concentration-dependent manner with a half-maximal inhibitory concentration (IC_{50}) in the nanomolar range, 0.6 ± 0.1 μM (Figure 1-4A). Cyclen appears to be a pure antagonist because it did not induce cAMP production when added alone (Figure 1-4B). To assess the specificity of cyclen as an antagonist of TAAR348, we tested cyclen on HEK293T cells expressing another sea lamprey TAAR-like receptor (TAAR346a), which we found responded to cadaverine (Figure 1-4C). TAAR346a and TAAR348 shared 47% identity at the amino acid level (Figure S1-7); however, cyclen treatment did not inhibit cAMP production induced by cadaverine in TAAR346a-expressing HEK293T cells (Figure 1-4D). The incomplete maximal inhibition (approximately 70% in Figure 1-4A) is consistent with an action as a negative allosteric modulator that may contribute to the specificity of its actions. Our data indicate that cyclen is a potent and selective antagonist for TAAR348.

Cyclen treatment also reduced olfactory responses to spermine in adult sea lampreys. The olfactory epithelium was exposed to cyclen for 5 minutes, and then the olfactory responses to cyclen mixed with various other stimuli—including spermine, L-arginine [29], 3-keto petromyzonol sulfate (3kPZS), which is a male sea lamprey sex pheromone released through the

gills [19], and spermidine, which is the immediate precursor of spermine biosynthesis [13]—were recorded. Treating the olfactory epithelium with cyclen reduced the response to spermine (p = 0.005) but not to other odorants ($p > 0.10$; Figure 1-5A).

Likewise, cyclen nullified attraction of ovulatory females to spermine. When both maze channels were perfused with cyclen (10^{-12} M), spermine at 10^{-12} M did not induce a preference in ovulatory females over the vehicle (Figure 1-5B, $p = 0.33$). As expected, cyclen did not alter the behavioral response of ovulatory females to the gill-released pheromone 3kPZS. 3kPZS attracted ovulatory females in the absence or presence of cyclen (Figure 1-5B, $p = 0.014$ and $p < 0.001$, respectively). Furthermore, inhibition of the behavioral response to spermine by cyclen was reversible. When cyclen application ceased, ovulatory females were attracted to spermine (Figure 1-5B, $p = 0.002$). The modification of the electrophysiological and behavioral responses to spermine in lampreys exposed to cyclen is consistent with the cyclen-mediated inhibition of the cAMP responses to spermine in HEK293T cells expressing TAAR348, the only receptor of the 46 tested that responds to spermine.

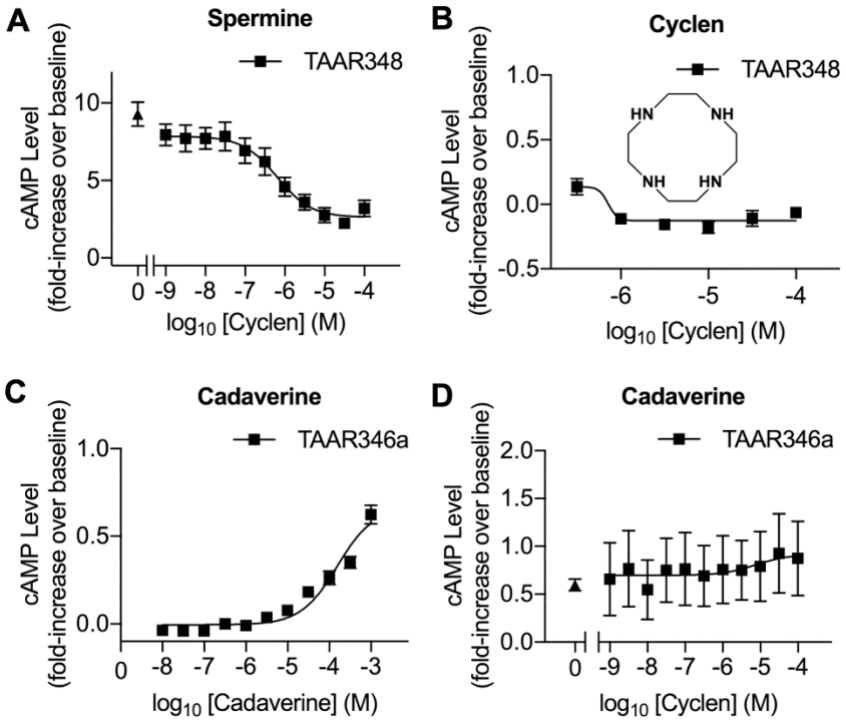

Figure 1-4. Cyclen antagonized spermine-induced cAMP responses to receptor TAAR348
(A) Cyclen treatment inhibited cAMP production induced by 0.1 mM spermine in TAAR348-expressing HEK293T cells as measured with a TR-FRET assay and normalized to the cAMP level in buffer-treated cells (mean ± SEM, n = 5). The filled triangle represents cAMP production induced by 0.1 mM spermine in the cells without exposure to cyclen. Fold increase over basal level was calculated as [(measured cAMP − basal cAMP) ÷ basal cAMP] − 1. (B) Cyclen did not induce cAMP production in HEK293T with TAAR348 (mean ± SEM; reads from triplicate wells). (Inset) Structure of cyclen (1,4,7,10-tetraazacyclododecane). (C) Cadaverine induced cAMP production in a concentration-dependent manner in HEK293T cells expressing another sea lamprey TAAR-like gene—TAAR346a (mean ± SEM, n = 5). (D) Cyclen treatment did not inhibit cAMP production induced by 1 mM of cadaverine in HEK293T cells expressing TAAR346a. The filled triangle represents the cAMP production induced by 1 mM of cadaverine in the cells without exposure to cyclen (mean ± SEM, n = 5).

Analog ID	CAS* number	Common name
SP1	109-76-2	1,3-Diaminopropane
SP2	110-60-1	1,4-Diaminobutane
SP3	462-94-2	1,5-Diaminopentane
SP4	646-19-5	1,7-Diaminoheptane
SP5	373-44-4	1,8-Diaminooctane
SP6	646-25-3	1,10-Diaminodecane
SP7	124-09-4	Hexamethylenediamine
SP8	4605-14-5	N,N′-Bis(3-aminopropyl)-1,3-propanediamine
SP9	4741-99-5	N,N′-Bis(2-aminoethyl)-1,3-propanediamine
SP10	10563-26-5	1,2-Bis(3-aminopropylamino)ethane
SP11	7209-38-3	1,4-Bis(3-aminopropyl)piperazine
SP12	295-37-4	1,4,8,11-Tetraazacyclotetradecane
SP13	15439-16-4	1,4,8,12-Tetraazacyclopentadecane
SP14	113812-15-0	N1,N12-Diethylspermine tetrahydrochloride
SP15	77928-70-2	N1-Acetylspermine trihydrochloride
SP16	177213-61-5	N4,N9-di-Boc-spermine
SP17	112-24-3	Triethylenetetramine
SP18	112-57-2	Tetraethylenepentamine
SP19	1310544-60-5	N,N'-Bis(2-pyridylmethyl)-1,2-ethylenediamine tetrahydrochloride
SP20	294-90-6	Cyclen (1,4,7,10-Tetraazacyclododecane)
SP21	122306-11-0	Nap-spermine (1-Naphthylacetyl spermine)
SP22	295-14-7	1,4,7,10-Tetraazacyclotridecane

Table 1-2. Spermine structural analogs screened as TAAR348 spermine receptor antagonists and agonists

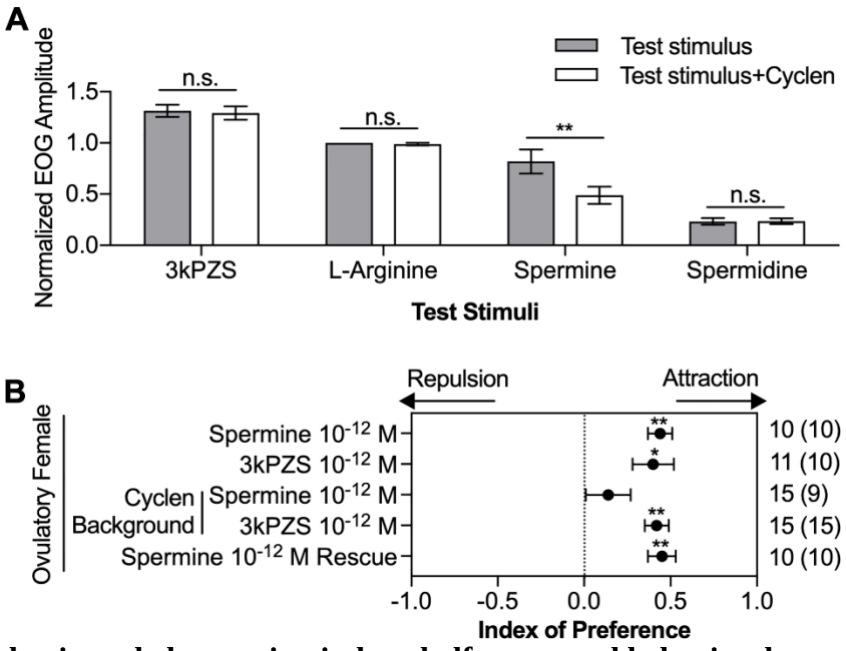

Figure 1-5. Cyclen impeded spermine-induced olfactory and behavioral responses
(A) Cyclen treatment (10^{-5} M) reduced the EOG response magnitude to spermine (10^{-5} M) but not to 3kPZS (10^{-7} M), spermidine (10^{-5} M), or L-arginine (10^{-5} M). EOG responses were blank-subtracted and normalized to the amplitude of the responses to 10^{-5} M L-arginine (mean ± SEM, n = 5). The difference in responses for each stimulus before (gray) and during (white) exposure of the naris to cyclen was evaluated with a paired *t* test. (B) Ovulatory female sea lamprey behavioral responses to spermine and 3kPZS (positive control) in the absence and presence of 10^{-12} M cyclen (cyclen background) in a two-choice maze assay (Figure S1-2). The effect of cyclen was reversible because the attraction to spermine was rescued when cyclen application ceased. For the definition of the index of preference, see Materials and methods. A positive index value indicates attraction, and a negative index value indicates repulsion. Significance was evaluated using a Wilcoxon signed-rank test. The number in the parentheses indicates the number of test subjects spending more time in the experimental channel out of the total sample size. *$p < 0.05$, **$p < 0.01$. n.s., not significant.

A spermine receptor agonist induced olfactory and behavioral responses comparable to those induced by spermine

In our final step to characterize a possible role of TAAR348 in mediating responses to spermine, we reasoned that another TAAR348 agonist, if found, should replicate the effects of spermine at the receptor, olfactory epithelia, and behavioral levels. From 22 structural analogs tested (Table 1-2), we found that 1-naphthylacetyl spermine (nap-spermine; see structure in the inset of Figure 1-6A) was an agonist of TAAR348 (Figure S1-6B). Nap-spermine induced robust cAMP production in cells expressing TAAR348, with an EC_{50} of 5 ± 1 μM, comparable to that of spermine (Figure 1-6A). As expected, nap-spermine induced EOG responses of magnitudes comparable to those induced by spermine (Figure 1-6B). Moreover, cyclen inhibited the nap-spermine-induced cAMP production with an IC_{50} of 0.5 ± 0.3 μM (Figure 1-6C), remarkably similar to the IC_{50} for spermine-induced activity. As was the case for spermine, prolonged exposure of the olfactory epithelium to cyclen reduced the olfactory response magnitude to nap-spermine (Figure 1-6D, $p = 0.01$). Consistent with the behavioral results of spermine, nap-spermine attracted ovulatory females when compared with the vehicle ($p = 0.008$) but did not attract spermiating males ($p = 0.38$; Figure 1-6E). In summary, cyclen consistently nullified the receptor, olfactory, and behavioral responses induced by spermine, whereas nap-spermine consistently induced responses that replicated those induced by spermine. These results, coupled with the lack of spermine-induced responses for 45 other sea lamprey olfactory chemoreceptors that we have tested, is consistent with a specific role for TAAR348 in mediating the pheromone function of spermine.

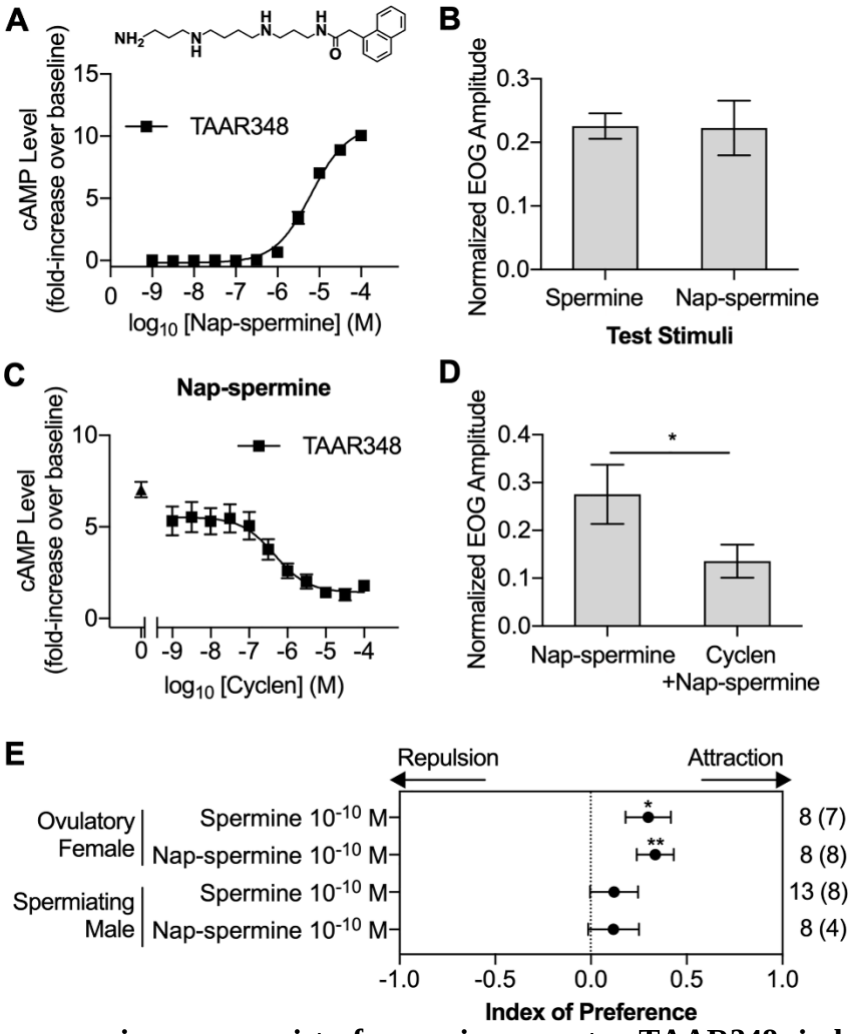

Figure 1-6. Nap-spermine, an agonist of spermine receptor TAAR348, induced responses virtually identical to those induced by spermine

(A) Nap-spermine induced cAMP production in a concentration-dependent manner in TAAR348-expressing HEK293T cells (mean ± SEM, n = 5). The cAMP assay was done as in Figure 1-3B. (Inset) Structure of nap-spermine. (B) EOG responses to 10^{-7} M spermine and 10^{-7} M nap-spermine (mean ± SEM, n = 12 and n = 6, respectively). Normalized EOG responses were blank-subtracted and normalized to the amplitude of the responses to 10^{-5} M L-arginine. (C) Cyclen inhibited cAMP production induced by 10^{-5} M nap-spermine in HEK293T cells with TAAR348. The filled triangle represents the cAMP production induced by TAAR348-expressing HEK293T cells exposed to only 10^{-5} M nap-spermine (mean ± SEM, n = 5). (D) Cyclen treatment (10^{-5} M) reduced the EOG response magnitude to nap-spermine (10^{-6} M). Cyclen exposure conditions are the same as in Figure 1-5A. EOG responses were blank-subtracted and normalized to the amplitude of the responses to 10^{-5} M L-arginine (mean ± SEM, n = 5). (E) Adult sea lamprey behavioral responses to spermine and nap-spermine in a two-choice maze (Figure S1-2). For definition of the index of preference, see Materials and methods. A positive index value indicates attraction, and a negative index value indicates repulsion. Significance was evaluated using a Wilcoxon signed-rank test. The number in the parentheses indicates the number of test subjects spending more time in the experimental channel out of the total sample size. *$p < 0.05$, **$p < 0.01$.

DISCUSSION

In this study, we show that sea lamprey milt is a source of the chemical cue spermine, which attracts ovulatory females, representing a chemically defined, semen-derived pheromone that stimulates reproductive behaviors. Pheromones are described as chemical signals that elicit stereotyped responses in certain conspecifics [6, 30]. Our chemical analyses linked the source of waterborne spermine to milt. Our biological assays demonstrated remarkable olfactory potency of spermine and a strong behavioral preference of ovulatory females for spermine. In addition, we showed that a sea lamprey TAAR-like receptor, TAAR348, responds to spermine when expressed in a heterologous system. Furthermore, a newly identified, selective TAAR348 antagonist reduced the olfactory response and completely nullified the female behavioral response to spermine. A distinct TAAR348 agonist replicated spermine effects, producing virtually identical responses at the receptor, olfactory epithelia, and whole-organism behavioral levels. These lines of evidence demonstrate that spermine is a pheromone that originates in the seminal plasma and attracts ready-to-mate female sea lampreys. Our data also support a model in which TAAR348 plays a key role in mediating the pheromone function of spermine.

The dichotomy in behavioral responses of adult female and male sea lampreys to spermine is consistent with our hypothesis that ovulatory females use spermine to identify males actively releasing sperm in a lek-like spawning aggregation. Spermine as a male signal is highly specific in its effects on individuals of the same species, attracting only ovulatory females and no other adults. On a typical nest, a male and one to several females often stay together and spawn many times [11]. Therefore, a signal such as spermine, released through the act of spawning, may contribute to the maintenance of the temporary spawning groups and attract additional female

mates. Although spermine elicits distinct sex-specific behavioral responses, both male and female sea lampreys detect spermine at the olfactory level with comparable potencies. This phenomenon is consistent with those responses observed for sex pheromones in sea lamprey [19, 31], goldfish [32, 33], tilapia [34, 35], and some insects [36].

In contrast to the highly specific pheromone effect of spermine on ovulatory females, milt itself attracted both males and females of various maturation stages. Although this has not been documented previously in other species, such a broad effect of milt on behaviors of conspecific adults is consistent with the promiscuous spawning system of sea lamprey. Other males and females, mature or immature, may detect milt odors to spy on spawning habitat and potential mates engaging in spawning activities. Therefore, we speculate that these additional odorants from semen may be chemical cues that do not directly benefit the releasing male. In fact, a previous study has shown that immature sea lampreys en route to spawning grounds track odorants of spermiating males [37]. Males may benefit from their attraction to milt because an aggregate of males in a lek-like system will collectively release more pheromone and attract more females than any one male can alone. The milt odorant(s) that attracts males and pre-ovulatory females remains to be identified. Future studies—particularly in natural spawning streams—on these aspects of milt function may further explain the fitness benefit of the incredible chemical complexity known to exist in seminal plasma [2, 7].

The remarkable olfactory potency of spermine is consistent with the effects of other sea lamprey pheromones and is likely a critical factor that enables this compound to function as a pheromone. Sea lampreys spawn in rapids with water velocities up to 1.5 m s^{-1} [11], where emitted milt containing spermine is likely quickly diluted, forming a steep spermine concentration gradient immediately downstream of a nest. Adult sea lampreys appear to be well adapted to detect and

respond to spermine at a wide range of concentrations. Sea lamprey have the ability to smell spermine from 10^{-14} or 10^{-13} M to 10^{-6} M, whereas the ovulatory females showed preference to spermine from 10^{-14} to 10^{-10} M. The behavioral attraction to a wide range of concentrations is consistent with those demonstrated for the lamprey mating pheromone [10]. The olfactory detection threshold of spermine is 1 to 2 orders of magnitude lower than those of either the lamprey mating or migratory pheromone [19, 38, 39]. Spermine is detected at much lower concentrations in vivo (i.e., EOG and behavioral responses) compared with in vitro (i.e., TAAR348 expressed in HEK293T), suggesting more optimized conditions for receptor expression and function in native sea lamprey neurons or possibly the presence of additional types of spermine receptors. Notably, spermine evokes olfactory responses in goldfish and zebrafish, 2 species that spawn in more stagnant water, but only at much higher concentrations of 10^{-8} M and 10^{-6} M, respectively [14, 15]. Whether spermine functions as an attractive pheromone in these 2 species has not been examined. Although spermine is known to be an odorant, its influence on behavior has not been examined in other animals.

The function of spermine as an odorant may be widespread because it is likely present in semen of many vertebrates. Pheromones are not necessarily species specific, and pheromone functions can be maintained through many mechanisms of species isolation [6]. If spermine is found to function as a pheromone in other species, it might exemplify convergent evolution of pheromone structures in distant species [40] constrained by common biochemical processes [6]. It is not surprising that spermine has been co-opted as a sex pheromone, which often evolve from compounds once originally intended for other functions linked to mate choice [41]. Spermine is abundant in semen [13, 17] and critical to male fertility [42]. It is possible that spermine is also critical to male fertility and sperm mobility in sea lamprey, as has been shown in mammals [16,

43]. An ovulatory female lamprey should be keenly attuned to such a signal that is a reliable indicator for sperm availability to maximize the fertilization rate and her fitness [44].

Our molecular and cellular data indicate that TAAR348 appears to be a narrowly tuned olfactory receptor. TAAR348 showed robust, concentration-dependent responses only to spermine and not to other biogenic amines. Spermine as a polyamine represents a new type of ligand for TAAR receptors, which have been shown to detect mono- and di-amines previously [45, 46]. Notably, the gene family encoding TAAR-like receptors first appeared in lampreys and evolved independently from the TAAR gene family of jawed vertebrates [47]. It would be interesting to determine whether spermine activates TAAR receptors of teleost fishes and humans [14, 15, 21, 22, 47].

Inhibition of multiple spermine functions by cyclen treatment shows that TAAR348 likely plays a role in sea lamprey responses to spermine. Cyclen specifically and potently inhibited TAAR348-mediated cAMP production in response to spermine but did not inhibit another polyamine-responsive receptor (TAAR346a). In the olfactory epithelia, cyclen treatment reduced the EOG responses to spermine but not to other odorants, including a known male lamprey pheromone 3kPZS and spermidine, a precursor to spermine. More importantly, cyclen treatment blocked the behavioral responses of ovulatory females to spermine, but not to 3kPZS, at equal concentrations (10^{-12} M). Furthermore, the spermine response was restored when cyclen treatment was removed. In addition, another TAAR348 agonist, nap-spermine, replicated the effects of spermine by inducing virtually identical responses at the receptor, olfactory epithelia, and behavioral levels. All this evidence lends strong support for the model that TAAR348 mediates olfactory detection of spermine. Our data, however, cannot exclude the possible involvement of additional receptors in the detection of spermine, because the cyclen treatment reduced but did not

completely eliminate EOG responses to spermine. Odorant perceptions are often encoded by the combinatorial activation of multiple receptors, particularly with TAARs [48]. In the future, the role of TAAR348 should be further examined through gene knockout experiments, when such techniques become feasible in adult lampreys [28].

Based on chemical, physiological, and behavioral evidence, we conclude that spermine is a male pheromone in sea lamprey. This discovery implicates a new strategy that male animals use to recruit mates through the release of chemical cues in ejaculates, as opposed to the commonly recognized strategy for males to deny further courtship to copulated females through seminal plasma compounds. Notably, the sea lamprey is an abundant and destructive invasive species in the Laurentian Great Lakes [49, 50] despite being imperiled in many countries throughout its native range [49]. Spermine, and our identification of cyclen as a spermine receptor antagonist, may provide approaches for either control or conservation of sea lamprey populations.

MATERIALS AND METHODS

Ethics statement

All procedures involving sea lampreys were approved by the Michigan State University Institutional Animal Use and Care Committee (03/14-054-00 and 02/17-031-00). Sea lamprey used for EOG recordings were anesthetized with exposure to 3-aminobenzoic acid ethyl ester (MS222; 100 mg/L; Sigma-Aldrich, St. Louis, MO) and immobilized with an intramuscular injection of gallamine triethiodide (3 mg/kg of body weight, in 0.9% saline). Gills were continuously irrigated with aerated water containing MS222 for the duration of recording, and sea lampreys were euthanized with MS222 followed by decapitation.

Animals

Reagents in the Materials and methods were purchased from Sigma-Aldrich (St. Louis, MO) unless stated otherwise. Immature adult sea lampreys (pre-spermiating males and pre-ovulatory females) were captured in tributaries of the Laurentian Great Lakes by the United States Fish and Wildlife Service and Fisheries and Oceans Canada; were transported to the US Geological Survey Hammond Bay Biological Station, Millersburg, Michigan; and were held in 500 to 1,000 L aerated flow-through tanks maintained at 15 to 19°C. Pre-spermiating male (232.1 g ± 29.3, 487.8 mm ± 14.2; mean ± SEM) and pre-ovulatory female (266.3 g ± 21.2, 509.6 mm ± 13.4) sea lampreys used for EOG recordings were transported to the University Research Containment Facility at Michigan State University, East Lansing, Michigan, held in flow-through tanks (250 L) supplied with aerated, chilled well water maintained at 7 to 9°C, and were used in April and May 2016 to 2018. To produce sexually mature adults (spermiating male and ovulatory females) for spermine quantification and behavioral assays conducted in June and July 2016 to 2018, immature adults

were held in cages constructed of polyurethane mesh and plastic pipe (0.5 m^3) located in the lower Ocqueoc River, Millersburg, Michigan, to allow natural maturation. These animals were monitored daily for signs of sexual maturation [11].

Cell line

HEK293T cells were maintained at 37°C with 5% CO_2 and grown in Dulbecco's Modified Eagle Medium (DMEM; Hyclone; Logan, UT) supplemented with 10% fetal bovine serum (FBS; Gibco; Waltham, MA) without antibiotic.

Quantification of spermine

Ovulatory female and spermiating male sea lampreys were separated by sex and held for 14 hours in two 500-L tanks supplied with continuous flow-through, aerated Lake Huron water at 17.7°C before samples were collected for the quantification of spermine. Each lamprey was transferred to a 20-L bucket supplied with continuous flow-through, aerated Lake Huron water and acclimated for 1 hour. All water was drained from the bucket, and 3 L of deionized water with an air stone was added. After 1 hour, the lamprey was removed from the bucket, and a conditioned water sample was collected. The water samples were concentrated 50 times using a CentriVap Cold Trap with CentriVap Concentrator (Labconco; Kansas City, MO) and then stored at −20°C until further analysis. Milt (sperm with seminal plasma) and eggs with ovarian fluid were collected from spermiating males or ovulatory females, respectively, by applying gentle pressure to the abdomen, resulting in expression of gametes from the cloacal opening. A subset of the milt samples were centrifuged (10 minutes, 1,020*g* at 4°C) to separate the seminal plasma from the sperm. The seminal plasma (supernatant) was transferred to a new tube. The samples were stored at −80°C until further analysis.

To prepare the stock solutions of spermine (≥99%, 85590) and [$^2H_8$] -spermine (Sp-d_8, 95%,

705330), each compound was dissolved in water/methanol (7:3, v/v) at a concentration of 1 mg mL^{-1}. The stock solution of internal standard (IS hereafter; Sp-d_8) was further diluted with water/methanol (7:3, v/v) to 500 ng mL^{-1}; 10-µl IS was added to each sample before extraction as described by Magnes and colleagues [51] with modification. Briefly, each 1 mL sample spiked with IS was treated with trichloroacetic acid (TCA; 4%, 100 µL) [52], vortexed (5 minutes), and centrifuged (10 minutes, 10,000*g*), resulting in 500 µL supernatant that was mixed with 500 µL deionized water. Subsequently, sodium carbonate buffer (0.1 M [pH 9], 125 µL) and isobutyl chloroformate (25 µL) were added and incubated at 35°C for 15 minutes. The isobutyl chloroformate residue was cleaned [53] and reconstituted to 100 µL with the initial mobile phase. A Waters ACQUITY H-Class UHPLC system connected to a Waters Xevo TQ-S triple quadrupole mass spectrometer was used to detect spermine in the conditioned water and gamete samples (Waters Corp.; Milford, MA). The mobile phase consisted of water (containing 0.1% formic acid) as (A) and acetonitrile (containing 0.1% formic acid) as (B). A Waters BEH C18 column (2.1 × 50 mm, 1.7 µm particle size) coupled with an Acquity UHPLC column in-line filter kit (0.2 µm filter) was used. Samples were separated with a gradient program at a flow rate of 250 µL min^{-1} for 12 minutes at 35°C: 70% A for 1 minute, decreased to 0% A from 1 to 7 minutes, and then maintained at 0% A from 7.01 to 9.0 minutes, increased to 70% A from 9.0 to 9.01 minutes, and then maintained at 70% A to 12 minutes for column equilibrium. The sample injection volume was 10 µL. Spermine was detected by Multiple Reaction Monitoring (MRM) mode and processed using Masslynx 4.1 software (Waters Corp.; http://www.waters.com/waters/en_US/MassLynx-MS-Software/nav.htm?locale=en_US&cid=513662). The UHPLC–MS/MS parameters were optimized for the transition of the spermine analyte as follows: $[M + H]^+$ *m/z* 603.4, MRM *m/z* 603.4 > 154.9, cone voltage 49 V, collision energy 40 eV, and retention time 6.92 minutes; and for

the spermine-d_8 analyte as follows: $[M + H]^+$ *m/z* 611.4, MRM *m/z* 611.4 > 163.1, cone voltage 36 V, collision energy 40 eV, and retention time 6.92 minutes.

The UHPLC effluent was introduced into the mass spectrometer with electrospray ionization in the negative mode. The electrospray ionization mass spectrometry (ESI–MS/MS) parameters were set as follows: capillary voltage, 2.60 kV; extractor voltage, 5 V; source temperature, 150°C; desolvation temperature, 500°C; and desolvation gas flow, 800 L h^{-1} (N_2, 99.9% purity). Argon (99.9999% purity) was introduced as the collision gas into the collision cell at a flow rate of 0.15 mL min^{-1}. Data were collected in centroid mode with a scan range of 50 to 1,000 *m/z*. The dwell time established for each transition was 0.2 seconds, and the interscan delay was set at 20 ms. Data acquisition was carried out using Masslynx 4.1 software and processed using TargetLynx (Waters Corp.). The limit of spermine quantification with the UHPLC–MS/MS was 1.0 ng mL^{-1}. Because the water samples were concentrated 50 times, the limit of spermine quantification of the water samples was 0.02 ng mL^{-1}.

EOG recordings

EOG setup and recordings were conducted following established procedures by Li and colleagues [54] to determine whether the adult sea lamprey olfactory organ was sensitive to spermine. Sea lampreys were anesthetized with MS222 (100 mg L^{-1}), immobilized with an intramuscular injection of gallamine triethiodide (3 mg kg^{-1} of body weight, in 0.9% saline), and placed in a V-shaped plastic stand. Gills were continuously irrigated with aerated water containing 50 mg L^{-1} MS222. The olfactory lamellae were surgically exposed by removing the skin on the surface of the olfactory capsule. The differential EOG response to each test stimulus was recorded using borosilicate electrodes filled with 0.04% agar in 0.9% saline connected to solid state electrodes with Ag/AgCl pellets (model ESP-M15N; Warner Instruments; Hamden, CT) in 3M

KCl. The recording electrode was placed between 2 olfactory lamellae and adjusted to maximize the response to L-arginine standard while minimizing the response to the blank control (vehicle in charcoal-filtered water handled in the same way as stimulus solution but without the addition of spermine), and the reference electrode was placed on the external skin near the naris. Electrical signals were amplified by a NeuroLog system (model NL102; Digitimer, England, UK), filtered with a low-pass 60 Hz filter (model NL125; Digitimer), digitized by Digidata 1440A (Molecular Devices, San Jose, CA), and recorded on a PC running AxoScope 10.4 software (Molecular Devices;http://mdc.custhelp.com/app/answers/detail/a_id/18779/~/axon%E2%84%A2pclamp%E2%84%A2-10-electrophysiology-data-acquisition-%26-analysis-software-download).

For the concentration-response recordings, the olfactory epithelia of sea lampreys were exposed to 10^{-15} M to 10^{-6} M solutions of spermine. A 10^{-3} M stock solution of spermine in water/methanol (1:1, v:v) was prepared, stored at −20°C, and then serially diluted with filtered water to yield 10^{-15} M to 10^{-6} M solutions. A 10^{-2} M stock solution of L-arginine in deionized water was prepared, stored at 4°C, and diluted with filtered water to yield a 10^{-5} M solution. A 10^{-5} M L-arginine solution was introduced to the olfactory epithelium for 4 seconds, and the response was recorded to correct for variations in olfactory sensitivity among fish. The olfactory epithelium was flushed with filtered water for 2 minutes, and then the blank control was introduced and recorded. Next, the test stimulus starting at 10^{-15} M to 10^{-6} M was applied in $\log_{10}$ molar increments, recorded, and flushed. Blank control and 10^{-5} M L-arginine standard were measured repeatedly (approximately after every 3 concentrations of stimuli) throughout each recording session. The EOG response magnitudes were measured in mV. The normalized EOG response was calculated as normalized EOG amplitude = (Rt − Rb) ÷ (Ra − Rb), where Rt is the response magnitude to the test stimulus, Rb is the response magnitude to the blank, and Ra is the response

magnitude to 10^{-5} M L-arginine. The responses to 10^{-5} M L-arginine standard (mean ± SEM, male: 2.75 ± 0.08, female: 3.41 ± 0.08) and blank (male: 0.17 ± 0.01, female: 0.13 ± 0.01) were comparable to previous studies [54–56]. The threshold of detection was defined as the lowest concentration in which the test stimulus elicited a larger response than the blank (paired *t* test, one tailed with a Bonferroni correction for 4 comparisons, $\alpha = 0.0125$).

For the cyclen treatment to the olfactory epithelium experiments, the EOG responses to the test stimuli (spermine, L-arginine, 3kPZS [Bridge Organics Co., Vicksburg, MI]), spermidine, and nap-spermine) were first recorded in a similar manner as the concentration-response recordings. Then, the naris was continuously exposed to 10^{-5} M cyclen for 5 minutes. Next, the EOG responses to mixtures of each test stimulus with the adapting solution of 10^{-5} M cyclen were recorded. The naris was rinsed with charcoal-filtered water for 2 minutes, and then the responses to the test stimuli were recorded to ensure recovery of the olfactory system. The normalized EOG response of each test stimuli before and during cyclen treatment was evaluated with a two-tailed paired *t* test.

Two-choice maze behavioral assay

The behavioral preferences of the sea lampreys to the test stimuli were evaluated using a two-choice maze assay that was described in a previous study [54] (Figure S1-2). Briefly, a single lamprey was introduced to the acclimation cage at the downstream end of the maze for 5 minutes. The lamprey was released, and the cumulative amount of time the lamprey spent in each channel was recorded for 10 minutes (pretreatment period before odorant application). The test stimulus was introduced to a randomly chosen channel and vehicle (water when milt was test stimulus and methanol for other test stimuli) to the other channel at constant rates of 200 ± 5 mL min^{-1}. The test stimulus and vehicle were pumped into the maze for 5 minutes. The cumulative amount of time

the lamprey spent in each channel was recorded for 10 minutes while continuing to apply the test stimulus and vehicle (odorant application period). The maze was flushed with water for 10 minutes before the start of the next experiment to remove any remaining test stimulus. The time spent in the control (Bc) and experimental (Be) channel before odorant application and in the control (Ac) and experimental (Ae) channel after odorant application were used to calculate an index of preference for each trial as defined by index of preference = [Ae ÷ (Ae + Be)–Ac ÷ (Ac + Bc)] [54]. The index of preference was evaluated using a Wilcoxon signed-rank test ($\alpha = 0.05$) to determine whether the index of preference was significantly different from zero. Differences were considered significant at $p < 0.05$. A significant positive value of the index of preference indicated attraction. A significant negative value of the index of preference indicated repulsion. A nonsignificant value of the index of preference indicated neutral. The trial was discarded if the sea lamprey failed to enter the control and experimental channel for at least 10 seconds during the 10-minute period before the odorant was applied because this was an indication of strong side bias or inactivity.

To assess the influence of cyclen on behavioral responses of ovulatory females to spermine, a modified behavioral assay was followed. Cyclen (10^{-12} M) was applied to the experimental and control channel during the acclimation and pretreatment period. The cumulative amount of time the lamprey spent in each channel during the pretreatment period was recorded. Then, a mixture of either cyclen (10^{-12} M) and spermine (10^{-12} M, test stimulus) or cyclen (10^{-12} M) and 3kPZS (10^{-12} M, control; Bridge Organics) was introduced to a randomly chosen channel and a mixture of cyclen (10^{-12} M) and vehicle to the other channel for 5 minutes. Then, the cumulative amount of time the lamprey spent in each channel was recorded for 10 minutes while the treatments continued to be administered. An index of preference was calculated as described above. To

determine whether the influence of cyclen on the spermine behavioral response was reversible, cyclen (10^{-12} M) was applied to the experimental and control channel during the acclimation and pretreatment periods. Next, cyclen application stopped, and spermine application (10^{-12} M) started. Spermine was applied to the experimental channel and vehicle to the control channel for the treatment period. The cumulative amount of time the lamprey spent in each channel during the pretreatment and treatment period was recorded, and an index of preference was calculated.

High-throughput ligand screening of TAARs

The open reading frames of TAARs were mined from the sea lamprey genome assembly (Pmarinus_7.0) [24]. A total of 26 TAARs were annotated, cloned from genomic DNA, and introduced into Rho-pCMV modified from pCMV-Tag-2B (211172; Agilent Technologies, Santa Clara, CA) by introducing a Rho-tag (the first 21 amino acids of bovine rhodopsin) at the N terminal to replace the intrinsic flag-tag [25].

HEK293T cells were seeded at 5,500 cells per well on a 384-well plate and cotransfected with 5-μL DNA-transfection mixture that contained 5 ng of a TAAR plasmid, 5 ng pCI-mRTPs (provided by Dr. H. Matsunami, Duke University, Durham, NC), and 5 ng pEGFP-N1 (6085–1, Clontech, Mountain View, CA). The empty plasmid, pCI-mRTPs, and pEGFP-N1 were cotransfected as a negative control. The plate was incubated for 48 hours at 37°C with 5% CO_2, fixed with 3 μL 37% formaldehyde per cell for 15 minutes at room temperature (RT), washed with 50 μL PBS 3 times, and incubated with 25 μL blocking buffer (1× PBS) with 5% bovine serum albumin (BSA) for 1 hour at RT. Subsequently, 25 μL mouse monoclonal anti-rhodopsin antibody (1:500, MABN15, Millipore, Burlington, MA) was added to each well and incubated at 4°C overnight. The antibody solution was aspirated, washed with 50 μL PBS 3 times, and incubated with Alexa Fluor 594 goat anti-mouse IgG (1:500, A11005, Thermo Scientific, Waltham, MA) for

1 hour at RT. Nuclei were counterstained with DAPI (1:1,000, D1306, Thermo Scientific). Images were acquired at 200× magnification under Cytation 3 Cell Imaging Multi-Mode Reader (BioTek, Winooski, VT) with DAPI, green fluorescent protein (GFP), and Texas Red filters. Additional images of TAAR348 membrane and total expression patterns were sequentially acquired on a Nikon A1 laser scanning confocal microscope with DAPI, GFP, and Texas Red filters. Images were sequentially acquired in single XY-plane and merged. Results indicated that 21 TAARs targeted to the plasma membrane, which were used in subsequent screening experiments.

The initial high-throughput screening (HTS) was performed in 384-well plates as described by Zhuang and colleagues [25] with the following modifications. For the reverse transfection, 5 μL DNA-transfection mixture (20 ng CRE-Luciferase vector pGL4.29 [E8471; Promega, Madison, WI], 5 ng of a TAAR plasmid, 5 ng pCI-mRTPs, 5 ng pCI-$G_{\alpha olf}$ [provided by Dr. H. Matsunami]), and 5,500 HEK293T cells in 25 μL 0.5% FBS DMEM medium were added to each well. The plates were incubated for 48 hours at 37°C with 5% CO_2. Each stimulus solution (either 150 nL of 2 mM in DMSO for a final concentration of 10 μM or 150 nL of 20 mM in DMSO for a final concentration of 100 μM) was dispensed into a designated well using Biomek FXP liquid handling automation workstation (Beckman Coulter; Brea, CA). The negative control stimulus was 150 nL DMSO. Plates were incubated for 4 hours at 37°C with 5% CO_2. Luciferase activity was measured using Steady Glo Luciferase Assay System (E2520, Promega), and luminescence was read on a Synergy Neo multi-mode microplate reader (BioTek). Luciferase activity was normalized by DMSO-stimulated luminescence value with the following formula: (Luc induced by Ligand) ÷ (Luc induced by DMSO).

Assay for cAMP production

The cAMP production assay was performed in 384-well plates as described in LANCE Ultra cAMP Kit manual (TRF0263, PerkinElmer; Waltham, MA) to characterize the cAMP production induced in HEK293T cells expressing TAAR348. Briefly, HEK293T cells were seeded in a 100-mm dish with 3×10^6 cells in 10-mL complete culture medium (DMEM medium with 10% FBS and 1 × Antibiotic-Antimycotic; Gibco) and incubated for 24 hours at 37°C with 5% CO_2. Cells were then transfected with 5 μg pGL4.29, 1 μg pCI-mRTPs, 1 μg pCI- $G_{\alpha olf}$, and 1 μg TAAR plasmid and incubated at 37°C with 5% CO_2 for 24 hours. Transfected cells were detached with Versene (15040066, Thermo Scientific) and transferred to 384-well plates at 5 μL (2,000 cells) per well; 5 μL of the 2 × spermine serial dilutions were added to each well and incubated for 30 minutes at RT. Afterwards, 5 μL 4 × Eu-cAMP tracer working solution and 5 μL 4 × ULight-anti-cAMP working solution were added to each well and incubated for 1 hour at RT. Plates were read with the Synergy Neo multi-mode microplate reader for TR-FRET emissions at 620 nm (as internal reference) and 665 nm (as biological response). The ratio of 665/620 allows normalization for the well-to-well variability and interference due to assay components.

Screening of agonists and antagonists of TAAR348

Twenty-two spermine structural analogs (Table 1-2) were screened to identify another agonist of TAAR348 using a strategy similar to the initial HTS with the following modifications. Briefly, 3×10^6 HEK293T cells were seeded in 10 mL complete culture medium and incubated for 24 hours on day 1. On day 2, the cells were cotransfected with 5 μg pGL4.29, 1 μg pCI-mRTPs, 1 μg pCI-$G_{\alpha olf}$, and 1 μg TAAR plasmid and then incubated for 24 hours. On day 3, the transfected cells were harvested and then reseeded in 384-well plates at a density of 9,000 cells per well in 30 μL 0.5% FBS DMEM medium and incubated for 24 hours. On day 4, 150 nL of each analog solution

(2 mM in DMSO; Table 1-2), or 150 nL DMSO as a negative control, was dispensed into a designated well and subsequently incubated for 4 hours. Luciferase activity was measured as the indicator for receptor activity as described in the HTS.

To identify antagonists of the spermine-induced responses in HEK293T cells expressing TAAR348, the screening procedure followed that of the agonist screening from day 1 through day 3. On day 4, 150 nL of analog solution (2 mM in DMSO, Table 1-2), or 150 nL DMSO as a negative control, was dispensed into each well and incubated for 30 minutes at 37°C with 5% CO_2. Afterward, 5 µL 6×10^{-5} M spermine was added to each well and incubated for 4 hours at 37°C with 5% CO_2 before the luciferase activity as described in the HTS.

To examine the inhibition of cyclen on spermine-induced cAMP production in HEK293T cells expressing TAAR348, HEK293T cells were transfected with 5 µg pGL4.29, 1 µg pCI-mRTPs, 1 µg pCI- $G_{\alpha olf}$, and 1 µg TAAR348. TAAR348-expressing HEK293T cells were stimulated with successive additions of cyclen serial dilutions and 0.1 mM spermine. The cAMP production assay was performed as described for characterization of TAAR348. Subsequently, Eu-cAMP tracer and ULight-anti-cAMP were added, incubated for 1 hour at RT, and read for TR-FRET emissions at 620 nm (as internal reference) and 665 nm (as biological response). To examine the inhibition specificity of cyclen, the effect of cyclen on another sea lamprey TAAR (TAAR346a) induced cAMP production was assessed. The cAMP production assay was performed as described for the cyclen inhibition of spermine-induced responses with the following modifications: HEK293T cells were transfected with 5 µg pGL4.29, 1 µg pCI-mRTPs, 1 µg pCI- $G_{\alpha olf}$, and 1 µg TAAR346a. TAAR346a-expressing HEK293T cells were stimulated with successive additions of cyclen serial dilutions and 1 mM cadaverine (TAAR346a agonist; Sigma-Aldrich D22606). Subsequently, Eu-cAMP tracer and ULight-anti-cAMP were added, incubated, and read for TR-FRET emissions at

620 nm (as internal reference) and 665 nm (as biological response).

In situ hybridizations of *taar348*

Probes (approximately 350–400 bp) were designed based on the coding region of *taar348*. The amplified DNA fragments were cloned into a pGEM-T vector (A3610, Promega), and the sequences were verified. Each plasmid was linearized using restriction enzyme Nco (antisense probe) or Spe (sense probe) and used for synthesis of digoxigenin (DIG)-labeled RNA probes with DIG RNA labeling kit (SP6/T7; 11175025910, Roche; Basel, Switzerland). In situ hybridization was conducted following previously described methods by Chung-Davidson and colleagues [57]. Briefly, 20-μm frozen sections of olfactory epithelium were hybridized with RNA probes (3 ng μL^{-1}) overnight at 65°C in the hybridization solution (50% deionized formamide, 1× Denhart's solution, 5% dextran sulfate, 750 mM sodium chloride, 25 mM ethylenediaminetetraacetic acid, 25 mM piperazine-N, N′-bis-2-ethanesulfonic acid, 0.25 mg mL^{-1} fish sperm DNA, 0.25 mg mL^{-1} poly A acid, and 0.2% sodium dodecyl sulfate). After hybridization, sections were washed 3 times for 5 minutes each in 4 × saline-sodium citrate (SSC). Subsequently, sections were washed sequentially in 2 × SSC containing 0.3% Tween-20 and 0.2 × SSC containing 0.3% Tween-20 3 times each for 15 minutes each at 68°C. Sections were washed in 0.1 × SSC containing 0.3% Tween-20 for 15 minutes followed by 3 washes of 5 minutes each in 0.1 M PBS containing 0.3% Tween-20 at RT. The sections were then incubated with blocking solution (1 × PBS, 2 mg/mL BSA, 0.3% Tween-20, and 10% normal sheep serum) for 1 hour at RT, followed by incubation with alkaline phosphatase-conjugated sheep anti-DIG Fab fragments (1:1,000 diluted in blocking solution, Roche 11093274910) overnight at 4°C. Hybridization signals were detected by incubating the sections in nitro blue tetrazolium and 5-bromo-4-chloro-3-indolyl phosphate (NBT/BCIP, 34042, Thermo Scientific) for 2 hours at RT and then counterstained with Nuclear

Fast Red (H3403, Vector Laboratories; Burlingame, CA) for 5 minutes at RT. The differential interference contrast (DIC) images displayed in the main text were acquired with a C2 Nikon microscope equipped with a 20 × and 60 × oil objective. Sections in Figure S1-5 were observed and photographed on Zeiss Axioskop2 mot plus microscope equipped with a 40 × objective. Control experiments (sense probe) were conducted simultaneously with identical procedure and conditions.

Sequence alignment

The sea lamprey TAAR348 sequence (348 amino acid residues) was aligned with the sea lamprey TAAR346a sequence (346 amino acid residues) using CLUSTAL X 1.83 with default parameters. The transmembrane (TM) segments, extracellular loops (ECLs), and intracellular loops (ICLs) of TAAR348 and TAAR346a were predicted by TMpred program. The conserved residues of the aminergic ligand motif, TAAR fingerprint, and rhodopsin-type GPCRs were predicted based on previously described approaches [58, 59].

SUPPORTING INFORMATION

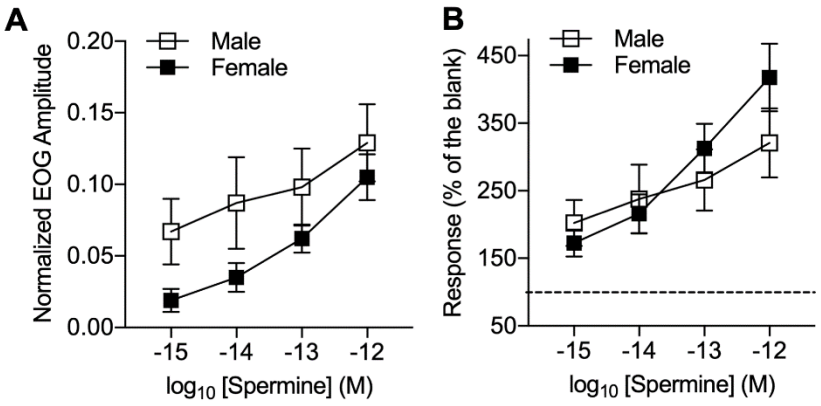

Figure S1-1. Expanded view of semi-logarithmic plot of EOG amplitude (mean ± SEM) elicited by spermine (10^{-15} M to 10^{-12} M) in pre-ovulatory female (n = 10) and pre-spermiating male (n = 11) sea lampreys

(A) Expanded view of Figure 1-1C. The EOG response to spermine at each concentration was blank-subtracted and normalized to the response of 10^{-5} M L-arginine (standard) for each fish. (B) The EOG response to spermine at each concentration expressed as a percentage of the response to blank (vehicle in charcoal-filtered water handled in the same way as stimulus solution but without the addition of spermine) for each fish. The dashed line represents 100% of the blank. Deviation above the dashed line indicates detection of spermine different than the blank.

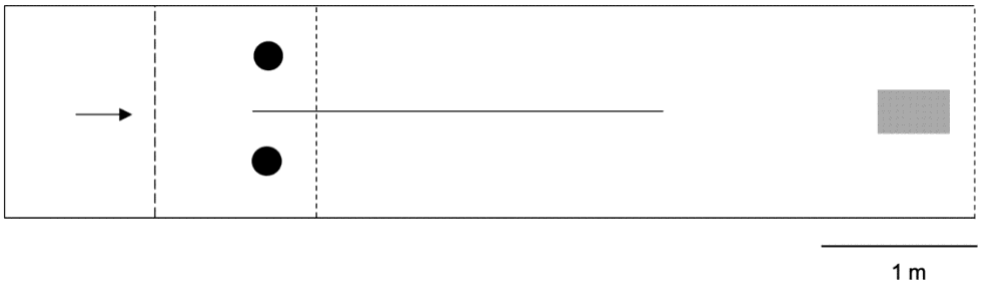

Figure S1-2. Two-choice maze used to evaluate behavioral responses of sea lamprey to test stimuli

The 2 black circles represent test stimuli administration points. The large dashed lines represent flow boards used to reduce water turbulence. The small dashed lines represent fine mesh used to restrict the movement of the sea lamprey. The gray rectangle represents the release cage. Arrow represents the direction of water flow (0.07 m s^{-1} ± 0.01). Scale bar: 1 m.

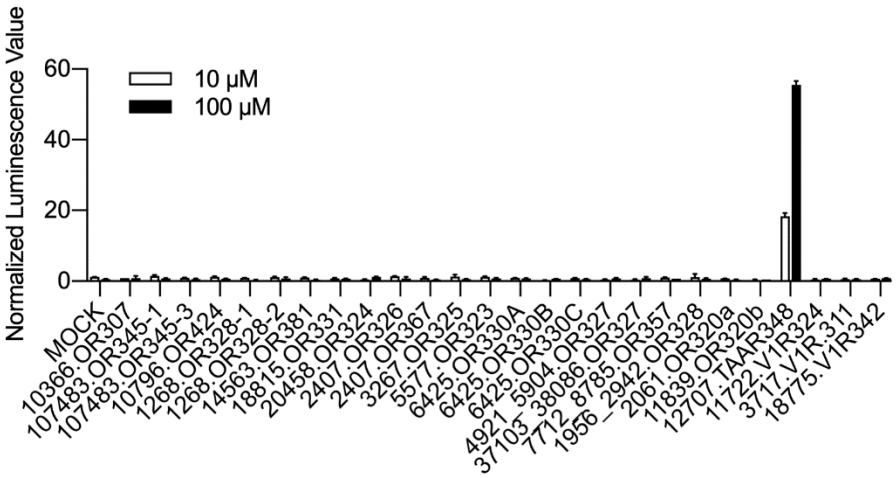

Figure S1-3. Spermine induced higher luciferase activity in TAAR348 compared with sea lamprey ORs or V1Rs

HEK293T cells were incubated with OR, TAAR, or V1R plasmids or mock (empty vector) along with a CRE-luciferase reporter vector for 48 hours and subsequently stimulated with 10 or 100 μM spermine for 4 hours. Luciferase activity was indicated by the luminescence value and was normalized to the responses from the control stimuli DMSO (mean ± SEM, n = 2).

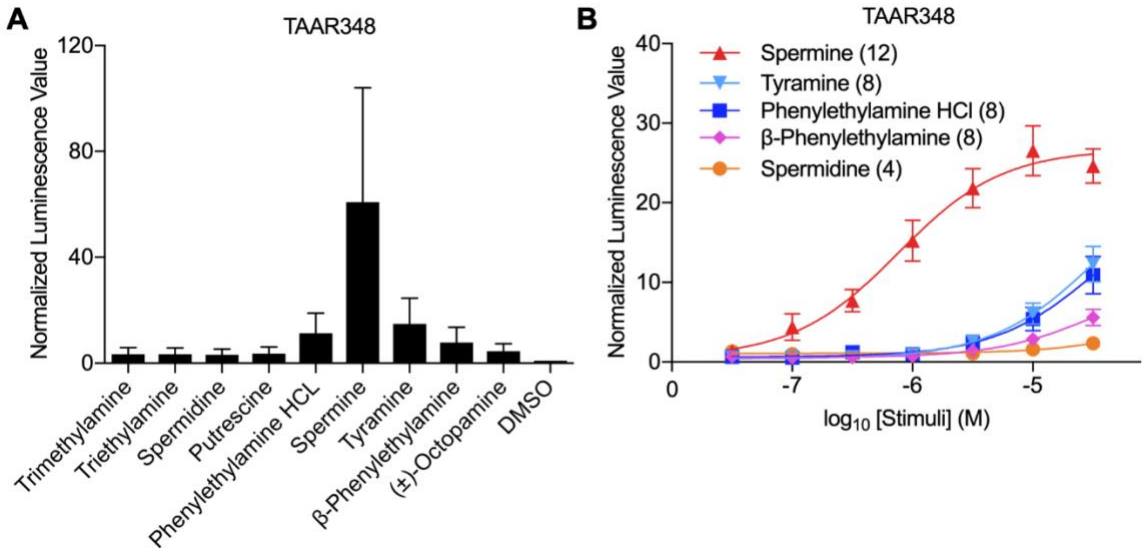

Figure S1-4. Spermine induced higher luciferase activity than other tested amines in TAAR348

(A) HEK293T cells were incubated with TAAR348 plasmid or vehicle (empty vector) along with a CRE-luciferase reporter vector for 48 hours and subsequently stimulated with 10 μM of an amine for 4 hours. Luciferase activity was indicated by luminescence value and was normalized to the responses to the control stimuli DMSO (mean ± SEM, n = 2). (B) Spermine induced dose-dependent activity in HEK293T cells expressing TAAR348. HEK293T cells were incubated with TAAR348 plasmid or vehicle (empty vector) along with a CRE-luciferase reporter vector for 48 hours, stimulated with increasing concentrations of the indicated amine, and assayed for luciferase activity. Luciferase activity was indicated by the luminescence value and was normalized to the responses from the control stimuli DMSO (mean ± SEM). The sample size is indicated by the number in the parentheses.

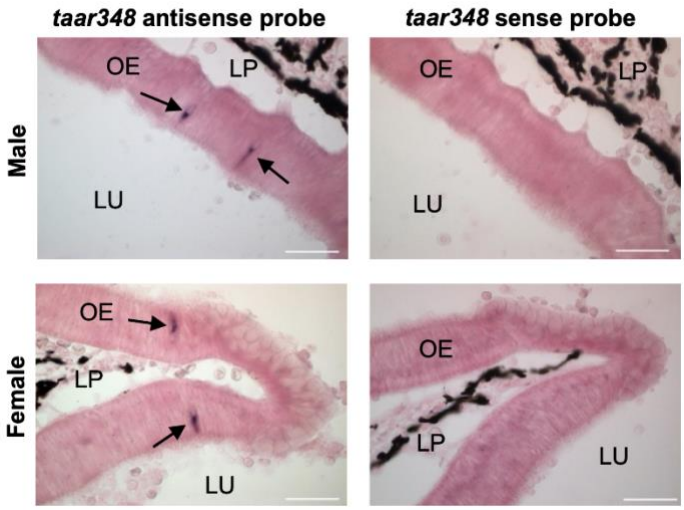

Figure S1-5. Representative olfactory receptor neurons with transcripts of sea lamprey *taar348*

taar348 mRNA positive cells are labeled with a DIG-labeled antisense RNA probe in the cross-sections of the main olfactory epithelium of adult male and female sea lampreys. These cells are denoted with purple stain (NBT/BCIP) and black arrows. Sections were counterstained with Nuclear Fast Red. Black melanophores in the lamina propria are characteristic of sea lamprey olfactory epithelia. Images were acquired with a Zeiss Axioskop2 mot plus microscope equipped with a 40 × Plan-Neuoflaur objective. Scale bar: 50 μm. LP, lamina propria; LU, lumen; OE, olfactory epithelium.

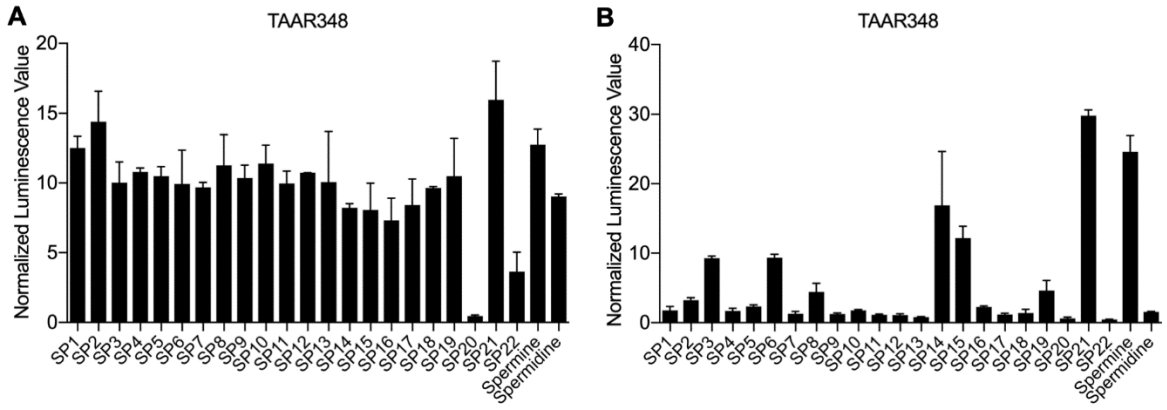

Figure S1-6. Cyclen (SP20) identified as an antagonist of spermine receptor TAAR348 and nap-spermine (SP21) as another agonist

(A) To identify antagonists, HEK293T cells were reverse transfected with a TAAR348 plasmid and CRE-luciferase reporter vector, incubated for 48 hours, then stimulated with simultaneous application of 10-μM spermine along with 10 μM of a series spermine analogs (see list in Table 1-2). After incubation for 4 hours, luciferase activity was assessed. Luciferase activity was normalized to the responses from the vehicle control stimulus DMSO (mean ± SEM, n = 2). Cyclen inhibited the spermine-induced luciferase activity in TAAR348-expressing HEK293T cells. (B) To assess agonist activity, HEK293T cells were reverse transfected with a TAAR348 plasmid and CRE-luciferase reporter vector and incubated for 48 hours. The cells were then stimulated with 10 μM of the spermine analogs alone (see list in Table 1-2), incubated 4 hours, and then assayed for luciferase activity. Luciferase activity normalized to the responses from the control stimulus DMSO (mean ± SEM, n = 2). SP21 (Nap-spermine) was identified as a full agonist of TAAR348.

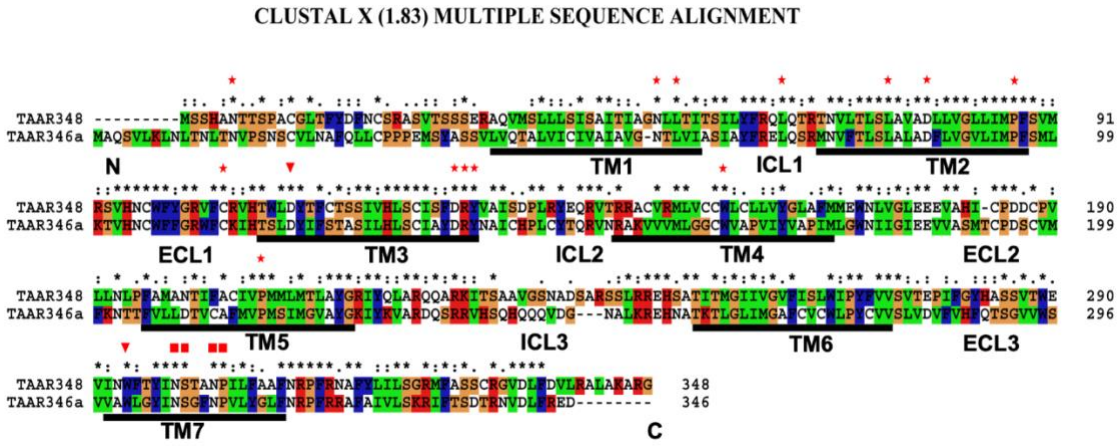

Figure S1-7. Sequence alignment of sea lamprey TAAR348 and TAAR346a

Sea lamprey TAAR348 (348 amino acid residues) was aligned with TAAR346a (346 amino acid residues) using CLUSTAL X 1.83 with default parameters. The amino acid sequences of the 2 receptors share 47% identity and 66% conservative substitutions. Marks for highly conserved amino acid substitutions: "*" residues which have a single, fully conserved residue; ":" residues with one of the following "strong" groups fully conserved: STA, NEQK, NHQK, NDEQ, QHRK, MILV, MILF, HY, FYW; and "." residues with one of the following "weak" groups fully conserved: CSA, ATV, SAG, STNK, STPA, SGND, SNDEQK, NDEQHK, NEQHRK, FVLIM, HFY. We used positive scores from the Gonnet Pam250 matrix to define strong (score > 0.5) and weak groups (score ≤ 0.5). Color assignment was based on the amino acid residue profile specified in Clustal X. Pentagrams indicate broadly conserved residues in rhodopsin-type GPCRs; triangles indicate the aminergic ligand motif; squares indicate the characteristic fingerprint of TAARs. ATV, Alanine Threonine Valine; CSA, Cysteine Serine Alanine; FYW, Phenylalanine Tyrosine Tryptophan; FVLIM, Phenylalanine Valine Leucine Isoleucine Methionine; HFY, Histidine Phenylalanine Tyrosine; HY, Histidine Tyrosine; MILF, Methionine Isoleucine Leucine Phenylalanine; MILV, Methionine Isoleucine Leucine Valine; NDEQ, Asparagine Aspartic acid Glutamic acid Glutamine; NDEQHK, Asparagine Aspartic acid Glutamic acid Glutamine Histidine Lysine; NEQHRK, Asparagine Glutamic acid Glutamine Histidine Arginine Lysine; NEQK, Asparagine Glutamic acid Glutamine Lysine; NHQK, Asparagine Histidine Glutamine Lysine; QHRK, Glutamine Histidine Arginine Lysine; SAG, Serine Alanine Glycine; SGND, Serine Glycine Asparagine Aspartic acid; SNDEQK, Serine Asparagine Aspartic acid Glutamic acid Glutamine Lysine; STA, Serine Threonine Alanine; STNK, Serine Threonine Asparagine Lysine; STPA, Serine Threonine Proline Alanine.

ACKNOWLEDGMENTS

We thank Joseph Riedy and Skye Fissette for technical assistance, Dr. H. Matsunami for providing pCI-mRTPs and pCI-$G_{\alpha olf}$, the US Geological Survey Hammond Bay Biological Station for the use of their research facilities, and the staff of US Fish and Wildlife Service and Fisheries and Oceans Canada for providing sea lampreys.

AUTHOR CONTRIBUTIONS

Conceptualization: Richard R. Neubig, Weiming Li.

Data curation: Anne M. Scott, Zhe Zhang, Liang Jia.

Formal analysis: Anne M. Scott, Zhe Zhang, Liang Jia, Ke Li, Thomas Dexheimer, Jianfeng Ren.

Funding acquisition: Weiming Li.

Investigation: Anne M. Scott, Zhe Zhang, Liang Jia, Ke Li, Qinghua Zhang, Thomas Dexheimer, Yu-Wen Chung-Davidson, Yao Zu.

Supervision: Richard R. Neubig, Weiming Li.

Validation: Anne M. Scott.

Visualization: Anne M. Scott, Zhe Zhang, Liang Jia.

Writing-original draft: Anne M. Scott, Zhe Zhang, Liang Jia, Ke Li, Weiming Li.

Writing-review and editing: Anne M. Scott, Zhe Zhang, Liang Jia, Yu-Wen Chung-Davidson, Richard R. Neubig, Weiming Li.

REFERENCES

REFERENCES

1. Shine R, Mason R. An airborne sex pheromone in snakes. Biol Lett. 2012;8(2):183–5.

2. Suarez S, Wolfner M. Seminal Plasma Plays Important Roles in Fertility. In: Jonge CD, Barratt C, editors. The Sperm Cell: Production, Maturation, Fertilization, Regeneration. Cambridge: Cambridge University Press; 2017. p.88–108.

3. Avila FW, Sirot LK, LaFlamme BA, Rubinstein CD, Wolfner MF. Insect seminal fluid proteins: identification and function. Annu Rev Entomol. 2011;56:21–40.

4. Gabrieli P, Kakani EG, Mitchell SN, Mameli E, Want EJ, Anton AM, et al. Sexual transfer of the steroid hormone 20E induces the postmating switch in Anopheles gambiae. Proc Natl Acad Sci U S A. 2014;111(46):16353–8.

5. Malouines C. Counter-perfume: using pheromones to prevent female remating. Biol Rev Camb Philos Soc. 2017;92(3):1570–81.

6. Wyatt TD. Pheromones and animal behavior: chemical signals and signatures: Cambridge University Press; 2014.

7. Perry JC, Sirot L, Wigby S. The seminal symphony: how to compose an ejaculate. Trends Ecol Evol. 2013;28(7):414–22.

8. Carolsfeld J, Tester M, Kreiberg H, Sherwood N. Pheromone-induced spawning of Pacific herring. Horm Behav. 1997;31(3):256–68.

9. Smith C, Spence R, Reichard M. Sperm is a sexual ornament in rose bitterling. J Evol Biol. 2018;31(11):1610–22.

10. Johnson NS, Yun S-S, Thompson HT, Brant CO, Li W. A synthesized pheromone induces upstream movement in female sea lamprey and summons them into traps. Proc Natl Acad Sci U S A. 2009;106.

11. Johnson NS, Buchinger TJ, Li W. Reproductive ecology of lampreys. In: Docker MF, editor. Lampreys: biology, conservation and control. Netherlands: Springer; 2015. p. 265–303.

12. Siefkes MJ, Winterstein SR, Li W. Evidence that 3-keto petromyzonol sulphate specifically attracts ovulating female sea lamprey Petromyzon marinus. Anim Behav. 2005;70.

13. Tabor CW, Tabor H. Polyamines. Annu Rev Biochem. 1984;53(1):749–90.

14. Michel W, Sanderson M, Olson J, Lipschitz D. Evidence of a novel transduction pathway mediating detection of polyamines by the zebrafish olfactory system. J Exp Biol. 2003;206(10): 1697–706.

15. Rolen SH, Sorensen P, Mattson D, Caprio J. Polyamines as olfactory stimuli in the goldfish Carassius auratus. J Exp Biol. 2003;206(10):1683–96.

16. Lefèvre PL, Palin M-F, Murphy BD. Polyamines on the reproductive landscape. Endocr Rev. 2011;32(5): 694–712.

17. Mann T. Secretory function of the prostate, seminal vesicle and other male accessory organs of reproduction. J Reprod Fertil. 1974;37(1):179–88.

18. Rosenthal SM, Tabor CW. The pharmacology of spermine and spermidine. Distribution and excretion. J Pharmacol Exp Ther. 1956;116(2):131–8.

19. Li W, Scott AP, Siefkes MJ, Yan H, Liu Q, Yun S-S. Bile acid secreted by male sea lamprey that acts as a sex pheromone. Science. 2002;296.

20. Hubbard P, Barata E, Canario AV. Olfactory sensitivity to catecholamines and their metabolites in the goldfish. Chemical senses. 2003;28(3):207–18.

21. Liberles SD, Buck LB. A second class of chemosensory receptors in the olfactory epithelium. Nature. 2006;442(7103):645–50.

22. Hussain A, Saraiva LR, Korsching SI. Positive Darwinian selection and the birth of an olfactory receptor clade in teleosts. Proc Natl Acad Sci U S A. 2009;106(11):4313–8.

23. Nishimura K, Utsumi K, Yuhara M, Fujitani Y, Iritani A. Identification of puberty-accelerating pheromones in male mouse urine. J Exp Zool. 1989;251(3):300–5.

24. Smith JJ, Kuraku S, Holt C, Sauka-Spengler T, Jiang N, Campbell MS. Sequencing of the sea lamprey (Petromyzon marinus) genome provides insights into vertebrate evolution. Nat Genet. 2013;45.

25. Zhuang H, Matsunami H. Evaluating cell-surface expression and measuring activation of mammalian odorant receptors in heterologous cells. Nat Protoc. 2008;3(9):1402.

26. Laframboise A, Ren X, Chang S, Dubuc R, Zielinski B. Olfactory sensory neurons in the sea lamprey display polymorphisms. Neurosci Lett. 2007;414(3):277–81.

27. Hansen A, Eckart Z. The peripheral olfactory organ of the zebrafish, Danio rerio: an ultrastructural study. Chem Senses. 1998;23(1):39–48.

28. Zu Y, Zhang X, Ren J, Dong X, Zhu Z, Jia L, et al. Biallelic editing of a lamprey genome using the CRISPR/Cas9 system. Sci Rep. 2016;6:23496.

29. Li W, Sorensen PW. Highly independent olfactory receptor sites for naturally occurring bile acids in the sea lamprey, Petromyzon marinus. J Comp Physiol A. 1997;180(4):429–38.

30. Karlson P, Lüscher M. ‘Pheromones’: a new term for a class of biologically active substances. Nature. 1959;183(4653):55–6.

31. Siefkes MJ, Li W. Electrophysiological evidence for detection and discrimination of pheromonal bile acids by the olfactory epithelium of female sea lampreys (Petromyzon marinus). J Comp Physiol A. 2004;190.

32. Kobayashi M, Sorensen PW, Stacey NE. Hormonal and pheromonal control of spawning behavior in the goldfish. Fish Physiol Biochem. 2002;26(1):71–84.

33. Stacey N. Hormonally-derived pheromones in teleost fishes. In: Sorensen PW, Wisenden BD, editors. Fish Pheromones and Related Cues. West Sussex, UK: John Wiley & Sons; 2015. p. 33–88.

34. Keller-Costa T, Hubbard PC, Paetz C, Nakamura Y, da Silva JP, Rato A, et al. Identity of a tilapia pheromone released by dominant males that primes females for reproduction. Curr Biol. 2014;24(18):2130–5.

35. Keller-Costa T, Canário AV, Hubbard PC. Olfactory sensitivity to steroid glucuronates in Mozambique tilapia suggests two distinct and specific receptors for pheromone detection. J Exp Biol. 2014;217(23):4203–12.

36. Gomez-Diaz C, Benton R. The joy of sex pheromones. EMBO reports. 2013;14(10):874–83.

37. Brant CO, Li K, Johnson NS, Li W. A pheromone outweighs temperature in influencing migration of sea lamprey. R Soc Open Sci. 2015;2.

38. Scott AM, Li K, Li W. The Identification of Sea Lamprey Pheromones Using Bioassay-Guided Fractionation. J Vis Exp. 2018;(137):e58059.

39. Sorensen PW, Fine JM, Dvornikovs V, Jeffrey CS, Shao F, Wang J. Mixture of new sulfated steroids functions as a migratory pheromone in the sea lamprey. Nat Chem Biol. 2005;1.

40. Kelly DR. When is a butterfly like an elephant? Chem Biol. 1996;3(8):595–602.

41. Johansson BG, Jones TM. The role of chemical communication in mate choice. Biol Rev Camb Philos Soc. 2007;82(2):265–89.

42. Shohat B, Maayan R, Singer R, Sagiv M, Kaufman H, Zukerman Z. Immunosuppressive activity and polyamine levels of seminal plasma in azo-ospermic, oligospermic, and normospermic men. Arch Androl. 1990;24(1):41–50.

43. Stanger J, Quinn P. Effect of polyamines on fertilization of mouse ova in vitro. J Exp Zool. 1982;220(3):377–80.

44. Taylor ML, Price TA, Wedell N. Polyandry in nature: a global analysis. Trends Ecol Evol. 2014;29(7):376–83.

45. Liberles SD. Trace amine-associated receptors: ligands, neural circuits, and behaviors. Curr Opin Neurobiol. 2015;34:1–7.

46. Hussain A, Saraiva LR, Ferrero DM, Ahuja G, Krishna VS, Liberles SD, et al. High-affinity olfactory receptor for the death-associated odor cadaverine. Proc Natl Acad Sci U S A. 2013;110(48):19579–84.

47. Hashiguchi Y, Nishida M. Evolution of trace amine–associated receptor (TAAR) gene family in vertebrates: lineage-specific expansions and degradations of a second class of vertebrate chemosensory receptors expressed in the olfactory epithelium. Mol Biol Evol. 2007;24(9):2099–107.

48. Saraiva LR, Kondoh K, Ye X, Yoon K-h, Hernandez M, Buck LB. Combinatorial effects of odorants on mouse behavior. Proc Natl Acad Sci U S A. 2016;113(23):E3300–E6.

49. Hansen MJ, Madenjian CP, Slade JW, Steeves TB, Almeida PR, Quintella BR. Population ecology of the sea lamprey (Petromyzon marinus) as an invasive species in the Laurentian Great Lakes and an imperiled species in Europe. Rev Fish Biol Fish. 2016;26(3):509–35.

50. Smith B, Tibbles J. Sea lamprey (Petromyzon marinus) in Lakes Huron, Michigan, and Superior: history of invasion and control, 1936–78. Can J Fish Aquat Sci. 1980;37(11):1780–801.

51. Magnes C, Fauland A, Gander E, Narath S, Ratzer M, Eisenberg T, et al. Polyamines in biological samples: Rapid and robust quantification by solid-phase extraction online-coupled to liquid chromatography–tandem mass spectrometry. J Chromatogr A. 2014;1331:44–51.

52. Glaubitz U, Erban A, Kopka J, Hincha DK, Zuther E. High night temperature strongly impacts TCA cycle, amino acid and polyamine biosynthetic pathways in rice in a sensitivity-dependent manner. J Exp Bot. 2015:erv352.

53. Byun JA, Lee SH, Jung BH, Choi MH, Moon MH, Chung BC. Analysis of polyamines as carbamoyl derivatives in urine and serum by liquid chromatography–tandem mass spectrometry. Biomed Chromatogr. 2008;22(1):73–80.

54. Li K, Scott AM, Riedy JJ, Fissette S, Middleton ZE, Li W. Three novel bile alcohols of mature male sea lamprey (Petromyzon marinus) act as chemical cues for conspecifics. J Chem Ecol. 2017;43(6):543–9.

55. Li K, Scott AM, Brant CO, Fissette SD, Riedy JJ, Hoye TR, et al. Bile salt-like dienones having a novel skeleton or a rare substitution pattern function as chemical cues in adult sea lamprey. Org Lett. 2017.

56. Li K, Brant CO, Siefkes MJ, Kruckman HG, Li W. Characterization of a novel bile alcohol sulfate released by sexually mature male Sea Lamprey (Petromyzon marinus). PLoS ONE. 2013;8.

57. Chung-Davidson Y-W, Rees CB, Wu H, Yun S-S, Li W. β-naphthoflavone induction of CYP1A in brain of juvenile lake trout (Salvelinus namaycush Walbaum). J Exp Biol. 2004;207(9):1533–42.

58. Huang ES. Construction of a sequence motif characteristic of aminergic G protein–coupled receptors. Protein Sci. 2003;12(7):1360–7.

59. Lindemann L, Hoener MC. A renaissance in trace amines inspired by a novel GPCR family. Trends Pharmacol Sci. 2005;26(5):274–81.

CHAPTER 2

CONVERGENT OLFACTORY TRACE AMINE-ASSOCIATED RECEPTORS DETECT BIOGENIC POLYAMINES WITH DISTINCT MOTIFS VIA A CONSERVED BINDING SITE

Jia L[#], **Li S**[#], Dai W, Guo L, Xu Z, Scott AM, Zhang Z, Ren J, Zhang Q, Dexheimer TS, Chung-Davidson YW, Neubig RR, Li Q, Li W. Convergent olfactory trace amine-associated receptors detect biogenic polyamines with distinct motifs via a conserved binding site. J Biol Chem. 2021 Nov;297(5):101268.
# These authors contributed equally to this work.

ABSTRACT

Biogenic amines activate G-protein-coupled receptors (GPCRs) in the central nervous system in vertebrate animals. Several biogenic amines, when excreted, stimulate trace amine-associated receptors (TAARs), a group of GPCRs in the main olfactory epithelium, and elicit innate behaviors. How TAARs recognize amines with varying numbers of amino groups is largely unknown. We reasoned that a comparison between lamprey and mammalian olfactory TAARs, which are thought to have evolved independently but show convergent responses to polyamines, may reveal structural determinants of amine recognition. Here, we demonstrate that sea lamprey TAAR365 (sTAAR365) responds strongly to biogenic polyamines cadaverine, putrescine, and spermine, and shares a similar response profile as a mammalian TAAR (mTAAR9). Docking and site-directed mutagenesis analyses show that both sTAAR365 and mTAAR9 recognize the two amino groups of cadaverine with the conserved $Asp^{3.32}$ and $Tyr^{6.51}$ residues. sTAAR365, which has remarkable sensitivity for cadaverine (EC_{50} = 4 nM), uses an extra residue, $Thr^{7.42}$, to stabilize ligand binding. These cadaverine recognition sites also interact with amines with four and three amino groups (spermine and spermidine, respectively). $Glu^{7.36}$ of sTAAR365 cooperates with $Asp^{3.32}$ and $Thr^{7.42}$ to recognize spermine, whereas mTAAR9 recognizes spermidine through an additional aromatic residue, $Tyr^{7.43}$. These results suggest a conserved mechanism whereby independently evolved TAAR receptors recognize amines with two, three, or four amino groups using the same recognition sites, at which sTAAR365 and mTAAR9 evolved distinct motifs. These motifs interact directly with the amino groups of the polyamines, a class of potent and ecologically important odorants, mediating olfactory signaling.

INTRODUCTION

Biogenic amines are a group of signaling molecules that activate G-protein-coupled receptors (GPCRs) and regulate a wide variety of neurophysiologic and behavioral functions. Recognition of amine neurotransmitters, which are often monoamines that activate the aminergic family of GPCRs in vertebrate central nervous systems, has been examined extensively [1–3]. Besides, some excreted biogenic amines function as odorants and are detected by another family of GPCRs, the olfactory trace amine-associated receptors (TAARs) [4–10]. These molecules are categorized based on the number of amino groups as either monoamine (one amino group, such as tyramine, tryptamine, phenylethylamine, and triethylamine) or polyamine (two or more amino groups, such as putrescine, cadaverine, spermidine, and spermine). To date, the structural basis of a TAAR receptor recognizes amines with one or two amino groups having been examined [11–13]. However, how TAAR receptors recognize polyamines with three or four amino groups has not been determined. Thus, exploring the mechanism whereby TAARs respond to polyamines with two three, or four amino groups will complete the story on how biogenic amines with one through four amino groups are recognized by GPCRs.

Odorous polyamines are found in natural excretions (urine, feces, and semen), decomposed tissues, and food sources, and can elicit significant physiological changes and behavioral responses in various species examined [4–15]. Cadaverine and putrescine, the foul-smelling diamines produced by microbial metabolism of putrefied animal tissue, repel zebrafish by activating an olfactory TAAR receptor (zTAAR13c) [9]. Similarly, cadaverine activates an olfactory TAAR receptor in mouse (mTAAR9) and elicits either neutral or aversive behavioral responses, depending on the particular behavioral paradigm [16, 17]. In contrast, putrescine is attractive to

mice, although the cognate receptor or receptors have not been identified [16]. Also, both cadaverine and putrescine can elicit feeding behaviors in rat and goldfish [18, 19]. In addition, spermine, an abundant polyamine in the semen of male sea lamprey, acts as a male sex pheromone that specifically attracts ovulated females [5]. A sea lamprey TAAR receptor, sTAAR348, is proposed to play a key role in mediating the pheromone function of spermine [5]. Likewise, spermine and spermidine (a biosynthetic precursor of spermine) activate mTAAR9 and elicit neutral or attractive behavioral preferences, respectively [16]. However, the mechanisms for TAARs in recognizing polyamines have not been fully determined. We argue that vertebrate TAARs have retained a conserved mechanism for polyamine recognition, even though the behavioral responses to the polyamines are species-specific and context-dependent.

Olfactory TAAR gene families are present in all vertebrate species [20, 21]. Phylogenetic analysis revealed that TAARs of sea lamprey (a jawless vertebrate) cluster into an independent clade that is distantly related to the TAAR clade of jawed animals [20–22]. Given that sea lamprey and mouse TAARs both detect the same group of polyamines, this provides an excellent opportunity to study the functional convergence of two independently evolved TAAR subfamilies. Many olfactory TAARs retain amine recognition motifs that are conserved in classical aminergic receptors, including an aspartate residue in transmembrane helix III ($Asp^{3.32}$; Ballesteros–Weinstein indexing) and a tryptophan residue in transmembrane helix VII ($Trp^{7.40}$) [22, 23]. Molecular docking and mutagenesis studies of mammalian TAAR1, mTAAR7e, and mTAAR7f demonstrate that the negatively charged residue Asp3.32 is critical for amine recognition and forms a salt bridge with the ligand amino group. Other highly variable residues in the transmembrane domains contribute to the selectivity for ligands and serve as scaffolds that stabilize ligand binding [12]. By contrast, a large number of teleost-TAARs lack $Asp^{3.32}$, and

instead, use Asp$^{5.42}$ to form a salt bridge with an amino group of the biogenic amine. Several TAARs such as zTAAR13c, contain both Asp$^{3.32}$ and Asp$^{5.42}$ and recognize di-cationic molecules including cadaverine and putrescine [13]. Notably, almost all sea lamprey and mouse TAARs have only a single negatively charged residue, Asp$^{3.32}$ or Glu$^{3.32}$ in transmembrane helix III that could theoretically recognize only one amino group of the polyamines. The structural basis for these TAARs to stabilize their interaction with the other amino groups in polyamines remains elusive. It is likely that vertebrate olfactory TAARs feature a salt bridge that engages a ligand amino group and have other scaffolds that contribute to the specificity of polyamine recognition. However, the structures of these predicted scaffolds and their function in recognizing amines with two or more amino groups have not been elucidated.

We hypothesized that vertebrate TAARs rely on residues that form a cation–pi interaction or a hydrogen bond with the amino groups in addition to the salt bridge formed by Asp$^{3.32}$ to recognize polyamines. In this study, we identified a sea lamprey olfactory TAAR receptor (sTAAR365) that shows a strikingly similar response profile to cadaverine, putrescine, and spermine as does mTAAR9. Through a systematic comparison of these two distant receptors with convergent functions, we show that sTAAR365 and mTAAR9 both possess conserved Asp$^{3.32}$ and Tyr$^{6.51}$ residues that interact with the two amino groups in cadaverine. In addition, sTAAR365 uses an extra Thr$^{7.42}$ that stabilizes the recognition of cadaverine, serving as part of the amine-binding motif. In sTAAR365, this motif uses an additional negatively charged residue Glu$^{7.36}$ that cooperates with Asp$^{3.32}$ and Thr$^{7.42}$ to recognize the tetraamine spermine. Likewise, mTAAR9 recognizes the triamine spermidine through an aromatic residue, Tyr$^{7.43}$. Thus, sTAAR365 and mTAAR9 recognize these polyamines through a novel motif located in the transmembrane α-helices VI and VII. Taken together, our results propose a mechanism that sTAAR365 and

mTAAR9 converged on their polyamine recognition through distinct motifs in a conserved binding site.

RESULTS

Mammalian TAAR9 orthologs recognize biogenic polyamines

We first asked whether mammalian TAAR9 orthologs are broadly tuned to triethylamine, cadaverine, spermidine, and spermine, as has been shown in mTAAR9 [16]. We examined the response of TAAR9s from rat, human, hamster, and rabbit to the stimulation of 1 mM amines using a well-established cAMP response element (CRE)-driven luciferase reporter assay based on G_{olf}-mediated cAMP signal transduction [5, 24]. In addition to the four mTAAR9 ligands, we included putrescine, which is also a polyamine and precursor of spermine/spermidine biosynthesis. The tested TAAR9s were not activated by putrescine but exhibited varying degrees of activation to the other four amines (Figure 2-1B). Rat TAAR9 showed the maximum responses to triethylamine, cadaverine, spermidine, and spermine compared with the other mammalian species. Cat TAAR9 displayed similar activation properties (potency and efficacy) to those of mTAAR9. These mTAAR9 ligands induced concentration-dependent activities in cells expressing mouse, rat, and cat TAAR9s (Figure 2-1C). In contrast, human, hamster, and rabbit TAAR9s showed minimal activities for this set of ligands.

We then sought to determine if other mouse olfactory TAARs are activated by the mTAAR9 ligands. Only mTAAR8c showed modest activity to 500 μM spermidine (Figure 2-1D). Triethylamine induced robust responses by mTAAR7f and moderate activities for mTAAR5 and mTAAR8c (Figure 2-1D). Other TAARs were not activated by cadaverine or spermidine. Based on these findings, we concluded that several mammalian TAAR9 orthologs detect polyamines. As the mouse is a model animal for olfactory studies, we focused the remainder of our studies on mouse TAAR9 to further characterize TAAR interactions with polyamines.

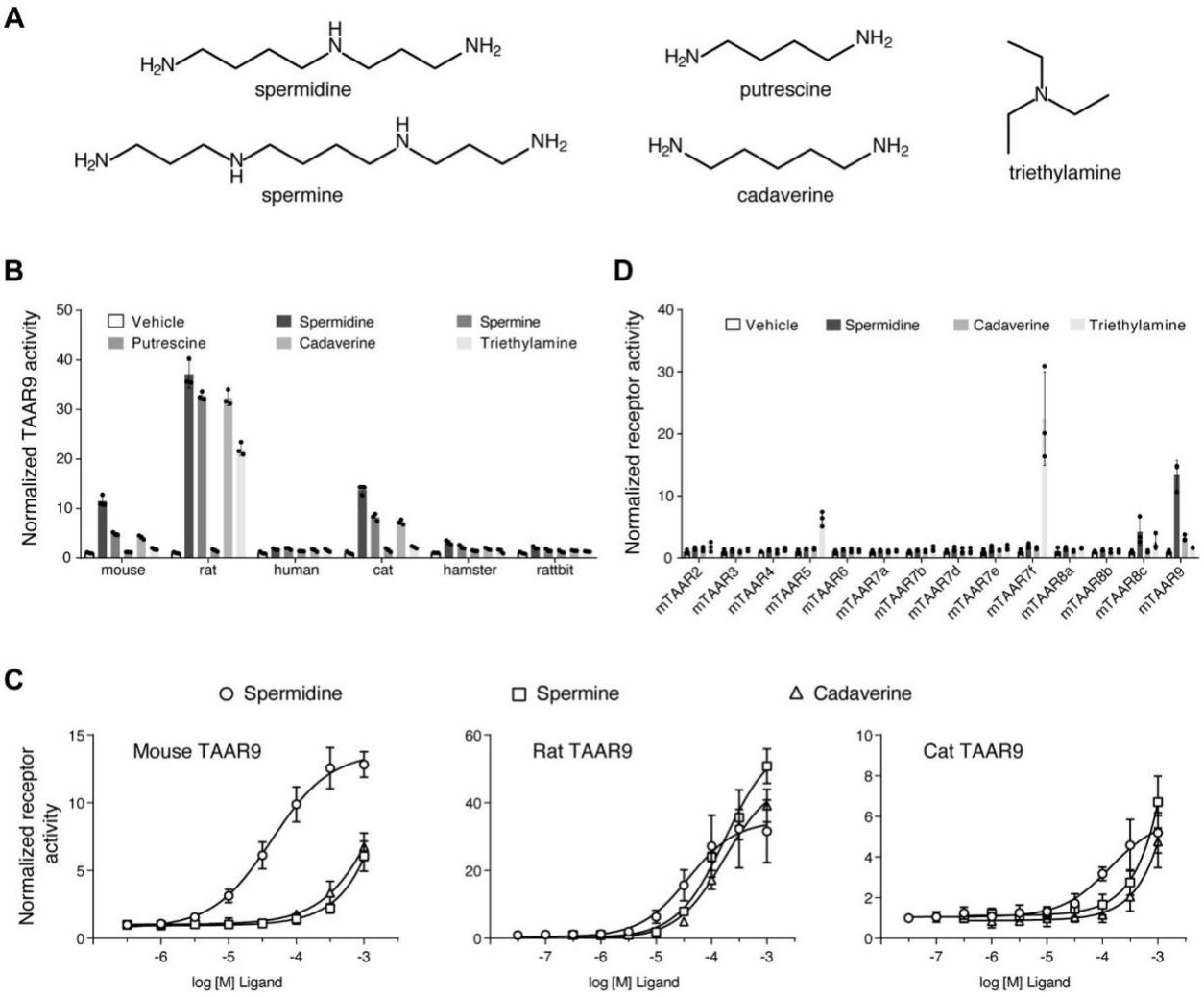

Figure 2-1. Mammalian TAAR9s are broadly tuned to respond to various volatile amines
Mammalian TAAR9 plasmids were transfected into Hana3A cells along with a cAMP-dependent luciferase reporter plasmid (CRE-Luc). Transfected cells were incubated with tested ligands, and luciferase activity was quantified with a fluorescent substrate as a reporter for G_{olf}-mediated TAAR activation. Luciferase activity was indicated by the luminescence value and normalized as a fold-increase over the response to the vehicle stimuli (mean ± S.D., n = 3). (A) Chemical structures of the tested ligands spermidine, spermine, putrescine, cadaverine, and triethylamine. (B) Hana3A cells expressing mouse, rat, human, cat, hamster, and rabbit TAAR9 were incubated with either vehicle or tested ligands (1 mM) and assayed for reporter activity. (C) Concentration-dependent luciferase activity in Hana3A cells expressing mouse, rat, and cat TAAR9 receptors stimulated with cadaverine, spermidine, and spermine. (D) Hana3A cells expressing 14 mouse olfactory TAARs were incubated with vehicle, spermidine, cadaverine, or triethylamine (500 μM) and assayed for reporter activity.

Sea lamprey olfactory sTAAR365 exhibits a similar polyamine response profile to mTAAR9

Next, we questioned whether the sea lamprey TAAR repertoire contains members that are broadly tuned to biogenic amines and that share similar response profiles with mTAAR9. In a previous study, we reported that sTAAR348 responds to spermine when expressed in HEK293T cells but not to other structurally related biogenic amines [5]. Sequence alignment analyses indicated that sTAAR365 shares 74% sequence identity with sTAAR348 (Figure S2-1). sTAAR348 and sTAAR365 showed 34.0% and 34.5% sequence identity, respectively, with mTAAR9 (Figure S2-1). We reasoned that sTAAR365 could be a candidate as a polyamine receptor. To test this hypothesis, we used an established cAMP assay to examine the amine response properties of sTAAR365 [5]. sTAAR365 was activated by cadaverine, putrescine, and spermine, but not by spermidine or triethylamine (Figure 2-2A). Putrescine and spermine elicited a half maximal response (EC_{50}) at concentrations of 56 μM and 28 μM, respectively, in cells expressing sTAAR365 (Figure 2-2B). These are comparable to the potency of odorant receptor agonists in similar assays, ranging from 100 nM to 100 μM [25, 26, 27]. Surprisingly, sTAAR365 was exquisitely sensitive to cadaverine, with EC_{50} of 4 nM, and a response threshold approaching 100 pM (Figure 2-2B). This level of sensitivity rivals the olfactory responses observed through in vivo recording [17]. Moreover, the maximal efficacy (E_{max}) of sTAAR365 response to cadaverine was comparable to that for putrescine, whereas spermine elicited a maximal response of only one-third as much, suggesting that spermine likely acts as a partial agonist for sTAAR365.

We confirmed expression of *sTaar365* and *mTaar9* in olfactory sensory neurons (OSNs) with in situ hybridization. For adult male and female sea lamprey, the antisense *sTaar365* labeled cells were sparsely distributed in lamellae along the rostral-caudal axis of the main olfactory epithelium, displaying tall cell bodies situated in the deeper epithelium and long dendrites coursing toward the

epithelium surface (Figure S2-2). In comparison, no labeling was observed with the sense probe. The expression pattern of *sTaar365* is very similar to that of *mTaar9* in the mouse olfactory epithelium (Figure S2-3). These results demonstrate that sTAAR365 and mTAAR9 are both broadly tuned and sparsely distributed in olfactory epithelia.

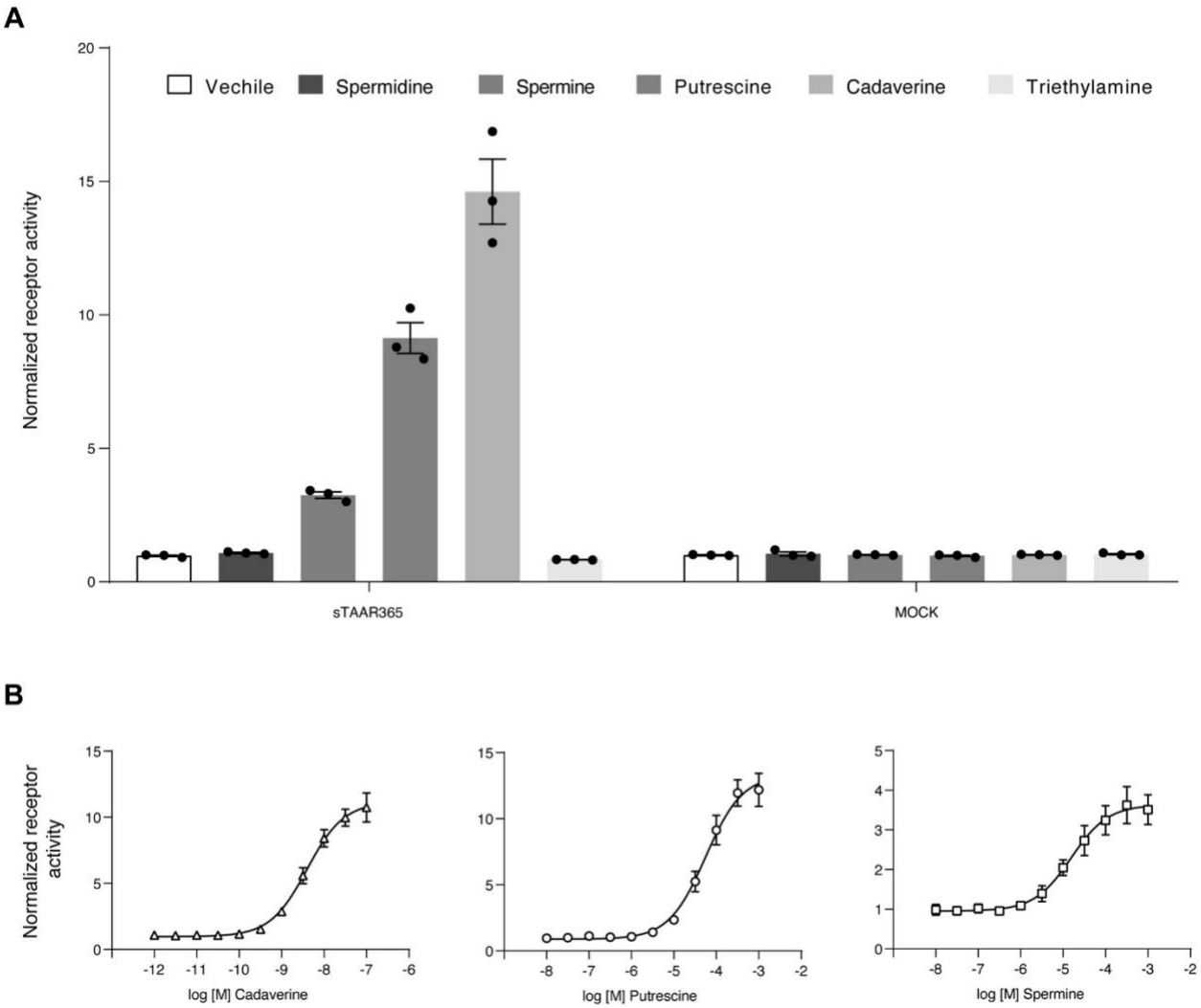

Figure 2-2. Sea lamprey sTAAR365 exhibits similar response profiles as mammalian TAAR9
HEK293T cells were transfected with sea lamprey sTAAR365 for 24 h and assayed for G_{olf}-mediated cAMP production with a TR-FRET assay at 30 min after ligand addition. Receptor activity was normalized to the cAMP level in buffer-treated cells (mean ± S.D., n = 3). (A) HEK293T cells expressing sTAAR365 or mock plasmid were incubated with either vehicle or tested ligands (1 mM). Spermine, putrescine, and cadaverine induced cAMP accumulation in HEK293T cells expressing sTAAR365. (B) concentration-dependent cAMP production of HEK293T cells expressing sTAAR365 stimulated with cadaverine, putrescine, and spermine.

sTAAR365 and mTAAR9 have convergent and divergent residues for polyamine recognition

A previous study of zTAAR13c by Li et al. [13] proposed that $Asp^{3.32}$ and $Asp^{5.42}$ each interact with one of the two amino groups in diamines, such as cadaverine and putrescine. However, it is not known how TAARs recognize polyamines with more than two amino groups. We sought to model the polyamine recognition sites, including residues that directly interact with additional amino groups, in sTAAR365 and mTAAR9. We speculated that TAARs use $Asp^{3.32}$ to confer critical and direct interactions with one amino group, while other nearby polar and/or aromatic residues stabilize polyamine binding by forming hydrogen bond or pi–cation interactions. To test this hypothesis, we generated sTAAR365 and mTAAR9 homology models using GPCR-I-TASSER to predict the putative recognition residues for biogenic polyamines. The models were based on the crystal structures of nine homologous templates. The primary models of sTAAR365 and mTAAR9 shared a maximal identity of 31% and 40%, respectively, to their closest homologous template, the human β2-adrenergic GPCR (Protein Data Bank Entry 2rh1A). The homology model with the highest C-score was chosen as the final structure for molecular docking. Both the sTAAR365 and mTAAR9 models displayed a canonical GPCR structure with seven hydrophobic transmembrane α-helices and an eighth intracellular helix (H8) in the C-terminus.

Using the homology models, we performed Induced Fit Docking (IFD) with Schrodinger Maestro 11.5 to predict the residues of sTAAR365 and mTAAR9 involved in polyamine binding. Several poses of ligand-receptor interactions were generated, and the top result was chosen according to docking scores and glide models. For sTAAR365, the highly conserved $Asp^{3.32}$ contacts both amino groups of cadaverine, one is docked 2.67 Å away from the highly conserved $Asp^{3.32}$, forming a salt bridge and a hydrogen bond with the carboxyl group of $Asp^{3.32}$ (Figure 2-3A). The second amino group of cadaverine also forms a pi-cation interaction with $Tyr^{6.51}$ and a

hydrogen bond with Thr$^{7.42}$ (Figure 2-3A). Similar to cadaverine, putrescine was predicted to interact with Asp$^{3.32}$, Tyr$^{6.51}$, and Thr$^{7.42}$ (Figure 2-3B). Notably, the distance between the carboxyl group of Asp$^{3.32}$ and its salt-bridged amino group of putrescine is predicted at 3.61 Å. The difference in the salt bridge distance predicted for cadaverine and putrescine likely explains the 1000-fold difference in their potency for sTAAR365.

We then docked spermine, a polyamine with four amino groups, into sTAAR365 homology model to infer how TAARs may interact with additional amino groups. As expected, the cadaverine recognition sites Asp$^{3.32}$ and Thr$^{7.42}$ are involved in spermine binding (Figure 2-3C). Asp$^{3.32}$ forms a salt bridge and a hydrogen bond with the two middle amino groups of spermine. The distance between the charged aspartate side chain and the further amino group of spermine is 4.22 Å. Meanwhile, an amino group at one end of spermine contacts the backbone of Thr$^{7.42}$ with a hydrogen bond, while the amino group at the other end is anchored on the negatively charged residue Glu$^{7.36}$, located in the extracellular vestibule of TM VII, through a salt bridge and a hydrogen bond. The distance between the carboxyl group of Glu$^{7.36}$ and the terminal amino group of spermine is predicted at 4.33 Å. The salt bridges involved in spermine recognition are longer than the typical cutoff value for a salt bridge at 4 Å. These relatively weak ionic interactions may explain the partial activation of sTAAR365 by spermine.

Docking cadaverine into mTAA9 homology model suggested that Asp$^{3.32}$ and Tyr$^{6.51}$ are the primary binding sites. The carboxyl group of Asp$^{3.32}$ forms a salt bridge with one amino group of cadaverine at a distance of 4.41 Å (Figure 2-4A) and a hydrogen bond with the second amino group of cadaverine. Likewise, Tyr$^{6.51}$ is predicted to be part of the cadaverine-binding pocket, forming a hydrogen bond with the amino group of cadaverine (Figure 2-4A). However, mTAAR9 differs from sTAAR365 by having Val$^{7.42}$ instead of Thr$^{7.42}$. The larger distance of the salt bridge

and the lack of scaffold interaction with Thr$^{7.42}$ may explain the much lower potency of cadaverine for mTAAR9 compared with sTAAR365. mTAAR9 exhibits robust responses to spermidine, a biosynthetic precursor of spermine. Results from docking spermidine (with three amino groups) into the mTAAR9 model suggested that an extra residue, Tyr$^{7.43}$, cooperates with Asp$^{3.32}$ and Tyr$^{6.51}$ to form the binding pocket (Figure 2-4B). Asp$^{3.32}$ recognizes the middle amino group of spermidine by a salt bridge, at a distance of 2.87 Å, and a hydrogen bond. Moreover, a pi-cation interaction is also predicted between the Tyr$^{6.51}$ residue and the middle amino group. For the amino groups at the ends of spermidine, Tyr$^{7.43}$ recognizes one and forms a pi-cation interaction, whereas Asp$^{3.32}$ recognizes the amino group at the other end and forms a hydrogen bond (Figure 2-4B). Furthermore, triethylamine, which has a similar potency as cadaverine for mTAAR9, forms a single salt bridge with the carboxyl group of Asp$^{3.32}$ at a distance of 2.81 Å (Figure 2-4C).

Taken together, these docking results suggest that sTAAR365 and mTAAR9 have the conserved Asp$^{3.32}$ and Tyr$^{6.51}$ that interact with two amino groups in diamines. In addition, sTAAR365 uses an extra Thr$^{7.42}$ to stabilize recognition of cadaverine and putrescine. The diamine recognition motifs, in addition to an extra Glu$^{7.36}$ in sTAAR365 or Tyr$^{7.43}$ in mTAAR9, enable the selective recognition of spermine and spermidine, respectively.

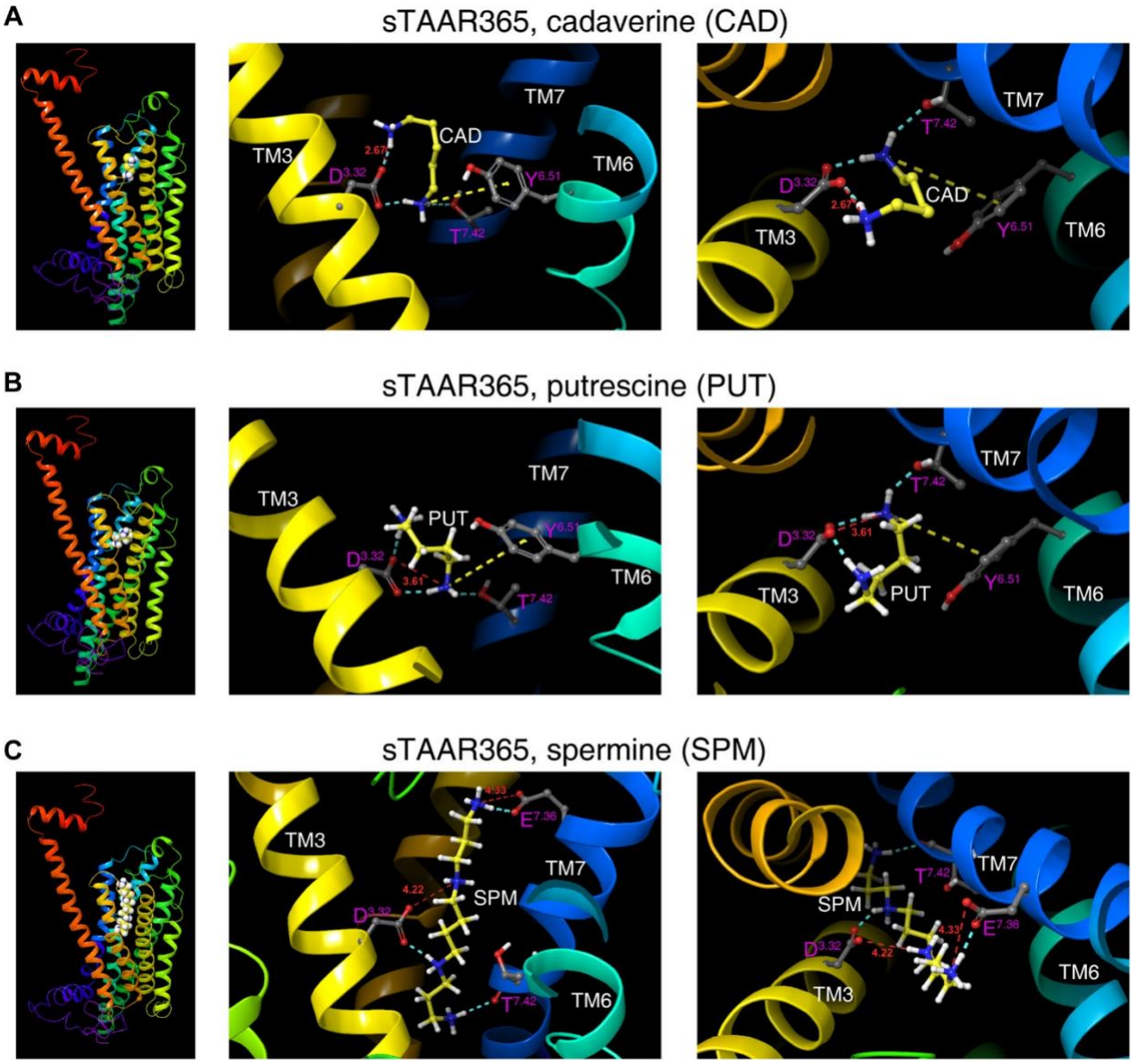

Figure 2-3. The binding sites for cadaverine, putrescine, and spermine predicted by docking into sTAAR365 homology model

Side profile and enlarged views of sTAAR365 homology model predicted spatial position of ligand (A) cadaverine (CAD), (B) putrescine (PUT), (C) spermine (SPM) and corresponding residues involved in ligand recognition. Side chains of key residues involved in ligand binding and major interactions between ligand and predicted binding residues were displayed. Red dashed line, salt bridge; cyan dashed line, hydrogen bond; yellow dashed line, Pi-cation interaction. Distances of the predicted salt bridges in Å were labeled in red.

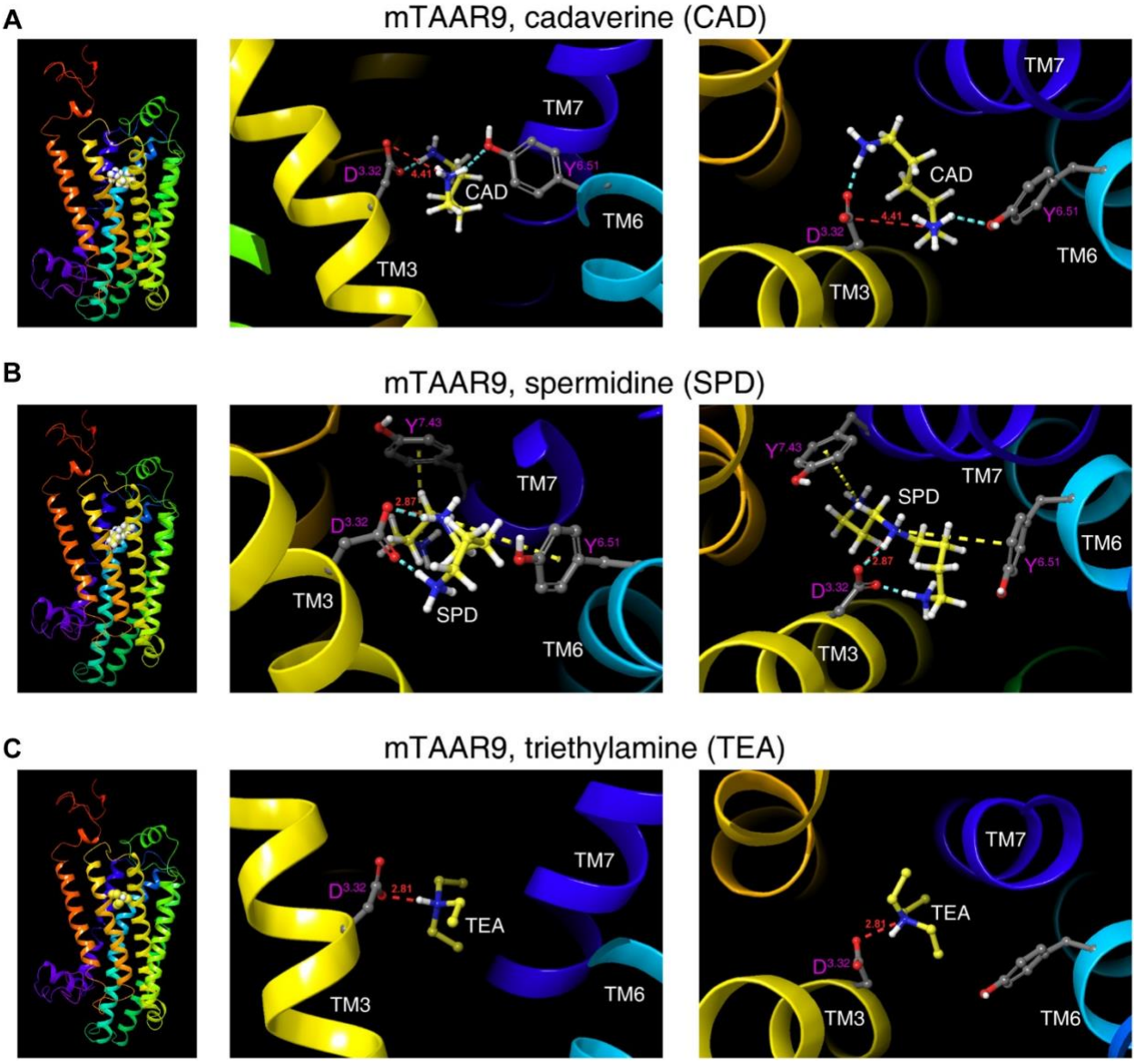

Figure 2-4. The binding sites for cadaverine, spermidine, and triethylamine predicted by docking to mTAAR9 homology model

Side profile and enlarged views of mTAAR9 homology model predicted spatial position of ligand (A) cadaverine (CAD), (B) spermidine (SPD), (C) triethylamine (TEA), and corresponding residues involved in ligand recognition. Side chains of key residues involved in ligand binding and major interactions between ligand and predicted binding residues were displayed. Red dashed line, salt bridge; cyan dashed line, hydrogen bond; yellow dashed line, Pi-cation interaction. Distances of the predicted salt bridges in Å were labeled in red.

The conserved Asp$^{3.32}$ is critical for TAAR activation

To confirm the role of Asp$^{3.32}$ in polyamine recognition by sTAAR365 and mTAAR9, we replaced their Asp$^{3.32}$ with alanine, asparagine, or glutamate. In sTAAR365, a charge-neutralizing mutation of Asp$^{3.32}$ (D3.32A or D3.32N) eliminated activation by cadaverine, putrescine, and spermine (Figure 2-5A). In contrast, the D3.32E mutant, with the most conservative exchange of Asp$^{3.32}$ to Glu, was activated by cadaverine and putrescine with comparable efficacy as wild-type, albeit with drastically decreased potency (Figure 2-5A and Table 2-1). The EC_{50} values of cadaverine and putrescine for the D3.32E mutant increased three and one orders of magnitude for sTAAR365, respectively (Table 2-1). However, spermine activity at the D3.32E mutant was almost eliminated, resulting in minimal cAMP accumulation at the highest concentration tested (1 mM) (Figure 2-5A).

Similar results were observed for mutations of Asp$^{3.32}$ in mTAAR9 for responses to spermidine. Activity was abolished for the D3.32A, D3.32N, and D3.32E mutants (Figure 2-5C). Likewise, cadaverine- and triethylamine-induced activities were abolished for mTAAR9 mutants (Figure 2-5C). These empirical findings are consistent with docking predictions that the highly conserved Asp$^{3.32}$ is a critical determinant for activation of sTAAR365 and mTAAR9 by various amines.

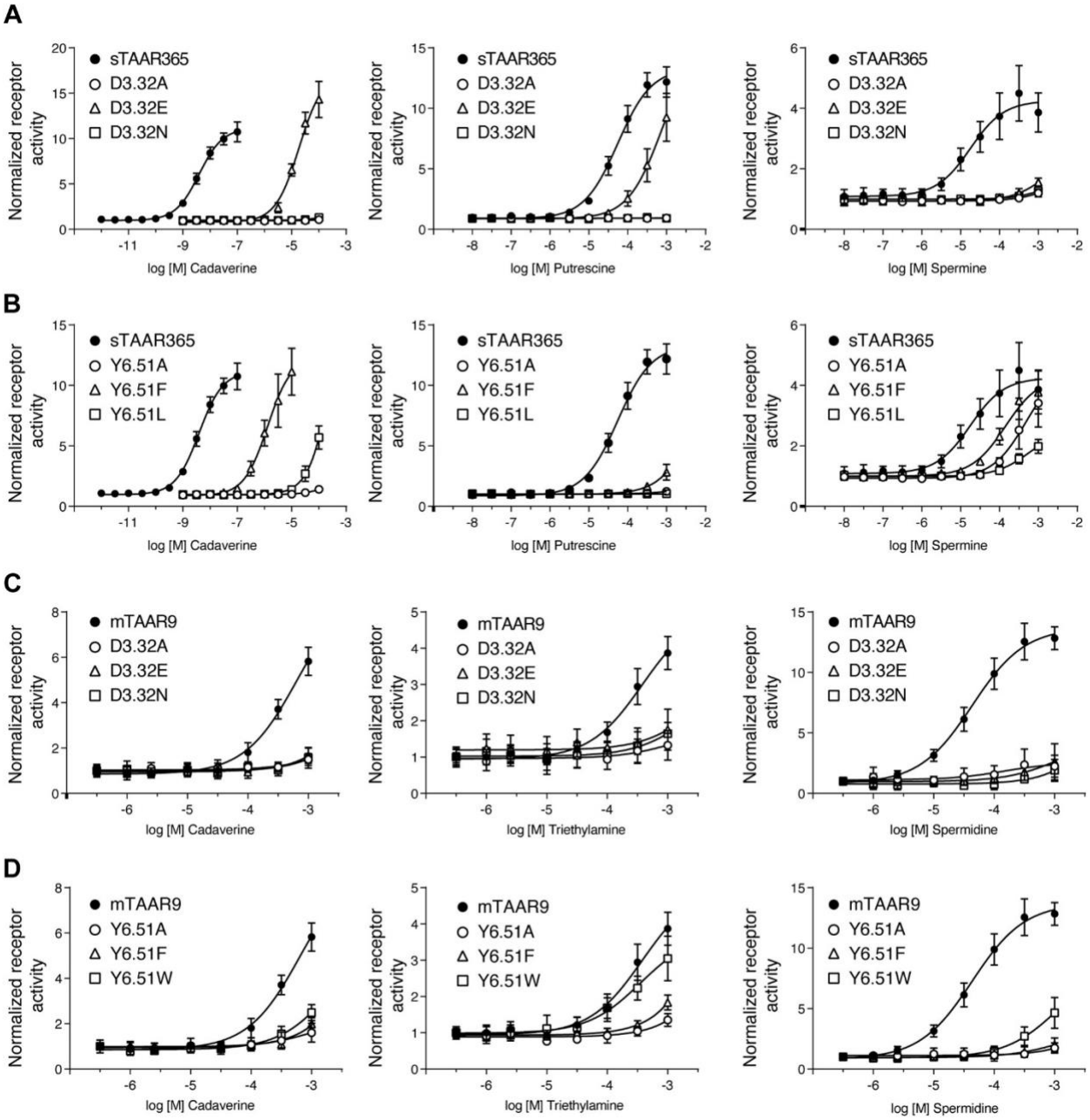

Figure 2-5. Effect of amino acid residue substitution at conservative binding sites ($Asp^{3.32}$ and $Tyr^{6.51}$) of sTAAR365 and mTAAR9

HEK293T or Hana3A cells were transfected with either wild-type sTAAR365, wild-type mTAAR9, or mutant receptors ($Asp^{3.32}$ or $Tyr^{6.51}$) of sTAAR365 and mTAAR9, and incubated with dilutions of ligands. Receptor activity was normalized to the basal activity of buffer-treated cells (mean ± S.D., n = 3). (A) Concentration-dependent cAMP production of HEK293T cells expressing sTAAR365 and its $D^{3.32}$ mutants stimulated with cadaverine, putrescine, and spermine. (B) Concentration-dependent cAMP production of HEK293T cells expressing sTAAR365 and its $Y^{6.51}$ mutants stimulated with cadaverine, putrescine, and spermine. (C) Concentration-dependent luciferase activity of Hana3A cells expressing mTAAR9 and its $D^{3.32}$ mutants stimulated with cadaverine, spermidine, and triethylamine.

Figure 2-5 (cont'd).
(D) Concentration-dependent luciferase activity of Hana3A cells expressing mTAAR9 and its $Y^{6.51}$ mutants stimulated with cadaverine, spermidine, and triethylamine.

Receptor	SPM	CAD	PUT
sTAAR365	28 ± 6 μM	4.0 ± 0.6 nM	56 ± 7 μM
sTAAR365 D3.32A	loss	loss	loss
sTAAR365 D3.32E	loss	14 ± 0.5 μM	>500 μM
sTAAR365 D3.32N	loss	loss	loss
sTAAR365 Y6.51A	319 ± 112 μM	loss	loss
sTAAR365 Y6.51F	114 ± 20 μM	1.7 ± 0.9 μM	>500 μM
sTAAR365 Y6.51L	>500 μM	>100 μM	loss
sTAAR365 T7.42A	loss	31 ± 24 μM	>500 μM
sTAAR365 T7.42M	loss	loss	loss
sTAAR365 T7.42S	64 ± 7 μM	126 ± 13 nM	260 ± 129 μM
sTAAR365 T7.42V	loss	9 ± 2 μM	>500 μM
sTAAR365 E7.36A	>500 μM	50 ± 20 nM	420 ± 87 μM
sTAAR365 E7.36D	>500 μM	7 ± 2 nM	72 ± 14 μM
sTAAR365 E7.36Q	>500 μM	60 ± 11 nM	325 ± 169 μM
sTAAR365 Y7.43A	loss	144 ± 11 μM	loss
sTAAR365 Y7.43F	loss	2 ± 0.2 μM	>1000 μM
sTAAR365 Y7.43Q	loss	7 ± 0.3 μM	loss
sTAAR365 Y7.43S	loss	124 ± 9 μM	loss
sTAAR365 Y7.43L	loss	1 ± 0.2 μM	>1000 μM
sTAAR365 W7.40F	564 ± 371 μM	223 ± 37 nM	>500 μM
sTAAR365 W7.40Y	530 ± 259 μM	127 ± 41 nM	>500 μM
sTAAR365 W7.40G	loss	12 ± 4 μM	loss
	SPD	**CAD**	**TEA**
mTAAR9	43 ± 7 μM	311 ± 109 μM	251 ± 82 μM
mTAAR9 D3.32A	loss	loss	loss
mTAAR9 D3.32E	loss	loss	loss
mTAAR9 D3.32N	loss	loss	loss
mTAAR9 Y6.51A	loss	loss	loss
mTAAR9 Y6.51F	loss	loss	loss
mTAAR9 Y6.51W	>1000 μM	>1000 μM	355 ± 80 μM
mTAAR9 V7.42T	loss	loss	loss
mTAAR9 E7.36A	loss	loss	loss
mTAAR9 E7.36D	142 ± 43 μM	>1000 μM	>1000μM
mTAAR9 E7.36Q	loss	loss	loss
mTAAR9 Y7.43A	loss	loss	loss
mTAAR9 Y7.43F	loss	loss	loss
mTAAR9 Y7.43Q	loss	loss	loss
mTAAR9 Y7.43S	loss	loss	loss
mTAAR9 W7.40F	9 ± 7 μM	83 ± 35 μM	36 ± 16 μM
mTAAR9 W7.40Y	2 ± 0.5 μM	28 ± 8 μM	11 ± 3 μM
mTAAR9 W7.40A	68 ± 48 μM	>1000 μM	>1000 μM

Table 2-1. EC_{50} values of CAD, PUT, SPD, SPM, and TEA for wildtype sTAAR365, wildtype mTAAR9, sTAAR365 mutants, and mTAAR9 mutants (mean ± S.D., n = 3)

Tyr$^{6.51}$ is another common binding partner for polyamine recognition in sTAAR365 and mTAAR9

As described above, the Tyr$^{6.51}$ residue of sTAAR365 was predicted to interact with cadaverine and putrescine. We substituted the Tyr$^{6.51}$ residue with phenylalanine, alanine, or leucine and examined the effect on receptor activity. These substitutions resulted in a loss of the hydrogen-bond interaction or pi-cation, or both. The sTAAR365 Y6.51A and Y6.51L mutants drastically reduced receptor responses to cadaverine and putrescine (Figure 2-5B). In contrast, cadaverine was able to activate the Y6.51F mutant but with a potency 350-fold lower than the wild-type sTAAR365 (Figure 2-5B and Table 2-1). These results strongly suggest that the pi-cation interaction formed by Tyr$^{6.51}$ is important for binding of cadaverine and putrescine to sTAAR365. Though Tyr$^{6.51}$ was not predicted to be directly involved in spermine recognition by sTAAR365, it is in proximity to spermine (within a cutoff value of 4.0 Å) and likely helps stabilize the spermine-binding pocket. Indeed, all three sTAAR365 Tyr$^{6.51}$ mutants were activated by spermine with reductions in potency, ranging from 5- to 20-fold (Figure 2-5B and Table 2-1).

To examine whether the Tyr$^{6.51}$ residue of mTAAR9 plays a similar role in polyamine recognition, we substituted Tyr$^{6.51}$ with alanine, phenylalanine, or tryptophan. The Y6.51W mutant showed reduced potency for cadaverine and spermidine, with only small residual activity induced at very high ligand concentrations (Figure 2-5D). The Y6.51A and Y6.51F mutants almost completely lost the receptor activity to cadaverine and spermidine (Figure 2-5D). Tyr$^{6.51}$ was not predicted to be a triethylamine recognition site. However, this residue is situated 5 Å from triethylamine in the docking model, well within the range of van der Waals interactions. For triethylamine, Tyr$^{6.51}$ mutants impaired the receptor activity (Figure 2-5D). In conclusion, results

from site-directed mutagenesis suggest that the $Tyr^{6.51}$ residue either constitutes or stabilizes an amine-binding pocket for polyamines in sTAAR365 and mTAAR9.

Thr$^{7.42}$ is a distinct polyamine recognition motif in sTAAR365

Our docking studies of sTAAR365 predicted that the polar residue Thr$^{7.42}$ is involved in amine recognition by forming a potential hydrogen bond. We substituted the Thr$^{7.42}$ residue with alanine, valine, methionine, or serine to examine the effect on receptor activity. As the most conservative exchange, T7.42S mutant retained a comparable maximum response to the wild-type when exposed to polyamines (Figure 2-6A). However, the potency of cadaverine, putrescine, and spermine for the mutant decreased about 32-fold, 5-fold, and 2-fold, respectively (Table 2-1). In contrast, T7.42A and T7.42V mutants showed drastic decreases in their response to cadaverine, increasing the EC_{50} values by over three orders of magnitude (Figure 2-6A and Table 2-1). Likewise, we observed that these two mutants showed a massive decrease in potency of putrescine (Figure 2-6A). Furthermore, spermine induced no receptor activity in these two mutants (Figure 2-6A). Finally, the T7.42M mutant, with a bulky side chain that blocks the binding site, lost receptor activity to all ligands tested (Figure 2-6A).

Since mTAAR9 possesses a hydrophobic Val$^{7.42}$, as opposed to a polar Thr$^{7.42}$ in sTAAR365, we determined whether a V7.42T mutant enhances the potency of polyamines for mTAAR9. Unexpectedly, the mTAAR9 V7.42T mutant lost activity to cadaverine and spermidine and showed a drastic reduction in its response to triethylamine (Figure 2-6B). Taken together, these results suggest that sTAAR365 utilizes a polar Thr$^{7.42}$ residue to form a hydrogen bond that recognizes polyamines, which is a mechanism distinct from mammalian TAAR9.

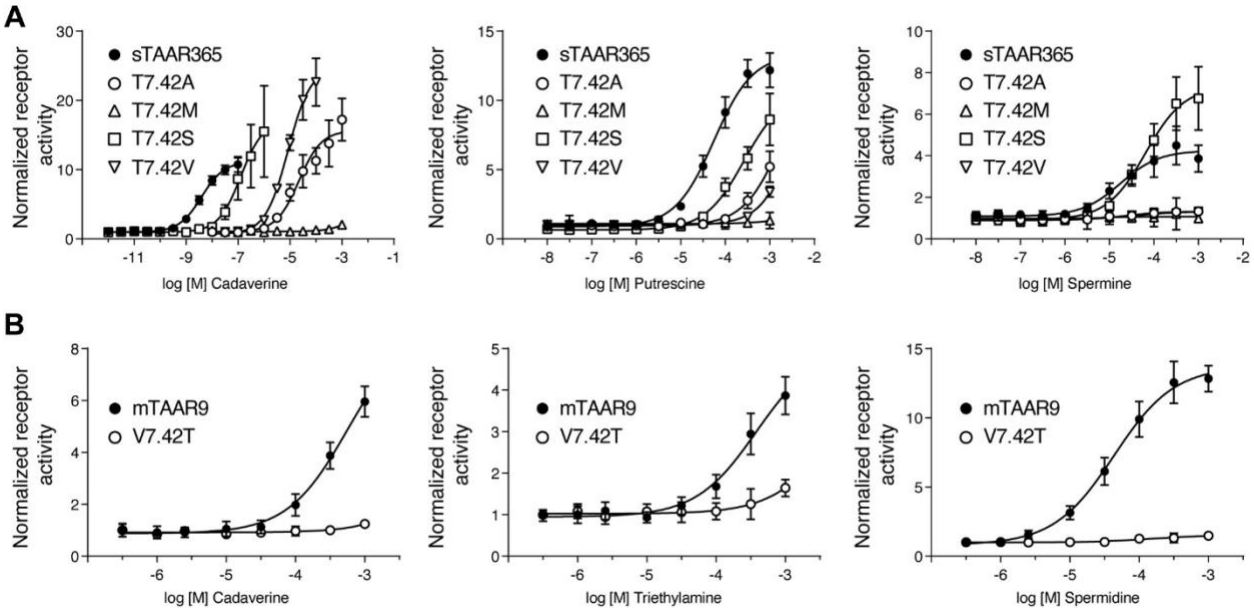

Figure 2-6. Concentration–response curves of sTAAR365 and mTAAR9 mutated at a sTAAR365 specific amine recognition site (Thr$^{7.42}$)

HEK293T or Hana3A cells were transfected with wild-type sTAAR365, wild-type mTAAR9, or Thr$^{7.42}$ mutants of sTAAR365 and mTAAR9, and incubated with dilutions of ligands. Receptor activity was normalized to the basal activity of buffer-treated cells (mean ± S.D., n = 3). (A) Concentration-dependent cAMP production of HEK293T cells expressing sTAAR365 and its T$^{7.42}$ mutants when stimulated with cadaverine, putrescine, and spermine. (B) Concentration-dependent luciferase activity of Hana3A cells expressing mTAAR9 and the V7.42T mutant stimulated with cadaverine, spermidine, and triethylamine.

Glu$^{7.36}$ in the extracellular vestibule contributes to spermine recognition in sTAAR365

Docking of spermine into sTAAR365 homology model suggested that the Glu$^{7.36}$ residue in the extracellular vestibule forms a salt bridge with an amino group at the distal end of spermine. However, Glu$^{7.36}$ was not predicted to interact directly with the docked cadaverine and putrescine. It could also form an interhelical salt bridge with the Arg$^{2.64}$ residue to potentially modulate structural stability of sTAAR365 (Figure S2-4). We reasoned that mutations of the Glu$^{7.36}$ residue may drastically reduce the potency of spermine but not cadaverine and putrescine. To test this hypothesis, we generated a series of mutants by replacing the Glu$^{7.36}$ residue with alanine, glutamine, or aspartate. As expected, E7.36A, E7.36Q, and E7.36D had decreased responses to spermine, with increases in EC50 values of more than 30-fold (Figure 2-7A and Table 2-1). In contrast, the most conservative substitution, the E7.36D mutant, was activated by cadaverine and putrescine with similar EC_{50} values as wild-type sTAAR365 (Figure 2-7A and Table 2-1). Similar results were observed in the charge-neutralizing mutants E7.36A and E7.36Q that showed a slight decrease in responses to cadaverine and putrescine, likely due to the loss of the interhelical salt bridge (Figure 2-7A).

Likewise, the interhelical salt bridge between Glu$^{7.36}$ and Arg$^{2.64}$ was observed in mTAAR9 docking models (Figure S2-5). We generated three mutants for the Glu$^{7.36}$ residue (E7.36A, E7.36G, and E7.36D) in mTAAR9 and examined their receptor activity. Triethylamine, cadaverine, and spermidine activated the E7.36D mutant with little loss of potency (Figure 2-7C). In sharp contrast, the charge-neutralizing mutants E7.36A and E7.36Q completely abolished mTAAR9 activation (Figure 2-7C). These results indicate that the interhelical salt bridge between Glu$^{7.36}$ and Arg$^{2.64}$ may play an important role in modulating the stability of amine recognition pocket or structural conformation of mTAAR9.

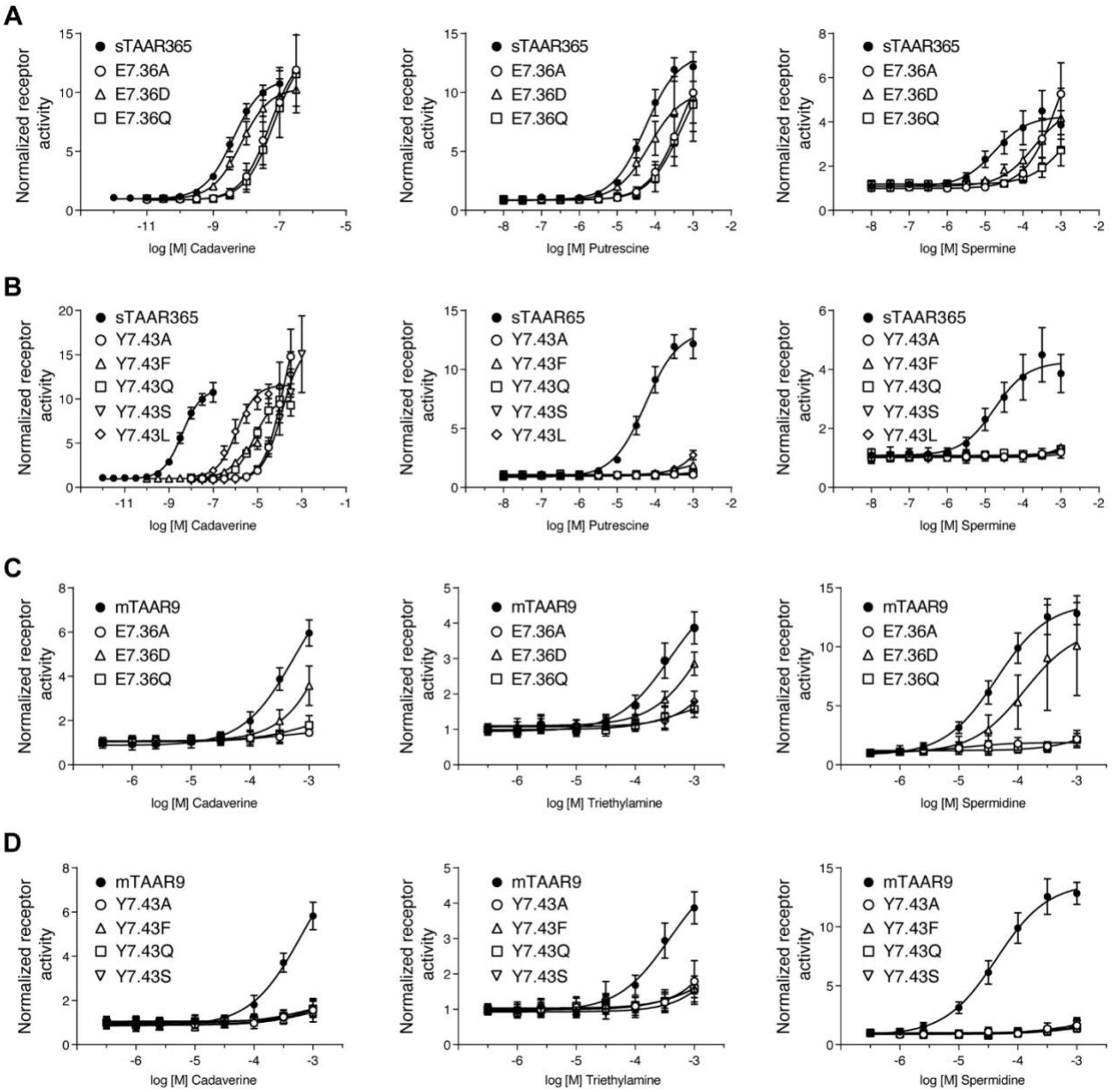

Figure 2-7. Altering sTAAR365 and mTAAR9 responses by mutation of divergent binding sites ($Glu^{7.36}$ and $Tyr^{7.43}$)

HEK293T or Hana3A cells were transfected with wild-type sTAAR365, wild-type mTAAR9, or mutant receptors ($Glu^{7.36}$ and $Tyr^{7.43}$) of sTAAR365 and mTAAR9, and incubated with dilutions of ligands. Receptor activity was normalized to the basal activity of buffer-treated cells (mean ± S.D., n = 3). (A) Concentration-dependent cAMP production of HEK293T cells expressing sTAAR365 and its $E^{7.36}$ mutants stimulated with cadaverine, putrescine, and spermine. (B) Concentration-dependent cAMP production of HEK293T cells expressing sTAAR365 and its $Y^{7.43}$ mutants stimulated with cadaverine, putrescine, and spermine. (C) Concentration-dependent luciferase activity of Hana3A cells expressing mTAAR9 and its $E^{7.36}$ mutants stimulated with cadaverine, spermidine, and triethylamine. (D) Concentration-dependent luciferase activity in Hana3A cells expressing mTAAR9 and its $Y^{7.43}$ mutants stimulated with cadaverine, spermidine, and triethylamine.

Tyr$^{7.43}$ either stabilizes or recognizes polyamines

Although the Tyr$^{7.43}$ residue was not predicted to be part of the polyamine recognition motif in sTAAR365 homology model, docking studies suggested that the hydroxyl group of Tyr$^{7.43}$ interacts with Asp$^{3.32}$ by a hydrogen bond that stabilizes the conformation of the essential amine recognition site (Figure S2-6). We posited that disruption of the hydrogen bond could drastically reduce the potency of ligands for sTAAR365. To test this hypothesis, we replaced the Tyr$^{7.43}$ residue with alanine, glutamine, phenylalanine, serine, or leucine. As expected, all five sTAAR365 mutants showed decreases in cadaverine potency, up to a 1000-fold (Table 2-1). In contrast, we observed that all mutants had a reduced maximum response when putrescine was applied (Figure 2-7B). The Y7.43F and Y7.43L mutants retained minimal putrescine-induced receptor activity, whereas the remaining Tyr$^{7.43}$ mutants completely abolished receptor activity. Likewise, all five mutants were inactive to spermine (Figure 2-7B). Taken together, all experimental data from the Tyr$^{7.43}$ mutants are consistent with the prediction that Asp$^{3.32}$ is anchored in place by a hydrogen bond to the hydroxyl group of Tyr$^{7.4}$3, which stabilizes polyamine recognition of sTAAR365.

A similar interhelical hydrogen bond was not observed in the mTAAR9 homology model; instead, the Tyr$^{7.43}$ residue was predicted to interact with an amino group at the distal end of spermidine through a pi-cation interaction. Functional testing with spermidine revealed that all four mTAA9 mutants of Tyr$^{7.43}$ (Y7.43A, Y7.43Q, Y7.43F, and Y7.43S) eliminated the activity of the receptor (Figure 2-7D). Furthermore, these mutants did not show receptor responses to cadaverine or triethylamine (Figure 2-7D). However, flow cytometry analysis showed that mutation of the mTAAR9 Tyr$^{7.43}$ residue to Ala (Y7.43A), Phe (Y7.43F), and Ser (Y7.43S) had impaired cell-surface expression of the receptor (Figure S2-10). None of the other tested sTAAR365 mutants exhibited reduced surface expression (Figure S2-9). These results suggest that

Tyr$^{7.43}$ has an important role in mediating the structural stability of mTAAR9, and mutation of Tyr$^{7.43}$ may result in detrimental conformational alternations. Indeed, we observed that the Tyr$^{7.43}$ residue forms an intramolecular pi-pi stacking interaction with Tyr$^{7.44}$ in docking models of cadaverine and triethylamine (Figure S2-7). In all, we speculate that Tyr$^{7.43}$ not only participates in spermidine recognition but also contributes to the structural stability of mTAAR9.

Trp$^{7.40}$ modulates the function of the aminergic DW motif

The Trp$^{7.40}$ residue of the aminergic DW motif has been shown to participate in ligand recognition in several aminergic receptors, including serotonin, histamine, muscarinic, adrenergic, and dopamine receptors [23, 28, 29, 30, 31]. However, this residue was not included in the polyamine recognition sites of our sTAAR365 or mTAAR9 homology model. To explore whether Trp$^{7.40}$ affects polyamine recognition in sTAAR365 and mTAAR9, we generated a series of mutants (sTAAR365: W7.40G, W7.40F, and W7.40Y; mTAAR9: W7.40A, W7.40F, and W7.40Y) for Trp$^{7.40}$. All three sTAAR365 mutants showed reduction in potency to cadaverine, with increases in EC_{50} values for about 56-fold, 32-fold, and 3000-fold, respectively (Figure 2-8A and Table 2-1). For spermine, the EC_{50} for the W7.40F and W7.40Y mutants increased by 20-fold (Figure 2-8A and Table 2-1). These two mutants also showed a drastic reduction in their responses to putrescine (Figure 2-8A). The W7.40G mutant lost receptor activity to putrescine and spermine (Figure 2-8A). All experimental results suggest that Trp$^{7.40}$ is critical for polyamine recognition by sTAAR365, potentially stabilizing a positively charged amino group via hydrophobic or aromatic/aromatic interactions. A close investigation of the docking model for cadaverine and spermine indicates that Trp$^{7.40}$ contacts Tyr$^{7.43}$ with a pi-pi stacking to stabilize Asp$^{3.32}$ in the polyamine-binding pocket (Figure S2-8).

In sharp contrast to sTAAR365 mutants, the mTAAR9 W7.40F and W7.40Y mutants displayed a marked increase in potency of cadaverine and spermidine, resulting in a shift of the concentration–response curves to lower concentrations by about one order of magnitude (Figure 2-8B). The efficacy of cadaverine for these two mutants was comparable to wild-type mTAAR9, whereas the efficacy of spermidine was significantly decreased (Figure 2-8B). For monoamine detection, similar results were observed for these two mutants with triethylamine activation, with

an 11-fold and 36-fold decrease of EC_{50}, respectively (Figure 2-8B and Table 2-1). On the other hand, we observed that the W7.40A mutant showed a decrease in efficacy and potency of cadaverine, spermidine, and triethylamine (Figure 2-8B). Thus, all experiments performed with the $Trp^{7.40}$ mutants showed that substituting $Trp^{7.40}$ with amino acid residues having a less bulky aromatic side chain increases the potency of ligands at mTAAR9. It is conceivable that the less bulky aromatic residue facilitates access of ligands into the internal binding pocket and generates a more sensitive receptor for amine detection. In contrast, the W7.40A mutation might result in a loss of structural stability by replacing the aromatic side chain with a methyl side chain, which abrogates potential aromatic interactions with neighboring amino acids, or it may reduce receptor overall stability. Taken together, these observations suggest that the $Trp^{7.40}$ residue of the aminergic DW motif plays different pharmacological roles in modulating amine response profiles in sTAAR365 and mTAAR9.

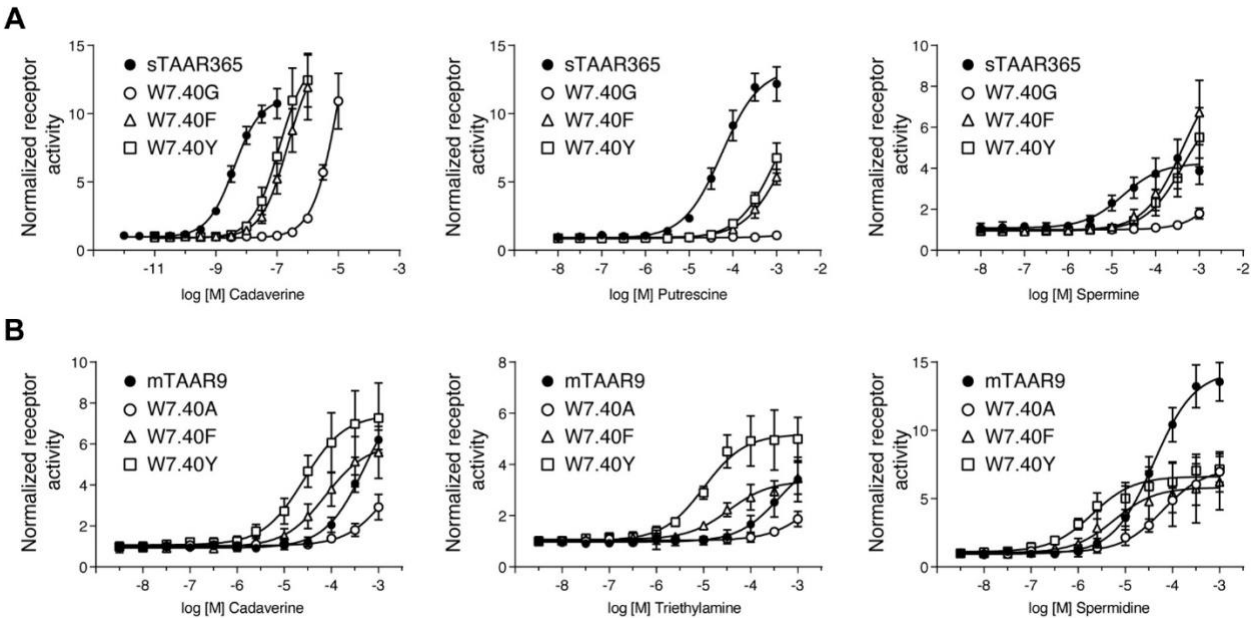

Figure 2-8. Altering sTAAR365 and mTAAR9 responses by mutation of $Trp^{7.40}$ in the conserved aminergic DW motif

HEK293T or Hana3A cells were transfected with wild-type sTAAR365, wild-type mTAAR9, or $Trp^{7.40}$ mutants of sTAAR365 and mTAAR9, and incubated with concentration-dependent ligands. Receptor activity was normalized to the basal activity of buffer-treated cells (mean ± S.D., n = 3). (A) Concentration-dependent cAMP production of HEK293T cells expressing sTAAR365 and its $W^{7.40}$ mutants stimulated with cadaverine, putrescine, and spermine. (B) Concentration-dependent luciferase activity of Hana3A cells expressing mTAAR9 and its $W^{7.40}$ mutants stimulated with cadaverine, spermidine, and triethylamine.

DISCUSSION

Olfactory TAARs enable vertebrates to detect volatile or soluble amines that are ubiquitous in their habitat. The structural determinants for TAARs that recognize amines with a wide range of amino groups have remained elusive, largely due to the lack of crystal structures for any olfactory receptor. In the present study, we examined the structural basis of sTAAR365 and mTAAR9 for detection of polyamines with up to four amino groups. The sea lamprey and jawed vertebrate TAARs are suggested to have evolved independently, forming distinct clades. Receptors from both clades recognize polyamines, providing a unique opportunity to characterize polyamine recognition sites across independently evolved vertebrate GPCRs. Previous studies have demonstrated that teleost TAARs utilize a canonical amine-detection site $Asp^{3.32}$ or a noncanonical amine-detection site $Asp^{5.42}$ (or both) to recognize various monoamines or diamines [13]. However, sTAAR365 and mammalian TAAR9s contain the canonical $Asp^{3.32}$ but lack the $Asp^{5.42}$, implying that these receptors may have evolved alternative mechanisms to recognize various polyamines with two or more amino groups. Based on the odotope theory [25], we propose a hypothetical structural model for polyamine recognition by two clades of independently evolved TAARs, represented by sTAAR365 and mTAAR9. The highly conserved $Asp^{3.32}$ is the primary site essential to binding to one amino group of polyamines. Near $Asp^{3.32}$ are secondary sites that either recognize other amino groups of polyamines (a common residue $Tyr^{6.51}$ for both sTAAR365 and mTAAR9 and a distinct residue $Thr^{7.42}$ for sTAAR365) or stabilize recognition of polyamines with more than two amino groups ($Glu^{7.36}$ and $Tyr^{7.43}$ for both sTAAR365 and mTAAR9). Our models provide strong evidence for a steric and functional odotope theory that sTAAR365 and mTAAR9 utilize convergent structural bases with distinct residues to detect various biogenic

polyamines. The convergent mechanism of polyamine recognition by TAARs reveals additional insights into amine detection by GPCRs.

Conserved and common amine recognition sites for polyamines

The olfactory system uses a combinatorial approach to encode odor identities in which each receptor recognizes multiple odorants, and each odorant activates a specific combination of receptors [25]. Interestingly, olfactory systems in different vertebrate species can evolve independently to detect particular odorants, probably through evolutionarily conserved and divergent recognition sites [12]. Prior to this study, the $Asp^{3.32}$ residue of the aminergic DW motif ($Asp^{3.32}$ and $Trp^{7.40}$) has been reported as a critical element for amine recognition by TAARs [11, 12, 13, 32]. This negatively charged $Asp^{3.32}$ is conserved in all jawless fish TAARs (sea lamprey, 26/26), most mammalian TAARs (mouse 13/15, rat 15/17, human 6/6), and some teleost TAARs (zebrafish 34/112). A few mammalian TAARs, such as two mouse TAARs (mTAAR7a and mTAAR7d) and two rat TAARs (rTAAR7a and rTAAR7c), contain a noncanonical amine-detection site $Glu^{3.32}$ on transmembrane III. Here, we also showed that $Asp^{3.32}$, but not $Trp^{7.4}0$, forms a salt bridge with one amino group in polyamines, which is an essential element for polyamine recognition by both sTAAR365 and mTAAR9. The $Asp^{3.32}$ residue is highly conserved among class A GPCRs, and a similar salt bridge between $Asp^{3.32}$ and the ligand amino group has been described in crystal structures of aminergic receptors, including β1 adrenergic receptor, β2 adrenergic receptor, and H1 histamine receptor [33, 34, 35]. Charge-neutralizing mutation of $Asp^{3.32}$ abolished the ability of sTAAR365 and mTAAR9 to detect polyamines. However, mutation of $Asp^{3.32}$ to Glu in sTAAR365 retained receptor activity to polyamines but reduced ligand potency. Thus, the salt bridge formed by the amino group of polyamines and the anionic carboxylate group of residue 3.32 is relatively flexible in sTAAR365, with $Asp^{3.32}$ having a

stronger interaction than Glu$^{3.32}$. This phenomenon is consistent with the fact that some mammalian TAARs use Glu$^{3.32}$ to detect amines [11, 13]. For mTAAR9, however, the same mutation of Asp$^{3.32}$ to Glu resulted in a nearly complete loss of receptor activity. The differences suggest that other distinct sites in the two receptors are also critical to stabilize polyamine binding. The polyamine detection mechanisms vary throughout TAAR clades. Previous studies have shown that several zebrafish family members TAAR13 and TAAR14 evolved a noncanonical Asp$^{5.42}$ along with Asp$^{3.32}$ to form a salt bridge with each amino group of di-cationic polyamines [11, 13]. However, Asp$^{5.42}$ is not present in sTAAR365 and mTAAR9, raising the possibility that alternative sites are involved. We combined homology modeling with mutagenesis experiments to show that sTAAR365 and mTAAR9 use a common polar Tyr$^{6.51}$ residue as another polyamine contact site. Notably, residue 6.51 is also considered as an interaction hotspot for aminergic receptors, by forming pi-cation, hydrogen-bond, or hydrophobic interaction with aminergic ligands [36]. Though TAARs are distantly related to aminergic receptors, the recognition function of Tyr$^{6.51}$ for polyamines seems to be well conserved in olfactory TAARs and the phylogenetically related aminergic receptors.

Distinct amine recognition sites for polyamine detection

Our docking and mutagenesis data indicate that a distinctive polar residue (Thr$^{7.42}$) at the same plane of Asp$^{3.32}$ serves as a binding site for polyamines in sTAAR365. Likewise, a polar residue at this position (Tyr$^{7.42}$) is predicted to be part of the amine recognition pocket in crystal structures of aminergic receptors. Indeed, phylogenetic and evolutionary analyses indicate a close relationship between lamprey TAARs and the aminergic serotonin (5-HT)-4 receptor, supporting the idea that lamprey TAARs and aminergic receptors may use a polar residue at 7.42 that selectively recognizes biogenic amines [37, 38, 39]. Mutation of this pivotal Thr$^{7.42}$ binding site to

hydrophobic residues resulted in a drastic reduction of ligand potency. In contrast, the subtle exchange for another polar residue (serine) showed minimal loss of potency to polyamines. Moreover, we observed that the maximal efficacy of spermine on the T7.42S mutant differs from that on the wild-type. The greater E_{max} value is likely imparted by the ability of GPCRs coupling to G proteins and the formation of agonist-induced active conformation. These findings encouraged us to examine the role of the hydrophobic $Val^{7.42}$ in mTAAR9. In contrast to the requirement for a polar residue at this position in sTAAR365, swapping $Thr^{7.42}$ for $Val^{7.42}$ in mTAAR9 failed to increase the potency of mTAAR9 ligands and impaired receptor activation, suggesting that the residue at position 7.42 plays disparate roles in sTAAR365 and mTAAR9. $Thr^{7.42}$ is involved in polyamine recognition by sTAAR365. In contrast, mTAAR9 has evolved a hydrophobic $Val^{7.42}$ that does not directly contribute to polyamine recognition but plays an important role in maintaining the structural stability of the receptor, conceivably due to effects of hydrophobic residues that point toward the lipid-protein interface.

In addition, $Asp^{3.32}$ is stabilized by a hydrogen bond to the hydroxyl group of $Tyr^{7.43}$ in sTAAR365 docking models that stabilizes polyamine recognition. The $Asp^{3.32}$ residue of mTAAR7e and mTAAR7f is also reported to anchor $Tyr^{7.43}$ with the same hydrogen bond that stabilizes the ionic interaction between $Asp^{3.32}$ and the ligand amino group [11]. A similar hydrogen bond between $Asp^{3.32}$ and $Tyr^{7.42}$ has been described in the crystal structures of various aminergic receptors [36], including muscarinic acetylcholine receptors and α1B adrenergic receptor [30, 40, 41, 42]. In most cases, impairment of this hydrogen bond between $Asp^{3.32}$ and $Tyr^{7.42}$ reduces potency of biogenic amines, possibly by destabilizing the interaction of ligand amino group with $Asp^{3.32}$ [36]. In accordance with these experimental results on aminergic receptors, the sTAAR365 $Tyr^{7.43}$ mutants had pronounced effects on potency of polyamine ligands,

suggesting that the hydrogen bond between $Tyr^{7.43}$ and $Asp^{3.32}$ is important in shaping a stabilized amine-binding pocket in sTAAR365. In contrast, this hydrogen bond was not predicted to be present in the mTAAR9 docking models. In mTAAR9, the $Tyr^{7.43}$ residue is demonstrated to either participate in spermidine recognition or stabilize the recognition pocket of cadaverine and triethylamine. These results suggest that $Tyr^{7.43}$ regulates ligand binding in both sTAAR365 and mTAAR9 albeit with different mechanisms.

Aside from the abovementioned key residues in the upper region of transmembrane domains, an extra negatively charged residue, $Glu^{7.36}$, located in the extracellular vestibule of sTAAR365, is predicted to be part of spermine-binding sites. Notably, $Glu^{7.36}$ contacts $Arg^{2.64}$ with an interhelical salt bridge in the homology modeling of sTAAR365 and mTAAR9. Likewise, a similar hydrogen bond is well maintained in all of the available crystal structures of activated muscarinic acetylcholine receptors (mAChRs), serving as a cryptic pocket for mAChR ligands [43]. More interestingly, ligand docking slightly shortens the length of the salt bridge in both sTAAR365 and mTAAR9, suggesting that the interaction between $Glu^{7.36}$ and $Arg^{2.64}$ appears to be essential in stabilizing the opening of the amine recognition pocket. Consistent with this, the E7.36D mutant retains the salt bridge with $Arg^{2.64}$ and shows similar ligand potency in sTAAR365 and mTAAR9 (except spermine for sTAAR365). While the more drastic substitutions, E7.63Q and E7.63A, either reduced potency of cadaverine or putrescine for sTAAR365, or radically diminished the magnitude of activation of mTAAR9. In contrast to cadaverine/putrescine, all three sTAAR365 mutants showed a significant loss of potency to spermine, conceivably because spermine has a much longer carbon chain and $Glu^{7.36}$ serves as an extracellular vestibular site to stabilize the terminal amino group of spermine.

We noticed that compared with the wild-type, some sTAAR365 mutants (such as D3.32E with Hill slope 1.44) show steeper slopes in their concentration-response curves for cadaverine. Overall, three mutant receptors with good responses (E_{max} > 0.5 of WT sTAAR365) gave Hill slopes >1.2. The pharmacological mechanism underlying this phenomenon remains to be examined. This may be due to the much lower potency and attendant artifacts of the high concentrations. However, there could be mutation-induced loss of major interaction, which then requires two separate ligands to contact the multiple sites needed to activate the receptor.

Polyamines are ecologically relevant odorants

Biogenic amines are potent odorants enriched in biological excretions and act as important social cues that elicit distinct behavioral responses in vertebrates [5, 9, 16, 17, 44]. TAARs not only play important roles in mediating aminergic signaling in the nervous system but also serve as olfactory receptors (except TAAR1) to specifically detect these odorous amines. We herein show that sea lamprey olfactory sTAAR365 and mammalian TAAR9 subfamily members are broadly tuned to detect multiple biogenic polyamines. Thus, the ability to detect biogenic polyamines is well conserved among vertebrates, from jawless fish to mammals, highlighting the ecological significance of polyamines. Though the broadly tuned sTAAR365 and narrowly tuned sTAA348 showed no response to spermidine in the heterologous expression system [5], in vivo calcium imaging experiments with sea lamprey olfactory sensory neurons revealed that spermine and spermidine can activate separate olfactory sensory neurons at high (10^{-5} M) and low (10^{-9} M) concentrations [45]. However, we cannot preclude the involvement of sTAAR365 in detecting spermidine because others have reported that amines can robustly activate TAAR3- and TAAR4-expressing OSNs but fail to activate these receptors in heterologous assays [16, 46]. On the other hand, TAAR9 can be activated by urine samples from different species (mouse, rat, human, and

other mammalian species) with similar sensitivity [7]. However, it is still unclear whether these specific polyamines and TAAR pairs are responsible for the observed instinctive animal behaviors. Nevertheless, these published studies together with our results strongly suggest that polyamines are ecologically relevant odorants for TAARs that mediate vertebrate physiology and behavior. It is worth noting that a previous study has revealed direct activation of G_i/G_o proteins by natural polyamines [47], suggesting that polyamines could potentially elicit physiological responses independent on TAARs.

Taken together, our deorphanization of sTAAR365 provided a unique avenue to examine the structural basis of polyamine recognition by TAARs. Different from the previous studies that identified $Asp^{3.32}$ and $Asp^{5.42}$ for diamine recognition, our results show that sTAAR365 and mTAAR9, two independently evolved vertebrate TAARs, utilize convergent ($Asp^{3.32}$ and $Tyr^{6.51}$) and divergent ($Thr^{7.42}$, $Glu^{7.36}$, and $Tyr^{7.43}$) motifs for recognition of polyamine odorants (Figure 2-9). These findings demonstrate a novel molecular mechanism for activation of vertebrate TAARs by polyamines. As sea lamprey is an abundant and destructive invasive species in the Laurentian Great Lakes, future studies are needed to examine the role of sTAAR365 and its ligands in mediating behavior.

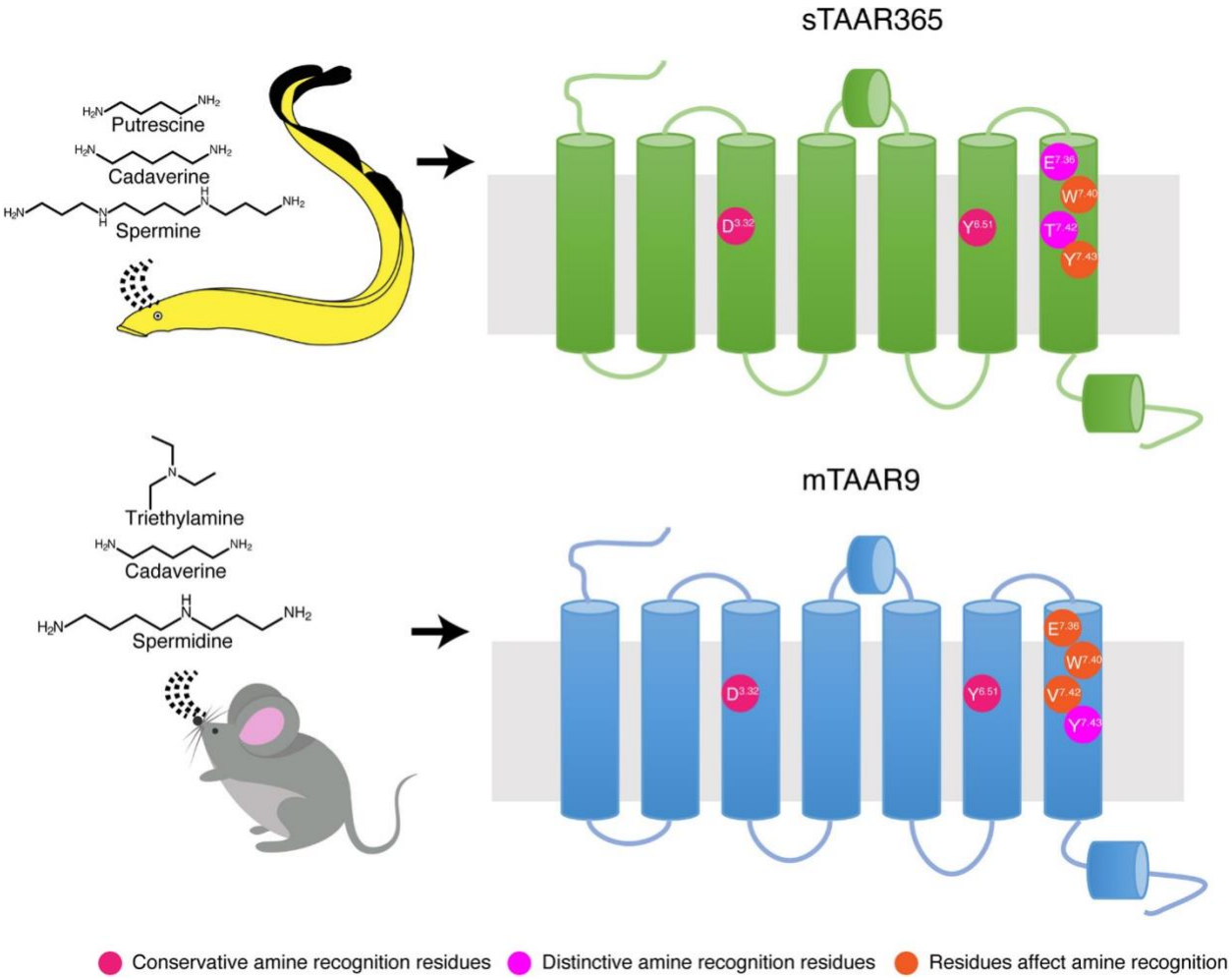

Figure 2-9. A schematic diagram describing the proposed polyamine recognition sites in convergent sTAAR365 and mTAAR9

Cartoon representations of sTAAR365 (green) and mTAAR9 (blue) structures show seven transmembrane domains and two short α-helices. Conservative amine recognition residues ($Asp^{3.32}$ and $Tyr^{6.51}$) are indicated with carnation circle dots. Distinctive amine recognition residues ($Glu^{7.36}$ and $Thr^{7.42}$ in sTAAR365; $Tyr^{7.43}$ in mTAAR9) are labeled with magenta circle dots. Tangerine circle dots represent residues ($Trp^{7.40}$ and $Tyr^{7.43}$ in sTAAR365; $Glu^{7.36}$, $Trp^{7.40}$, and $Val^{7.42}$ in mTAAR9) that affect amine recognition.

MATERIALS AND METHODS

Ethics statement

All procedures involving sea lamprey (*Petromyzon marinus*) were approved by the Michigan State University Institutional Animal Use and Care Committee (03/14-054-00 and 02/17-031-00). Sea lamprey used for in situ hybridization was euthanized with 3-aminobenzoic acid ethyl ester (MS222; 100 mg/l; Sigma-Aldrich) followed by dissection of the olfactory organ.

All mouse experiments were approved by the Animal Ethics Committee of Shanghai Jiao Tong University School of Medicine and the Institutional Animal Care and Use Committee (Department of Laboratory Animal Science, Shanghai Jiao Tong University School of Medicine, animal protocol number A-2016-049). Mice used for in situ hybridization were euthanized with carbon dioxide followed by dissection of the olfactory epithelium.

Chemicals

Amine compounds of the highest purity available were purchased from Sigma-Aldrich. All chemicals were dissolved in dimethyl sulfoxide (DMSO; Sigma-Aldrich) at a final concentration of 200 mM and stored at −20 °C.

Cell lines

HEK293T cells used for all sTAAR365 experiments were maintained at 37 °C with 5% CO_2 and grown in Dulbecco's Modified Eagle Medium (DMEM; Hyclone) supplemented with 10% fetal bovine serum (FBS; Gibco) and 1 × Antibiotic-Antimycotic (Gibco) Hana3A cells derived from HEK293 used for all mTAAR9 experiments were maintained at 37 °C with 5% CO_2 and grown in DMEM supplemented with 10% fetal bovine serum and 1 × Antibiotic-Antimycotic.

Cloning of mammalian and sea lamprey TAAR genes

All mammalian TAAR genes were cloned from genomic DNA inserted into a modified pcDNA3.1- (Invitrogen) vector containing a Rho-tag (the first 20 amino acids of bovine rhodopsin) as described previously (Table S2-1) [6]. The open reading frame of sTAAR365 was mined from the sea lamprey genome assembly (Pmarinus_7.0). sTAAR365 was cloned from sea lamprey genomic DNA and inserted into Rho-pCMV modified from pCMV-Tag-2B (Agilent Technologies) by introducing a Rho-tag (the first 21 amino acids of bovine rhodopsin) at the N-terminal replacing the intrinsic Flag-tag (Table S2-1).

Site-directed mutagenesis of sTAAR365 and mTAAR9

Site-directed mutations of sTAAR365 and mTAAR9 were introduced following the protocol of QuikChange site-directed mutagenesis kit (Agilent Technologies). In brief, PCR primers were designed by Agilent QuikChange Primer Design (Table S2-2 and Table S2-3) and PCR reactions were performed using PfuUltra High-Fidelity DNA Polymerase with wild-type sTAAR365 and mTAAR9 plasmids as templates. The methylated parental strands were selectively digested with 1 μL DpnI enzyme, and the DpnI-treated PCR products were transformed into DMT chemically competent cells (Transgen Biotech). All mutants were verified by DNA sequencing. Positive colonies for the desired substitutions were grown in LB broth and the plasmids were isolated using an EndoFree mini plasmid DNA purification kit (Tiangen Biotech).

Functional assay of mTAAR9 and mutants in the Hana3A heterologous system

Hana3A cells were seeded in poly-D-lysine pre-coated 96-well plates at a density of 1×10^4 cells per well with 50 μL DMEM medium with 10% FBS and incubated for 24 h at 37 °C with 5% CO_2. Cells in each well were transfected with 10 ng CRE-Luc, 10 ng pRL-SV40, 10 ng olfactory mRTPs, and 50 ng mTAAR9 or mutants by Lipofectamine 2000 (Invitrogen), and then incubated

for 18 h at 37 °C with 5% CO_2. Subsequently, the media was aspirated and replaced with 50 µL fresh CD293 media (with 1% glutamine) and incubated for 30 min at 37 °C with 5% CO_2. Then, cells were stimulated with serial dilutions of compounds (diluted in CD293 media) and incubated for 4 h at 37 °C with 5% CO_2. The firefly luciferase and renilla luciferase activity was measured with a BioTek microplate reader following manufacturer's instructions.

Functional assay of sTAAR365 and mutants in the HEK293T heterologous system

HEK293T cells were maintained at 37 °C with 5% CO_2 and grown in DMEM supplemented with 10% FBS with 1 × Antibiotic-Antimycotic. The cAMP production assay was performed in 384-well plates as described in LANCE Ultra cAMP Kit manual (PerkinElmer) to characterize the cAMP production induced in HEK293T cells expressing sTAAR365 and its mutants. Briefly, HEK293T cells were seeded in a 100 mm dish with 3×10^6 cells in 10 mL DMEM medium with 10% FBS and incubated for 24 h at 37 °C with 5% CO^2. Cells were then transfected with 5 µg pGL4.29, 1 µg pCI-mRTPs, 1 µg pCI-$G_{\alpha olf}$, and 1 µg sTAAR365 plasmid or sTAAR365 mutants and incubated at 37 °C with 5% CO_2 for 24 h. Transfected cells were detached with 2 mL Versene (Gibco) and transferred to 384-well plates at 5 µL (2000 cells) per well. Then, 5 µL of the 2 × compound serial dilutions was added to each well and incubated for 30 min at room temperature. Afterward, 5 µL 4 × Eu-cAMP tracer working solution and 5 µL 4 × ULight-anti-cAMP working solution were added to each well and incubated for 1 h at room temperature. Plates were read in the Synergy Neo multimode microplate reader for TR-FRET emissions at 620 nm (as internal reference) and 665 nm (as biological response). The ratio of 665/620 allows normalization for the well-to-well variability and interference due to assay components.

In situ hybridizations of *sTaar365* and *mTaar9*

sTaar365 anti-sense probes were designed against the 372 bp nucleotide sequences of sTAAR365 open reading frame. Amplified fragments were cloned into the pGEM-T vector (Promega) for sequence verification. Plasmids were linearized using restriction enzyme NcoI (anti-sense probe) or SpeI (sense probe) and used for synthesis of digoxigenin (DIG)-labeled RNA probes with DIG RNA labeling kit (SP6/T7) (Roche). *mTAAR9* anti-sense probe was designed against the entire coding region of mTAAR9 (1044 bp). Amplified fragments were cloned into the TOPO TA cloning vector (Invitrogen) for sequence verification. Plasmids were linearized using restriction enzyme NotI and used for synthesis of digoxigenin-labeled RNA probes with DIG RNA labeling kit (SP6/T7).

In situ hybridization was conducted following previously described methods by Chung-Davidson and colleagues [48]. Briefly, 20 μm frozen sections of olfactory epithelium were hybridized with RNA probes (3 ng/μL) overnight at 65 °C in the hybridization solution (50% deionized formamide, 1 × Denhart's solution, 5% dextran sulfate, 750 mM sodium chloride, 25 mM ethylenediaminetetraacetic acid, 25 mM piperazine-N, N′-bis-2-ethanesulfonic acid, 0.25 mg/mL fish sperm DNA, 0.25 mg/mL poly A acid, and 0.2% sodium dodecyl sulfate). Sections were washed three times (5 min each) in 4 × saline-sodium citrate (SSC). For high stringency conditions, sections were washed sequentially in 2 × SSC with 0.3% Tween-20 and 0.2 × SSC with 0.3% Tween-20 three times (15 min each) at 68 °C. Sections were washed in 0.1 × SSC with 0.3% Tween-20 for 15 min followed by three washes (5 min each) in 0.1 M phosphate buffered saline (PBS) with 0.3% Tween-20 at room temperature. The sections were then incubated with blocking solution (1 × PBS, 2 mg/mL bovine serum albumin (BSA), 0.3% Tween-20, and 10% normal sheep serum) for 1 h at room temperature, followed by incubation with alkaline

phosphatase-conjugated sheep-anti-digoxigenin Fab fragments (1:1000 diluted in blocking solution; Roche) overnight at 4 °C. Hybridization signals were detected by incubating the sections in nitro blue tetrazolium and 5-bromo-4-chloro-3-indolyl phosphate (NBT/BCIP; Thermo Fisher Scientific) for 2 h at room temperature. sTAAR365 slides were counterstained with nuclear fast red (Vector Laboratories) for 5 min at room temperature. The images were captured with a Zeiss Axioskop2 mot plus microscope with a 20 × or 40 × objective. Control experiments (*sTaar365* and *mTaar9* sense probe) were conducted simultaneously.

Homology modeling and ligand docking of sTAAR365 and mTAAR9

Homology models of sTAAR365 and mTAAR9 were generated using GPCR-I-TASSER based on the crystal structure of nine homologous templates (Protein Data Bank Entries: 6oijR, 4amjA, 6kuwA, 5zbh, 3d4s, 2rh1A, 6hlpA, 4ib4, and 5uenA) [49]. Rank of templates represented the top threading templates selected by GPCR-I-TASSER. The primary models of sTAAR36 and mTAAR9 shared a maximal identity of 31% and 40%, respectively, to their closest homologous template, the human beta 2-adrenergic G protein-coupled receptor (Protein Data Bank Entry 2rh1A). The model with the highest C-score (sTAAR365: 0.19 and mTAAR9: 0.06) was chosen as the final structure.

The homology models of sTAAR365 and mTAAR9 for ligand docking were refined to prepared states by using Protein Preparation Wizard module integrated in Schrodinger Suite [50]. Protons were added or eliminated according to physiological pH and restrained minimization was performed. The structures of triethylamine, cadaverine, putrescine, spermidine, and spermine were retrieved from PubChem (https://pubchem.ncbi.nlm.nih.gov) and prepared by LigPrep in Maestro [51] with environment adjusted to a physiological pH of 7.0. We then performed receptor-ligand docking in the Induced-Fit Docking module of Schrodinger [52]. The center of binding pocket was

set to $Asp^{3.32}$ in both mTAAR9 and sTAAR365. Several poses of ligand-receptor interactions were generated, and the final pose was chosen according to the docking score and glide model.

Immunocytochemistry assay of sTAAR365 and mutants

HEK293T cells were seeded in collagen I coated 24-well glass bottom plates at a density of 5×10^4 cells per well with 1 mL DMEM medium with 10% FBS and incubated for 24 h at 37 °C with 5% CO_2. Cells were then transfected with 375 ng pGL4.29, 75 ng pCI-mRTPs, 75 ng pEGFP-N1 (Clontech), and 75 ng sTAAR365 plasmid or sTAAR365 mutants and incubated at 37 °C with 5% CO_2 for 24 h. The null plasmid, pGL4.29, pCI-mRTPs, and pEGFP-N1 were cotransfected as a negative control. Subsequently, 100 μL of 37% formaldehyde was added to each well and incubated for 15 min at room temperature and then washed with 500 μL of PBS three times (5 min each). Cells were permeabilized or not permeabilized with 0.5% Triton X-100 for 10 min at room temperature to label the whole cell or only cell membrane, respectively. Then, cells were washed with 500 μL of PBS three times (5 min each). Permeabilized cells were treated with 500 μL blocking buffer (5% BSA and 0.3% Triton X-100 in PBS) for 1 h at room temperature. Nonpermeabilized cells were treated with 500 μL blocking buffer (5% BSA in PBS) for 1 h at room temperature. Then, the blocking buffer was removed and 300 μL mouse monoclonal anti-rhodopsin antibody (MABN15, Millipore; 1:500 diluted in dilution buffer: 1% BSA in PBS for nonpermeabilized cells or 1% BSA, 0.3% Triton X-100 in PBS for permeabilized cells) was added to each well and incubated at 4 °C overnight. The antibody solution was aspirated and washed five times for 5 min each with 500 μL of PBS. Cells were incubated with 300 μL red-fluorescent Alexa Fluor 594 goat anti-mouse IgG (Invitrogen; 1:500 diluted in dilution buffer: 1% BSA in PBS for nonpermeabilized cells or 1% BSA, 0.3% Triton X-100 in PBS for permeabilized cells) for 1 h at room temperature. Cells were washed three times for 5 min each with 500 μL of PBS. Cells were

counterstained with 300 μL DAPI (Invitrogen; 1:5000 diluted in PBS) and incubated in the dark for 5 min. Cells were washed three times for 5 min each with 500 μL of PBS. Images were acquired at 400 × magnification under DMI8 Thunder (Leica) with DAPI filter, GFP filter, and Texas Red filter (ten random views/well, n = 3). The mean value of the red fluorescent signal was quantified with LAS X software (Leica).

Fluorescence cytometry analysis

Hana3A or HEK293T cells were seeded in 6-well plates at a density of 3×10^5 cells per well with 2 mL DMEM medium with 10% FBS and incubated for 24 h at 37 °C with 5% CO_2. Cells were then transfected with 0.4 μg pCI-mRTPs, 0.3 μg pEGFP-N1, and 2 μg wild-type receptor plasmid (mTAAR9 or sTAAR365) or mutant receptor plasmid, and incubated at 37 °C with 5% CO_2 for 24 h. The null pCI plasmid, pCI-mRTPs, and pEGFP-N1 were cotransfected as a negative control. Subsequently, transfected cells were dissociated with CellstripperTM (Corning) and transferred into 5 mL tubes for antibody incubation. 100 μL mouse monoclonal anti-rhodopsin antibody (MABN15, Millipore; 1:100 diluted in staining buffer: 5% BSA, 1% NaN3 in PBS) was added to each tube and incubated at 4 °C for 45 min. Cells were washed twice by adding 2 mL staining buffer and centrifuged at 200*g* for 3 min at 4 °C. In the next step, 100 μL phycoerythrin-conjugated donkey anti-mouse IgG (Jackson ImmunoResearch; 1:100 diluted in staining buffer: 5% BSA, 1% NaN3 in PBS) was added and incubated at 4 °C for 30 min. Cells were washed twice by adding 2 mL staining buffer and then centrifuged at 200*g* for 3 min at 4 °C. Cell pellets were resuspended in 500 μL staining buffer for flow cytometry analysis (BD LSRFortessaTM X-20, Becton, Dickinson and Company).

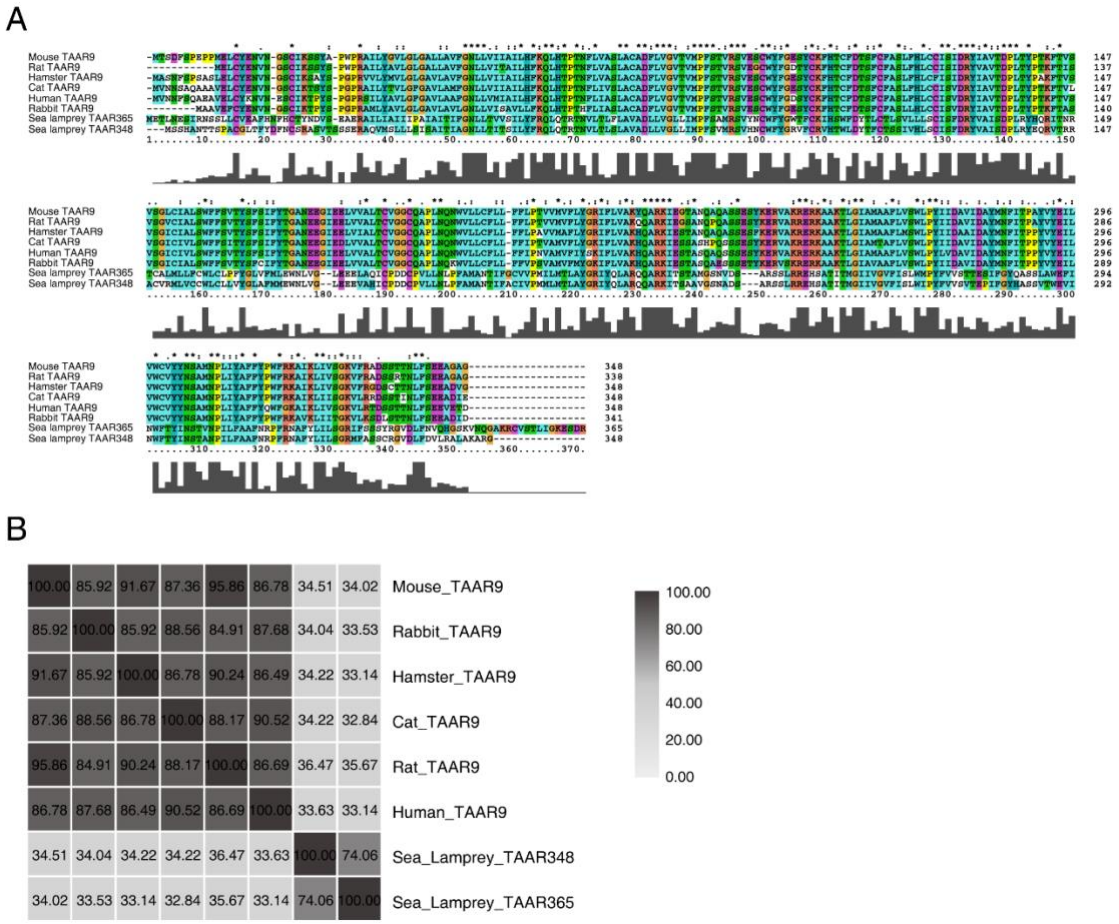

Figure S2-1. Comparison of primary structures of mammalian TAAR9 with sea lamprey sTAAR365 and sTAAR348

(A) Mouse TAAR9 (NP_001010831.1, 348 amino acid residues), rat TAAR9 (NP_783192.1, 338 amino acid residues), hamster TAAR9 (XP_005088204.1, 348 amino acid residues), cat TAAR9 (XP_003986636.1, 348 amino acid residues), human TAAR9 (NP_778227.3, 348 amino acid residues), and rabbit TAA9 (XP_002714783.1, 341 amino acid residues) were aligned with sea lamprey sTAAR365 (365 amino acid residues) and sTAAR348 (348 amino acid residues) by using CLUSTAL 2.1 with default parameters. We used positive scores from the Gonnet Pam250 matrix to define strong (score > 0.5) and weak groups (score ≤ 0.5). Color assignment was based on the amino acid residue profile. (B) The percentage of identical amino acid residues among mammalian TAAR9 receptors, sea lamprey sTAAR365, and sTAAR348 was calculated using NCBI blast2seq (a pairwise sequence alignment tool, https://blast.ncbi.nlm.nih.gov/Blast.cgi) and plotted.

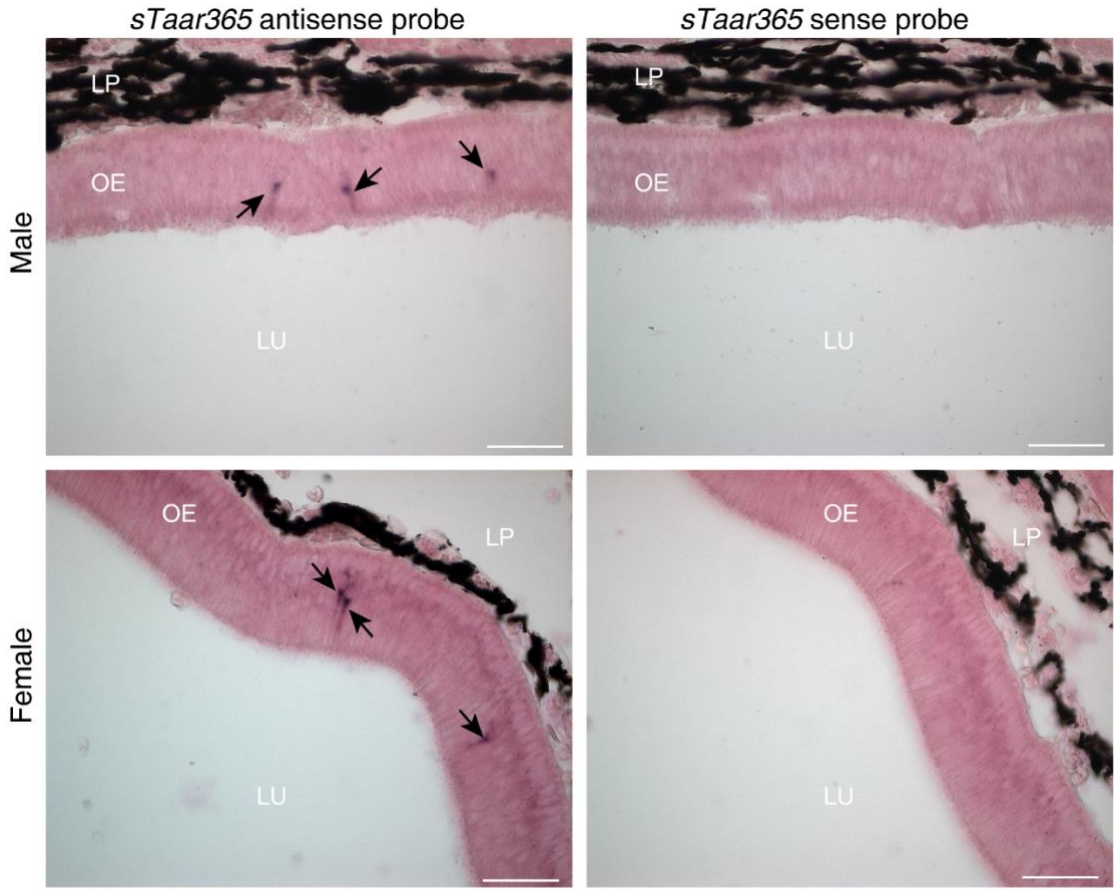

Figure S2-2. Representative olfactory receptor neurons expressing *sTaar365* in a cross-sectional view of the main olfactory epithelium of adult sea lamprey

Representative olfactory receptor neurons expressing *sTaar365* (purple), labeled with a DIG-labeled antisense RNA probe in a cross-sectional view of the main olfactory epithelium of an adult male and female sea lamprey. Sections were counterstained with Nuclear Fast Red. Positive neurons expressing *sTaar365* indicated with purple stain (NBT/BCIP) are marked by black arrows. No positive neurons were observed in the cross sections with digoxigenin-labeled *sTaar365* sense RNA probe. Black melanophores in the lamina propria are characteristic of sea lamprey olfactory epithelia. Scale bars: 50 μm. LP, lamina propria; LU, lumen; OE, olfactory epithelium.

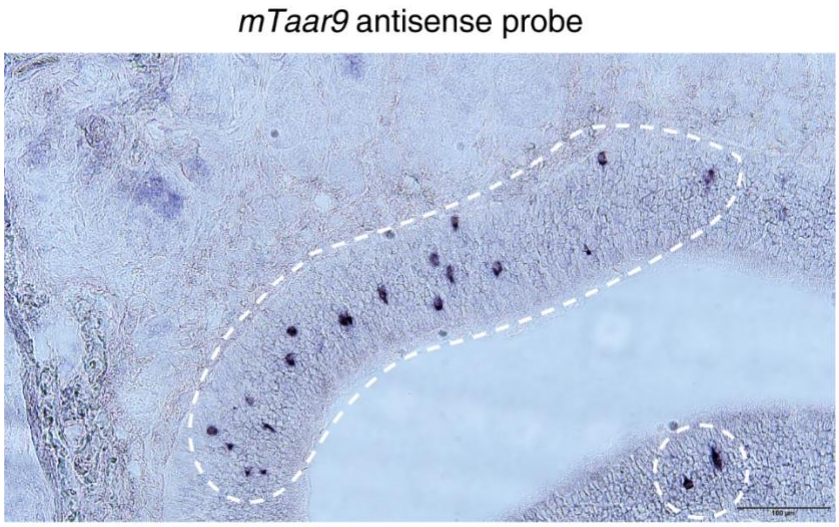

Figure S2-3. Representative olfactory receptor neurons expressing *mTaar9* in a coronal-sectional view of mouse olfactory epithelium

Representative olfactory receptor neurons expressing *mTaar9* (purple), labeled with a DIG-labeled antisense RNA probe in a coronal-sectional view of mouse olfactory epithelium. Positive neurons expressing *mTaar9* indicated with purple stain (NBT/BCIP) are circled with white dashed lines. Scale bar: 100 μm.

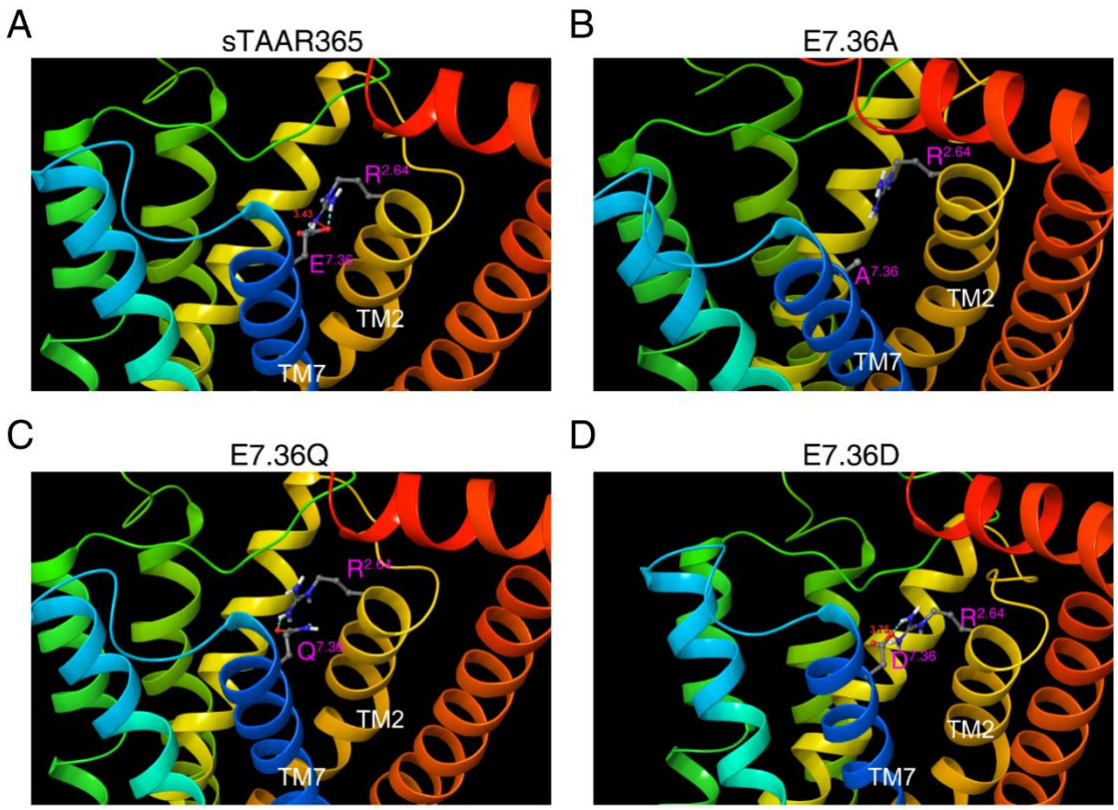

Figure S2-4. Interhelical interactions between Glu$^{7.36}$ and Arg$^{2.64}$ predicted in the homology models of sTAAR365 and its Glu$^{7.36}$ mutants

Side chains of Glu$^{7.36}$ and Arg$^{2.64}$ and major interactions between these two residues were displayed. Red dashed line, salt bridge; cyan dashed line, hydrogen-bond. Distances of the predicted salt bridges in Å were labeled in red. (A) Enlarged view of sTAAR365 predicted interhelical interactions between Glu$^{7.36}$ and Arg$^{2.64}$. (B) Enlarged view of mutant E7.36A predicted spatial position of Arg$^{2.64}$ and mutated Ala$^{7.36}$. (C) Enlarged view of mutant E7.36Q predicted interhelical interactions between Arg$^{2.64}$ and mutated Gln$^{7.36}$. (D) Enlarged view of mutant E7.36D predicted interhelical interactions between Arg$^{2.64}$ and mutated Asp$^{7.36}$.

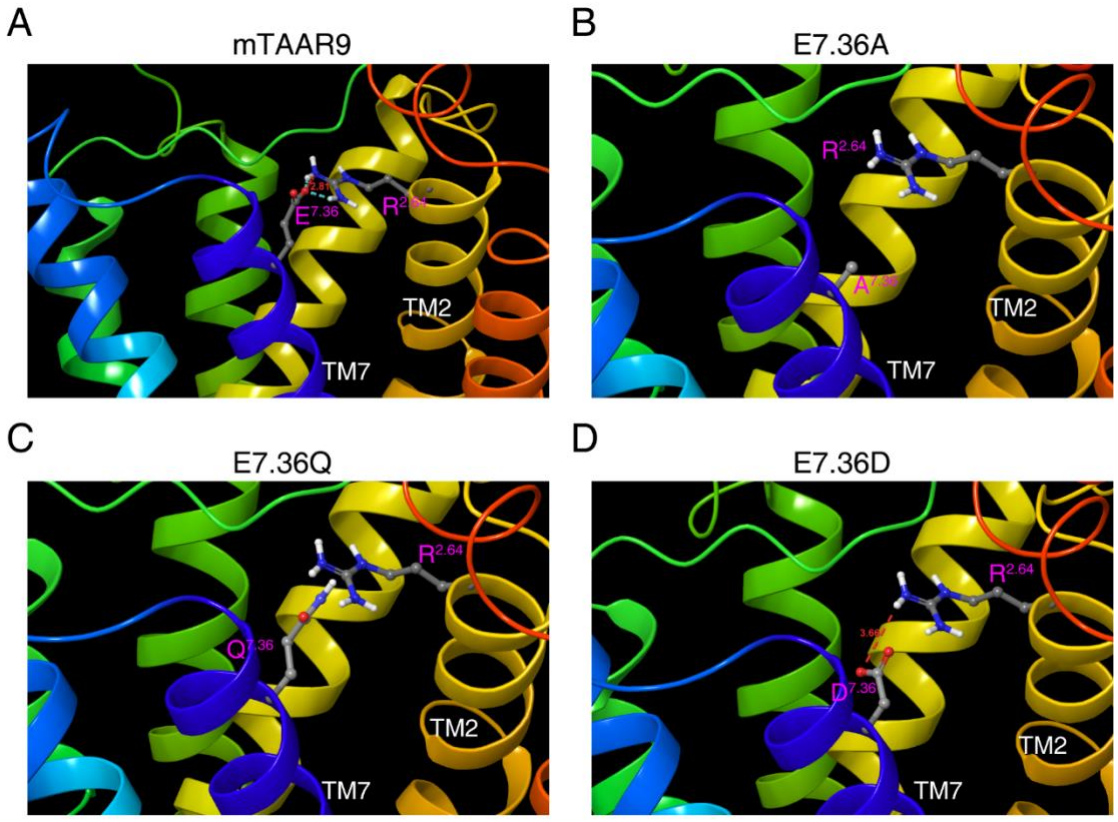

Figure S2-5. Interhelical interactions between Glu$^{7.36}$ and Arg$^{2.64}$ predicted in the homology models of mTAAR9 and its Glu$^{7.36}$ mutants

Side chains of Glu$^{7.36}$ and Arg$^{2.64}$ and major interactions between these two residues were displayed. Red dashed line, salt bridge; cyan dashed line, hydrogen-bond. Distances of the predicted salt bridges in Å were labeled in red. (A) Enlarged view of mTAAR9 predicted interhelical interactions between Glu$^{7.36}$ and Arg$^{2.64}$. (B) Enlarged view of mutant E7.36A predicted spatial position of Arg$^{2.64}$ and mutated Ala$^{7.36}$. (C) Enlarged view of mutant E7.36Q predicted spatial position of Arg$^{2.64}$ and mutated Gln$^{7.36}$. (D) Enlarged view of mutant E7.36D predicted interhelical interactions between Arg$^{2.64}$ and mutated Asp$^{7.36}$.

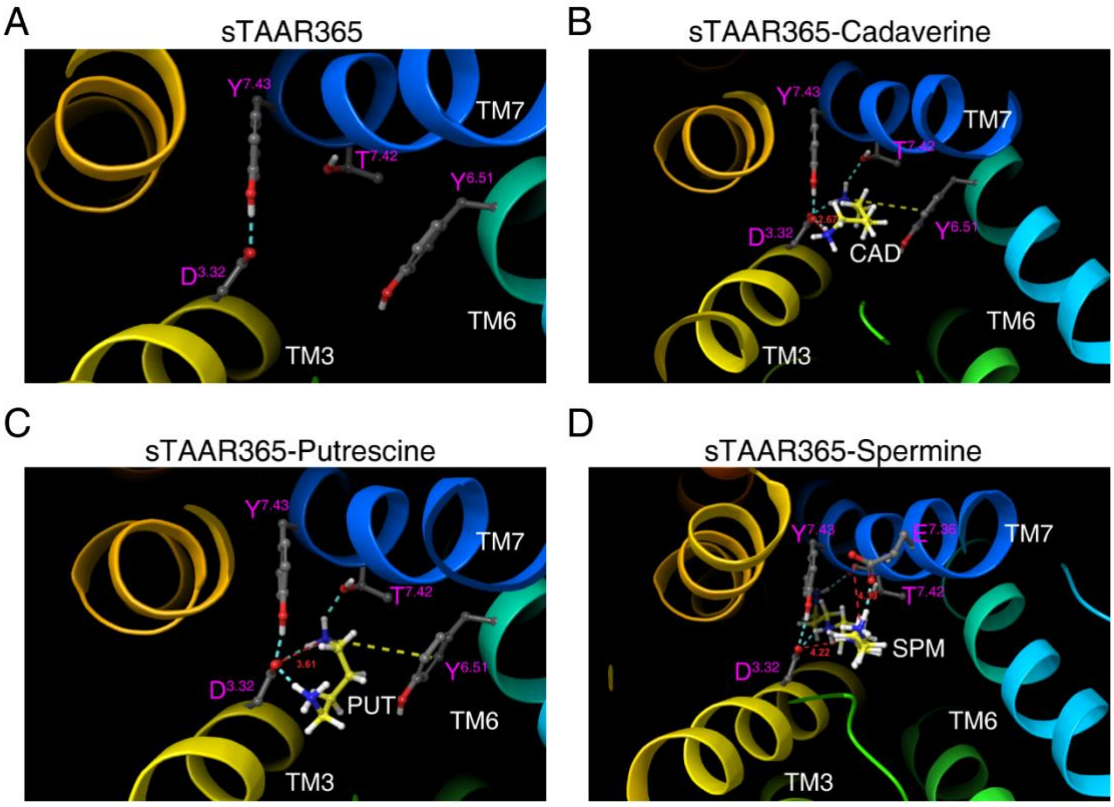

Figure S2-6. Asp$^{3.32}$ is stabilized by an interhelical hydrogen-bond to the hydroxyl group of Tyr$^{7.43}$ in the sTAAR365 homology modeling

Side chains of key residues, ligand, and major interactions were displayed. Red dashed line, salt bridge; cyan dashed line, hydrogen-bond; yellow dashed line, Pi-cation interaction. Distances of the predicted salt bridges in Å were labeled in red. (A) sTAAR365 homology modeling predicted an interhelical hydrogen-bond between Asp$^{3.32}$ and Tyr$^{7.43}$. (B) Docking of cadaverine into sTAAR365 homology model predicted an interhelical hydrogen-bond between Asp$^{3.32}$ and Tyr$^{7.43}$. (C) Docking of putrescine into sTAAR365 homology model predicted an interhelical hydrogen-bond between Asp$^{3.32}$ and Tyr$^{7.43}$. (D) Docking of spermine into sTAAR365 homology model predicted an interhelical hydrogen-bond between Asp$^{3.32}$ and Tyr$^{7.43}$.

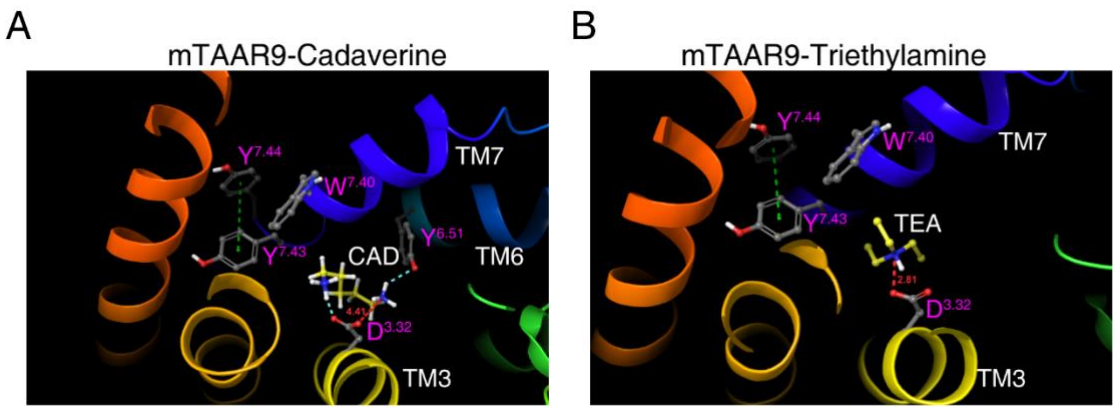

Figure S2-7. Tyr$^{7.43}$ is stabilized by an intramolecular pi-pi stacking to the aromatic side chain of Tyr$^{7.44}$ in mTAAR9 docking models

Side chains of key residues, ligand, and major interactions were displayed. Red dashed line, salt bridge; cyan dashed line, hydrogen-bond; green dashed line, Pi-pi stacking interaction. Distances of the predicted salt bridges in Å were labeled in red. (A) Docking of cadaverine into mTAA9 homology model predicted an intramolecular pi-pi stacking interaction between Tyr$^{7.43}$ and Tyr$^{7.44}$. (B) Docking of triethylamine into mTAA9 homology model predicted an intramolecular pi-pi stacking interaction between Tyr$^{7.43}$ and Tyr$^{7.44}$.

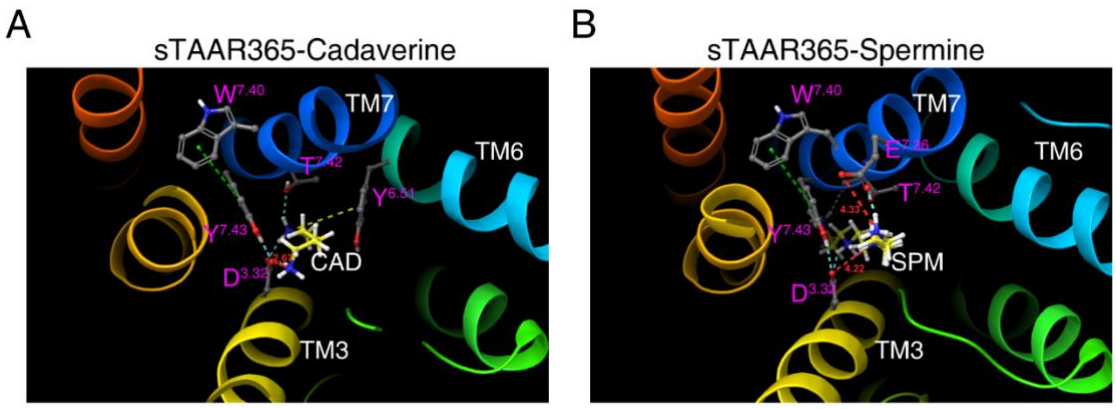

Figure S2-8. Trp$^{7.40}$ contacts Tyr$^{7.43}$ with an intramolecular pi-pi stacking to stabilize Asp$^{3.32}$ in sTAAR365 docking models

Side chains of key residues, ligand, and major interactions were displayed. Red dashed line, salt bridge; cyan dashed line, hydrogen-bond; green dashed line, Pi-pi stacking interaction; yellow dashed line, Pi-cation interaction. Distances of the predicted salt bridges in Å were labeled in red. (A) Docking of cadaverine into sTAAR365 homology model predicted an intramolecular pi-pi stacking interaction between Trp$^{7.40}$ and Tyr$^{7.43}$. (B) Docking of spermine into sTAAR365 homology model predicted an intramolecular pi-pi stacking interaction between Trp$^{7.40}$ and Tyr$^{7.43}$.

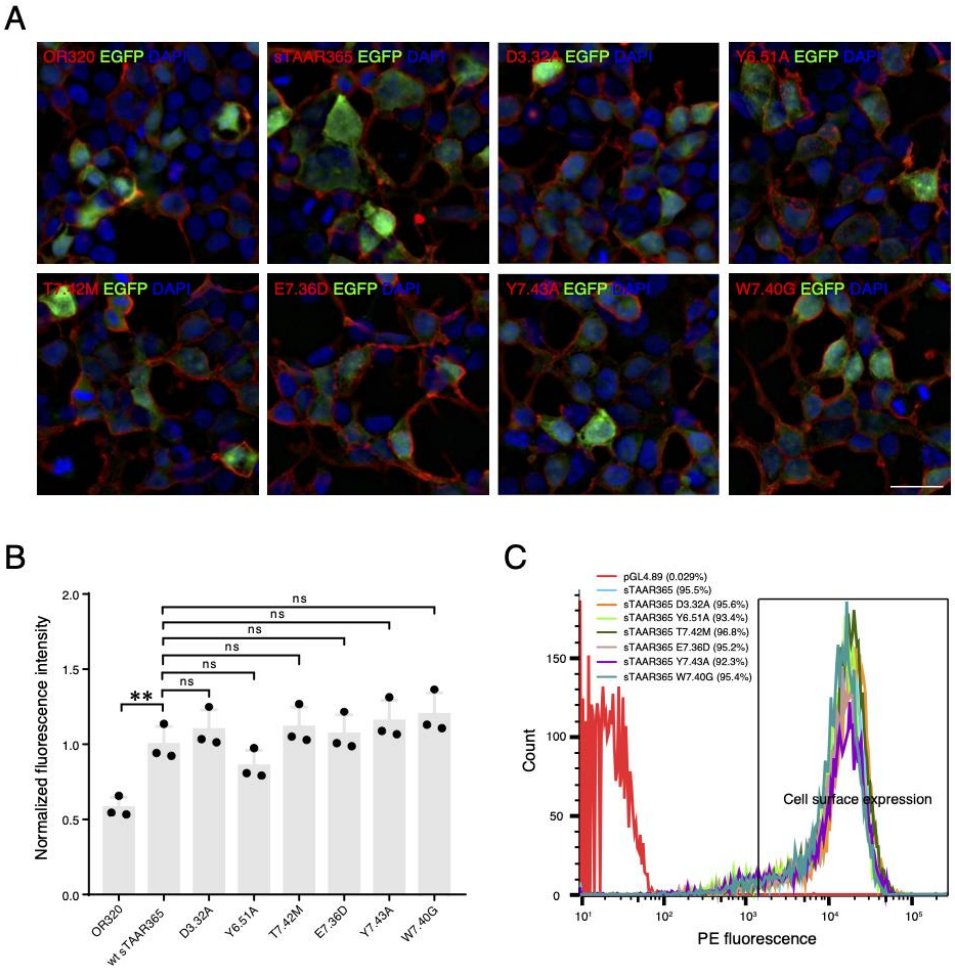

Figure S2-9. sTAAR365 mutants are well-expressed on the surface of HEK293T cells with comparable expression level to wildtype sTAAR365

(A) sTAAR365 and its mutants are well-expressed on the cytomembrane of HEK293T cells as shown by the immunostained Rho-tag antibody (red) for membrane-bound expression. HEK293T cells expressing sTAAR365, sTAA365 mutants, and OR320 were labeled with mouse monoclonal anti-Rho-tag antibody (without permeation) and incubated with red-fluorescent Alexa Fluor 594 goat anti-mouse IgG. Receptors located on the cell surface appeared as red rings around the nucleus. The nucleus was counterstained with DAPI (blue). EGFP was used as a control to evaluate transfection efficiency (green). Scale bar: 30 μm. (B) The mean value of red fluorescent signals of sTAAR365, mutants, and control OR320 were quantified by LAS X software (Leica). Red fluorescent intensity of sTAAR365 mutants and control OR320 was normalized to fluorescence value of wildtype sTAAR365. All mutants showed no significant difference in membrane expression level from wildtype sTAAR365 (mean ± S.D., n = 3; One-way ANOVA, $p > 0.25$). (C) HEK293T cells expressing sTAAR365 and sTAAR365 mutant receptors were labeled with mouse monoclonal anti-Rho-tag antibody (without permeation) and incubated with phycoerythrin-conjugated donkey anti-mouse IgG to perform flow cytometry analysis. The numbers inside the parentheses represent the percent of phycoerythrin positive cells among EGFP positive cells. D3.32A, Y6.51A, T7.42M, E7.36D, Y7.43A, and W7.40G mutants showed comparable cell-surface expression level to wildtype sTAAR365.

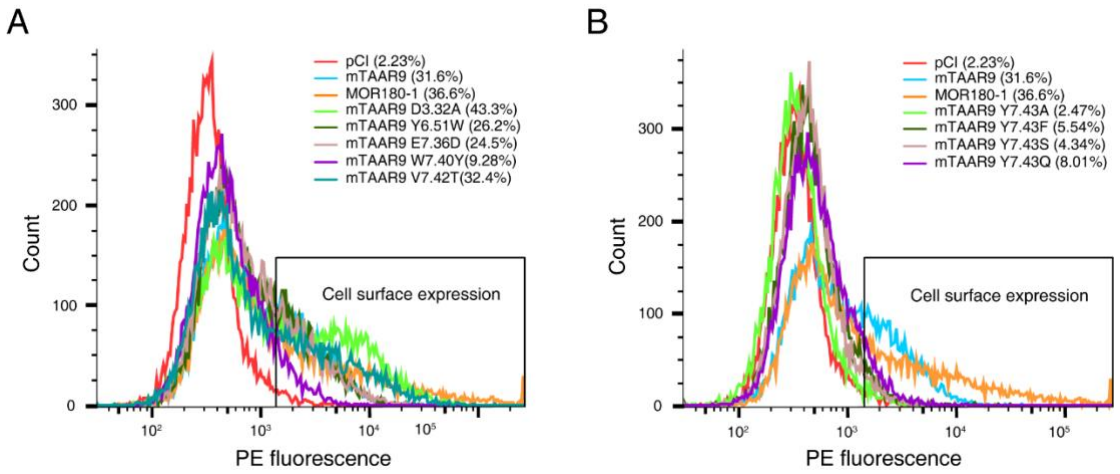

Figure S2-10. Flow cytometry analysis of mTAAR9 and its mutants
Hana3A cells expressing mTAAR9, mTAA9 mutants, and controls were labeled with mouse monoclonal anti-Rho-tag antibody (without permeation) and incubated with phycoerythrin-conjugated donkey anti-mouse IgG to perform flow cytometry analysis. The numbers inside the parentheses represent the percent of phycoerythrin positive cells among EGFP positive cells. (A) D3.32A, Y6.51W, E7.36D, and V7.42T mutants showed comparable cell-surface expression level to wildtype mTAAR9. W7.40Y mutant showed significant decrease in cell-surface expression level compared to wildtype mTAAR9. (B) Y7.43A, Y7.43F, Y7.43S, and Y7.43Q mutants showed drastic decrease in cell-surface expression level compared to the wildtype mTAAR9.

Receptor	Sequence (5'-3')
mTAAR2-F	TTGCGGCCGCGATGGCATCTTTTGAAGCCCAG
mTAAR2-R	CGGAATTCCTATTCTGTTTCTTTTTGAGT
mTAAR3-F	TTGCGGCCGCGATGGATCTAATATACATTCCC
mTAAR3-R	CGGAATTCTTAATGTGCTTCAGGAAAAAG
mTAAR4-F	TTGCGGCCGCGATGAATACACCCGACCCCTGG
mTAAR4-R	CGGAATTCCTAAGGATGTGCAGGATGCAG
mTAAR5-F	TTGCGGCCGCGATGAGAGCTGTCCTCCTCCCGG
mTAAR5-R	CGGAATTCCTCAGTCATGGTATAAATCAACA
mTAAR6-F	TTGCGGCCGCGATGGGCAGTAACTCGTCTCCG
mTAAR6-R	CGGAATTCTTATATTTGCTCAGAGAACAAG
mTAAR7a-F	TTGCGGCCGCGATGGACAAATTGGTTGACCATT
mTAAR7a-R	CCCTCGAGCTACTCAGGAAACAAGTTGGTG
mTAAR7b-F	TTGCGGCCGCGATGGCTACAGATAATGACAGTT
mTAAR7b-R	CCCTCGAGCTACTCAGGAAACAAGTTGGTG
mTAAR7d-F	TTGCGGCCGCGATGGCTACAGGTGATGACAGTT
mTAAR7d-R	CCCTCGAGCTATTCAGGAAACAGGTTGGTG
mTAAR7e-F	TTGCGGCCGCGATGGCTACAGGTGATGACAGT
mTAAR7e-R	CGGAATTCCTACTCAGGAAACAGGTTGGT
mTAAR7f-F	TTGCGGCCGCGATGTCTATAGCTGATGAAACTG
mTAAR7f-R	CGGAATTCCTACTCAGAAAACAGATTGGT
mTAAR8a-F	TTGCGGCCGCGATGACCAGCAACTTTTCCCAA
mTAAR8a-R	CGGAATTCTTACTCTGAAAATAAATTTGCA
mTAAR8b-F	TTGCGGCCGCGATGACCAGCAACTTTTCCCAA
mTAAR8b-R	CGGAATTCTTACTCTGAAAACAAACTCATG
mTAAR8c-F	TTGCGGCCGCGATGACCAGCAACTTTTCCCAA
mTAAR8c-R	CGGAATTCTTACTCTGAAAATAAATTTGT
mTAAR9-F	TTGCGGCCGCGATGACAAGCGACTTCTCCCCA
mTAAR9-R	CGGAATTCTTAACCTGCACCTGCCTCTTC
human TAAR9-F	TTGCGGCCGCGATGGTGAACAATTTCTCCCA
human TAAR9-R	CGGAATTCTTAATCTGTCTCTACTTCTT
hamster TAAR9-F	TTGCGGCCGCGATGGCAAGCAACTTCTCCCCT
hamster TAAR9-R	CGGAATTCTTAACCTACATCTGCCTCTTC
rat TAAR9-F	TTGCGGCCGCGATGGAGCTCTGCTACGAGAAC
rat TAAR9-R	CGGAATTCTTAACCTGCACCTGCTTCTT
cat TAAR9-F	TTGCGGCCGCGATGGTGAACAATTCCGCCCA
cat TAAR9-R	CGGAATTCTCACTCTATATCTGCTTCCT
rabbit TAAR9-F	TTGCGGCCGCGATGGCAGCTGTGGAGTTCTG
rabbit TAAR9-R	CGGAATTCTTAATCTATATCTGCCTCTTC
sTAAR365-F	TTGCGGCCGCGATGGAAACACTGAACGAGTCC
sTAAR365-R	CGGAATTCTCACCTATCTGACTCCTTGCC

Table S2-1. Primers of PCR for mouse olfactory TAARs, mammalian TAAR9 and sTAAR365

mTAAR9 Mutant	Sequence (5'-3')
D3.32A-F	TTCCACACGTGTTTCGCCACCTCCTTCTGT
D3.32A-R	GCGAAACACGTGTGGAACTTACAGTAACTC
D3.32E-F	TTCCACACGTGTTTCGAAACCTCCTTCTGT
D3.32E-R	TTCGAAACACGTGTGGAACTTACAGTAACT
D3.32N-F	TTCCACACGTGTTTCCAAACCTCCTTCTGT
D3.32N-R	TTGGAAACACGTGTGGAACTTACAGTAACT
Y6.51A-F	CGTGTCCTGGCTGCCAGCCATTATTGATGC
Y6.51A-R	GCTGGCAGCCAGGACACGAGAAATGCAGCC
Y6.51F-F	CGTGTCCTGGCTGCCATTCATTATTGATGC
Y6.51F-R	AATGGCAGCCAGGACACGAGAAATGCAGCC
Y6.51W-F	CGTGTCCTGGCTGCCATGGATTATTGATGC
Y6.51W-R	CCATGGCAGCCAGGACACGAGAAATGCAGC
V7.42T-F	ATTAGTGTGGTGTACTTACTACAATTCAG
V7.42T-R	AGTACACCACACTAATATCTCATAGACGT
E7.36A-F	TGCGTACGTCTATGCGATATTAGTGTG
E7.36A-R	CGCATAGACGTACGCAGGAGTTATGAAG
E7.36D-F	TGCGTACGTCTATGACATATTAGTGTG
E7.36D-R	GTCATAGACGTACGCAGGAGTTATGAAG
E7.36Q-F	CCTGCGTACGTCTATCAGATATTAGTGTGG
E7.36Q-R	GATAGACGTACGCAGGAGTTATGAAGTTCA
Y7.43A-F	ATATTAGTGTGGTGTGTTGCCTACAATTCAGCTATGAACC
Y7.43A-R	GGTTCATAGCTGAATTGTAGGCAACACACCACACTAATAT
Y7.43F-F	TAGTGTGGTGTGTTTTCTACAATTCAGCTA
Y7.43F-R	AAAACACACCACACTAATATCTCATAGACG
Y7.43Q-F	AGTGTGGTGTGTTCAATACAATTCAGCTA
Y7.43Q-R	TTGAACACACCACACTAATATCTCATAGA
Y7.43S-F	AGTGTGGTGTGTTTCCTACAATTCAGCTA
Y7.43S-R	GGAAACACACCACACTAATATCTCATAGA
W7.40A-F	GTCTATGAGATATTAGTGGCGTGTGTTTACTACAATTCAG
W7.40A-R	CTGAATTGTAGTAAACACACGCCACTAATATCTCATAGAC
W7.40F-F	GTCTATGAGATATTAGTGTTCTGTGTTTACTACAATTCAG
W7.40F-R	CTGAATTGTAGTAAACACAGAACACTAATATCTCATAGAC
W7.40Y-F	GTCTATGAGATATTAGTGTATTGTGTTTACTACAATTCAG
W7.40Y-R	CTGAATTGTAGTAAACACAATACACTAATATCTCATAGAC

Table S2-2. Primers of PCR for mTAAR9 mutants

sTAAR365 Mutant	Sequence (5'-3')
D3.32A-F	GAGTGCAAAGTGTGTAGGCGAACCACGAGTGTATC
D3.32A-R	GATACACTCGTGGTTCGCCTACACACTTTGCACTC
D3.32E-F	AGAGTGCAAAGTGTGTACTCGAACCACGAGTGTAT
D3.32E-R	ATACACTCGTGGTTCGAGTACACACTTTGCACTCT
D3.32N-F	GAGTGCAAAGTGTGTAGTTGAACCACGAGTGTATCTT
D3.32N-R	AAGATACACTCGTGGTTCAACTACACACTTTGCACTC
Y6.51A-F	GTCGACACCACGAAGGCCGGCATCCAGAGCGA
Y6.51A-R	TCGCTCTGGATGCCGGCCTTCGTGGTGTCGAC
Y6.51F-F	TCGACACCACGAAGAACGGCATCCAGAGC
Y6.51F-R	GCTCTGGATGCCGTTCTTCGTGGTGTCGA
Y6.51L-F	GTTGTCGACACCACGAATAACGGCATCCAGAGCGAG
Y6.51L-R	CTCGCTCTGGATGCCGTTATTCGTGGTGTCGACAAC
T7.42A-F	CCGTTGAGTTGATGTACGCGAACCAGTTGATGAACTC
T7.42A-R	GAGTTCATCAACTGGTTCGCGTACATCAACTCAACGG
T7.42M-F	CACCGTTGAGTTGATGTACATGAACCAGTTGATGAACTC
T7.42M-R	GAGTTCATCAACTGGTTCATGTACATCAACTCAACGGTG
T7.42S-F	CCGTTGAGTTGATGTACGAGAACCAGTTGATGAACTC
T7.42S-R	GAGTTCATCAACTGGTTCTCGTACATCAACTCAACGG
T7.42V-F	CACCGTTGAGTTGATGTACACGAACCAGTTGATGAACTCC
T7.42V-R	GGAGTTCATCAACTGGTTCGTGTACATCAACTCAACGGTG
E7.36A-F	AACCAGTTGATGAACGCCCACGCCAACGAGC
E7.36A-R	GCTCGTTGGCGTGGGCGTTCATCAACTGGTT
E7.36D-F	TGAACCAGTTGATGAAATCCCACGCCAACGAGC
E7.36D-R	GCTCGTTGGCGTGGGATTTCATCAACTGGTTCA
E7.36Q-F	CCAGTTGATGAACTGCCACGCCAACGAGC
E7.36Q-R	GCTCGTTGGCGTGGCAGTTCATCAACTGG
Y7.43A-F	GATTCACCGTTGAGTTGATGGCCGTGAACCAGTTGATGAACT
Y7.43A-R	AGTTCATCAACTGGTTCACGGCCATCAACTCAACGGTGAATC
Y7.43F-F	TCACCGTTGAGTTGATGAACGTGAACCAGTTGATG
Y7.43F-R	CATCAACTGGTTCACGTTCATCAACTCAACGGTGA
Y7.43Q-F	GATTCACCGTTGAGTTGATCTGCGTGAACCAGTTGATGAAC
Y7.43Q-R	GTTCATCAACTGGTTCACGCAGATCAACTCAACGGTGAATC
Y7.43S-F	GATTCACCGTTGAGTTGATGCTCGTGAACCAGTTGATGAACT
Y7.43S-R	AGTTCATCAACTGGTTCACGAGCATCAACTCAACGGTGAATC
Y7.43L-F	GGATTCACCGTTGAGTTGATTAACGTGAACCAGTTGATGAAC
Y7.43L-R	GTTCATCAACTGGTTCACGTTAATCAACTCAACGGTGAATCC
W7.40G-F	GTTGATGTACGTGAACCCGTTGATGAACTCCCACG
W7.40G-R	CGTGGGAGTTCATCAACGGGTTCACGTACATCAAC
W7.40F-F	TTGAGTTGATGTACGTGAAGAAGTTGATGAACTCCCACGC
W7.40F-R	GCGTGGGAGTTCATCAACTTCTTCACGTACATCAACTCAA
W7.40Y-F	GGCGTGGGAGTTCATCAACTATTTCACGTACATCAACTCAAC
W7.40Y-R	GTTGAGTTGATGTACGTGAAATAGTTGATGAACTCCCACGCC

Table S2-3. Primers of PCR for sTAAR365 mutants

ACKNOWLEDGMENTS

We thank Dr H. Matsunami for providing pCI-mRTPs and pCI-$G_{\alpha olf}$ and staff members of US Fish and Wildlife Service and Fisheries and Oceans Canada for providing sea lamprey.

AUTHOR CONTRIBUTIONS

Conceptualization: Liang Jia, Shengju Li, Wenxuan Dai, Lingna Guo, Zhengrong Xu, Richard R. Neubig, Qian Li, Weiming Li.

Data curation: Liang Jia, Shengju Li, Wenxuan Dai, Richard R. Neubig, Qian Li, Weiming Li.

Formal analysis: Liang Jia, Shengju Li, Wenxuan Dai, Qian Li.

Funding acquisition: Qian Li, Weiming Li.

Investigation: Liang Jia, Shengju Li, Wenxuan Dai, Lingna Guo, Zhengrong Xu, Anne M. Scott, Zhe Zhang, Jianfeng Ren, Qinghua Zhang, Yu-Wen Chung-Davidson.

Supervision: Richard R. Neubig, Qian Li, Weiming Li.

Validation: Liang Jia, Shengju Li, Richard R. Neubig.

Visualization: Liang Jia.

Writing-original draft: Liang Jia, Shengju Li, Qian Li.

Writing-review and editing: Liang Jia, Anne M. Scott, Richard R. Neubig, Qian Li, Weiming Li.

REFERENCES

REFERENCES

1. Kandel, E. R., Schwartz, J. H., Jessell, T. M., Siegelbaum, S. A., and Hudspeth, A. J. Principles of Neural Science, McGraw-Hill Medical, New York, NY; 2000.

2. Liu, Y., Zhao, J., and Guo, W. Emotional roles of mono-aminergic neurotransmitters in major depressive disorder and anxiety disorders. Front. Psychol. 2018;9,2201.

3. Liu, Y., Zhao, J., Fan, X., and Guo, W. Dysfunction in serotonergic and noradrenergic systems and somatic symptoms in psychiatric disorders. Front. Psychiatry. 2019;10, 286.

4. Andersen, G., Marcinek, P., Sulzinger, N., Schieberle, P., and Krautwurst, D. Food sources and biomolecular targets of tyramine. Nutr. Rev. 2019;77,107–115.

5. Scott, A. M., Zhang, Z., Jia, L., Li, K., Zhang, Q., Dexheimer, T., Ellsworth, E., Ren, J., Chung-Davidson, Y. W., Zu, Y., Neubig, R. R., and Li, W. Spermine in semen of male sea lamprey acts as a sex pheromone. PLoS Biol. 2019;17,e3000332.

6. Liberles, S. D., and Buck, L. B. A second class of chemosensory receptors in the olfactory epithelium. Nature. 2006;442,645–650.

7. Ferrero, D. M., Lemon, J. K., Fluegge, D., Pashkovski, S. L., Korzan, W. J., Datta, S. R., Spehr, M., Fendt, M., and Liberles, S. D. Detection and avoidance of a carnivore odor by prey. Proc. Natl. Acad. Sci. U. S. A. 2011;108,11235–11240.

8. Ferrero, D. M., and Liberles, S. D. The secret codes of mammalian scents. Wiley Interdiscip. Rev. Syst. Biol. Med. 2010;2,23–33.

9. Hussain, A., Saraiva, L. R., Ferrero, D. M., Ahuja, G., Krishna, V. S., Liberles, S. D., and Korsching, S. I. High-affinity olfactory receptor for the death-associated odor cadaverine. Proc. Natl. Acad. Sci. U. S. A. 2013;110,19579–19584.

10. Muñoz-Esparza, N. C., Latorre-Moratalla, M. L., Comas-Basté, O., Toro-Funes, N., Veciana-Nogués, M. T., and Vidal-Carou, M. C. Polyamines in food. Front. Nutr. 2019;6,108.

11. Sharma, K., Ahuja, G., Hussain, A., Balfanz, S., Baumann, A., and Korsching, S. I. Elimination of a ligand gating site generates a supersensitive olfactory receptor. Sci. Rep. 2016;6,28359.

12. Ferrero, D. M., Wacker, D., Roque, M. A., Baldwin, M. W., Stevens, R. C., and Liberles, S. D. Agonists for 13 trace amine-associated receptors provide insight into the molecular basis of odor selectivity. ACS Chem. Biol. 2012;7,1184–1189.

13. Li, Q., Tachie-Baffour, Y., Liu, Z., Baldwin, M. W., Kruse, A. C., and Liberles, S. D. Non-classical amine recognition evolved in a large clade of olfactory receptors. Elife, 2015;4,e10441.

14. Li, Q., and Liberles, S. D. Aversion and attraction through olfaction. Curr. Biol. 2015;25,R120–R129.

15. Li, Q., Korzan, W. J., Ferrero, D. M., Chang, R. B., Roy, D. S., Buchi, M., Lemon, J. K., Kaur, A. W., Stowers, L., Fendt, M., and Liberles, S. D. Synchronous evolution of an odor biosynthesis pathway and behavioral response. Curr. Biol. 2013;23,11–20.

16. Saraiva, L. R., Kondoh, K., Ye, X., Yoon, K. H., Hernandez, M., and Buck, L. B. Combinatorial effects of odorants on mouse behavior. Proc. Natl. Acad. Sci. U. S. A. 2016;113, E3300–E3306.

17. Dewan, A., Pacifico, R., Zhan, R., Rinberg, D., and Bozza, T. Nonredundant coding of aversive odours in the main olfactory pathway. Nature. 2013;497,486–489.

18. Heale, V. R., Petersen, K., and Vanderwolf, C. H. Effect of colchicine-induced cell loss in the dentate gyrus and Ammon's horn on the olfactory control of feeding in rats. Brain Res. 1996;712, 213–220.

19. Rolen, S. H., Sorensen, P. W., Mattson, D., and Caprio, J. Polyaminesas olfactory stimuli in the goldfish Carassius auratus. J. Exp. Biol. 2003;206,1683–1696.

20. Eyun, S. I., Moriyama, H., Hoffmann, F. G., and Moriyama, E. N. Molecular evolution and functional divergence of trace amine-associated receptors. PLoS One. 2016;11,e0151023.

21. Hussain, A., Saraiva, L. R., and Korsching, S. I. Positive Darwinian selection and the birth of an olfactory receptor clade in teleosts. Proc. Natl. Acad. Sci. U. S. A. 2009;106,4313–4318.

22. Li, Q. Chapter 4-odor sensing by trace amine-associated receptors. In: Zufall, F., Munger, S. D., eds. Chemosensory Transduction. In Methods Mol Biol, Academic Press, Cambridge, MA: 2018;21–31.

23. Huang, E. S. Construction of a sequence motif characteristic of aminergic G protein-coupled receptors. Protein Sci. 2003;12,1360–1367.

24. Saito, H., Kubota, M., Roberts, R. W., Chi, Q., and Matsunami, H. RTP family members induce functional expression of mammalian odorant receptors. Cell. 2004;119,679–691.

25. Rinaldi, A. The scent of life. The exquisite complexity of the sense of smell in animals and humans. EMBO Rep. 2007;8,629–633.

26. Saito, H., Chi, Q., Zhuang, H., Matsunami, H., and Mainland, J. D. Odor coding by a Mammalian receptor repertoire. Sci. Signal. 2009;2,ra9.

27. Katada, S., Hirokawa, T., Oka, Y., Suwa, M., and Touhara, K. Structural basis for a broad but selective ligand spectrum of a mouse olfactory receptor: Mapping the odorant-binding site. J. Neurosci. 2005;25,1806–1815.

28. Roth, B. L., Shoham, M., Choudhary, M. S., and Khan, N. Identification of conserved aromatic residues essential for agonist binding and second messenger production at 5-hydroxytryptamine2A receptors. Mol. Pharmacol. 1997;52,259–266.

29. Fu, D., Ballesteros, J. A., Weinstein, H., Chen, J., and Javitch, J. A. Residues in the seventh membrane-spanning segment of the dopamine D2 receptor accessible in the binding-site crevice. Biochemistry. 1996;35,11278–11285.

30. Wess, J., Nanavati, S., Vogel, Z., and Maggio, R. Functional role of proline and tryptophan residues highly conserved among G protein-coupled receptors studied by mutational analysis of the m3 muscarinic receptor. EMBO J. 1993;12,331–338.

31. Strader, C. D., Sigal, I. S., and Dixon, R. A. Structural basis of beta-adrenergic receptor function. FASEB J. 1989;3,1825–1832.

32. Izquierdo, C., Gomez-Tamayo, J. C., Nebel, J. C., Pardo, L., and Gonzalez, A. Identifying human diamine sensors for death related putrescine and cadaverine molecules. PLoS Comput. Biol. 2018;14,e1005945.

33. Rosenbaum, D. M., Cherezov, V., Hanson, M. A., Rasmussen, S. G., Thian, F. S., Kobilka, T. S., Choi, H. J., Yao, X. J., Weis, W. I., Stevens, R. C., and Kobilka, B. K. GPCR engineering yields high-resolution structural insights into beta2-adrenergic receptor function. Science. 2007;318,1266–1273.

34. Rosenbaum, D. M., Rasmussen, S. G., and Kobilka, B. K. The structure and function of G-protein-coupled receptors. Nature. 2009;459,356–363.

35. Shimamura, T., Shiroishi, M., Weyand, S., Tsujimoto, H., Winter, G., Katritch, V., Abagyan, R., Cherezov, V., Liu, W., Han, G. W., Kobayashi, T., Stevens, R. C., and Iwata, S. Structure of the human histamine H1 receptor complex with doxepin. Nature. 2011;475,65–70.

36. Vass, M., Podlewska, S., de Esch, I. J. P., Bojarski, A. J., Leurs, R., Kooistra, A. J., and de Graaf, C. Aminergic GPCR-ligand interactions: A chemical and structural map of receptor mutation data. J. Med. Chem. 2019;62,3784–3839.

37. Borowsky, B., Adham, N., Jones, K. A., Raddatz, R., Artymyshyn, R., Ogozalek, K. L., Durkin, M. M., Lakhlani, P. P., Bonini, J. A., Pathirana, S., Boyle, N., Pu, X., Kouranova, E., Lichtblau, H., Ochoa, F. Y., et al. (2001) Trace amines: Identification of a family of mammalian G protein-coupled receptors. Proc. Natl. Acad. Sci. U. S. A. 2001;98,8966– 8971.

38. Lindemann, L., Ebeling, M., Kratochwil, N. A., Bunzow, J. R., Grandy, D. K., and Hoener, M. C. Trace amine-associated receptors form structurally and functionally distinct subfamilies of novel G protein-coupled receptors. Genomics. 2005;85,372–385.

39. Hashiguchi, Y., and Nishida, M. Evolution of trace amine associated receptor (TAAR) gene family in vertebrates: Lineage-specific expansions and degradations of a second class of vertebrate chemosensory receptors expressed in the olfactory epithelium. Mol. Biol. Evol. 2007;24, 2099–2107.

40. Thal, D. M., Sun, B., Feng, D., Nawaratne, V., Leach, K., Felder, C. C., Bures, M. G., Evans, D. A., Weis, W. I., Bachhawat, P., Kobilka, T. S., Sexton, P. M., Kobilka, B. K., and Christopoulos, A. Crystal structures of the M1 and M4 muscarinic acetylcholine receptors. Nature. 2016;531,335–340.

41. Takahashi, K., Hossain, M., Ahmed, M., Bhuiyan, M. A., Ohnuki, T., and Nagatomo, T. Asp^{125} and Thr^{130} in transmembrane domain 3 are major sites of alpha1b-adrenergic receptor antagonist binding. Biol. Pharm. Bull. 2007;30,1891–1894.

42. Porter, J. E., Hwa, J., and Perez, D. M. Activation of the alpha1badrenergic receptor is initiated by disruption of an interhelical salt bridge constraint. J. Biol. Chem. 1996;271,28318–28323.

43. Hollingsworth, S. A., Kelly, B., Valant, C., Michaelis, J. A., Mastromihalis, O., Thompson, G., Venkatakrishnan, A. J., Hertig, S., Scammells, P. J., Sexton, P. M., Felder, C. C., Christopoulos, A., and Dror, R. O. Cryptic pocket formation underlies allosteric modulator selectivity at muscarinic GPCRs. Nat. Commun. 2019;10,3289.

44. Xu, Z., and Li, Q. TAAR agonists. Cell. Mol. Neurobiol. 2020;40,257–272.

45. Aurangzeb, Z. Studies of Cells within Three Chemosensory Structures in the Sea Lamprey (Petromyzon marinus), University of Windsor. Master thesis; 2019.

46. Zhang, J., Pacifico, R., Cawley, D., Feinstein, P., and Bozza, T. Ultrasensitive detection of amines by a trace amine-associated receptor. J. Neurosci. 2013;33,3228–3239.

47. Bueb, J. L., Da Silva, A., Mousli, M., and Landry, Y. Natural polyamines stimulate G-proteins. Biochem. J. 1992;282,545–550.

48. Chung-Davidson, Y. W., Rees, C. B., Wu, H., Yun, S. S., and Li, W. beta-naphthoflavone induction of CYP1A in brain of juvenile lake trout (*Salvelinus namaycush Walbaum*). J. Exp. Biol. 2004;207,1533–1542.

49. Zhang, J., Yang, J., Jang, R., and Zhang, Y. GPCR-I-TASSER: A hybrid approach to G protein-coupled receptor structure modeling and the application to the human genome. Structure. 2015;23,1538–1549.

50. Sastry, G. M., Adzhigirey, M., Day, T., Annabhimoju, R., and Sherman, W. Protein and ligand preparation: Parameters, protocols, and influence on virtual screening enrichments. J. Comput. Aided Mol. Des. 2013;27,221–234.

51. Maestro. Schrödinger Release, Schrödinger, LLC, New York, NY; 2020.

52. Farid, R., Day, T., Friesner, R. A., and Pearlstein, R. A. New insights about HERG blockade obtained from protein modeling, potential energy mapping, and docking studies. Bioorg. Med. Chem. 2006;14,3160–3173.

CHAPTER 3

STRUCTURAL DETERMINANTS OF LIGAND-DEPENDENT AND LIGAND-INDEPENDENT ACTIVATION OF AN OLFACTORY TRACE AMINE-ASSOCIATED RECEPTOR

Jia L, Scott AM, Zhang Z, Ren J, Zhang Q, Chung-Davidson YW, Li W, Neubig RR. (2022) Structural determinants of ligand-dependent and ligand-independent activation of an olfactory trace amine-associated receptor. Manuscript in preparation.

ABSTRACT

G protein-coupled receptors can exhibit constitutive activity and accumulate second messengers in an agonist-independent manner. Also, olfactory sensory neurons display varying degrees of intrinsic spike firing, suggesting that the constitutive activity of olfactory receptors may modulate olfactory function (1-3). Here, we report that a cadaverine-responsive sea lamprey olfactory trace amine-associated receptor, TAAR346a, displays robust constitutive activity when heterologously expressed in HEK293T cells. Moreover, triethylamine is identified as an inverse agonist to TAAR346a that can specifically attenuate the constitutive activity of the receptor. Combining the application of the inverse agonist and agonist, we show that one negatively-charged residue in TM5, $Asp^{5.42}$, is required for the inverse agonist action of triethylamine. Along with $Asp^{5.42}$, a highly conserved aspartate in TM3, $Asp^{3.32}$, is identified to compose a di-cationic recognition motif for cadaverine binding. By integrating data with homology modeling and mutational analyses, we suggest a novel action of the predicted hydrogen bond $Thr^{3.37}$/$Ala^{5.46}$ which is highly important for the constitutive signaling of TAAR346a, whereas another predicted hydrogen bond $Asn^{1.50}$/$Asp^{2.50}$ contains conserved function as that in other class A constitutively active GPCRs, mediating both agonist-induced and constitutive signaling of the receptor. In contrast, mutation of residues at the proposed hydrophobic barrier and ionic lock between TM3 and TM6 generates variants with a massive increase in constitutive activity. These findings indicate that interhelical interactions may serve different roles in modulating the GPCR activation. Taken together, our results define structural determinants for ligand-dependent and ligand-independent activation of an olfactory trace amine-associated receptor.

INTRODUCTION

Olfaction contributes to a wide variety of critical physiological functions in animals, including predation, mating, predator avoidance, and navigation [4-8]. Odor detection by olfactory sensory neurons (OSNs) in the vertebrate main olfactory epithelium critically relies on the specific binding of divergent odorants to different olfactory receptors. Olfactory receptors make up the largest family of G protein-coupled receptors (GPCRs) and transduce extracellular chemical stimuli into intracellular signals that are ultimately conveyed to the central nervous system [9-12]. Using combinatorial inputs, the olfactory system is able to detect and discriminate various odors. Upon odorant binding, receptors expressed on the cilia of OSNs in the main olfactory epithelium switch into an active conformation that couples with the intracellular olfactory-specific G-protein ($G_{\alpha olf}$) to trigger the cyclic adenosine monophosphate (cAMP) second messenger cascade. cAMP opens cyclic nucleotide gated ion channels (CNGs) enhancing inward Ca^{2+} and Na^{+} currents, which also activate Ca^{2+}-activated Cl^{-} channels, and generate an action potential [13, 14].

Although activation of most GPCRs is agonist-dependent, a number of wild-type GPCRs, such as opioid receptors, cannabinoid receptors, and biogenic amine receptors, exhibit considerable constitutive activity [15]. In the absence of agonist, receptors having low basal activity are constrained to a relatively inactive conformation with a high energy well. Whereas, constitutively active GPCRs with high basal activity have a lower energy barrier and spontaneously flip between active and inactive conformations, resulting in accumulation of second messengers. Binding of an inverse agonist stabilizes the receptor in an inactive conformation, thereby decreasing the constitutive activity. In contrast, binding of an agonist shifts the receptor into an active conformation. Likewise, individual OSNs have been shown to be intrinsically noisy

with varying degrees of basal current in the absence of stimuli. Physiological evidence with mouse OSNs showed that an odorant receptor antagonist can inhibit the agonist-independent OSN activity, thus likely serving as an inverse agonist [2]. Moreover, odorant receptors also play an important role in mediating formation of the topographic projection of activated glomeruli in the olfactory bulb. Agonist-independent GPCR activity can determine anterior-posterior axon targeting of OSNs [3], indicating that the constitutive activity of olfactory receptor could be essential for modulating both short- and long-term olfactory functions. In addition to the odorant receptors, trace amine-associated receptors (TAARs), a distinct subfamily of GPCRs, are highly expressed in a unique subset of ciliated OSNs and function as olfactory receptors with a high affinity for volatile amines (exclusive of the non-olfactory TAAR1) [16, 17]. Ligands identified for TAARs, including cadaverine, putrescine, spermine, and spermidine, can elicit strong innate behavioral responses in a variety of species examined, such as attraction and repulsion [18-23]. The phylogeny of TAARs shows a distant relation to biogenic amine receptors, so we reasoned that olfactory TAARs also may have varying degrees of constitutive activity [24]. Although the odorant selectivity of TAARs and corresponding innate behaviors have been examined, little is known about the molecular and structural basis underlying ligand-independent and ligand-dependent activation of olfactory TAARs.

GPCR activation is associated with the reorientation of transmembrane domains (TMs) [15, 25]. The crystal structures of active class A GPCRs provide evidence that agonist-induced movements of TMs break an intracellular ionic lock and hydrophobic barrier which enable the receptor to form interhelical hydrogen bond networks that transiently stabilize the active conformation [25]. Thus, constitutively active GPCR mutants (CAMs) are thought to disrupt the interactions stabilizing the inactive conformation and to create new interaction networks that shift

the receptor into the active conformation. In addition, the constitutively active receptor maintains an active conformation for ligand binding while coupled with its cognate G protein. These structural changes suggest that the hydrogen bond networks within TMs may act as an essential factor to preserve GPCRs in a relatively active state.

We herein report that a previously deorphanized cadaverine-responsive sea lamprey trace amine-associated receptor [20], TAAR346a, exhibits constitutive activity with considerable basal cAMP production in receptor-expressing HEK293T cells. We conducted a chemical screening and found that triethylamine functions as an inverse agonist to inhibit the TAAR346a constitutive activity in a concentration-dependent manner. Using a joint approach of site-directed mutagenesis, computational modeling, and pharmacologic analysis with the inverse agonist and agonist, we investigated the molecular and structural basis underlying ligand-dependent and ligand-independent activation of TAAR346a. Our results support a model in which the inverse agonist recognizes only one ($Asp^{5.42}$) of the two orthosteric sites ($Asp^{3.32}$ and $Asp^{5.42}$) used by the agonist as it elicits its inhibitory effect on the basal activity of the receptor. We showed that in TAAR346a, a model-predicted hydrogen bond ($Thr^{3.37}$/$Ala^{5.46}$) is highly important for the constitutive signaling of TAAR346a, whereas it serves the opposite function in other class A GPCRs. Also, the others ($Asn^{1.50}$/$Asp^{2.50}$ and $Asp^{5.42}$/$Tyr^{3.33}$) were shown to be critical for both constitutive and agonist-induced activity of TAAR346a. More remarkably, a massive increase in basal activity was observed in mutant receptors which have lost the predicted ionic lock and hydrophobic barrier between TM3 and TM6. These results suggest that residues of these interhelical interactions may act in different functions in the activation of TAAR346a, synergistically stabilizing the receptor in a partially constitutively active state. Taken together, our results provide molecular and structural determinants for activation of a constitutively active olfactory trace amine-associated receptor,

both by ligand-dependent and ligand-independent means.

RESULTS

TAAR346a shows constitutive activity in HEK293T cells

In our previous study [20], we screened 21 putative sea lamprey TAARs for responses to an array of potential ligands. Of those 21 receptors, two (TAAR346a and TAAR365) showed dramatic increases in the cAMP response element (CRE)-driven luciferase signal without olfactory mediators added (Figure S3-1A). Since basal luciferase activity reflects an amplified cAMP signal and could be dependent on the level of receptor expression on the cytomembrane [26], we performed immunocytochemistry to evaluate the membrane expression levels of TAAR346a and TAAR365 (Figure 3-1A and Figure 3-1B). Also, using a well-established LANCE cAMP assay, we directly evaluated basal cAMP levels induced by TAAR346a and TAAR365 and reaffirmed that TAAR346a exhibits constitutive activity with robust basal cAMP production. The basal level of cAMP with TAAR346a was dozens of times higher than that of the mock-transfected control or for cells transfected with the non-constitutively active TAAR348 which expresses at a similar level (Figure 3-1C and Figure S3-1B). However, TAAR365 only showed moderately increased basal cAMP production compared to the non-constitutively active TAAR348 (Figure 3-1C), even while TAAR365 showed a 10-fold higher expression level than TAAR348. Thus, high receptor expression is not a prerequisite for high constitutive activity. In contrast, high luciferase activity generated by TAAR365 is likely related to its high membrane expression level. Since TAAR346a appears to have a higher endogenous basal activity, we have focused the remainder of our studies on TAAR346a.

To understand the potential biological significance of TAAR346a, we asked whether *taar346a* transcripts were expressed in olfactory sensory neurons in the main olfactory epithelium.

The *taar346a* anti-sense probe hybridized to mRNA in a small subset of olfactory sensory neurons in the main olfactory epithelium of adult sea lamprey as is observed for most functional olfactory receptors (Figure S3-1C). Digoxigenin-labeled intact neurons showed a short, thick morphology, with the cell bodies situated deep in the olfactory epithelium and long dendrites projecting towards the epithelial surface. In comparison, no labeling was observed with the control *taar346a* sense probe. Taken together, these results suggest that TAAR346a, which exhibits constitutive activity in a heterologous expression system and is expressed in a population of OSNs in the main olfactory epithelium that functions as a cognate receptor for cadaverine responsiveness.

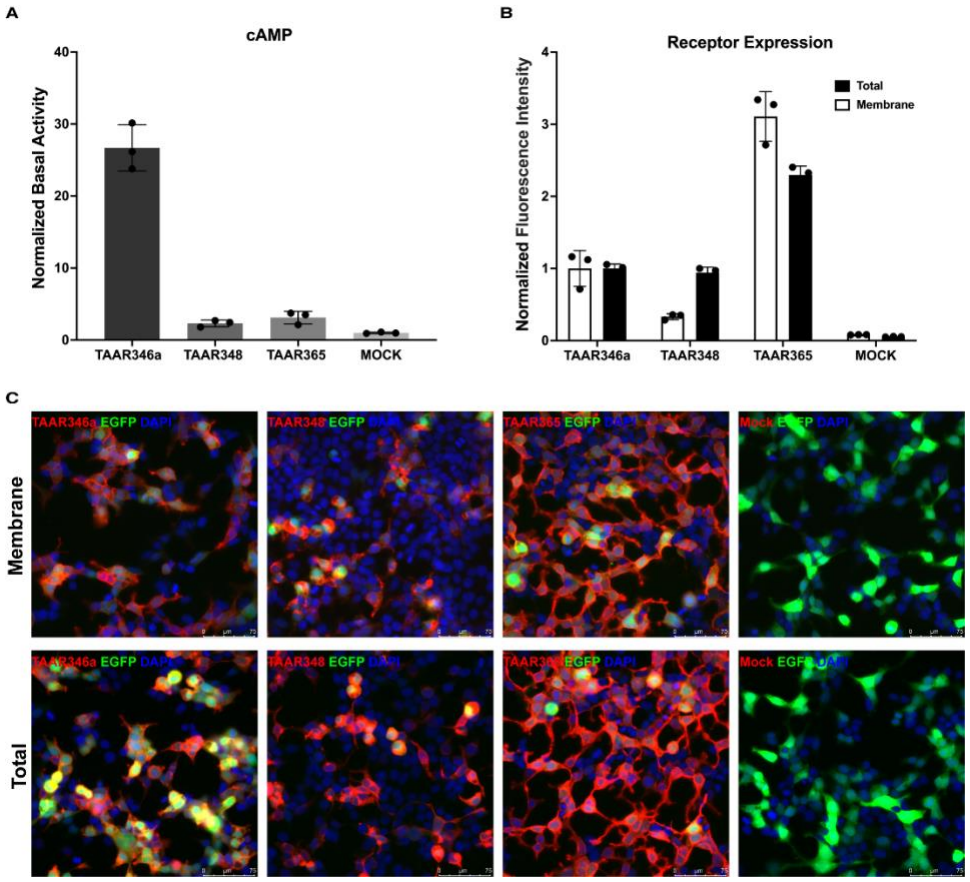

Figure 3-1. TAAR346a showed constitutive activity in TAAR346a expressed HEK293T cells (A) Buffer-stimulated HEK293T cells (ligand-independent) exhibited robust cAMP production when expressing TAAR346a, with 25-fold higher basal activity over the mock transfected cells. The basal cAMP levels were measured with a TR-FRET assay and normalized to the basal cAMP level of mock control (mean ± S.D., n=3). (B) HEK293T cells were transfected with 75ng TAAR 346a, TAAR348, TAAR365, and mock receptor, respectively, together with 375ng pGL4.29, 75ng mRTPs, and 75ng EGFP. Transfected cells were incubated for 24 hours for immunocytochemistry assay. TAAR 346a, TAAR348, TAAR365, and mock receptor were labeled with anti-Rho-tag antibody that colored with red-fluorescent Alexa Fluor 594. Cells were permeabilized or not permeabilized with Triton X-100 to label the whole cell or only cell membrane. Images were acquired at 400 × magnification under DMI8 Thunder (Leica) with DAPA filter, GFP filter, and Texas Red filter, respectively (10 random views/well, mean ± S.D., n=3). The mean value of red-fluorescent signal was quantified with LAS X software (Leica). (C) TAAR346a, TAAR348, and TAAR365 are expressed on cytomembrane of HEK293T cells as shown by the immunostained Rho-tag antibody (red) for membrane-bound (top panel, without permeation) expression. Receptors located on the cell surface appeared as red rings around the nucleus or total (bottom panel, with permeation using Triton X-100). The nucleus was counterstained with DAPI (blue). EGFP was used as the negative control to evaluate transfection efficiency (green). Scale bar: 75 μm.

Triethylamine is an inverse agonist of TAAR346a

We next sought to identify ligands that could modulate the constitutive activity of TAAR346a. As cadaverine is an agonist of TAAR346a (Figure S3-1B) and has been reported to stimulate the mouse receptor TAAR9 and the zebrafish receptor TAAR13c [14, 18, 19, 21, 23], we reasoned that other ligands that affect mTAAR9 and zTAAR13c might be able to modulate the activation of TAAR346a. To this end, we measured the cAMP response of TAAR346a expressing HEK293T cells to compounds that had been shown to activate mTAAR9 and zTAAR13c, including triethylamine, putrescine, spermine, and spermidine. We found minimal stimulation of cAMP accumulation in HEK293T cells expressing TAAR346a in the presence of putrescine, spermine, and spermidine (Figure S3-2). Strikingly, triethylamine (1mM) drastically reduced the constitutive activity of TAAR346a (Figure 3-2A). Further tests showed that triethylamine could attenuate the constitutive activity of TAAR346a in a concentration-dependent manner, with a half maximal inhibitory concentration (IC_{50}) of 495 ± 154 μM (mean ± S.D., n=3) (Figure 3-2B). To ensure that the effect of triethylamine was not due to pH changes in the medium from high concentrations of the bases, we examined cAMP responses of TAAR348 and TAAR365 in HEK293T cells treated by triethylamine. We found that triethylamine is ineffective in modulating either the basal activity or the stimulated activity of cells expressing the other two deorphanized lamprey TAARs (TAAR348 and TAAR365) (Figure S3-3A). Furthermore, triethylamine had no inhibitory effect on the agonist-induced cAMP level with TAAR365 (Figure S3-3B). Thus, we conclude that triethylamine is an inverse agonist of the constitutively active TAAR346a.

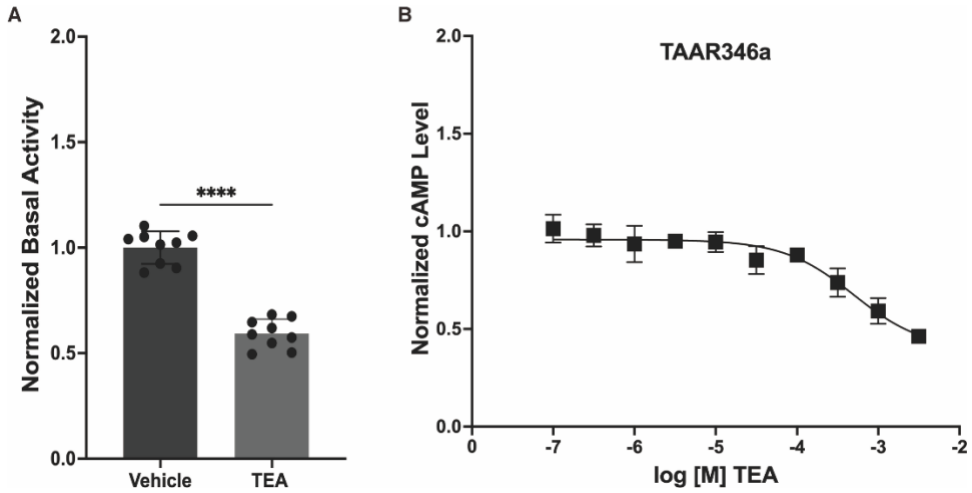

Figure 3-2. Triethylamine significantly attenuated the constitutive activity of TAAR346a
HEK293 cells expressed TAAR346a were incubated with concentration series of triethylamine (100nM to 3.3 mM). Changes in intracellular cAMP production were detected by TR-FRET and normalized to the WT basal cAMP production. The cAMP levels were normalized as measured cAMP /WT basal cAMP. (A) The considerable basal activity of TAAR346a was significantly attenuated by application of 1mM triethylamine (mean ± S.D., n=9; unpaired t test with Welch's correction, two tailed **** *p* value <0.0001). (B) The basal activity of TAAR346a was attenuated after pre-incubation with concentration-dependent triethylamine in TAAR346a expressed HEK293T cells, with a half maximal inhibitory concentration (IC_{50}) occurring at 500 ± 89 μM (mean ± S.D., n=3).

Docking of cadaverine and triethylamine predicts a binding pocket in TM3 and TM5

We then set about exploring the structural basis of TAAR346a for ligand recognition. To do so, we generated a TAAR346a homology model with GPCR-I-TASSER to predict putative residues for cadaverine and triethylamine recognition. The TAAR346a homology model was based on the crystal structures of eight homologous templates and exhibited a canonical GPCR structure with seven hydrophobic transmembrane α-helices and an eighth intracellular helix (H8) in the C-terminus (Figure S3-4B). The TAAR346a shares a maximal identity of 34% and a sequence coverage of 82% to the closest homologous template, the human beta 2-adrenergic G_s-protein complex (Protein Data Bank Entry 3SN6) (Figure S3-4A). In light of the substantial constitutive activity of TAAR346a, it is intriguing that the best homology model comes from an active (G_s-coupled) receptor structure. The homology model with the highest C-score (0.3) was chosen as the final structure for molecular docking.

Based on the homology model, we initially performed docking by using Schrodinger Maestro 11.5 to predict putative residues for cadaverine recognition. The classical amine-binding motif ($Asp^{3.32}$ and $Trp^{7.40}$) of aminergic receptors was defined as the centroid of an enclosing box to perform cadaverine docking within 20 Å of selected residues. The docking model placed cadaverine in close proximity to the highly conserved $Asp^{3.32}$, with a salt bridge to the carboxylic group of $Asp^{3.32}$ (Figure 3-3B and Figure 3-3C). However, docking did not predict $Trp^{7.40}$ to be a binding partner for cadaverine recognition in TAAR346a. The $Trp^{7.40}$ residue was 12.3 Å away from cadaverine excluding any interactions with the ligand (Figure 3-3B and Figure 3-3C). Therefore, we set $Asp^{3.32}$ as the centroid of an enclosing box for further examination of adjacent residues involved in cadaverine recognition. Docking results predicted that $Asp^{3.32}$ and $Asp^{5.42}$, two nearby negatively charged residues in the receptor structure, constitute a di-cationic motif to

contact with the two amine groups of cadaverine. Asp$^{3.32}$ formed a salt bridge with one protonated amino group at a distance of 2.96 Å (Figure 3-3E and Figure 3-3F), meanwhile, the second protonated amino group of cadaverine interacted with the Asp$^{5.42}$ carboxylate through another salt bridge and a hydrogen bond, at a distance of 2.84 Å (Figure 3-3E and Figure 3-3F). The salt bridges between cadaverine and both Asp$^{3.32}$and Asp$^{5.42}$ had distances within the proper range of a salt bridge from 1.75 Å to 4.0 Å [24]. Notably, Trp$^{7.40}$ of the conserved DW motif was 13.4 Å away from cadaverine located at the side of TM7 facing outwards toward membrane lipids (Figure 3-3F). In addition, several other residues were in proximity to cadaverine within the cutoff value of 4.0 Å (Figure S3-5) and thus likely serve to stabilize cadaverine in the binding pocket.

Following a similar strategy as described above, we next performed docking of triethylamine into the TAAR346a homology model. However, docking did not predict Asp$^{3.32}$ to be a binding site for triethylamine, Asp$^{3.32}$ was 8.22 Å away from the docked triethylamine (Figure 3-3H and Figure 3-3I). In contrast, triethylamine was docked in proximity to Asp$^{5.42}$ at a distance of 3.50 Å, forming a salt bridge with the carboxylate group of Asp$^{5.42}$ (Figure 3-3H and Figure 3-3I). The greater length of this salt bridge as well as the existence of only a single contact could explain the much lower potency of triethylamine for TAAR346a. In conclusion, these data suggest that TAAR346a relies on two negatively charged aspartates, Asp$^{3.32}$ and Asp$^{5.42}$, to interact with the two amino groups of cadaverine, while it utilizes only one of the orthosteric sites (Asp$^{5.42}$) for cadaverine to recognize triethylamine. In contrast, the conserved Trp$^{7.40}$ is not involved in the binding of either cadaverine or triethylamine in the docking models.

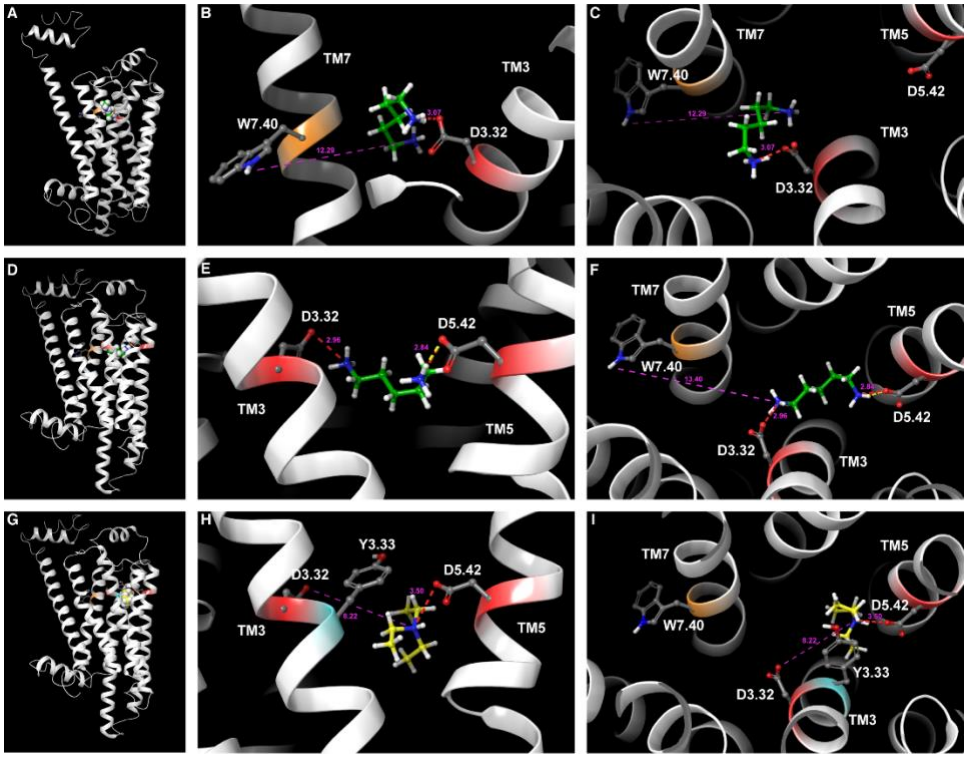

Figure 3-3. The binding sites for cadaverine and triethylamine predicted by docking to wildtype TAAR346a

TAAR346a structure (white) was showed with coordinating residues (aspartate: red; tryptophan: orange; tyrosine: cyan) and docking ligands (cadaverine: green, backbone; blue, amino groups; triethylamine: yellow, backbone; blue, amino group). Red dashed line, salt bridge; yellow dashed line, hydrogen-bond. The distance in Å was visualized as magenta. (A-C) Side profile and enlarged views of TAAR346a structure showed spatial position of cadaverine docking into the classical amine-binding motif ($D^{3.32}$ and $W^{7.40}$). (D-F) Side profile and enlarged views of TAAR346a structure with cadaverine and corresponding residues involved in ligand recognition. Side chains of key residues involved in ligand binding and major interactions between ligand and predicted binding residues were displayed. (G-I) Side profile and enlarged views of TAAR346a structure with triethylamine and corresponding residues involved in ligand recognition. Side chains of key residues involved in ligand binding and major interactions between ligand and predicted binding residues were displayed.

The aspartate Asp$^{5.42}$ in TM5 is required for the inverse agonism of triethylamine

Docking predicted the involvement of the Asp$^{5.42}$ but not the conserved Asp$^{3.32}$ in triethylamine recognition. We therefore hypothesized that mutations of Asp$^{5.42}$ should completely abrogate the inverse agonism of triethylamine. To test this hypothesis, we substituted the Asp$^{5.42}$ residue with asparagine (keep the polarity) or glutamate (keep the charge) to examine their effects on receptor activity, as both mutants retained comparable constitutive activity with wild-type TAAR346a (see baseline values in Figure S3-6A). HEK293T cells were transfected with mutant receptors and triethylamine was added to assess changes in cAMP levels. As predicted by the hypothesis, the D5.42N mutation resulted in complete loss-of-function of triethylamine on the constitutive activity of TAAR346a (Figure 3-4A). We even found that triethylamine induces a minimal increase in the cAMP production at the highest concentration tested. More interestingly, instead of reducing constitutive activity, triethylamine was converted into a weak agonist for the D5.42E mutant, with an EC_{50} value of 447 ± 228 μM (mean ± S.D., n=3) (Figure 3-4A and Figure S3-6B). This is quite similar to the IC_{50} of 495 ± 154 μM for inhibition of the constitutive activity. This retained potency even with the loss of a major contact may be due to new contacts (see modeling results below).

Although the highly conserved Asp$^{3.32}$ residue was not predicted to be triethylamine binding site, we were intrigued whether Asp$^{3.32}$ may contribute to triethylamine function. Two mutants of Asp$^{3.32}$ (D3.32N and D3.32E) were generated to test for triethylamine responses. The D3.32N mutant showed a significant reduction in potency of triethylamine (Figure 3-4B). In contrast, triethylamine, as with the D5.42E mutant, was converted into an agonist for the D3.32E mutant, with an EC_{50} value of 446 ± 167 μM (mean ± S.D., n=3) (Figure 3-4B and Figure S3-6B).

To understand how triethylamine affects the activation of these mutants, we performed

docking into the TAAR346a homology model in which the two aspartate residues were changed to glutamate or asparagine. Indeed, the wild-type salt bridge between the residue 5.42 and triethylamine was absent in the docking model of D5.42E and D3.32E mutants (Figure 3-4C and Figure 3-4D). However, docking studies suggested a pi-cation interaction of $Tyr^{3.33}$ with the amino group of triethylamine. Likewise, the wild-type salt bridge with triethylamine was not observed in the docking model of D5.42N mutant, but triethylamine was predicted to interact with $Tyr^{3.33}$ and $Ser^{3.36}$ forming a pi-cation interaction and a hydrogen bond, respectively (Figure 3-4C). In contrast, docking of triethylamine into the D3.32N mutant predicted the presence of the wild-type salt bridge and a new pi-cation interaction with $Tyr^{3.33}$ (Figure 3-4D). Taken together, all docking studies are consistent with our experimental results that $Asp^{5.42}$ is required for the exertion of an inhibitory effect on the constitutive activity of TAAR346a, potentially by forming a salt bridge with the triethylamine amino group.

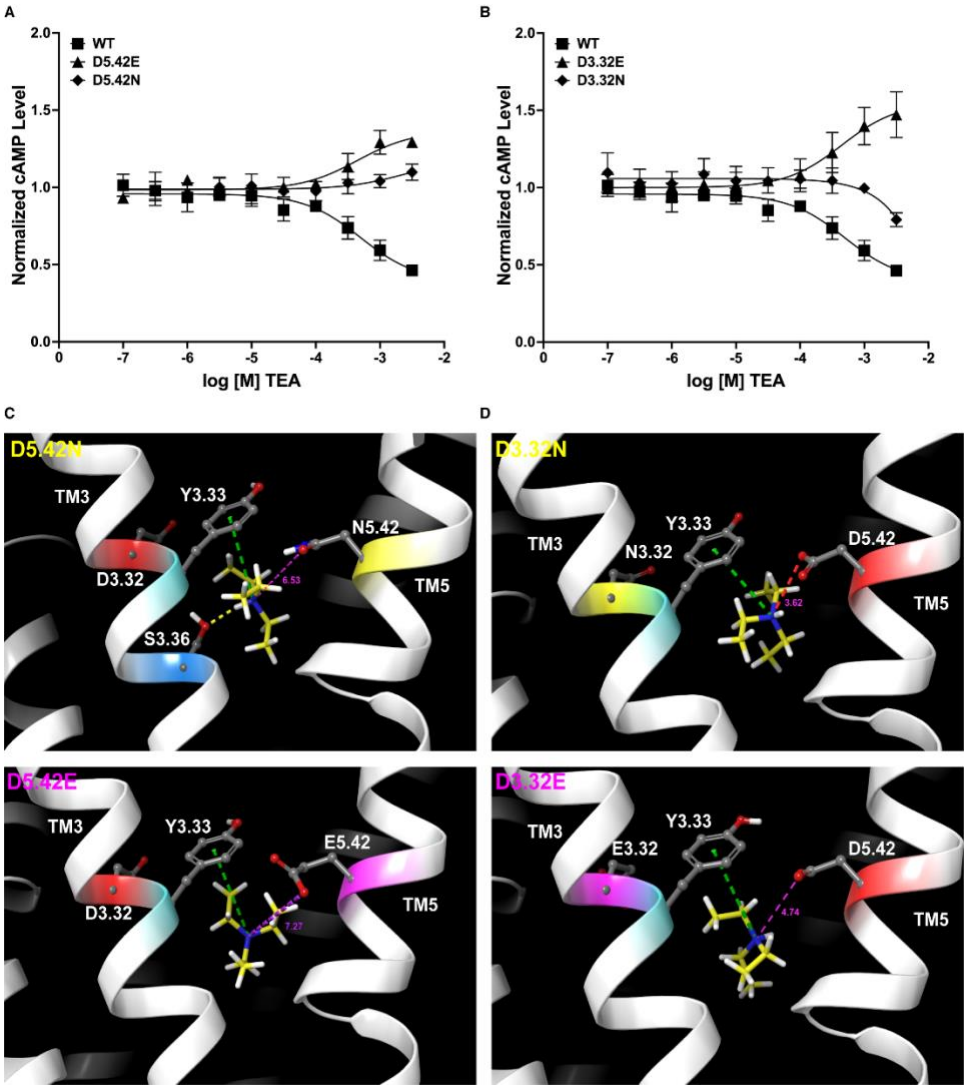

Figure 3-4. Concentration-response curves and docking model of TAAR346a characterized the critical role of $D^{5.42}$ in mediating the inverse agonism of triethylamine

HEK293 cells expressed TAAR346a, $D^{5.42}$ mutants, and $D^{3.32}$ mutants were incubated with concentration-dependent triethylamine (100nM to 3.3 mM). Changes in intracellular cAMP production were detected by TR-FRET and normalized to the basal cAMP production of each receptor. The cAMP levels were normalized as measured cAMP/basal cAMP. TAAR346a mutant structure (white) was showed with coordinating residues (aspartate: red; glutamate: magenta; alanine: violet; asparagine: yellow; tyrosine: cyan; serine: azure) and docking ligand triethylamine (yellow, backbone; blue, amino groups). Red dashed line, salt bridge; yellow dashed line, hydrogen-bond; green dashed line, Pi-interaction. The distance in Å was visualized as magenta. (A) Triethylamine-induced cAMP production in HEK293T cells expressing TAAR346a and its $D^{5.42}$ mutants (D5.42E and D5.42N) (mean ±S.D., n=3). (B) Triethylamine-induced cAMP production in HEK293T cells expressing TAAR346a and its $D^{3.32}$ mutants (D3.32E and D3.32N) (mean ±S.D., n=3). (C) Enlarged views of $D^{5.42}$ mutant structures with triethylamine and corresponding residues involved in ligand recognition. Side chains of key residues involved in ligand binding and major interactions between ligand and predicted binding residues were displayed.

Figure 3-4 (cont'd).
(D) Enlarged views of $D^{3.32}$ mutant structures with triethylamine and corresponding residues involved in ligand recognition. Side chains of key residues involved in ligand binding and major interactions between ligand and predicted binding residues were displayed.

The aspartates Asp$^{3.32}$ and Asp$^{5.42}$ are critical for activation of TAAR346a by cadaverine

As described above, docking with cadaverine suggested that TAAR346a utilizes Asp$^{3.32}$ and Asp$^{5.42}$ to recognize its two amino groups. Following the above-mentioned strategy, we generated mutants (alanine, asparagine, and glutamate) for both aspartates Asp$^{3.32}$ and Asp$^{5.42}$ to validate docking predictions. HEK293T cells expressing mutant receptors were stimulated with cadaverine to assess effects on cAMP levels. Functional testing showed that mutation to alanine (D3.32A and D5.42A) completely abolished cadaverine-evoked responses (Figure 3-5A). Notably, the D5.42A mutant exhibited a drastic decrease in its basal activity, but not the D3.32A mutant (Figure 3-5A and Figure S3-6A). Immunocytochemistry analysis revealed that the D5.42A mutant did not impair cell surface trafficking (Figure S3-8), suggesting that there may be a conformational change due to the major alteration in side-chain properties (e.g. charge and H-bonding) rather than complete loss of receptor expression and localization.

We then examined the effects of the conservative changes, from aspartate to glutamate or asparagine, on receptor activity. The D3.32N and D5.42N mutants retained comparable basal activity as wild-type TAAR346a, but showed nearly complete abolition of cadaverine responses (Figure 3-5A and Figure 3-5B). In contrast, the most conservative substitutions, D5.42E, retained cadaverine-evoked activity, with a similar potency as wild-type TAAR346a (Figure 3-5B). The same result was obtained for the D3.32E mutant, but showing a substantial decrease in potency (15-fold). Furthermore, a modest (40-50%) increase of basal activity was observed for the D5.42E mutant, while the D3.32E mutant showed a slight reduction (20-30%) of basal activity compared to the wild-type TAAR346a (Figure S3-6A).

As expected, docking with cadaverine predicted the absence of the wild-type salt bridge between the asparagine and the amino group of cadaverine in the D3.32N and D5.42N mutants

(Figure 3-5C and Figure 3-5D). The distance between the polar asparagine side chain and the amino group of cadaverine was predicted to be 6.55 Å and 6.46 Å, respectively, well beyond the range of a salt bridge. However, two polar residues ($Ser^{6.55}$ and $Ser^{3.36}$), respectively, was predicted to interact with one amino group of cadaverine by forming a hydrogen bond, which may contribute to the residual cadaverine responses (Figure 3-5C and Figure 3-5D). Also, the wild-type salt bridge between the aspartate and the amino group of cadaverine was not predicted in the D3.32E and D5.42E mutants. Docking studies suggested a pi-cation interaction of $Tyr^{3.33}$ with one amino group of cadaverine that functions as part of cadaverine binding motif (Figure 3-5C and Figure 3-5D). These findings would explain the activation of these two glutamate mutants by cadaverine. Taken together we conclude that TAAR346 utilizes a di-cationic motif ($Asp^{3.32}$ and $Asp^{5.42}$) for the recognition of cadaverine.

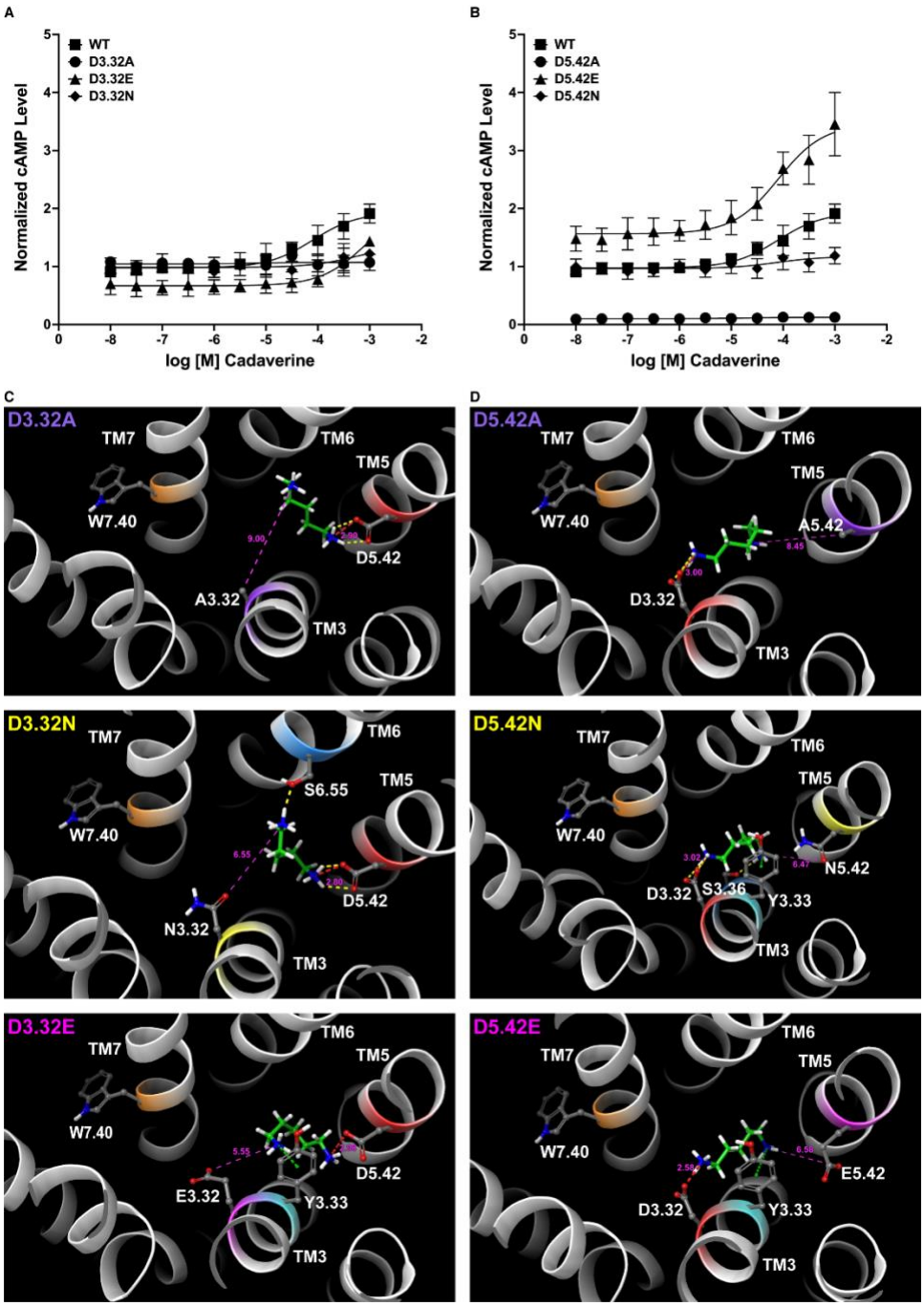

Figure 3-5. Concentration-response curves and docking model of TAAR346a mutated in the predicted cadaverine recognition sites $D^{3.32}$ and $D^{5.42}$

HEK293 cells expressed TAAR346a, $D^{3.32}$ mutants, or $D^{5.42}$ mutants were incubated with concentration-dependent cadaverine (10 nM to 1 mM). Changes in intracellular cAMP production were detected by TR-FRET and normalized to the WT basal cAMP production. The cAMP levels were normalized as measured cAMP /WT basal cAMP. TAAR346a mutant structure (white) was shown with coordinating residues (aspartate: red; glutamate: magenta; alanine: violet; asparagine: yellow; tryptophan: orange; tyrosine: cyan; serine: azure) and docking ligand cadaverine (green, backbone; blue, amino groups). Red dashed line, salt bridge; yellow dashed line, hydrogen-bond; green dashed line, Pi-interaction. The distance in Å was visualized as magenta.

Figure 3-5 (cont'd).
(A) Concentration-dependent responses of TAAR346a and its $D^{3.32}$ mutants for cadaverine (mean ±S.D., n=3). (B) Concentration-dependent responses of TAAR346a and its $D^{5.42}$ mutants for cadaverine (mean ±S.D., n=3). (C) Enlarged views of $D^{3.32}$ mutant structures with cadaverine and corresponding residues involved in ligand recognition. Side chains of key residues involved in ligand binding and major interactions between ligand and predicted binding residues were displayed. (D) Enlarged views of $D^{5.42}$ mutant structures with cadaverine and corresponding residues involved in ligand recognition. Side chains of key residues involved in ligand binding and major interactions between ligand and predicted binding residues were displayed.

The tryptophan Trp$^{7.40}$ of the DW motif is not involved in cadaverine binding

Docking studies suggested the irrelevance of the tryptophan residue Trp$^{7.40}$ of the DW motif in cadaverine binding. Trp$^{7.40}$ is highly conserved in class A GPCRs and thought to serve as part of amine recognition motif in aminergic receptors [27]. Therefore, we generated a series of Trp$^{7.40}$ mutants (phenylalanine, tyrosine, and glycine) to examine their effects on receptor activity. All three mutants exhibited comparable basal activity to wild-type TAAR346a. Cadaverine was able to activate these mutants with a similar potency as for wildtype, but showing a significant increase of efficacy (Figure S3-7A). Thus, functional experiments for all three mutnats suggest that Trp$^{7.40}$ is not involved in cadaverine recognition by TAAR346a.

Since a negatively charged asparatate Asp$^{6.58}$ of zTAAR13c has been reported to serve as an external binding site for cadaverine recognition [28], we then asked whether replacement of Asp$^{6.58}$ in TAAR346a may affect its activity. To validate our docking predictions, three Asp$^{6.58}$ mutants (alanine, asparagine, and glutamate) were generated to test receptor responses to cadaverine. Cadaverine was able to activate all three mutants, with a similar potency and efficacy as wild-type TAAR346a (Figure S3-7B). Taken together we conclude that Trp$^{7.40}$ and Asp$^{6.58}$ are irrelevant for activation of TAAR346a by cadaverine.

	(mean ± S.D.; n=3)		Predicted Interactions	
	CAD (EC_{50})	**TEA (IC_{50})**	**CAD**	**TEA**
TAAR346a	79 ± 94 μM	495 ± 154 μM	salt bridge: $D^{3.32}$ salt bridge: $D^{5.42}$	salt bridge: $D^{5.42}$
D3.32A	loss	—	salt bridge: $D^{5.42}$	—
D5.42A	loss	—	salt bridge: $D^{3.32}$	—
D3.32N	almost loss	>1000 μM	H-bond: $S^{6.55}$ salt bridge: $D^{5.42}$	salt bridge: $D^{5.42}$ pi-interaction: $Y^{3.33}$
D5.42N	almost loss	loss	salt bridge: $D^{3.32}$ H-bond: $S^{3.36}$	pi-interaction: $Y^{3.33}$ H-bond: $S^{3.36}$
D3.32E	>300	agonist EC_{50} = 446 ± 167	salt bridge: $D^{5.42}$ pi-interaction: $Y^{3.33}$	pi-interaction: $Y^{3.33}$
D5.42E	81 ± 329 μM	agonist EC_{50} = 447 ± 228	salt bridge: $D^{3.32}$ pi-interaction: $Y^{3.33}$	pi-interaction: $Y^{3.33}$

Table 3-1. Predicted interactions, detailed EC_{50} and IC_{50} values in the wild-type TAAR346a and mutant receptors

Interhelical hydrogen bond network among TMs plays important roles in mediating the constitutive activity of TAAR346a

Although the structural determinants for activation of various GPCRs have been examined, the structural basis of constitutively active olfactory receptors remains elusive. We next set about to characterize the structural basis for the constitutive activity of TAAR346a. Given that conformational changes in GPCR seven-transmembrane domains potentially underlie the molecular mechanisms of constitutively active receptors, we examined the TAAR346a homology model for interhelical interactions that could affect the constitutive activity of the receptor. Analysis of the TAAR346a homology model predicted the presence of several interhelical hydrogen bonds among the TMs, including key interactions between the side chains of paired residues $Asn^{1.50}$/$Asp^{2.50}$ and $Tyr^{3.33}$/$Asp^{5.42}$, as well as the side chain of $Thr^{3.37}$ and the backbone carbonyl of $Ala^{5.46}$ (Figure 3-6A and Figure 3-6B). As shown above, the D5.42A mutant completely abolished the constitutive activity of the receptor. In contrast, a conservative exchange from aspartate to asparagine or glutamate retained comparable basal activity to wild-type TAAR346a. Notably, similar interhelical hydrogen bonds have been reported to play essential roles in mediating the activation of several GPCRs [29-35]. Thus, we reasoned that these hydrogen bonds predicted by the TAAR346a homology model appear to be responsible for the constitutive activity of TAAR346a. To support this possibility, we first generated a series of mutants (N1.50G, D2.50A, D2.50N, D2.50E, and T3.37E) to test for their effects on receptor basal activity. In order to eliminate a role of impaired cell surface targeting in any change to the constitutive activity of mutant receptors, we immunostained transfected HEK293T cells with antibodies against the N-terminal Rho-tag on all of our mutant constructs, and found that all tested mutants were detected on the cell surface at a comparable level to that of wild-type TAAR346a (Figure S3-7). Measured

basal activities were normalized to the surface expression levels for further studies. The four mutations of the first residue pair ($Asn^{1.50}$/$Asp^{2.50}$) showed a massive reduction in the basal level of cAMP (Figure 3-6C). More notably, these mutants also resulted in complete loss of activation by cadaverine (Figure 3-6D). Docking studies did not predict the involvement of these two highly conserved residues in cadaverine binding, however, mutant receptors which have lost the predicted hydrogen bond at that residue pair show significantly reduced agonist-independent and agonist-dependent receptor activity.

Notably, the hydrogen bond between $Thr^{3.37}$ and $Ala^{5.46}$ is only present in the inactive state of class A GPCRs (37-40). The functional role of this hydrogen bond between $Thr^{3.37}$ and $Ala^{5.46}$ was evaluated by assessing the basal and cadaverine-induced cAMP production in the T3.37E mutant. As expected, hardly any constitutive activity was observed in HEK293T cells expressing the T3.37E mutant (Figure 3-6E). However, the T3.37E mutation did not impair cellular responses to cadaverine. The potency for cadaverine decreased about 4-fold, with a half-maximal response occurring at 287 ± 34 μM (mean ± S.E.M., n=3) vs 79 ± 94 μM (mean ± S.E.M., n=3) for the intact receptor (Figure 3-6F).

We further reasoned that these predicted hydrogen bonds should be absent in all mutant receptors, and therefore we examined the mutant structural differences. Indeed, the wild-type hydrogen bond between $Tyr^{3.33}$ and $Asp^{5.42}$ was absent from the homology model of the D5.42A mutant but was retained in the D5.42N and D5.42E mutants (Figure S3-10A, Figure S3-10B, and Figure S3-10C). Also, the other mutants lacked the wild-type hydrogen bonds between residue pairs $Thr^{3.37}$/$Ala^{5.46}$ and $Asn^{1.50}$/$Asp^{2.50}$ (Figure S3-10D, Figure S3-10E, Figure S3-10F, and Figure S3-10G). These observations are consistent with the hypothesis that these predicted hydrogen bonds function as an activation switch to stabilize the receptor in an active conformation.

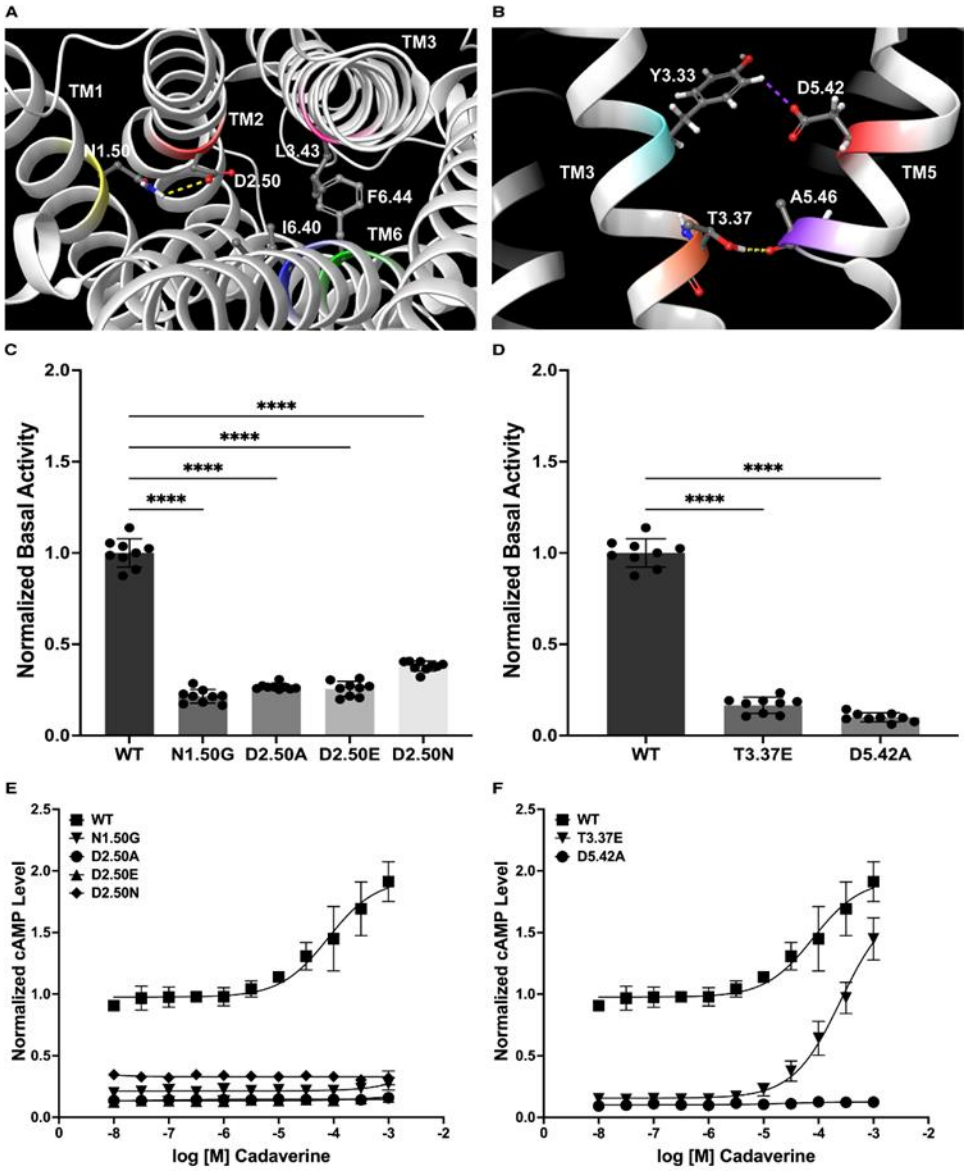

Figure 3-6. Disruption of interhelical hydrogen bond networks drastically eliminates the constitutively activity of TAAR346a

HEK293 cells expressed TAAR346a or TAAR346a mutants were incubated with concentration-dependent cadaverine (10 nM to 1 mM). Changes in intracellular cAMP production were detected by TR-FRET and normalized to the WT basal cAMP production. The cAMP levels were normalized as measured cAMP/WT basal cAMP. TAAR346a structure (white) was showed with coordinating residues forming interhelical hydrogen bond networks (aspartate: red; alanine: violet; asparagine: yellow; tyrosine: cyan; phenylalanine: green; leucine: pink; isoleucine: teal). Violet dashed line, aromatic hydrogen bond; yellow dashed line, hydrogen bond. (A) TAAR346a homology modeling predicted an interhelical hydrogen bond between the highly conserved $Asn^{1.50}$ and $Asp^{2.50}$. (B) TAAR346a homology modeling TAAR346a showed two hydrogen bond networks between the TM3 and TM5 segments. (C) Mutation of the $N^{1.50}$ and $D^{2.50}$ residues resulted in a significant reduction of the receptor's basal activity, by comparing with wildtype TAAR346a (mean ± S.D., n=9; Ordinary one-way ANOVA *p* value < 0.0001, Dunnett's multiple comparisons test **** *p* value <0.0001).

Figure 3-6 (cont'd).
(D) Mutation of the $T^{3.37}$ and $D^{5.42}$ residues almost completely eliminated the basal activity of the receptor (mean ± S.D., n=9; Ordinary one-way ANOVA *p* value < 0.0001, Dunnett's multiple comparisons test **** *p* value < 0.0001). (E) Mutation of the $N^{1.50}$ and $D^{2.50}$ residues resulted in complete loss of activation by cadaverine (mean ± S.D., n=3). (F) The T3.37E mutant was able to be activated by cadaverine in a concentration-dependent manner (mean ± S.D., n=3).

An introduced hydrogen bond with Asp$^{2.50}$ constrains the activation of TAAR346a

We subsequently asked whether introducing an extra hydrogen bond to contact with the above-mentioned residues could constrain the activation of TAAR346a. Structural modeling suggested that the substitution of residue Phe$^{6.44}$ by an arginine can form an interhelical salt bridge and a hydrogen bond with the highly conserved Asp$^{2.50}$ (Figure 3-7A). The introduction of a powerful salt bridge with Asp$^{2.50}$ from a different direction could mimic breaking the hydrogen bond between Asn$^{1.50}$ and Asp$^{2.50}$ that suppressed agonist-independent and agonist-dependent receptor activity. To support this hypothesis, we generated a F6.44R mutant to examine the effect of an added salt bridge on receptor activity. Immunocytochemistry indicated that the mutant receptor was properly targeted to the cell surface (Figure S3-8). As predicted, the F6.44R mutant not only completely abrogated the constitutive activity of TAAR346a, but also abolished cellular responses to cadaverine (Figure 3-7B), supporting our hypothesis on the role of an introduced interaction with Asp$^{2.50}$.

Furthermore, Phe$^{6.44}$ is proposed to constitute a hydrophobic core with two other hydrophobic residues at positions 3.43 and 6.40 that stabilize class A GPCRs in an inactive state [25]. Substitutions of these residues for a smaller hydrophobic residue or a polar residue could shift the receptor into an active conformation [25]. To test the functional properties of these hydrophobic residues, we generated a series of mutants by changing Leu$^{3.43}$, Ile$^{6.40}$, and Phe$^{6.44}$ into a smaller hydrophobic residue (alanine), a polar residue (serine), or a positively charged residue (arginine). Immunocytochemistry testing with all nine mutants showed no significant difference in cell surface targeting (Figure S3-8). Most mutants (exclusive of F6.44S and L3.43R) showed a significant increase in basal level of cAMP, and the basal activity of cells expressing the other two mutants (F6.44S and L3.43R) was not significantly different from that of the wild-type TAAR346a

(Figure 3-7C). More interestingly, stimulation of the L3.43A and L3.43S mutants with cadaverine hardly produced any increase in cAMP level (Figure S3-9A). It is possible that the basal activity is so high that no further cadaverine-induced cAMP accumulation could be detected. Cadaverine, however, was able to activate mutants I6.40A, I6.40S, F6.44A, and F6.44S, with a similar potency as wild-type TAAR346a (Figure S3-9B and Figure S3-9C). As observed in the F6.44R mutant, cadaverine-induced cAMP production was completely blunted in cells expressing the L3.43R and I6.40R mutants (Figure S3-9D). Hence, we conclude that residues involved in the hydrophobic core play important roles in the activation process of TAAR346a, possibly by holding the TM3 and TM6 in place for a relatively inactive conformation.

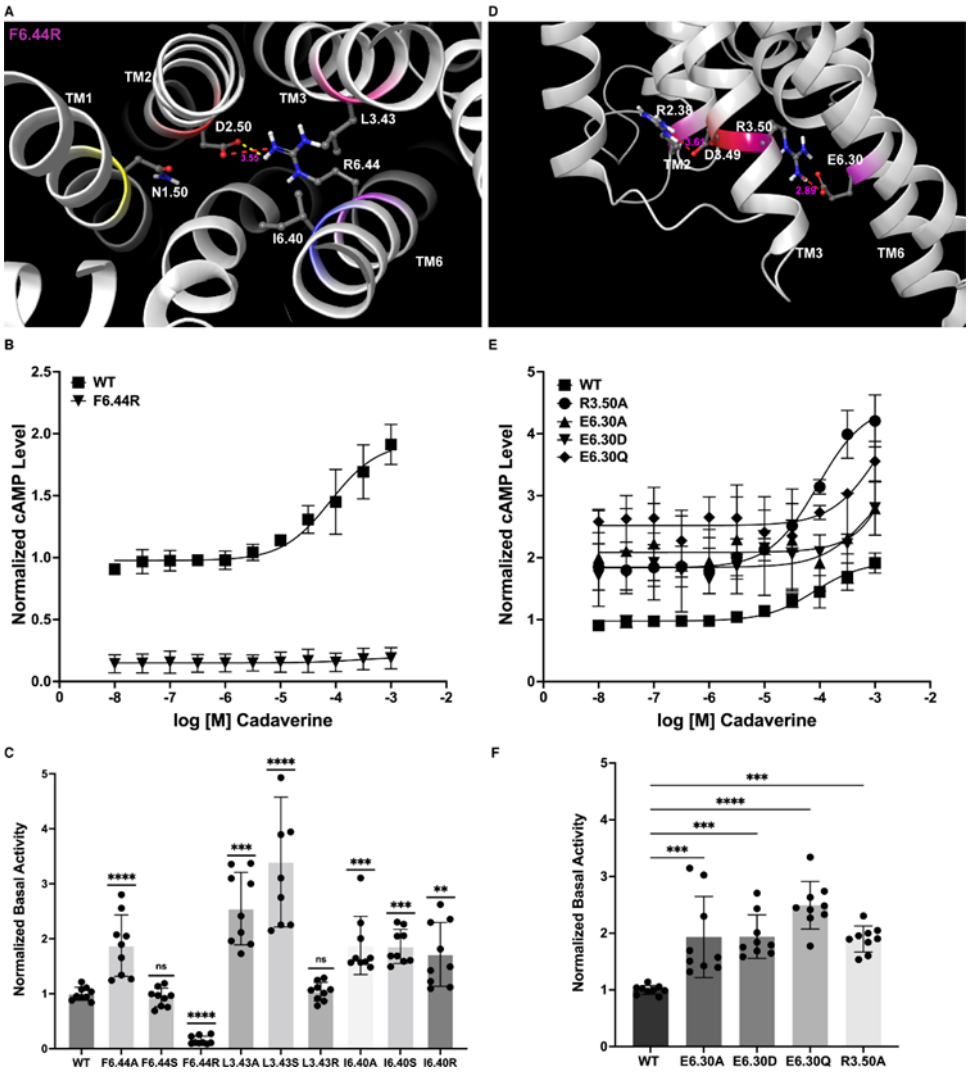

Figure 3-7. Influence of the hydrophobic core and ionic lock on activation of the constitutively active TAAR346a

HEK293 cells expressed TAAR346a or its mutants were incubated with concentration series of cadaverine (10 nM to 1 mM). Changes in intracellular cAMP production were detected by TR-FRET and normalized to the WT basal cAMP production. The cAMP levels were normalized as measured cAMP/WT basal cAMP. TAAR346a mutant structure (white) showed interhelical interactions within TMs (aspartate: red; asparagine: yellow; arginine: maroon; leucine: pink; isoleucine: teal; glutamate: magenta). Red dashed line, salt bridge; yellow dashed line, hydrogen bond. The distance in Å was visualized as magenta. (A) The F6.46R mutation introduced a salt bridge and a hydrogen bond with the highly conserved $Asp^{2.50}$, breaking the wild-type $Asn^{1.50}$-$Asp^{2.50}$ hydrogen bond. (B) Mutation of the $Phe^{6.46}$ residue to F6.46R completely abolished the constitutive and agonist-induced receptor activity (mean ± S.D., n=3). (C) Mutations (with the exception of F6.44S and L3.43R) in hydrophobic residues $Leu^{3.43}$, $Ile^{6.40}$, and $Phe^{6.46}$ showed a significant increase in basal level of cAMP (mean ± S.D, n=9; Ordinary one-way ANOVA p value <0.0001, Dunnett's multiple comparisons test **** p value < 0.0001, *** p value < 0.001, ** p value < 0.01, ns p value > 0.05). The basal level of cAMP in cells expressing the other two mutants (F6.44S and L3.43R) was not significantly different from that of wild-type TAAR346a.

Figure 3-7 (cont'd).
(D) The TAAR346a model showed a pair of salt bridges between the amino group of $Arg^{3.50}$ and the carboxylic group of $Glu^{6.30}$, and the side chains of $Asp^{3.49}$ and $Arg^{2.38}$. (E) Mutation of the $Arg^{3.50}$ residue to R3.50A exhibited a similar response to cadaverine as wildtype, whereas the three $Glu^{6.30}$ mutants drastically reduced cadaverine-induced TAAR346a activation (mean ± S.D., n=3). (F) All four mutant receptors at the ionic lock ($Arg^{3.50}$ and $Glu^{6.30}$) showed significant increases in basal activity (mean ± S.D, n=9; Ordinary one-way ANOVA *p* value <0.0001, Dunnett's multiple comparisons test **** *p* value < 0.0001, *** *p* value < 0.001, ** *p* value < 0.01).

Breaking the ionic lock between Arg$^{3.50}$ and Glu$^{6.30}$ leads to a significant increase in TAAR346a basal activity

GPCR activation requires a conformational change to cleave the ionic lock between TM3 (DRY motif) and TM6 (residue 6.30). This ionic interaction is primarily present in the trace amine, purinergic, opsin and aminergic subfamilies of class A GPCRs, and stabilizes the receptor in an inactive conformation [25]. However, it is not known whether a constitutively active TAAR receptor retains the ionic lock that stabilizes the receptor in a relatively inactive conformation. To address this question, we examined the homology model of TAAR346a to identify potential interactions between the DRY motif and Glu$^{6.30}$. The TAAR346a model predicted a salt bridge between the amino group of Arg$^{3.50}$ and the carboxylic group of Glu$^{6.30}$, at a distance of 2.89 Å (Figure 3-7D). In addition, we observed another salt bridge between the side chains of Asp$^{3.49}$ and Arg$^{2.38}$, at a distance of 3.61 Å (Figure 3-7D). These results suggested that the constitutively active TAAR346a retains the ionic lock that primarily exists in inactive GPCRs, holding the receptor in a partially constitutively active state. We then reasoned that disruption of the ionic lock should result in a significant increase of the receptor basal activity.

To test this hypothesis, we generated a series of mutants (R3.50A, E6.30A, E6.30D, E6.30Q, D3.49A, D3.49E, and D3.49N) to examine their effects on receptor activity. As expected, the four mutant receptors (R3.50A, E6.30A, E6.30D, E6.30Q) at the ionic lock showed significant increases in basal activity (Figure 3-7F). The R3.50A mutant was activated by cadaverine with a similar EC_{50} value as wildtype TAAR346a, suggesting that Arg$^{3.50}$ is involved in regulating the receptor basal activity rather than cadaverine recognition (Figure 3-7E). More interestingly, the three Glu$^{6.30}$ mutants showed a substantial decrease in potency of cadaverine (Figure 3-7E), probably due to an effect when disruption of the ionic lock at Glu$^{6.30}$ results in an outward

movement of TM6 relative to TM3 that destabilizes the structural basis for cadaverine binding. Furthermore, functional testing with the D3.49A and D3.49N mutants showed a robust increase in basal activity (Figure S3-11A). Hardly any cadaverine-induced cAMP accumulation was observed in the two mutants, conceivably due to such high basal activity that no further cAMP accumulation could be detected. In sharp contrast to charge-neutralizing mutations, the most conservative exchange, D3.49E, exhibited similarly basal activity and cadaverine response as wildtype (Figure S3-11B). These results suggest that the DRY/ERY motif plays a critical role in mediating GPCR activation. Structurally, the substitution of $Asp^{3.49}$ to glutamate in the DRY motif retained interhelical interactions between $Arg^{3.50}$ and $Glu^{6.30}$, $Glu^{3.49}$and $Arg^{2.38}$, which are consistent with the results that was observed in the wild-type TAAR346a (Figure S3-10J). Therefore, we conclude that the ionic lock appears to be important between TM3 and TM6 in TAARs, even a constitutively active TAAR, to stabilize the receptor in a relatively inactive conformation.

DISCUSSION

Although the molecular and structural basis of the activation of non-olfactory GPCRs has been explored more completely, those mechanisms for olfactory receptors still remain elusive. To date, only a few studies elucidated molecular interactions between an odorant and its responding receptor by applying a combined approach of structural modeling and site-directed mutagenesis, in part due to the unavailability of crystal structures [41-44, 47]. In this study, we apply an inverse agonist and an agonist to examine the structural basis of activation for TAAR346a, a constitutively active sea lamprey olfactory TAAR receptor. The inverse agonist (triethylamine) selectively binds to one ($Asp^{5.42}$) of the two orthosteric sites ($Asp^{3.32}$ and $Asp^{5.42}$ used by the agonist cadaverine) to attenuate the constitutive activity of TAAR346a. Moreover, the predicted interhelical hydrogen bonds ($Aan^{1.50}$/$Asp^{2.50}$, $Thr^{3.37}$/$Ala^{5.46}$, and $Tyr^{3.33}$/$Asp^{5.42}$) among TMs of TAAR346a function as an activation switch that contributes to the constitutive activation of the receptor. In contrast, the ionic lock between $Arg^{3.50}$ and $Glu^{6.30}$ appears to hold the receptor in a relatively inactive conformation. Remarkably, the F6.44R mutation right in the hydrophobic core of the receptor appears to introduce a hydrogen bond with $Asp^{2.50}$ and abolishes agonist-dependent and agonist-independent activation of TAAR346a. Thus, all of our experimental results highlight the importance of interhelical interactions in the activation of an olfactory TAAR receptor, both by agonist-dependent and agonist-independent means.

Independently evolved TAARs recognize cadaverine via an identical motif

The cadaverine-responsive TAAR346a exhibits considerable constitutive activity that can be drastically attenuated by the inverse agonist triethylamine, providing an opportunity to study the activation mechanism of a GPCR, in both ligand-dependent and ligand-independent state. Most

vertebrate TAARs utilize the highly conserved $Asp^{3.32}$ as a primary site to recognize the amino group of biogenic amines. In contrast, a large number of teleost-specific TAARs lack this conserved $Asp^{3.32}$ and use a non-canonical $Asp^{5.42}$ to interact with the amino group of amines. A minority of vertebrate TAARs, (i.e. zebrafish TAAR13c and TAAR13d) have evolved both $Asp^{3.32}$ and $Asp^{5.42}$ for the detection of di-cationic amines [44]. The characteristic fingerprint for jawed vertebrate TAARs is not well-conserved in sea lamprey TAARs, suggesting independent evolutionary processes of TAARs in lamprey and jawed animals [45]. Phylogenetic analysis indicates that lamprey TAARs cluster into an independent outgroup of TAAR genes vs those in jawed vertebrates [45]. In spite of the evolutionary distance, our results suggest that TAAR346a, like the zebrafish receptors, utilizes $Asp^{3.32}$ and $Asp^{5.42}$ as critical binding sites to recognize cadaverine. The results obtained from mutations of these two aspartates are consistent with the findings for zebrafish TAARs in previous studies [44]. Notably, cadaverine is a potent odorant of mammalian TAARs that do not contain the $Asp^{5.42}$, so it appears that additional residues are required for cadaverine recognition by mammalian TAARs, with a cation-pi interaction or a hydrogen-bond [44, 46]. Indeed, a recent study has shown that independently evolved TAARs utilize an aromatic residue and a polar residue to recognize cadaverine via a cation-pi interaction and a hydrogen-bond, respectively [47].

An inverse agonist can decrease the basal activity by binding one of the orthosteric sites for the agonist

Inverse agonism is very common among GPCR antagonists. An inverse agonist can bind to the orthosteric pocket to attenuate the receptor basal activity [2]. The results obtained from the $Asp^{5.42}$ mutants with triethylamine illustrate a similar molecular mechanism. Triethylamine interacts with $Asp^{5.42}$, but not the canonical amine recognition site $Asp^{3.32}$, to attenuate the

constitutive activity of TAAR346a. The substitution of $Asp^{5.42}$ with a glutamate or an asparagine allows triethylamine recognition, but converts it into an agonist. Likewise, a charge-neutralizing mutation of $Asp^{5.42}$ turns the zebrafish diamine receptor TAAR13c into a monoamine receptor [44]. More interestingly, triethylamine serves as an agonist at mouse TAAR9, in which the $Asp^{5.42}$ residue is not retained [21]. These results reveal the extensive landscape of ligand recognition among GPCRs and may help explain ligand selectivity at TAARs. Thus, we propose a structural model for inverse agonist recognition by GPCRs in which one of the orthosteric sites for an agonist can be involved in inverse agonist recognition. The ancestral TAARs use the conserved $Asp^{3.32}$ as a primary amine recognition site, and while another clade of TAARs evolved to utilize $Asp^{5.42}$ during a convergent evolution process, thereby gaining the ability to recognize both monoamine and diamine ligands.

Interhelical hydrogen bonds contribute to the constitutive activation of GPCRs

Interhelical hydrogen bonds involving residues 1.50, 2.50, 3.37, 5.42, and 5.46, have been reported to be responsible for the activation of GPCRs [30-40]. Here, we applied an approach combining structural modeling, site-directed mutagenesis, and pharmacological analysis to probe the proposed role of interhelical hydrogen bond network in GPCR activation. We have identified a novel function of the hydrogen bond between the side chain of $Thr^{3.37}$ and the backbone carbonyl of $Ala^{5.46}$ that has a positive effect on the constitutive activity, but does not affect receptor responses to cadaverine. However, the role of this hydrogen bond in other class A GPCRs appears to be different from its role in TAAR346a. This hydrogen bond is only present in the inactive crystal structures of rhodopsin, adenosine A2A receptor, and histamine$_1$ mutant receptor (T3.37E), and appears to have a negative effect on agonist-independent signaling activity [25, 32, 37]. Indeed, it is absent in the CAM of rhodopsin ($Glu^{3.37}$ mutants) and adenosine A2A receptor (Q3.37A),

implying that this hydrogen bond functions as a molecular constraint to stabilize the inactive state of the receptor [37-40]. Nevertheless, our findings suggest that the $Thr^{3.37}$/$Ala^{5.46}$ hydrogen bond may also serve as an activation switch for constitutively active GPCRs, by stabilizing the receptor in an active conformation.

Besides the $Thr^{3.37}$/$Ala^{5.46}$ hydrogen bond, disruption of the hydrogen bonds ($Aan^{1.50}$/$Asp^{2.50}$ and $Tyr^{3.33}$/$Asp^{5.42}$) also resulted in a drastic reduction in constitutive activity of TAAR346a. As with our results, the hydrogen bond between $Asn^{1.50}$ and $Asp^{2.50}$ has been shown to be present in the constitutively active mutant (CAM) of angiotensin II type 1 receptor (N3.35G-AT1), as well as the activated thyrotropin-releasing hormone receptor and chemokine receptor type 1 [30-32]. Moreover, crystal structures of constitutively active opioid receptors exhibited a similar hydrogen bond between $Asp^{2.50}$ and $Ser^{7.46}$ [48], suggesting that the hydrogen bond with $Asp^{2.50}$ is likely to be broadly present in activated GPCRs. Notably, mutations of the two involved residues resulted in a complete loss of cadaverine responses, suggesting that the $Aan^{1.50}$/$Asp^{2.50}$ hydrogen bond may play an important role in mediating agonist-independent and agonist-dependent activation of GPCRs. Similar results were observed in the AT1 mutants when angiotensin II was applied as an agonist. Thus, breakage of this hydrogen bond likely reorients the conformation of TM1 and TM2 and introduces a new interhelical interaction that functions as a molecular switch (such as the ionic lock or toggle switch) to constrain agonist-induced receptor activation. Indeed, our results with the F6.44R mutant appear to support this speculation. Introduction of a salt bridge with $Asp^{2.50}$ constrains agonist-independent and agonist-dependent activation of TAAR346a. In contrast, an increase of agonist-independent activity was observed in β_2-adrenergic receptor when removed the polar side chain of $Asp^{2.50}$ [49]. Taken together, these findings suggest that depending on the receptor, the hydrogen bond network is highly important for constitutive and agonist-induced

signaling in GPCRs.

The hydrophobic core and ionic lock contribute to holding the receptor in a relatively inactive state

In contrast to hydrogen bonds that stabilize the receptor in an active conformation, several hydrophobic residues (Leu$^{3.43}$, Ile$^{6.40}$, and Phe$^{6.64}$) at TM3 and TM6 right in the core of the receptor are proposed to comprise a hydrophobic barrier holding the TM3 and TM6 in place in the inactive receptor [25]. Curiously, although these hydrophobic residues do not predict to be involved in cadaverine binding, mutations from hydrophobic to a positively charged arginine completely abolished receptor responses to cadaverine. These results suggest that the introduction of an arginine right in the hydrophobic core is likely to form an extra interhelical interaction that prevents the receptor from being activated by cadaverine. Indeed, the structural modeling supports our hypothesis. Replacing Leu$^{3.43}$ and Ile$^{6.40}$ with arginine in the models predicts a new interaction between Arg$^{3.43}$/Asn$^{7.49}$ and Arg$^{6.40}$/Tyr$^{7.53}$, respectively (Figure S3-10H and Figure S3-10I). Notably, a similar interaction between Asp$^{6.44}$ and Asn$^{7.49}$ was observed in the inactive thyrotropin receptor where breaking the interaction results in constitutive activation of the receptor [33]. These results suggest that interactions with Asn$^{7.49}$ and Tyr$^{7.53}$ of the conserved NPxxY motif are required for the activation of GPCRs and may serve as a toggle switch that shifts the receptor into an inactive conformation by stopping the rotation of TM6 and the upward movement of TM3.

Apart from the hydrophobic core, the highly conserved D/ERY motif on the intracellular end of TM3 has been shown to be important for GPCR activation. The ionic lock between Arg$^{3.50}$ and Asp/Glu$^{6.30}$, along with an intrahelical salt bridge between Asp/Glu$^{3.49}$ and Arg$^{3.50}$, have long been presented in many inactive GPCRs [50-52]. However, the homology model did not include an intrahelical salt bridge between Asp$^{3.49}$ and Arg$^{3.50}$, but instead there was an interhelical salt bridge

between $Asp^{3.49}$ and $Arg^{2.38}$. Notably, similar interhelical interactions ($Arg^{3.50}$/$Asp^{6.30}$ and $Asp^{3.49}$/$Arg^{2.37}$) are observed in the structure of a constitutively active cannabinoid CB1 receptor [50]. Disruption of the ionic lock between $Arg^{3.50}$ and $Glu^{6.30}$ creates a mutant with high constitutive activity. The results of molecular dynamics stimulations of inactive opioid and rhodopsin-like receptors showed that the intrahelical salt bridge between $Asp^{3.49}$ and $Arg^{3.50}$ is more stable than the ionic lock between $Arg^{3.50}$ and Asp/$Glu^{6.30}$ [51, 52]. Thus, these results suggest that the ionic lock $Arg^{3.50}$/$Glu^{6.30}$ could be present in the constitutively active GPCRs, holding the receptor in a relatively inactive conformation. In contrast, the intrahelical salt bridge between Asp/$Glu^{3.49}$ and $Arg^{3.50}$ may represent a hallmark of inactive GPCRs. However, it is worth noting that we cannot rule out the possibility the constitutive activity of olfactory TAAR346a is also G_{α} dependent.

In conclusion, all modeling and functional analyses provide structural insights into ligand-dependent and ligand-independent activation of the sea lamprey olfactory TAAR346a. This discovery implicates a molecular mechanism that an inverse agonist could recognize one of the orthosteric sites for the agonist to elicit a completely inversed pharmacological effect. Furthermore, our results suggest that the constitutive activity of GPCRs is concomitantly orchestrated by interhelical interactions by flipping the receptor between active and inactive conformations; the interhelical hydrogen bond serves as an activation switch to stabilize the receptor in an active conformation, whereas the ionic lock and hydrophobic barrier are proposed to hold TM3 and TM6 in place for an inactive conformation. In the future, the physiological significance of the constitutively active lamprey TAAR346a should be examined and our identification of triethylamine as an inverse agonist may help with that goal.

MATERIALS AND METHODS

Ethics statement

All procedures involving sea lamprey (*Petromyzon marinus*) were approved by the Michigan State University Institutional Animal Use and Care Committee (03/14-054-00 and 02/17-031-00). Sea lamprey used for in situ hybridization were euthanized with 3-aminobenzoic acid ethyl ester (100 mg/L; MS222, Sigma-Aldrich, USA) followed by dissection of the olfactory organ.

Chemicals

Amine compounds of the highest purity available were purchased from Sigma-Aldrich. All chemicals were dissolved in dimethyl sulfoxide (DMSO; D4540, Sigma-Aldrich, USA) at a final concentration of 200 mM and stored at -20 ˚C.

Cell lines

HEK293T cells used for all TAAR346a experiments were maintained at 37 ˚C with 5% CO_2 and grown in Dulbecco's Modified Eagle Medium (DMEM; SH30243.01, Hyclone, USA) supplemented with 10% fetal bovine serum (FBS; 10437-028, Gibco, USA) and 1 × Antibiotic-Antimycotic (15240062, Gibco, USA).

High-throughput ligand screening of TAAR346a

The open reading frame of TAAR346a was mined from the sea lamprey genome assembly (Pmarinus_7.0) [53]. TAAR346a was cloned from sea lamprey genomic DNA, and was inserted into Rho-pCMV modified from pCMV-Tag-2B (211172, Agilent Technologies, USA) by harboring a Rho-tag (the first 21 amino acids of bovine rhodopsin) at the N terminal replacing the intrinsic flag-tag.

The initial high-throughput screening (HTS) was performed in 384-well plates as described by Zhuang and colleagues with the following modifications [54]. For the reverse transfection, 5 μL DNA-transfection mixture (25 ng CRE-Luciferase vector pGL4.29 [E8471, Promega, USA], 5 ng of a TAAR plasmid, 5 ng pCI-mRTPs, 5 ng pCI-Gαolf [provided by Dr. H. Matsunami]), and 5,500 HEK293T cells in 25 μL 0.5% FBS DMEM medium were added to each well. The plates were incubated for 48 hours at 37˚C with 5% CO_2. Each stimulus solution (ligands final concentration 10 μM or 100 μM) was dispensed into a designated well using Biomek FXP liquid handling automation workstation (Beckman Coulter, USA). The negative control stimulus was 150 nL DMSO. Plates were incubated for 4 hours at 37˚C with 5% CO_2. Luciferase activity was measured using Steady Glo Luciferase Assay System (E2520, Promega, USA), and luminescence was read on a Synergy Neo multi-mode microplate reader (BioTek). Luciferase activity was normalized by DMSO-stimulated luminescence value with the following formula: (Luc induced by Ligand) / (Luc induced by DMSO).

In situ hybridizations of *taar346a*

Probes were designed against nucleotide sequences in *taar346a* spanning 278bp of the coding regions. Amplified fragments were cloned into a pGEM-T vector (A3610, Promega, USA) for sequence verification. Plasmid was linearized using restriction enzyme NcoI (anti-sense probe) or SpeI (sense probe), and used for synthesis of digoxigenin-labeled RNA probes with DIG RNA labeling kit (SP6/T7) (11175025910, Roche, Germany). In situ hybridization was conducted following the previously described methods [20]. Briefly, 20 μm frozen sections of olfactory epithelium were hybridized with RNA probes (3 ng/μL) overnight at 65°C in the hybridization solution (50% deionized formamide, 1 × Denhart's solution, 5% dextran sulfate, 750 mM sodium chloride, 25 mM ethylenediaminetetraacetic acid, 25 mM piperazine-N, N′-bis-2-ethanesulfonic

acid, 0.25 mg/mL fish sperm DNA, 0.25 mg/mL poly A acid, and 0.2% sodium dodecyl sulfate). After hybridization, sections were washed three times for 5 minutes each in 4 × saline-sodium citrate (SSC). For high stringency conditions, sections were washed sequentially in 2 × SSC (containing 0.3% Tween-20) and 0.2 × SSC (containing 0.3% Tween-20) three times each for 15 minutes each at 68 °C. Sections were washed in 0.1 × SSC (containing 0.3% Tween-20) for 15 minutes followed by three washes for 5 minutes each in 0.1M PBS (containing 0.3% Tween-20) at room temperature. The sections were then incubated with blocking solution (1 × PBS, 2 mg/mL bovine albumin serum, 0.3% Tween-20, and 10% normal sheep serum) for 1 hour at room temperature, followed by incubation with alkaline phosphatase-conjugated sheep-anti-digoxigenin Fab fragments (1:1000 diluted in blocking solution; 11093274910, Roche, Germany) overnight at 4 °C. Hybridization signals were detected by incubating the sections in nitro blue tetrazolium and 5-bromo-4-chloro-3-indolyl phosphate (NBT/BCIP, 34042, Thermo Scientific, USA) for 2 hours at room temperature and then counterstained with nuclear fast red (H3403, Vector Laboratories, USA) for 5 minutes at room temperature. All images were observed and photographed with a Zeiss Axioskop2 mot plus microscope with a 40 × objective. Control experiments (sense probe) were conducted simultaneously to confirm the absence of staining when incubated with the anti-digoxigenin antibody alone.

Site-directed mutagenesis of TAAR346a

Site-directed mutations were introduced following the protocol of QuikChange Site-directed mutagenesis kit (200524, Agilent Technologies, USA). In brief, PCR primers were designed by Agilent QuikChange Primer Design (primers listed in Table S3-1), and PCR reactions were performed using PfuUltra High-Fidelity DNA Polymerase with wild-type TAAR346a plasmid as a template. The methylated parental strands were selectively digested with 1μL DpnI enzyme, and

the DpnI treated PCR products were transformed into DMT chemically competent cells (CD511-02, TRANSGEN BIOTECH, China). All mutants were verified by DNA sequencing, and positive colonies for the desired substitutions were grown in LB broth and the plasmids were isolated using an EndoFree mini plasmid DNA purification kit (DP118-02, TIANGEN BIOTECH, China).

Immunocytochemistry assay of TAAR346a and its mutants

HEK293T cells were seeded in collagen I coated 24 well glass bottom plates with a density of 5×10^4 cells per well in 1mL growth medium (DMEM medium with 10% FBS) and incubated for 24 hours at 37˚C with 5% CO_2. Cells were then transfected with 375 ng pGL4.29, 75 ng pCI-mRTPs, 75 ng pEGFP-N1 (6085–1, Clontech, USA), and 75 ng TAAR346a plasmid or TAAR346 mutants, incubating at 37˚C with 5% CO_2 for 24 hours. The null plasmid, pGL4.29, pCI-mRTPs, and pEGFP-N1 were co-transfected as a negative control. Subsequently, 100 μL 37% formaldehyde was added to each well and incubated for 15 minutes at room temperature, and then washed the wells three times for 5 minutes each with 500 μL PBS. Cells were permeabilized or not permeabilized with 0.5% Triton X-100 for 10 minutes at room temperature to label the whole cell or only cell membrane, and cells were washed three times for 5 minutes each with 500 μL PBS. Permeabilized cells were treated with 500 μL blocking buffer (5% BSA and 0.3% Triton X-100 in PBS) for 1 hour at room temperature, and non-permeabilized cells were treated with 500 μL blocking buffer (5% BSA in PBS) for 1 hour at room temperature. Then the blocking buffer was removed and 300 μL mouse monoclonal anti-rhodopsin antibody (MABN15, Millipore, USA; 1:500 diluted in dilution buffer: 1% BSA in PBS for non-permeabilized cells and 1% BSA, 0.3% Triton X-100 in PBS for permeabilized cells) was added to each well and incubated at 4 °C overnight. The antibody solution was aspirated and washed five times for 5 minutes each with 500 μL PBS, followed by adding 300 μL red-fluorescent Alexa Fluor 594 goat anti-mouse IgG (A11005,

Invitrogen, USA; 1:500 diluted in dilution buffer: 1% BSA in PBS for non-permeabilized cells and 1% BSA, 0.3% Triton X-100 in PBS for permeabilized cells) for 1 hour at room temperature. Cells were washed three times for 5 minutes each with 500 μL PBS, and cells were counterstained with 300 μL DAPI (D1306, Life Technologies, USA; 1:5000 diluted in PBS) and incubated in the dark for 5 minutes. Cells were washed three times for 5 minutes each with 500 μL PBS. Images were acquired at 400 × magnification under DMI8 Thunder (Leica) with DAPA filter, GFP filter, and Texas Red filter, respectively (10 random views/well, n=3). The mean value of red-fluorescent signal was quantified with LAS X software (Leica).

Functional assay of TAAR346a and its mutants in the HEK293T heterologous system

HEK293T cells were maintained at 37˚C with 5% CO_2 and grown in DMEM supplemented with 10% FBS and 1 × Antibiotic-Antimycotic. The cAMP production assay was performed in 384-well plates as described in LANCE Ultra cAMP Kit manual (TRF0263, PerkinElmer, USA) to characterize the cAMP production induced in HEK293T cells expressing TAAR346a and its mutants. Briefly, HEK293T cells were seeded in a 100 mm dish with 3×10^6 cells in 10 mL growth medium (DMEM medium with 10% FBS) and incubated for 24 hours at 37˚C with 5% CO_2. Cells were then transfected with 5 μg pGL4.29, 1 μg pCI-mRTPs, 1 μg pCI-$G_{\alpha olf}$, and 1 μg TAAR346a plasmid or TAAR346 mutants, incubating at 37˚C with 5% CO_2 for 24 hours. Transfected cells were detached with 2 mL Versene (15040066, Gibco, USA) and transferred to 384-well plates at 5 μL (2,000 cells) per well; 5 μL of the 2 × cadaverine serial dilutions were added to each well and incubated for 30 minutes at room temperature. Afterwards, 5 μL 4 × Eu-cAMP tracer working solution and 5 μL 4 × ULight-anti-cAMP working solution were added to each well and incubated for 1 hour at room temperature. Plates were read with the Synergy Neo multi-mode microplate reader for TR-FRET emissions at 620 nm (as internal reference) and 665 nm (as biological

response). The ratio of 665/620 allows normalization for the well-to-well variability and interference due to assay components.

Homology modeling and ligand docking of TAAR346a

We first performed sequence alignments of templates in the Protein Data Bank with TAAR346a, and identified that TAAR346a shares a maximal identity of 34% and a sequence coverage of 82% to the template 3SN6. We next chose the crystal structure of template 3SN6 to generate homology model of TAAR346a by using Modeller v9.18 [55]. The homology model was evaluated by Ramachandran plot and ERRAT, the score of Ramachandran plot and ERRAT was 95.4% and 95.02, which is well fitted in the reasonable range and was chosen to be the final homology model. Ligand docking of TAAR346a was generated using Schrodinger Maestro 11.5 to predict putative binding residues. The homology model was prepared for docking to optimize H-bond assignment and subject to restrained minimization by using the Protein Preparation Wizard function in Maestro 11.5. For mutant structure, homology models for mutants subsequently were generated by residue substitution in the wild-type homology model and prepared with the above described protocol. Then, docking ligand was introduced into the workspace by using the LigPrep function in Maestro 11.5. Subsequently, the docked ligand was confined to the enclosing box in the centroid of conserved $Asp^{3.32}$ to perform the Receptor Grid Generation function, and ligand was docked in the centroid of selected residues within the length of 20 Å. The ligand was used with flexible structure and was docked into the enclosing box with extra precision using Ligand Docking function with default parameter setting in Maestro 11.5.

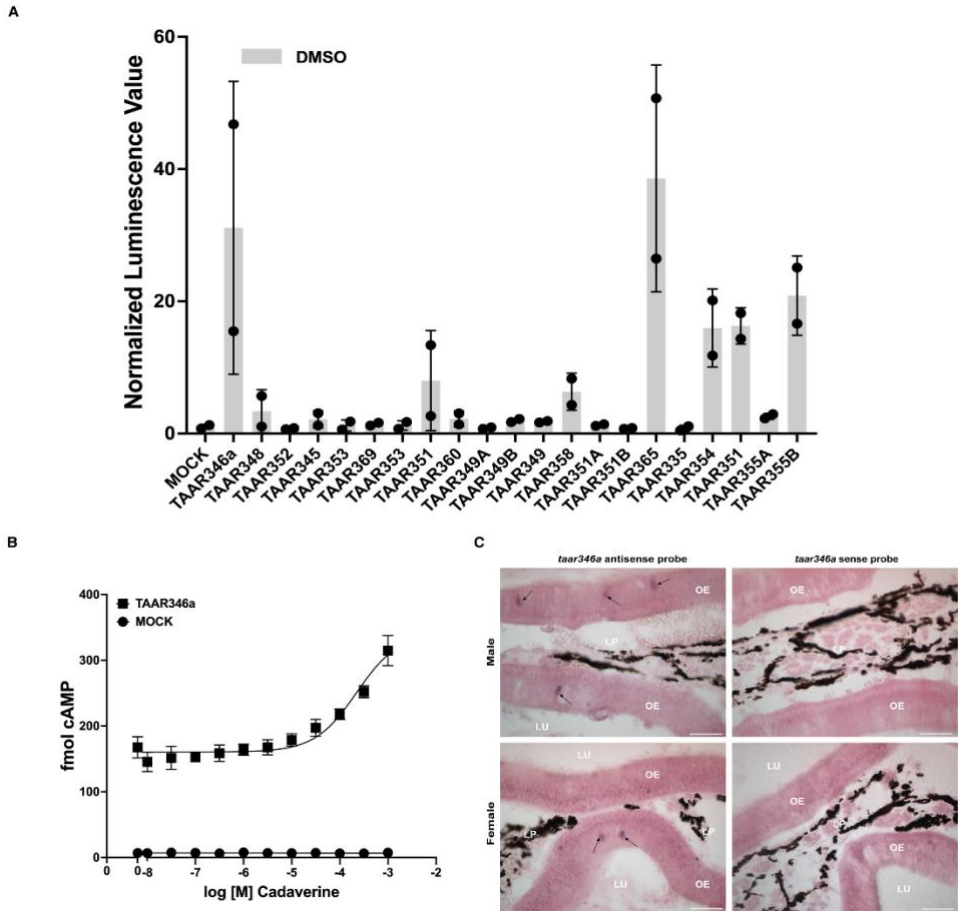

Figure S3-1. The basal luciferase activity and cadaverine-induced cAMP responses of the lamprey olfactory TAAR346a

(A) The normalized basal luciferase activity of 21 lamprey TAARs. HEK293T cells were transfected with TAAR plasmids or mock (empty vector) along with a CRE-luciferase reporter plasmid and incubated for 48 hours and subsequently stimulated with DMSO for 4 hours. Luciferase activity was indicated by luminescence value and was normalized to the response of DMSO from mock control (mean ± S.D., n=2). (B) Concentration-dependent responses of TAAR346a and mock receptor for cadaverine. The cAMP levels were measured with a TR-FRET assay (mean ± S.D., n=5). (C) Representative olfactory receptor neurons expressing *taar346a* (purple) labeled with a digoxigenin-labeled anti-sense RNA probe in a cross-sectional view of the main olfactory epithelium of adult male and female sea lampreys. Sections were counterstained with Nuclear Fast Red. The positive neurons are denoted with purple stain (NBT/BCIP) with black arrows, no positive neurons were observed in the cross sections with digoxigenin-labeled *taar346a* sense RNA probe. Black melanophores in the lamina propria are characteristic of sea lamprey olfactory epithelia. Images were acquired with a Zeiss Axioskop2 mot plus microscope equipped with a 40x Plan-Neuoflaur objective. Scale bars: 50 µm. LP, lamina propria; LU, lumen; OE, olfactory epithelium.

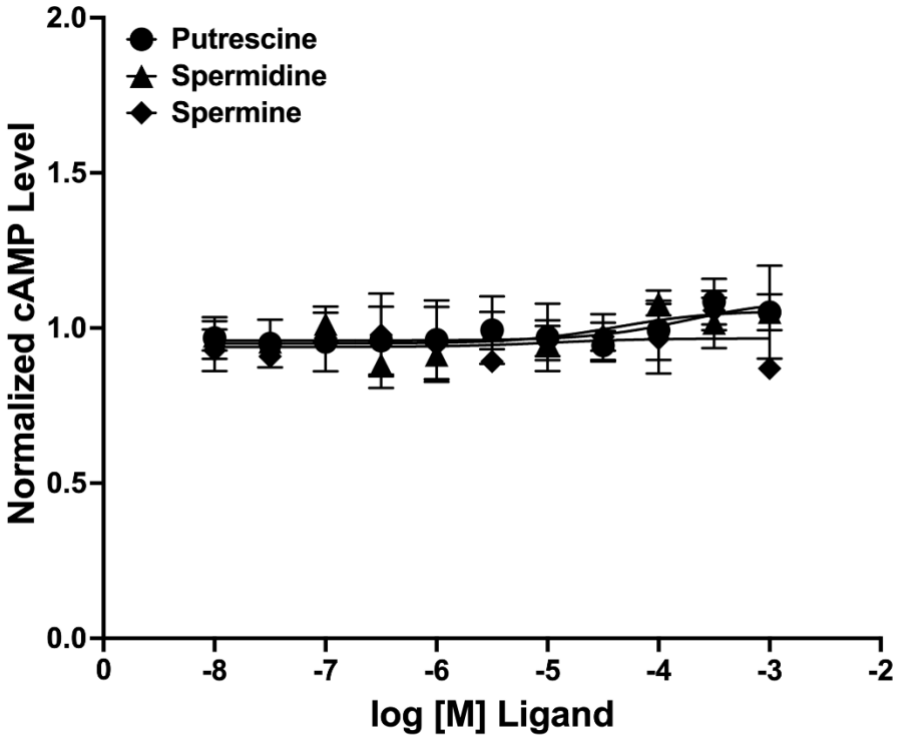

Figure S3-2. Concentration-dependent responses of TAAR346a for putrescine, spermidine, and spermine

HEK293 cells expressed TAAR346a were incubated with concentration series of putrescine, spermidine, and spermine (10 nM to 1 mM). The cAMP levels were measured with a TR-FRET assay and normalized to the basal cAMP level in buffer-treated cells (mean ± S.D., n=3). Stimulation of putrescine, spermine, and spermidine induced a minimal cAMP accumulation in HEK293T cells expressing TAAR346a.

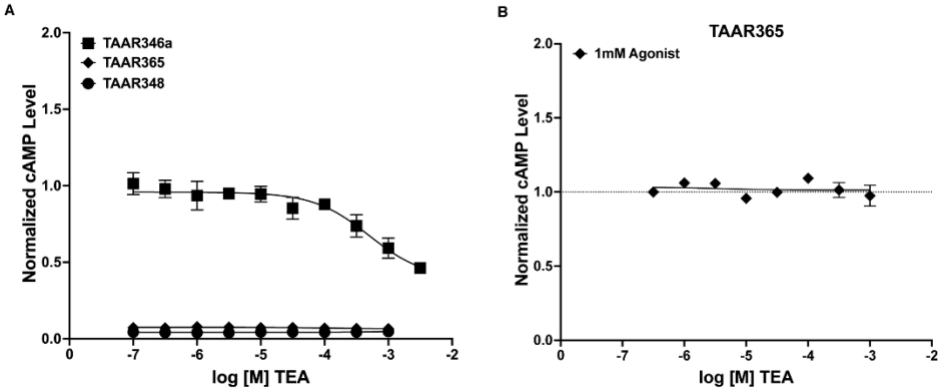

Figure S3-3. Triethylamine shows no inhibitory effect on the basal activity of the other two lamprey TAARs, TAAR348 and TAAR365

HEK293 cells expressed TAAR346a, TAAR348, and TAAR365 were incubated with concentration-dependent triethylamine (100nM to 3.3 mM). Changes in intracellular cAMP production were detected by TR-FRET and normalized to the WT basal cAMP production. The cAMP levels were normalized as measured cAMP /WT basal cAMP. (A) Concentration-dependent responses of TAAR346a, TAAR348, and TAAR365 for triethylamine (mean ± S.D., n=3). (B) Triethylamine treatment did not inhibit cAMP production induced by 1 mM TAAR365 agonist in HEK293T cells expressing TAAR365 (mean ± S.D., n=3). The dashed line represents the cAMP production induced by 1 mM TAAR365 agonist in the cells without exposure to triethylamine.

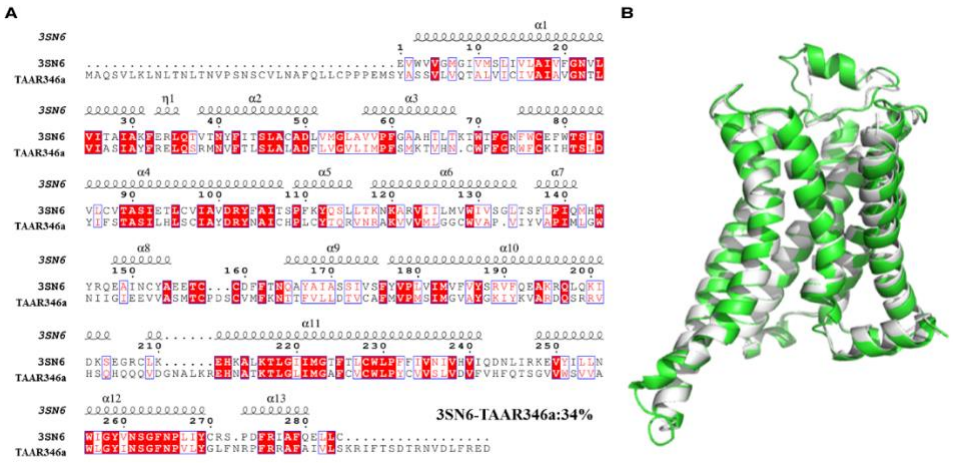

Figure S3-4. Sequence alignment and structural comparison of TAAR346a and its homologous template

(A) The TAAR346a homology model shares a maximal identity of 34% and a sequence coverage of 82% to its homologous template β2-adrenergic receptor-G_s protein complex (3SN6). (B) Cartoon representation of the TAAR346a homology model (green) based on comparison with its homologous template 3SN6 (white) exhibits the canonical seven hydrophobic transmembrane α-helices and an eighth intracellular helix (H8) in the C-terminus paralleled to the membrane plane.

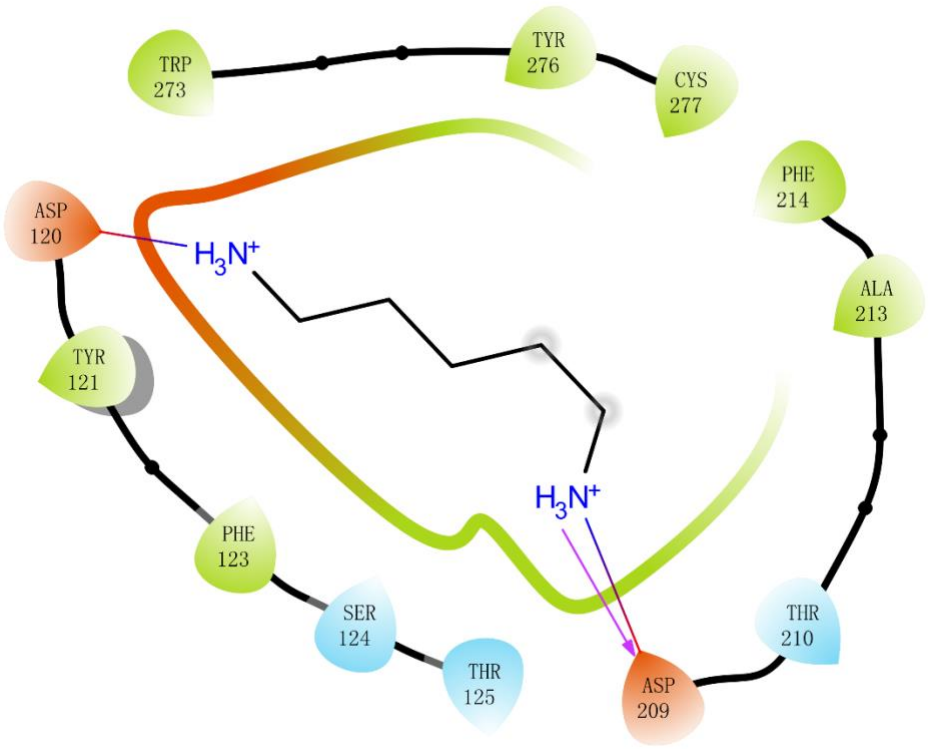

Figure S3-5. The 2D workspace of cadaverine interactions predicted by docking to wildtype TAAR346a

The 2D-diagram shows cadaverine, the major interacting residues ($Asp^{3.32}$ and $Asp^{5.42}$) and the surrounding residues embracing the predicted cadaverine binding pocket. Salt bridge is visualized as blue solid line. Hydrogen bond is visualized as magenta arrow.

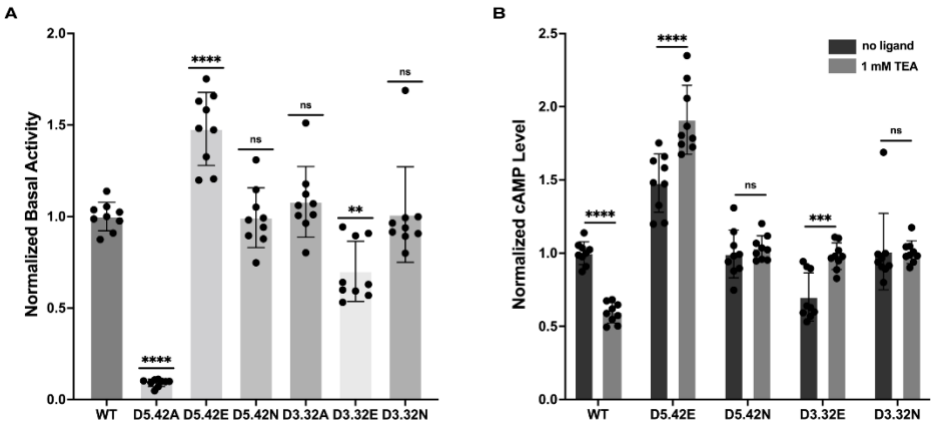

Figure S3-6. The basal activity of TAAR346a mutated in the di-cationic recognition motif
HEK293 cells expressed TAAR346a, $D^{5.42}$ mutants, and $D^{3.32}$ mutants were incubated with buffer or 1 mM triethylamine. Changes in intracellular cAMP production were detected by TR-FRET and normalized to the WT basal cAMP production. The cAMP levels were normalized as measured cAMP /WT basal cAMP. (A) The normalized basal activity of TAAR346a mutant receptors mutated in the cadaverine binding sites (mean ± S.D., n=9; Ordinary one-way ANOVA *p* value <0.0001, Dunnett's multiple comparisons test **** *p* value < 0.0001, ** *p* value < 0.01, ns *p* value > 0.05). (B) The D5.42E and D3.32E mutants showed a significant increase of cAMP production when 1 mM triethylamine was administrated (mean ± S.D., n=9; Two-way ANOVA *p* value < 0.0001, Šídák's multiple comparisons test **** *p* value < 0.0001, *** *p* value < 0.001, ns *p* value > 0.05).

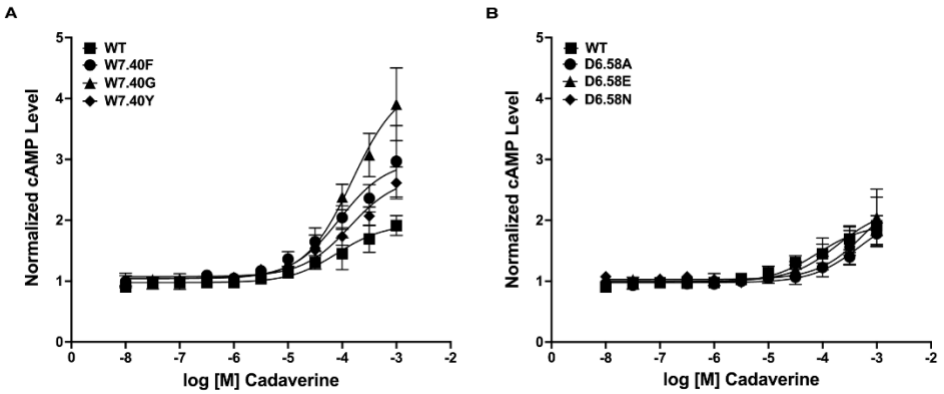

Figure S3-7. Concentration-response curves of TAAR346a mutated in Trp$^{7.40}$ and Asp$^{6.58}$
HEK293 cells expressed TAAR346a, W$^{7.40}$ mutants, and D$^{6.58}$ mutants were incubated with concentration series of cadaverine (100nM to 1 mM). Changes in intracellular cAMP production were detected by TR-FRET and normalized to the WT basal cAMP production. The cAMP levels were normalized as measured cAMP /WT basal cAMP. (A) All three Trp$^{7.40}$ mutants were activated by cadaverine, at a similar EC_{50} value as wildtype TAAR346a (mean ± S.D., n=3). Efficacy was strongly increased in these mutants. (B) Cadaverine was able to activate all three Asp$^{6.58}$ mutants, with similar potency and efficacy as wildtype (mean ± S.D., n=3).

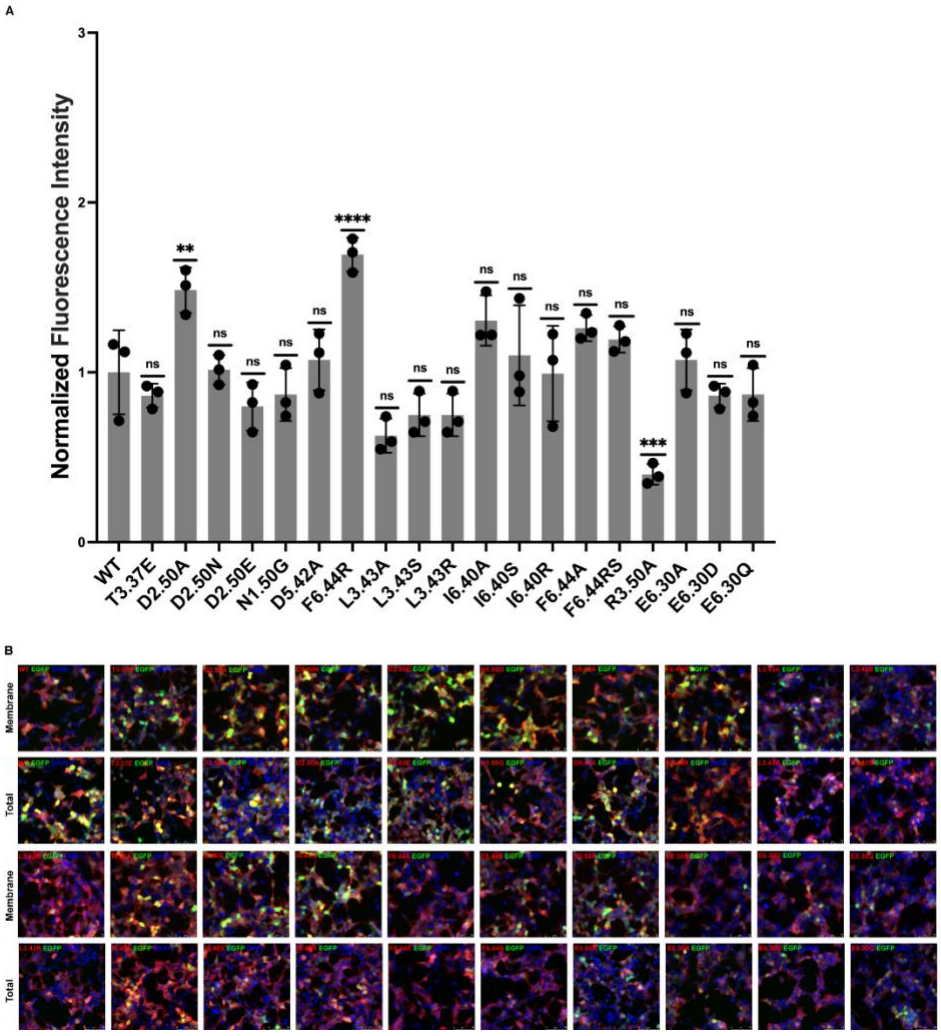

Figure S3-8. All TAAR346a mutants examined for basal activity are well-expressed on the cytomembrane

(A) HEK293T cells were transfected 75ng TAAR 346a and its mutant receptors, along with 375ng pGL4.29, 75ng mRTPs, and 75ng EGFP. Transfected cells were incubated for 24 hours for immunocytochemistry assay. TAAR 346a, TAAR348, TAAR365, and mock receptor were labeled with anti-Rho-tag antibody that colored with red-fluorescent Alexa Fluor 594. Cells were permeabilized or not permeabilized with Triton X-100 to label the whole cell or only cell membrane. Images were acquired at 400×magnification under DMI8 Thunder (Leica) with DAPI filter, GFP filter, and Texas Red filter, respectively (10 random views/well, mean ± S.D., n=3; Ordinary one-way ANOVA *p* value <0.0001, Dunnett's multiple comparisons test **** *p* value < 0.0001, ** *p* value < 0.01, ns *p* value > 0.05). The mean value of red-fluorescent signal was quantified with LAS X software (Leica). (B) TAAR346a and its mutant receptors are expressed on cytomembrane of HEK293T cell as shown by the immunostained Rho-tag antibody (red) for membrane-bound (top panel, without permeation) expression. Receptors located on the cell surface appeared as red rings around the nucleus or total (bottom panel, with permeation using Triton X-100). The nucleus was counterstained with DAPI (blue). EGFP was used as the negative control to evaluate transfection efficiency (green). Scale bar: 75 μm.

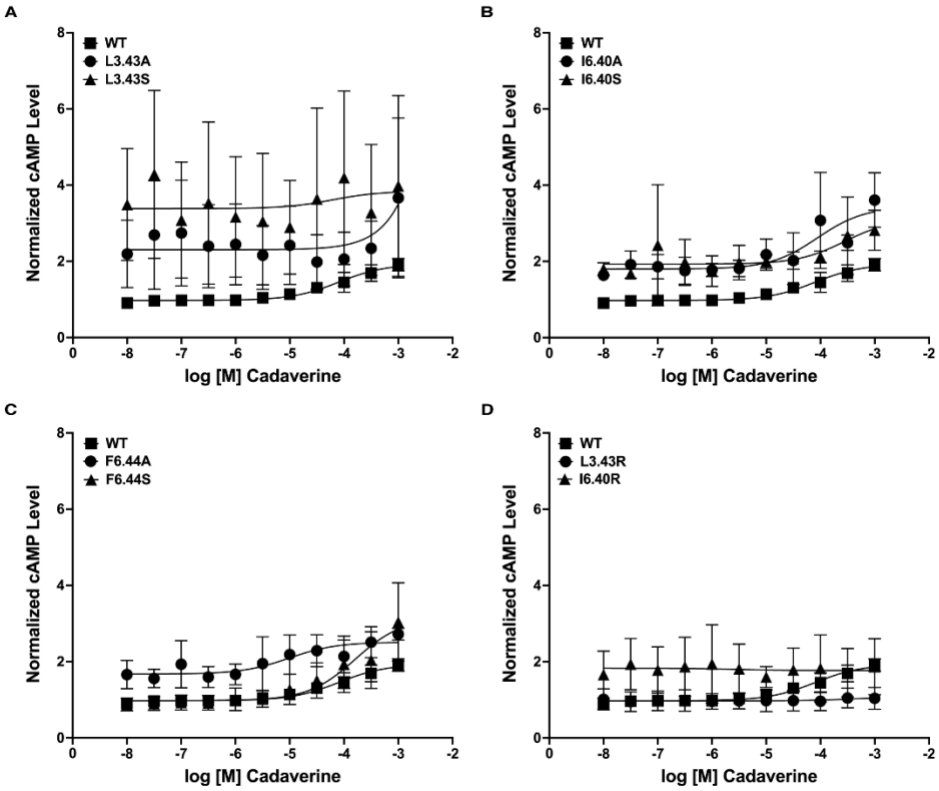

Figure S3-9. Concentration-response curves of TAAR346a mutated in hydrophobic residues Leu$^{3.43}$, Ile$^{6.40}$, and Phe$^{6.44}$

HEK293 cells expressed TAAR346a and its mutant receptors were incubated with concentration-dependent cadaverine (100nM to 1 mM). Changes in intracellular cAMP production were detected by TR-FRET and normalized to the WT basal cAMP production. The cAMP levels were normalized as measured cAMP /WT basal cAMP. (A) Hardly any cAMP production was induced by cadaverine in the L3.43A and L3.43S mutants (mean ± S.D, n=3). (B) Cadaverine induced cAMP production in a concentration-dependent manner in HEK293T cells expressing the I6.40A and I6.40S mutants, with a similar EC_{50} value as wild-type TAAR346a (mean ± S.D., n=3). (C) Cadaverine was able to activate HEK293T cells expressing the F6.44A and F6.44S mutants, with similar potency as wild-type TAAR346a (mean ± S.D., n=3). (D) The L3.43R and I6.40R mutants showed no responses to the stimulation of cadaverine (mean ± S.D., n=3).

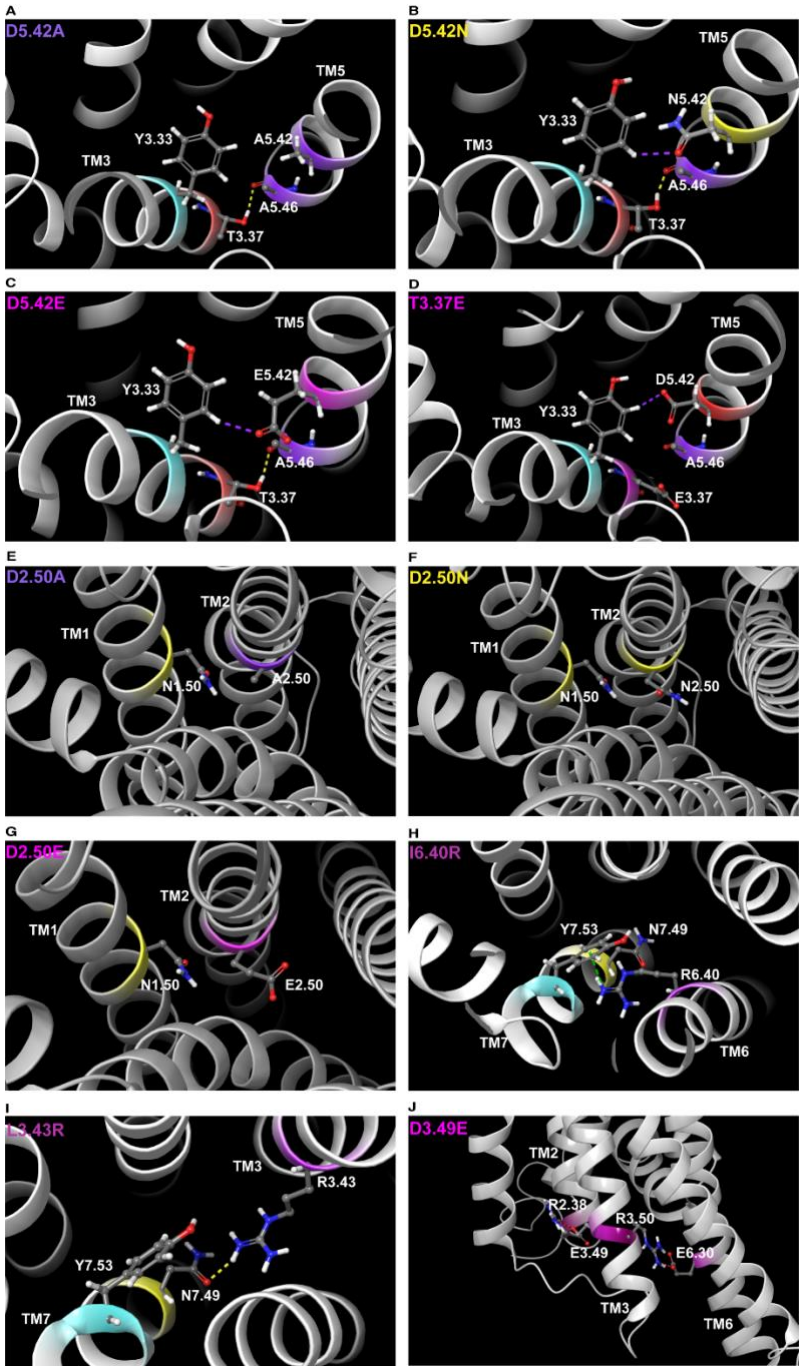

Figure S3-10. Rearrangement of interhelical interactions in the homology modeling of TAAR346a mutants

(A-C) Predicted structure of the D5.42A mutant showed the absence of the predicted wildtype hydrogen bond between $Y^{3.33}$ and $D^{5.42}$. In contrast, the wildtype hydrogen bond was retained in the D5.42E and D5.42N mutants. (D) Mutation of the $T^{3.37}$ residue to glutamate eliminated the wildtype hydrogen bond between $T^{3.37}$ and $A^{5.46}$. (E-G) Homology modeling of the $D^{2.50}$ mutants showed the absence of the wildtype hydrogen bond between $N^{1.50}$ and $D^{2.50}$. (H) Mutation of the $I^{6.40}$ residue to arginine formed a pi-cation interaction with $Y^{7.53}$. (I) Homology modeling of the L3.43R mutant predicted a hydrogen bond between $R^{3.43}$ and $N^{7.49}$.

Figure S3-10 (cont'd).
(J) The predicted interhelical interactions between paired residues $Arg^{3.50}/Glu^{6.30}$ and $Asp^{3.49}/Arg^{2.38}$ were retained in the D3.49E mutant.

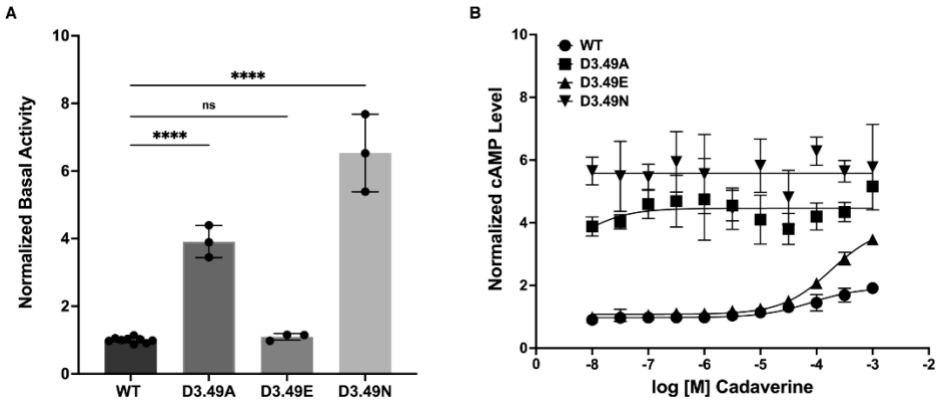

Figure S3-11. The DRY/ERY motif is involved in mediating constitutive activity of the receptor

HEK293 cells expressed TAAR346a and its mutant receptors were incubated with stimulation-buffer or concentration-dependent cadaverine (100nM to 1 mM). Changes in intracellular cAMP production were detected by TR-FRET and normalized to the WT basal cAMP production. The cAMP levels were normalized as measured cAMP /WT basal cAMP. (A) Charge-neutralizing mutation of $Asp^{3.49}$ resulted in a significant increase of receptor basal activity (mean ± S.D., n=3; Ordinary one-way ANOVA *p* value < 0.0001, Dunnett's multiple comparisons test **** *p* value <0.0001). The most conservative replacement, D3.49E, showed no difference in basal activity by comparing to wildtype TAAR346a (mean ± S.D., n=3; ns *p* value > 0.05). (B) Concentration-dependent responses of TAAR346a and its $Asp^{3.49}$ mutants for cadaverine (mean ± S.D., n=3).

	Sequence (5’-3’)
TAAR346a-F	TTGCGGCCGCGATGGCACAGAGCGTGTTGAAAC
TAAR346a-R	CGGAATTCTTAATCTTCTCTGAAAAGATCC
D3.32A-F	CGTGGAGAAGATGTAGGCGAGGCTCGTGTGAAT
D3.32A-R	ATTCACACGAGCCTCGCCTACATCTTCTCCACG
D3.32E-F	CGTGGAGAAGATGTACTCGAGGCTCGTGTGA
D3.32E-R	TCACACGAGCCTCGAGTACATCTTCTCCACG
D3.32N-F	CGTGGAGAAGATGTAGTTGAGGCTCGTGTGAATCT
D3.32N-R	AGATTCACACGAGCCTCAACTACATCTTCTCCACG
D5.42A-F	AAGGCACACACCGTGGCCAGAAGCACAAAGG
D5.42A-R	CCTTTGTGCTTCTGGCCACGGTGTGTGCCTT
D5.42E-F	GGCACACACCGTCTCCAGAAGCACAAAGGTA
D5.42E-R	TACCTTTGTGCTTCTGGAGACGGTGTGTGCC
D5.42N-F	GAAGGCACACACCGTGTTCAGAAGCACAAAGGTAG
D5.42N-R	CTACCTTTGTGCTTCTGAACACGGTGTGTGCCTTC
N1.50G-F	GCGATGACCAGCGTGCCGCCAACAGCGATGGC
N1.50G-R	GCCATCGCTGTTGGCGGCACGCTGGTCATCGC
D2.50A-F	CCACGAGGAAGGCGGCGAGCGCC
D2.50A-R	GGCGCTCGCCGCCTTCCTCGTGG
D2.50E-F	CCCACGAGGAACTCGGCGAGCGC
D2.50E-R	GCGCTCGCCGAGTTCCTCGTGGG
D2.50N-F	CCACGAGGAAGTTGGCGAGCGCCAG
D2.50N-R	CTGGCGCTCGCCAACTTCCTCGTGG
T3.37E-F	GTGCAGGATGGACGCCTCGGAGAAGATGTAGTCG
T3.37E-R	CGACTACATCTTCTCCGAGGCGTCCATCCTGCAC
L3.43A-F	TATGCGATGCAGCTGGCGTGCAGGATGGACGC
L3.43A-R	GCGTCCATCCTGCACGCCAGCTGCATCGCATA
L3.43S-F	GTATGCGATGCAGCTGCTGTGCAGGATGGACGCC
L3.43S-R	GGCGTCCATCCTGCACAGCAGCTGCATCGCATAC
L3.43R-F	ATGCGATGCAGCTGCGGTGCAGGATGGAC
L3.43R-R	GTCCATCCTGCACCGCAGCTGCATCGCAT

Table S3-1. Primers of PCR for TAAR346a and its mutants

ACKNOWLEDGMENTS

We thank Dr. H. Matsunami for providing pCI-mRTPs and pCI-Gα_{olf}, and staff members of US Fish and Wildlife Service and Fisheries and Oceans Canada for providing sea lamprey.

AUTHOR CONTRIBUTIONS

Conceptualization: Liang Jia, Weiming Li, Richard R. Neubig.

Data curation: Liang Jia, Weiming Li, Richard R. Neubig.

Formal analysis: Liang Jia, Richard R. Neubig.

Funding acquisition: Weiming Li.

Investigation: Liang Jia, Anne M. Scott, Zhe Zhang, Jianfeng Ren, Qinghua Zhang, Yu-Wen Chung-Davidson.

Supervision: Weiming Li, Richard R. Neubig.

Validation: Liang Jia, Richard R. Neubig.

Visualization: Liang Jia.

Writing-original draft: Liang Jia.

Writing-review and editing: Liang Jia, Weiming Li, Richard R. Neubig.

REFERENCES

REFERENCES

1. Lowe, G., & Gold, G. H. Olfactory transduction is intrinsically noisy. Proceedings of the National Academy of Sciences of the United States of America. 1995;92(17),7864–7868.

2.Reisert J. Origin of basal activity in mammalian olfactory receptor neurons. The Journal of general physiology. 2010;136(5),529–540.

3. H., Kiyonari, H., Abe, T., Chen, M., Weinstein, L. S., Yu, C. R., Storm, D. R., Nishizumi, H., & Sakano, H. Agonist-independent GPCR activity regulates anterior-posterior targeting of olfactory sensory neurons. Cell. 2013;154(6),1314–1325.

4. Wallace, K. J., & Rosen, J. B. Predator odor as an unconditioned fear stimulus in rats: elicitation of freezing by trimethylthiazoline, a component of fox feces. Behavioral neuroscience. 2000; 114(5),912–922.

5. Johnson, N. S., Yun, S. S., Thompson, H. T., Brant, C. O., & Li, W. A synthesized pheromone induces upstream movement in female sea lamprey and summons them into traps. Proceedings of the National Academy of Sciences of the United States of America. 2009;106(4),1021–1026.

6. Li, K., Brant, C. O., Huertas, M., Hessler, E. J., Mezei, G., Scott, A. M., Hoye, T. R., & Li, W. Fatty-acid derivative acts as a sea lamprey migratory pheromone. Proceedings of the National Academy of Sciences of the United States of America. 2018;115(34),8603–8608.

7. McMeniman, C. J., Corfas, R. A., Matthews, B. J., Ritchie, S. A., & Vosshall, L. B. Multimodal integration of carbon dioxide and other sensory cues drives mosquito attraction to humans. Cell. 2014;156(5),1060–1071.

8. Vickers N. J. Mechanisms of animal navigation in odor plumes. The Biological bulletin. 2000; 198(2),203–212.

9. Libants, S., Carr, K., Wu, H., Teeter, J. H., Chung-Davidson, Y. W., Zhang, Z., Wilkerson, C., & Li, W. The sea lamprey Petromyzon marinus genome reveals the early origin of several chemosensory receptor families in the vertebrate lineage. BMC evolutionary biology. 2009;9,180.

10. Borowsky, B., Adham, N., Jones, K. A., Raddatz, R., Artymyshyn, R., Ogozalek, K. L., Durkin, M. M., Lakhlani, P. P., Bonini, J. A., Pathirana, S., Boyle, N., Pu, X., Kouranova, E., Lichtblau, H., Ochoa, F. Y., Branchek, T. A., & Gerald, C. Trace amines: identification of a family of mammalian G protein-coupled receptors. Proceedings of the National Academy of Sciences of the United States of America, 2001;98(16),8966–8971.

11. Bunzow, J. R., Sonders, M. S., Arttamangkul, S., Harrison, L. M., Zhang, G., Quigley, D. I., Darland, T., Suchland, K. L., Pasumamula, S., Kennedy, J. L., Olson, S. B., Magenis, R. E., Amara, S. G., & Grandy, D. K. Amphetamine, 3,4-methylenedioxymethamphetamine, lysergic acid diethylamide, and metabolites of the catecholamine neurotransmitters are agonists of a rat trace amine receptor. Molecular pharmacology. 2001;60(6),1181–1188.

12. Nei, M., Niimura, Y., & Nozawa, M. The evolution of animal chemosensory receptor gene repertoires: roles of chance and necessity. Nature reviews. Genetics. 2008;9(12),951–963.

13. Firestein S. (2001). How the olfactory system makes sense of scents. Nature. 2001; 413(6852),211–218.

14. Restrepo, D., Teeter, J. H., & Schild, D. Second messenger signaling in olfactory transduction. Journal of neurobiology. 1996;30(1),37–48.

15. Tao Y. X. Constitutive activation of G protein-coupled receptors and diseases: insights into mechanisms of activation and therapeutics. Pharmacology & therapeutics. 2008;120(2),129–148.

16. Liberles, S. D., & Buck, L. B. A second class of chemosensory receptors in the olfactory epithelium. Nature. 2006;442(7103),645–650.

17. Liberles S. D. Trace amine-associated receptors: ligands, neural circuits, and behaviors. Current opinion in neurobiology. 2015;34,1–7.

18. Ferrero, D. M., Lemon, J. K., Fluegge, D., Pashkovski, S. L., Korzan, W. J., Datta, S. R., Spehr, M., Fendt, M., & Liberles, S. D. Detection and avoidance of a carnivore odor by prey. Proceedings of the National Academy of Sciences of the United States of America. 2011;108(27),11235–11240.

19. Li, Q., Korzan, W. J., Ferrero, D. M., Chang, R. B., Roy, D. S., Buchi, M., Lemon, J. K., Kaur, A. W., Stowers, L., Fendt, M., & Liberles, S. D. Synchronous evolution of an odor biosynthesis pathway and behavioral response. Current biology. 2013;23(1),11–20.

20. Scott, A. M., Zhang, Z., Jia, L., Li, K., Zhang, Q., Dexheimer, T., Ellsworth, E., Ren, J., Chung-Davidson, Y. W., Zu, Y., Neubig, R. R., & Li, W. Spermine in semen of male sea lamprey acts as a sex pheromone. PLoS biology. 2019;17(7),e3000332.

21. Saraiva, L. R., Kondoh, K., Ye, X., Yoon, K. H., Hernandez, M., & Buck, L. B. Combinatorial effects of odorants on mouse behavior. Proceedings of the National Academy of Sciences of the United States of America. 2016,113(23),E3300–E3306.

22. Adams, T. S, Holman, G. M, & Nelson, D R. Amines that induce monocoitic behavior in the house fly, *Muscadomestica*. Chemosphere. 1972;1(1),39-42.

23. Hussain, A., Saraiva, L. R., Ferrero, D. M., Ahuja, G., Krishna, V. S., Liberles, S. D., & Korsching, S. I. High-affinity olfactory receptor for the death-associated odor cadaverine. Proceedings of the National Academy of Sciences of the United States of America. 2013; 110(48),19579–19584.

24. Dinter, J., Mühlhaus, J., Wienchol, C. L., Yi, C. X., Nürnberg, D., Morin, S., Grüters, A., Köhrle, J., Schöneberg, T., Tschöp, M., Krude, H., Kleinau, G., & Biebermann, H. Inverse agonistic action of 3-iodothyronamine at the human trace amine-associated receptor 5. PloS one. 2015;10(2),e0117774.

25. Tehan, B. G., Bortolato, A., Blaney, F. E., Weir, M. P., & Mason, J. S. Unifying family A GPCR theories of activation. Pharmacology & therapeutics. 2014;143(1),51–60.

26. Parnot, C., Miserey-Lenkei, S., Bardin, S., Corvol, P., & Clauser, E. Lessons from constitutively active mutants of G protein-coupled receptors. Trends in endocrinology and metabolism: TEM. 2002;13(8),336–343.

27. Huang E. S. Construction of a sequence motif characteristic of aminergic G protein-coupled receptors. Protein science: a publication of the Protein Society. 2003;12(7),1360–1367.

28. Sharma, K., Ahuja, G., Hussain, A., Balfanz, S., Baumann, A., & Korsching, S. I. Elimination of a ligand gating site generates a supersensitive olfactory receptor. Scientific reports. 2016; 6,28359. 10.1038/srep28359.

29. Blundell, T., Barlow, D., Borkakoti, N., & Thornton, J. Solvent-induced distortions and the curvature of alpha-helices. Nature. 1983;306(5940),281–283.

30. Cabana, J., Holleran, B., Beaulieu, M. È., Leduc, R., Escher, E., Guillemette, G., & Lavigne, P. Critical hydrogen bond formation for activation of the angiotensin II type 1 receptor. The Journal of biological chemistry. 2013;288(4),2593–2604.

31. Park, S. H., Das, B. B., Casagrande, F., Tian, Y., Nothnagel, H. J., Chu, M., Kiefer, H., Maier, K., De Angelis, A. A., Marassi, F. M., & Opella, S. J. Structure of the chemokine receptor CXCR1 in phospholipid bilayers. Nature. 2012;491(7426),779–783.

32. Sansuk, K., Deupi, X., Torrecillas, I. R., Jongejan, A., Nijmeijer, S., Bakker, R. A., Pardo, L., & Leurs, R. A structural insight into the reorientation of transmembrane domains 3 and 5 during family A G protein-coupled receptor activation. Molecular pharmacology. 2011;79(2),262–269.

33. Perlman, J. H., Colson, A. O., Wang, W., Bence, K., Osman, R., & Gershengorn, M. C. Interactions between conserved residues in transmembrane helices 1, 2, and 7 of the thyrotropin-releasing hormone receptor. The Journal of biological chemistry. 1997;272(18),7–11942.

34. Ballesteros, J. A., Jensen, A. D., Liapakis, G., Rasmussen, S. G., Shi, L., Gether, U., & Javitch, J. A. Activation of the beta 2-adrenergic receptor involves disruption of an ionic lock between the cytoplasmic ends of transmembrane segments 3 and 6. The Journal of biological chemistry. 2001; 276(31),29171–29177.

35. Li, J., Edwards, P. C., Burghammer, M., Villa, C., & Schertler, G. F. Structure of bovine rhodopsin in a trigonal crystal form. Journal of molecular biology. 2004;343(5),1409–1438.

36. Deupi, X., Dölker, N., López-Rodríguez, M. L., Campillo, M., Ballesteros, J. A., & Pardo, L. Structural models of class A G protein-coupled receptors as a tool for drug design: insights on transmembrane bundle plasticity. Current topics in medicinal chemistry. 2007;7(10),991–998.

37. Lebon, G., Warne, T., Edwards, P. C., Bennett, K., Langmead, C. J., Leslie, A. G., & Tate, C. G. Agonist-bound adenosine A2A receptor structures reveal common features of GPCR activation. Nature. 2011;474(7352),521–525.

38. Standfuss, J., Edwards, P. C., D'Antona, A., Fransen, M., Xie, G., Oprian, D. D., & Schertler, G. F. The structural basis of agonist-induced activation in constitutively active rhodopsin. Nature. 2011; 471(7340),656–660.

39. Park, J. H., Scheerer, P., Hofmann, K. P., Choe, H. W., & Ernst, O. P. Crystal structure of the ligand-free G-protein-coupled receptor opsin. Nature. 2008;454(7201),183–187.

40. Xu, F., Wu, H., Katritch, V., Han, G. W., Jacobson, K. A., Gao, Z. G., Cherezov, V., & Stevens, R. C. Structure of an agonist-bound human A2A adenosine receptor. Science. 2011;332(6027), 322–327.

41. Sharma, K., Balfanz, S., Baumann, A., & Korsching, S. Full rescue of an inactive olfactory receptor mutant by elimination of an allosteric ligand-gating site. Scientific reports. 2018;8(1), 9631. 10.1038/s41598-018-27790-7.

42. Ferrero, D. M., Wacker, D., Roque, M. A., Baldwin, M. W., Stevens, R. C., & Liberles, S. D. Agonists for 13 trace amine-associated receptors provide insight into the molecular basis of odor selectivity. ACS chemical biology. 2012;7(7),1184–1189.

43. Bradaia, A., Trube, G., Stalder, H., Norcross, R. D., Ozmen, L., Wettstein, J. G., Pinard, A., Buchy, D., Gassmann, M., Hoener, M. C., & Bettler, B. The selective antagonist EPPTB reveals TAAR1-mediated regulatory mechanisms in dopaminergic neurons of the mesolimbic system. Proceedings of the National Academy of Sciences of the United States of America. 2009;106(47), 20081–20086.

44. Li, Q., Tachie-Baffour, Y., Liu, Z., Baldwin, M. W., Kruse, A. C., & Liberles, S. D. Non-classical amine recognition evolved in a large clade of olfactory receptors. eLife. 2015;4,e10441. 10.7554/eLife.10441.

45. Hussain, A., Saraiva, L. R., & Korsching, S. I. Positive Darwinian selection and the birth of an olfactory receptor clade in teleosts. Proceedings of the National Academy of Sciences of the United States of America. 2009;106(11),4313–4318.

46. Revel, F. G., Moreau, J. L., Gainetdinov, R. R., Bradaia, A., Sotnikova, T. D., Mory, R., Durkin, S., Zbinden, K. G., Norcross, R., Meyer, C. A., Metzler, V., Chaboz, S., Ozmen, L., Trube, G., Pouzet, B., Bettler, B., Caron, M. G., Wettstein, J. G., & Hoener, M. C. TAAR1 activation modulates monoaminergic neurotransmission, preventing hyperdopaminergic and hypoglutamatergic activity. Proceedings of the National Academy of Sciences of the United States of America. 2011;108(20),8485–8490.

47. Jia, L., Li, S., Dai, W., Guo, L., Xu, Z., Scott, A. M., Zhang, Z., Ren, J., Zhang, Q., Dexheimer, T. S., Chung-Davidson, Y. W., Neubig, R. R., Li, Q., & Li, W. Convergent olfactory trace amine-associated receptors detect biogenic polyamines with distinct motifs via a conserved binding site. The Journal of biological chemistry. 2021;297(5),101268.

48. Sanchez-Reyes, O. B., Cooke, A., Tranter, D. B., Rashid, D., Eilers, M., Reeves, P. J., & Smith, S. O. G Protein-Coupled Receptors Contain Two Conserved Packing Clusters. Biophysical journal. 2017;112(11),2315–2326.

49. Nygaard, R., Valentin-Hansen, L., Mokrosinski, J., Frimurer, T. M., & Schwartz, T. W. Conserved water-mediated hydrogen bond network between TM-I, -II, -VI, and -VII in 7TM receptor activation. The Journal of biological chemistry. 2010;285(25),19625–19636.

50. Scott, C. E., Abrol, R., Ahn, K. H., Kendall, D. A., & Goddard, W. A., III. Molecular basis for dramatic changes in cannabinoid CB1 G protein-coupled receptor activation upon single- and double-point mutations. Protein science. 2013;22(1),101–113.

51. Marino, K. A., Shang, Y., & Filizola, M. Insights into the function of opioid receptors from molecular dynamics simulations of available crystal structures. British journal of pharmacology. 2018;175(14),2834–2845.

52. Vogel, R., Mahalingam, M., Lüdeke, S., Huber, T., Siebert, F., & Sakmar, T. P. Functional role of the "ionic lock"- an interhelical hydrogen-bond network in family A heptahelical receptors. Journal of molecular biology. 2008;380(4),648–655.

53. Smith, J. J., Kuraku, S., Holt, C., Sauka-Spengler, T., Jiang, N., Campbell, M. S., Yandell, M. D., Manousaki, T., Meyer, A., Bloom, O. E., Morgan, J. R., Buxbaum, J. D., Sachidanandam, R., Sims, C., Garruss, A. S., Cook, M., Krumlauf, R., Wiedemann, L. M., Sower, S. A., Decatur, W. A., … Li, W. Sequencing of the sea lamprey (Petromyzon marinus) genome provides insights into vertebrate evolution. Nature genetics. 2013; 45(4), 415–421e4212.

54. Zhuang H, Matsunami H. Evaluating cell-surface expression and measuring activation of mammalian odorant receptors in heterologous cells. Nature Protocols. 2008;3(9):1402-1413.

55. Sali, A., & Blundell, T. L. Comparative protein modelling by satisfaction of spatial restraints. Journal of molecular biology. 1993;234(3),779–815.

CONCLUSIONS TO DISSERTATION

The sea lamprey relies heavily on a simple but well-developed olfactory system to detect chemical cues and mediate behavioral output. Studies presented in this dissertation provides physiological and molecular evidence showing that biogenic polyamines are potent odorants for sea lamprey olfactory trace amine-associated receptors (TAARs) that play important roles in mediating physiological changes and behavioral responses. The structural basis of sea lamprey TAARs recognize biogenic polyamines will contribute to our understanding of how GPCRs detect biogenic amines.

The results presented in Chapter 1 exhibit cellular, olfactory, and behavioral evidence to support that ovulated females utilize spermine, a semen-derived male sex pheromone, to locate and seek potential mates. The waterborne spermine is linked to the milt of spermiating males and shows a strong behavioral preference in ovulated females, but not in pre-ovulated females, pre-spermiating males, and spermiating males. In addition, a sea lamprey trace amine-associated receptor, TAAR348, appears to be a narrowly tuned olfactory receptor that showed robust, concentration-dependent responses only to spermine and not to other biogenic amines. Inhibition of spermine functions by a selective antagonist (cyclen) at cellular, olfactory, and behavioral levels appears to support a specific role of TAAR348 in mediating the pheromone function of spermine. Consistently, another TAAR348 agonist, nap-spermine replicated identical responses as with spermine at the receptor, olfactory epithelia, and behavioral levels. These lines of data demonstrate that spermine released with milt acts as a male sex pheromone that specifically attracts ovulated females. Our results support a model in which TAAR348 may play an essential role in mediating the olfactory detection of spermine. However, all this evidence cannot exclude the possibility for the involvement of additional receptors in the detection of spermine, because olfactory receptors are usually encoded in a combinatorial fashion to detect structurally diverse odorants. Moreover,

cyclen did not completely eliminate the olfactory responses to spermine and the incomplete maximal inhibition is consistent with an action as a negative allosteric modulator.

The deorphanization of sea lamprey TAAR365 in Chapter 2 provided us an ideal opportunity to characterize the functional convergence of two independently evolved TAAR subfamilies in detection of biogenic polyamines. We propose a hypothetical structural model for polyamine recognition by two clades of independently evolved TAARs, represented by sTAAR365 and mTAAR9. The highly conserved $Asp^{3.32}$ is the primary site essential to binding to one amino group of polyamines. sTAAR365 and mTAAR9 utilize other scaffolds that contribute to the specificity of polyamine recognition (a common residue $Tyr^{6.51}$ for both sTAAR365 and mTAAR9 and a distinct residue $Thr^{7.42}$ for sTAAR365) or stabilize recognition of polyamines with more than two amino groups ($Glu^{7.36}$ and $Tyr^{7.43}$ for both sTAAR365 and mTAAR9). Thus, this model provides strong evidence for a steric and functional odotope theory that sTAAR365 and mTAAR9 utilize convergent structural bases with distinct residues to detect various biogenic polyamines. The convergent mechanism of polyamine recognition by TAARs reveals additional insights into amine detection by GPCRs.

The identification of a lamprey constitutively active cadaverine-responsiveness trace amine-associated receptor (TAAR346a) in Chapter 3 allowed me to define structural determinants for ligand-independent and ligand-dependent activation of olfactory receptors. Triethylamine was identified as an inverse agonist of TAAR346a that inhibits the receptor constitutive activity in a concentration-dependent manner. By combining the data with the inverse agonist and agonist, I propose a model in which the inverse agonist triethylamine recognizes only one ($Asp^{5.42}$) of the two orthosteric sites ($Asp^{3.32}$ and $Asp^{5.42}$) used by the agonist cadaverine as it elicits its inhibitory effect on the basal activity of the receptor. For the ligand-independent activation, I show that a

model-predicted hydrogen bond ($Thr^{3.37}$/$Ala^{5.46}$) is highly important for the constitutive signaling of TAAR346a, whereas it holds the receptor in an inactive conformation in other class A GPCRs. Moreover, another model-predicted hydrogen bond ($Asn^{1.50}$/$Asp^{2.50}$) acts in a molecular switch that is critical for both constitutive and agonist-induced activity of TAAR346a. In contrast, residues at the predicted ionic lock and hydrophobic core between TM3 and TM6 are preferred to hold the receptor in a relative inactive conformation. Therefore, all of the homology modeling and site-directed mutagenesis results provide multiple lines of evidence that directly support the overall hypothesis that interhelical interactions may serve different roles in modulating the GPCR activation, synergistically holding the receptor in a partially constitutively active conformation.

In conclusion, my dissertation integrates chemical, physiological, and behavioral evidence to support the pheromone function of spermine in sea lamprey. The deorphanization of sea lamprey TAARs advances the structural basis of biogenic amine recognition by TAARs and provides the structural insights into the constitutively activation of olfactory TAARs. The ligands identified in the dissertation, including agonist, antagonist, and inverse agonist, may have potential applications for sea lamprey control in the Laurentian Great Lakes. Future studies are needed to examine the roles of identified ligands and paired TAARs in mediating physiological changes and behavioral responses.

CONTROL IMPLICATIONS

The sea lamprey (*Petromyzon marinus*) is an incredibly destructive invasive species in the Laurentian Great Lakes and has caused enormous economic and ecological damages on the Great Lakes fishery. To protect the integrity of the Great Lakes native ecosystem, the Great Lakes Fishery Commission (GLFC) and its cooperative partners carried out a sea lamprey control program that combines a series of control tactics to reduce the sea lamprey populations in the Great Lakes. Currently, the control tactics mainly aim at either the larval (lampricides) or adult stages (barriers traps, and pheromone) of the sea lamprey lifecycle [1-4]. Biogenic amines are potent odorants enriched in biological excretions (urine, feces, and semen), decomposed tissues, and food sources, and act as important odor cues that elicit distinct physiological changes and behavioral responses in vertebrates [5-10]. The data presented herein characterize a semen-derived male pheromone and odorous biogenic amines that advance our understanding of pheromone repertoire in sea lamprey and could be integrated into the sea lamprey control program for the reduction of sea lamprey populations in the Great Lakes.

Since the 1990s, scientists have been studying the application of pheromones in the sea lamprey management that can mediate migratory and spawning behavioral responses in adult sea lamprey [11, 12]. After over 20-years of research, 3kPZS has been shown to be a major component of sea lamprey mating pheromone and was registered as the first vertebrate pheromone biopesticide by the U.S. Environmental Protection Agency in 2015 [4, 12-14]. 3kPZS-baited sea lamprey traps have been shown to be more efficacy on capture rate [4]. The Chapter 1 of this dissertation unveils a novel male sex pheromone (spermine) in milt that is attractive for ovulatory females and no other adults. Prior to this study, almost all of the identified sea lamprey pheromones

(migratory pheromone and mating pheromone) belong to bile acids [15]. The identification of male pheromone spermine broadened the spectrum of sea lamprey pheromone repertoire. Unlike the anti-aphrodisiac molecules in insects, spermine released along milt appears to serve as an aphrodisiac that likely mediates mating aggregations and facilitates reproduction. The ovulatory females may use spermine as a reliable signal to identify the presence of spermiating males and assess sexual maturity. In contrast to the sex-specific and maturation-specific behavioral response of spermine, milt itself can attract all adults of various maturation stages. Milt odors are made up of multiple components that may serve as mating signals allowing males and females at various maturation stages to spy on spawning habitat and mating aggregations. Immature adults may benefit from milt odors to tract spawning grounds. Males may take the advantage of milt odors to aggregate in a lek-like system that allows males collectively releasing more pheromone to attract more mating partners. However, the pheromone function of milt odorant that attracts males remains to be examined in the future. The identification of milt pheromones may also have management implications for sea lamprey control in the Great Lakes.

In Chapter 2 and Chapter 3, several other biogenic amines are identified as ligands for two sea lamprey olfactory TAARs that may influence behavioral responses of sea lamprey and provide management approaches for sea lamprey control in the Great Lakes. These odorous biogenic amines are found in biological excretions (urine, feces, and semen), decomposed tissues, and food sources, and can elicit significant physiological changes and behavioral responses in various species examined. Cadaverine and putrescine, the foul-smelling diamines produced by microbial metabolism of putrefied animal tissue, can serve as alarm, feeding, and social cues in several vertebrate species and mediate innate aversion or attraction behavioral responses [5, 9, 16-18]. Also, these two diamines are endogenously present in urine and also contribute to the smell of

semen [19]. However, whether these two diamines are present in the lamprey milt and contribute to the pheromone function of milt in spawning adults remain to be examined in the future. However, cadaverine and putrescine likely have different roles in mediating larval behavior. As larval sea lamprey filter plankton and detritus, we suspect that cadaverine and putrescine from detritus may function as feeding cues and are attractive for larvae. Given that sea lamprey die shortly after spawning, carcasses would be a reliable source of feeding cues for larvae. Meanwhile, males and females may benefit from cadaverine and putrescine to spy on suitable spawning habitat. Future studies on behavioral aspects of cadaverine and putrescine may further explain the fitness benefit of biogenic amines in sea lamprey.

Inhibition of pheromone functions by applying an antagonist will likely block spawning behavior. Cyclen is a selective antagonist to spermine that can specifically disrupt the olfactory and behavioral responses of ovulatory females to spermine. Cyclen can specifically reduce the olfactory response to spermine in a concentration dependent manner and neutralize the behavioral preference of ovulatory females to spermine in a two-choice maze. More importantly, the spermine response in ovulatory females is reversible when cyclen treatment was removed. These results suggest that cyclen may have important management implications for sea lamprey control in the future. The neutralizing effect of cyclen on spermine-induced behavioral preference should be further examined in a natural spawning habitat. Additional field trials are needed to assess the utility of cyclen on spermine-induced nest approach, nest extension, and spawning behaviors in ovulated females.

Aside from the spermine antagonist, triethylamine is identified as an inverse agonist to another sea lamprey cadaverine-responsive TAAR receptor (TAAR346a). Triethylamine is a potent odorant in rodents [9], whereas few biological activates and behavioral responses have been

reported for this odorant. Thus, our identification of triethylamine as an inverse agonist may help to examine the physiological significance of the constitutively active TAAR346a. Moreover, many inverse agonists are also thought to be antagonists at GPCRs [20]. In the future, it would be interesting to determine whether cadaverine-induced response could be affected by triethylamine at the receptor, olfactory epithelia, and behavioral levels. Notably, triethylamine partially inhibits the constitutive activity of TAAR346a, indicating that triethylamine likely acts as a partial inverse agonist for TAAR346a. The pharmacological and physiological effects of triethylamine on the constitutively active TAAR346a should be further investigated in a natural environment. Therefore, it would be necessary to identify optimized inverse agonists with higher potency (full inverse agonists) for TAAR346a. An effective inverse agonist should completely nullify the constitutive activity and neutralize the physiological significance of the receptor. The identification of more potent inverse agonist will provide a better understanding of mechanisms whereby inverse agonists interact with constitutively active olfactory receptors and likely further alters olfactory responses to agonists, which will in turn facilitate the development of effective antagonists for sea lamprey control.

Taken together, the sea lamprey male pheromone, pheromone antagonist, odorous biogenic amines, and inverse agonist identified in this dissertation may have management implications for the sea lamprey control program in the Laurentian Great Lakes. The combination of pheromone with other control tactics will protect the integrity of ecosystem, sustain the native biodiversity, and ensure sustainable fishery in the Great Lakes.

REFERENCES

REFERENCES

1. Smith B, Tibbles J. Sea lamprey (Petromyzon marinus) in Lakes Huron, Michigan, and Superior: history of invasion and control, 1936–78. Can J Fish Aquat Sci. 1980;37(11):1780–801.

2. Christie G C, Goddard C I. Sea Lamprey International Symposium (SLIS II): advances in the integrated management of sea lamprey in the Great Lakes. Journal of Great Lakes Research. 2003, 29:1-14.

3. Li W, Twohey M, Jones M, et al. Research to guide use of pheromones to control sea lamprey. Journal of Great Lakes Research. 2007, 33: 70-86.

4. Johnson N S, Siefkes M J, Wagner C M, et al. A synthesized mating pheromone component increases adult sea lamprey (Petromyzon marinus) trap capture in management scenarios. Canadian Journal of Fisheries and Aquatic Sciences. 2013, 70(7): 1101-1108.

5. Hussain, A., Saraiva, L. R., Ferrero, D. M., Ahuja, G., Krishna, V. S., Liberles, S. D., & Korsching, S. I. High-affinity olfactory receptor for the death-associated odor cadaverine. Proceedings of the National Academy of Sciences of the United States of America. 2013; 110(48),19579–19584.

6. Li, Q., Korzan, W. J., Ferrero, D. M., Chang, R. B., Roy, D. S., Buchi, M., Lemon, J. K., Kaur, A. W., Stowers, L., Fendt, M., & Liberles, S. D. Synchronous evolution of an odor biosynthesis pathway and behavioral response. Current biology. 2013;23(1),11–20.

7. Dewan, A., Pacifico, R., Zhan, R., Rinberg, D., and Bozza, T. Nonredundant coding of aversive odours in the main olfactory pathway. Nature. 2013;497,486–489.

8. Li, Q., and Liberles, S. D. Aversion and attraction through olfaction. Curr. Biol. 2015;25,R120–R129.

9. Saraiva, L. R., Kondoh, K., Ye, X., Yoon, K. H., Hernandez, M., & Buck, L. B. Combinatorial effects of odorants on mouse behavior. Proceedings of the National Academy of Sciences of the United States of America. 2016,113(23),E3300–E3306.

10. Xu, Z., and Li, Q. TAAR agonists. Cell. Mol. Neurobiol. 2020;40,257–272.

11. Teeter J. Pheromone communication in sea lampreys (Petromyzon marinus): implications for population management. Canadian Journal of Fisheries and Aquatic Sciences. 1980, 37(11): 2123-2132.

12. Li W, Scott A P, Siefkes M J, et al. Bile acid secreted by male sea lamprey that acts as a sex pheromone. Science. 2002, 296(5565): 138-141.

13. Johnson, N. S., Yun, S. S., Thompson, H. T., Brant, C. O., & Li, W. A synthesized pheromone induces upstream movement in female sea lamprey and summons them into traps. Proceedings of the National Academy of Sciences of the United States of America. 2009;106(4),1021–1026.

14. Fredricks K, Johnson N, Hubert T, et al. Registration and application of sea lamprey pheromones for sea lamprey control in the United States and Canada. Journal of Great Lakes Research. 2021, 47: S448-S454.

15. Fissette S D, Buchinger T J, Wagner C M, et al. Progress towards integrating an understanding of chemical ecology into sea lamprey control. Journal of Great Lakes Research. 2021, 47: S660-S672.

16. Pinel J P J, Gorzalka B B, Ladak F. Cadaverine and putrescine initiate the burial of dead conspecifics by rats. Physiology & Behavior. 1981, 27(5): 819-824.

17. Heale V R, Petersen K, Vanderwolf C H. Effect of colchicine-induced cell loss in the dentate gyrus and Ammon's horn on the olfactory control of feeding in rats. Brain research. 1996, 712(2): 213-220.

18. Rolen S H, Sorensen P W, Mattson D, et al. Polyamines as olfactory stimuli in the goldfish Carassius auratus. Journal of Experimental Biology. 2003, 206(10): 1683-1696.

19. Heidari A, Gobato R. Putrescine, Cadaverine, Spermine and Spermidine–Enhanced Precatalyst Preparation Stabilization and Initiation (EPPSI) Nano Molecules. Parana Journal of Science and Education. 2018;4(5):1-14.

20. Costa T, Cotecchia S. Historical review: Negative efficacy and the constitutive activity of G-protein-coupled receptors. Trends in pharmacological sciences. 2005, 26(12): 618-624.